Forces, Stresses, and the (Thermo?) Dynamics of Active Matter: The Swim Pressure

Thesis by
Sho C Takatori

In Partial Fulfillment of the Requirements for the
degree of
Doctor of Philosophy

CALIFORNIA INSTITUTE OF TECHNOLOGY
Pasadena, California

2017
Defended May 8, 2017

Sho C Takatori
ORCID: 0000-0002-7839-3399

ACKNOWLEDGEMENTS

I would like to express my sincere gratitude for the support of many amazing people during my PhD studies at Caltech. First, I would like to thank my thesis advisor, John Brady. Aside from his exceptional scientific guidance and his remarkable ability to know the answer to a problem before actually solving it, the quality I appreciate most about Professor Brady's advising is his deep respect and trust for my independence. When I declared one day, "I will pursue experiments" (in an all-theory and simulation group), he allowed me to conduct experiments across three different research groups at Caltech and at ETH Zürich. When I incorporated Disney hats and references into conference presentations, he suggested that I go pursue 'experiments' at Disneyland. I am very fortunate to have learned from a world-class researcher; his academic curiosity, integrity, and rigor have set a high standard that I will continuously aim for as I begin my academic career.

I would like to thank the members of my thesis committee – Zhen-Gang Wang, Rob Phillips, and Mikhail Shapiro. Professor Phillips and Professor Shapiro have generously allowed me to use their lab resources to pursue my experimental studies, which would not have been possible without their support. I would like to thank Dr. Heun-Jin Lee in Professor Phillips' group for teaching me various techniques of experimental biophysics and microscopy. His extensive knowledge in the biophysical behavior of cells have sparked my curiosity in a variety of fields.

I would like to express my great gratitude for Professor Jan Vermant and Dr. Raf De Dier at ETH Zürich, who had the heroic patience and dedication to teach a theorist with an $\sim \mathcal{O}(\epsilon)$ knowledge of basic wet lab techniques how to conduct experiments in soft matter. Raf was the best sensei I could have wished for.

I thank the members of the Brady group: Nick Hoh, Charlie Slominski, Mu Wang, Wen Yan, Isaac Fees, Kevin Marshall, Mikey Phan, Marco Heinen, Eric Burkholder, Mateo Martinez, Luis Nieves, Camilla Kjeldbjerg, and Austin Dulaney. In particular, I thank Mikey for sharing many laughs, weekly runs, and the highs and lows of graduate school over the years. My time here would not have been complete without all of the epic triathlons and outdoor adventures with Kevin and Isaac. I would like to thank every member of the Chemical Engineering staff, in particular Martha Hepworth and Kathy Bubash, for their assistance. I thank the members of the Caltech Toastmasters club for wonderful speech competitions.

Words cannot express how much I have been supported by the love and support from friends and family outside of Caltech. My parents have made tremendous sacrifices throughout my life, just to help me be the best and happiest I could be, and I strive to do the same for them in the coming years. I would like to express my heartfelt gratitude to Gigi for always putting a smile on my face and being willing to lend a sympathetic ear. My life would not be the same without her optimism, sense of humor, and ever-enduring kindness. Thank you to Kevin for a continuous source of the best, funniest, and most legendary stories and adventures. Finally, I thank my sister and gastroenterologist, Dr. Takatori, for her unwavering support and love. I cannot be more proud of having a sister who saves the lives of patients suffering from hideous diseases like Inflammatory Bowel Disease.

Lastly, I would also like to express my deep gratitude for the Bill & Melinda Gates Foundation, which has supported me during my undergraduate and graduate school studies through the Gates Millennium Scholar Program. The research in this thesis was also supported by the National Science Foundation (NSF) Graduate Research Fellowship under Grant No. DGE-1144469 and by NSF Grant CBET 1437570.

ABSTRACT

A core feature of many living systems is their ability to move, self-propel, and be active. From bird flocks to bacteria swarms, to even cytoskeletal networks, active matter systems exhibit collective and emergent dynamics owing to their constituents' ability to convert chemical fuel into mechanical activity. Active matter systems generate their own internal stress, which drives them far from equilibrium and thus frees them from conventional thermodynamic constraints, and by so doing they can control and direct their own behavior and that of their surrounding environment. This gives rise to fascinating behaviors such as spontaneous self-assembly and pattern formation, but also makes the theoretical understanding of their complex dynamical behaviors a challenging problem in the statistical physics of soft matter.

In this thesis, I present a new principle that all active matter systems display—namely, through their self-motion they generate an intrinsic 'swim pressure' that impacts their dynamic and collective behavior. I combine experimental and computational methods to demonstrate how intrinsic activity imparts new behaviors to soft materials that explain a variety of complex phenomena, including the collective motion of self-propelled particles and the complete loss of shear viscosity in fluid suspensions. These nonequilibrium phenomena are driven fundamentally by the active constituent's tendency to diffuse, undergo a random walk, and exert a mechanical force or a pressure on a confining wall. The swim pressure theory is conceptually similar to the kinetic theory of gases, where molecular collisions with the container walls exert a pressure, or to the Brownian osmotic pressure exerted by molecular or colloidal solutes in solution. In contrast to thermodynamic quantities such as the chemical potential and free energy, the mechanical pressure (or stress) is valid out of equilibrium because it comes directly from the micromechanical equations of motion. I apply this swim pressure framework in a broad context to interpret living matter as a material and understand its complex behavior using tools of hydrodynamics, kinetic theory, and nonequilibrium statistical mechanics. The present theory is applied to active systems that are driven by self-propulsion and motility, but there are other types of nonequilibrium driving work that may fit into this general theoretical framework, like driven autocatalytic reactions in electrochemical and biochemical systems.

PUBLISHED CONTENT AND CONTRIBUTIONS

[1] S. C. Takatori, W. Yan, and J. F. Brady. "Swim pressure: stress generation in active matter". *Phys Rev Lett* 113.2 (2014), p. 028103. DOI: 10.1103/PhysRevLett.113.028103.
S.C.T. participated in the conception of the project, conducted simulations, analyzed the data, and participated in the writing of the manuscript.

[2] S. C. Takatori and J. F. Brady. "Swim stress, motion, and deformation of active matter: effect of an external field". *Soft Matter* 10.47 (2014), pp. 9433–9445. DOI: 10.1039/C4SM01409J.
S.C.T. participated in the conception of the project, conducted simulations, analyzed the data, and participated in the writing of the manuscript.

[3] S. C. Takatori and J. F. Brady. "Towards a thermodynamics of active matter". *Phys Rev E* 91.3 (2015), p. 032117. DOI: 10.1103/PhysRevE.91.032117.
S.C.T. participated in the conception of the project, conducted simulations, analyzed the data, and participated in the writing of the manuscript.

[4] S. C. Takatori and J. F. Brady. "A theory for the phase behavior of mixtures of active particles". *Soft Matter* 11.40 (2015), pp. 7920–7931. DOI: 10.1039/C5SM01792K.
S.C.T. participated in the conception of the project, conducted simulations, analyzed the data, and participated in the writing of the manuscript.

[5] S. C. Takatori and J. F. Brady. "Forces, stresses and the (thermo?) dynamics of active matter". *Curr Opin Colloid Interface Sci* 21 (2016), pp. 24–33. DOI: 10.1016/j.cocis.2015.12.003.
S.C.T. participated in the conception of the project, conducted simulations, analyzed the data, and participated in the writing of the manuscript.

[6] S. C. Takatori*, R. De Dier*, J. Vermant, and J. F. Brady. "Acoustic trapping of active matter". *Nat Commun* 7 (2016). DOI: 10.1038/ncomms10694.
S.C.T. participated in the conception of the project, participated in the development of the experiments and simulations, analyzed the data, and participated in the writing of the manuscript. (* equal contribution).

[7] S. C. Takatori and J. F. Brady. "Superfluid behavior of active suspensions from diffusive stretching". *Phys Rev Lett* 118.1 (2017), p. 018003. DOI: 10.1103/PhysRevLett.118.018003.
S.C.T. participated in the conception of the project, conducted simulations, analyzed the data, and participated in the writing of the manuscript.

TABLE OF CONTENTS

LIST OF ILLUSTRATIONS

Chapter 1

INTRODUCTION TO THE DYNAMICS OF ACTIVE MATTER

This thesis consists of independent chapters that are presented in a form suitable for publication, with Chapters 1-7 already published. This introductory chapter provides an overview of the basic features of active matter systems and a few of the main results of the thesis. Subsequent chapters provide a more in-depth analysis of the dynamics of collective motion exhibited by active matter, as well as additional topics not covered in this introduction. I lay the groundwork in Chapter 2 for all of the work in this thesis by introducing the principle of a unique mechanical swim pressure exerted by active matter systems. I present in Chapter 3 an experimental measurement of the swim pressure by employing the novel use of an acoustic tweezer to confine self-propelled particles in a potential well. In Chapters 4 and 5, I use the swim pressure framework to construct an equation of state of active matter and predict its self-organization and unusual phase behavior. I analyze in Chapter 6 the effect of an external orienting field on the dynamics of self-propelled bodies, and provide potential applications of active matter for nano/micromechanical devices and motors with tunable material properties. In Chapter 7, I discover that active self-propulsion engenders an additional contribution to the suspension shear stress, and explain why and how fluids containing motile bacteria can exhibit superfluid-like behaviors with zero effective shear viscosity. Lastly, I analyze in Chapter 8 the effects of finite particle inertia on the stress generation of active matter to extend the swim pressure framework to larger swimmers such as fish and birds.

This introductory chapter includes content from our previously published article:

[1] S. C. Takatori and J. F. Brady. “Forces, stresses and the (thermo?) dynamics of active matter”. *Curr Opin Colloid Interface Sci* 21 (2016), pp. 24–33. DOI: 10.1016/j.cocis.2015.12.003.

1.1 Introduction

The statistical mechanics and microhydrodynamics of active matter systems have been studied intensively during the past several years by various soft matter physicists, chemists, engineers, and biologists around the world. Recent attention has focused on the fascinating nonequilibrium behaviors of active matter that cannot

be observed in equilibrium thermodynamic systems, such as spontaneous collective motion and swarming. Even minimal kinetic models of active Brownian particles exhibit self-assembly that resembles a gas-liquid phase separation from classical equilibrium systems. Self-propulsion allows active systems to generate internal stresses that enable them to control and direct their own behavior and that of their surroundings. In this introduction we discuss the forces that govern the motion of active Brownian microswimmers, the stress (or pressure) they generate, and the implication of these concepts on their collective behavior. We focus on recent work involving the unique 'swim pressure' exerted by active systems, and discuss how this perspective may be the basic underlying physical mechanism responsible for self-assembly and pattern formation in all active matter. We discuss the utility of the swim pressure concept to quantify the forces, stresses, and the (thermo?) dynamics of active matter.

A distinguishing feature of many living organisms is their ability to move, to self-propel, to be active. Constituents of "active matter" systems are capable of independent self-propulsion by converting fuel into mechanical motion, and include both microscopic entities like microorganisms and motor proteins within our cells to large bodies like fishes and birds. Inanimate, nonliving bodies can also achieve self-propulsion using mechanisms that are different than living organisms, but the outcome of their collective behavior is not necessarily different between living and nonliving active systems. Indeed, active matter systems of all scales have the tendency to associate together and move collectively, from colonies of bacteria, swarms of insects, flocks of birds, schools of fish, and herds of cattle. A question arises as to the micromechanical origin for living organisms to exhibit collective and coherent motion, and whether it can be explained and expressed using basic physical quantities.

All active matter systems are intrinsically out of equilibrium, a trait which allows self-propelled entities to display fascinating behaviors that cannot be observed in thermodynamic systems in equilibrium such as spontaneous self-assembly and pattern formation [1, 2, 3, 4]. At the same time, nonequilibrium systems like active matter have very complex and specialized networks relating the input to the response, and which make the theoretical understanding of their behaviors a challenging and intriguing problem in soft matter and statistical mechanics.

In this chapter, we discuss the unique forces, stresses, and (thermo)dynamics of active matter, in an effort to offer a simple perspective to help explain many of the

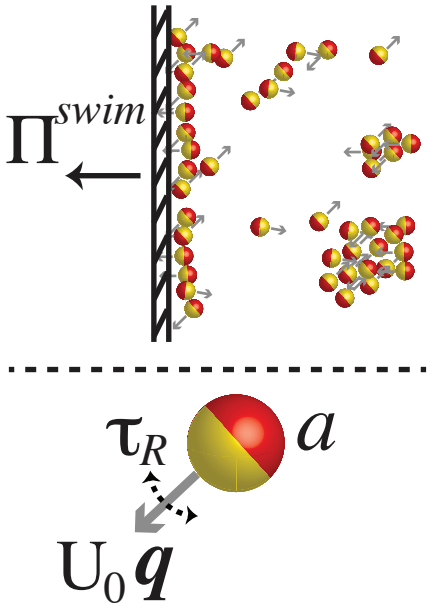

Figure 1.1: Self-propelled bodies exert a unique mechanical 'swim pressure' (Takatori, Yan, and Brady, *Phys Rev Lett*, 2014), Π^{swim}, on an osmotic boundary owing to their self-motion. In a simple model of active matter, particles of size a translate with a swim velocity $U_0\boldsymbol{q}$ and reorient with a reorientation time scale τ_R, where the unit orientation vector $\boldsymbol{q}$ indicates the direction of swimming.

intriguing behaviors exhibited by active systems. In particular, we focus on a new 'swim pressure' principle [5, 6] to explain the self-assembly of active particles and analyze the applicability of conventional thermodynamic concepts to a nonequilibrium system. First, in Sec 1.2 we review the different classes of active swimmers including both living microorganisms and inanimate, synthetic self-propelled entities, and the methods to control and manipulate their motion. Next, we discuss the forces that govern the motion of microswimmers at low Reynolds number, explaining why and how microorganisms are able to move while being 'force-free.' Because of their ability to self-propel and reorient, active swimmers have an enhanced effective translational diffusivity, which we explain in Sec 1.5. Owing to the swimmer's tendency to wander away and diffuse, a swimmer enclosed inside a container would exert a pressure on the surrounding boundaries of the container as it interacts with the walls. As described in Sec 1.6, this is the physical origin of the 'swim pressure,' a unique mechanical pressure generated by all active systems as a result of their self-motion. In Sec 1.7 we consider different approaches in the literature that have analyzed the fascinating collective behavior exhibited by active matter. We focus on the swim pressure perspective to predict the onset of phase

separation in a simple active Brownian suspension. Next, we discuss whether the notion of an effective 'temperature' of active matter can be used to describe the activity of an active suspension. In Sec 1.8 we explain how active systems may exert an 'internal' force that behaves just like an external body force like gravity and how one can describe active systems using a microscopic theory. Finally, in Sec 1.9, we conclude with suggestions for future research.

1.2 Active matter systems

Among a large class of active matter systems, we focus our attention on microscopic swimmers whose size a and swimming speed U_0 are such that the Reynolds number associated with their self-motion is negligibly small $Re \equiv U_0 a/\nu \sim O(10^{-6} - 10^{-2})$ (ν is the fluid kinematic viscosity, taken to be that of water), and hence their dynamics are governed by the Stokes equations. Unlike large organisms like fish that self-propel by making use of inertia in the surrounding fluid, bodies at low-Reynolds number must break time-reversal symmetry to move. Active matter systems need not be living, and in fact intensive research has gone into the fabrication of nonliving, synthetic microswimmers, as described below.

Inanimate, synthetic particles

Despite a recent increase in active matter research, fabrication of artificial systems of autonomously moving and self-assembling bodies have been done for some time. Purcell's three-link swimmer [7] and Taylor's toroidal swimmer [8] are a few early examples which illustrate the importance of breaking symmetry to move in the Stokes regime. An asymmetric chemical reaction occurring around a body's surface also results in self-motion from symmetry breaking; a famous example is camphor crystals placed on an water/air interface that self-propel by an asymmetric dissolution of camphor creating surface tension gradients that induce motion [9]. Aside from gradients in surface tension, Ismagilov et al [10] fabricated a micro-plate that self-propelled on a water surface by having an asymmetric coating of platinum that reacted in a solution of hydrogen peroxide. These plates moved by releasing bubbles generated by the decomposition of hydrogen peroxide at the platinum surface. Others [11, 12] created micron-sized particles that had half of the particle surface coated with a thin layer of platinum. Called 'Janus particles,' only the areas coated with platinum decompose hydrogen peroxide, which result in an asymmetric distribution of reactants and products along their surface. In self-electrophoresis [13, 14], bimetallic particles composed of two different metals (e.g., Au/Pt) can gener-

ate self-propulsion due to an ionic current resulting from a difference in electron affinities of the two metals. In self-diffusiophoresis [15], autonomous motion is attributed to the osmotic pressure gradient induced by an asymmetric distribution of solutes around the particle [16]. However, the full mechanism behind the motion of self-diffusiophoretic particles is not fully understood [17]. Nonetheless, Janus microswimmers have become a standard model for active Brownian colloids and are used frequently by researchers around the world.

Active Janus particles swim roughly at a fixed speed U_0 in a direction specified by a body-fixed unit orientation vector $\boldsymbol{q}$, as shown in Fig 1.1. The orientation $\boldsymbol{q}$ changes by Brownian motion with rotational diffusivity D_R so the Janus particle has a characteristic reorientation timescale given by $\tau_R \sim 1/D_R$.

Light-activated Janus particles [18, 19, 20] offer a convenient method to control the speed U_0 of the particles—the chemical reaction taking place at the particle surface is trigged by light, which allows researchers to instantly turn on or off the particle motion. Researchers have also fabricated Janus motors with layers of ferromagnetic material that allow for magnetic alignment of the swimmer orientation to move in a directed fashion [21], providing a method to control the reorientation time τ_R in addition to the speed U_0.

Living microorganisms

In addition to artificial microswimmers, another large class of active matter include living microorganisms, which can be divided into 4 sub-categories based upon their swimming mechanism: ciliates such as *Paramecium* mobilize small flagella around their body; flagellates such as *E. coli* activate a single or multiple flagella; spirochetes such as *Leptospira* use axial filaments to undergo a twisting, corkscrew motion; and amoebas such as *Amoeba proteus* deform their entire body. Many motile microorganisms like *E. coli* undergo a run-and-tumble where they alternate between a "run," where they swim straight towards a given orientation with speed U_0, and a "tumble" which aligns them into a new random direction with frequency ω [22]. Like a synthetic active Janus particle, the activity of a motile microorganism may be described by an average speed U_0 and reorientation time $\tau_R \sim 1/\omega$.

Similar to synthetic particles that allow for magnetic control, external fields like chemical and thermal gradients, and magnetic and gravitational fields can cause living microorganisms to modify their swimming behavior to facilitate movement to a favorable region. *E. coli* have been known to undergo chemotaxis by pref-

erentially swimming towards (or away from) chemical gradients of nutrients (or toxins) [23]. Magnetotactic microorganisms such as *Magnetospirillum* have organelles called magnetosomes that contain magnetic crystals that help the organism align along imposed magnetic field lines [24]. Other common examples of taxis swimmers include phototactic [25] and gravitactic [26] bacteria. *Chlamydomonas reinhardtii* is a green alga that swims with a breast-stroke motion and possesses an eyespot that allows the alga to orient itself and swim toward a light source [27].

Molecular motors and active gels

Sub-cellular metabolic processes and energy-consuming enzymes like motor proteins are another important class of active soft matter that has been studied intensively and is of significant biological relevance[28, 4, 2, 29]. Molecular motors consume chemical fuel (like ATP) to generate active stresses that are responsible for cell locomotion, muscle contraction, mechanotransduction, and many other critical cellular processes. In particular, simplified model systems of filaments and motors that constitute the eukaryotic cellular cytoskeleton have led to a deeper fundamental understanding of the inner workings of the cell. Hydrodynamic theories for active polar and nematic gels [30, 31, 32, 33, 34] were developed by invoking linear irreversible thermodynamics [35, 36] for systems perturbed slightly away from equilibrium. The resulting theory gives a relationship between the active stress, suspension flux on a continuum level, and the chemical potential difference of ATP and its reaction products generated by the motor. By providing an extension to soft matter physics, active gels and hydrodynamic theories have successfully elucidated a variety of nonequilibrium biological phenomena, including the prediction of cell polarity and pattern formation [37, 38, 39, 40], actin cortex flows in developing embryos [41], and microtubule-based pronuclear motion [42]. Active gel theory has the potential to explain other areas of physics, including mechanical fracture, jamming, and wetting [28].

1.3 Other open driven systems

Systems that are subject to an open flow of mass and energy can lose their thermodynamic stability and evolve to one of many possible nonequilibrium states called dissipative structures [43]. These irreversible processes can be driven by internal fluctuations or other environmental influences. In this thesis, I focus on active systems that are driven by self-propulsion and motility, but there are other types of nonequilibrium driving work that may fit into the general theoretical framework.

One example is driven reactive mixtures in electrochemical systems, where externally controlled chemical reactions can control the onset of phase separation [44]. Another example is the autocatalytic reactions in biochemical systems, where chemically-driven phase separations can control patterns that lead to membraneless organelles [37, 45]. The thermodynamic stability of dissipative structures have been studied using concepts of irreversible thermodynamics and entropy generation [43]. A very interesting extension of the present swim pressure theory would be to understand how it relates to the formalism of linear irreversible thermodynamics and the associated ideas on entropy production.

Now that we have briefly reviewed the different classes of active systems within a broader class of open driven systems, in the next section we discuss the self-propulsive forces that govern their motion in the Stokes regime, explaining why and how microorganisms are able to move while being 'force-free.'

1.4 'Force-free' motion

Swimming microorganisms and inanimate self-propelled particles move in the Stokes regime and undergo so-called 'force-free' motion. This phrase is somewhat ambiguous, as all non-accelerating bodies are by definition force-free, i.e., $m(d\boldsymbol{U}/dt) = \sum \boldsymbol{F} = \boldsymbol{0}$. This is true for an airplane traveling at constant speed, where its propulsive force is balanced by the frictional forces acting against the body. The same applies for microscopic bodies swimming at low-Reynolds number. What researchers actually mean when they say active matter undergoes force-free motion is that the body experiences no *external* force causing the body to move.

What force then, if any, induces the body to swim? Suppose we have a ciliated microorganism (such as *Paramecium*) which swims by beating many small flagella cooperatively along its body surface, such that the velocity of the surrounding fluid at any point on the swimmer surface is $\boldsymbol{u}(\boldsymbol{x}) = \boldsymbol{U} + \Omega \times (\boldsymbol{x} - \boldsymbol{X}) + \boldsymbol{u}^s(\boldsymbol{x})$, where $\boldsymbol{U}$ and $\boldsymbol{\Omega}$ are translational and angular velocities of the body (about its center), $\boldsymbol{X}$ is the position of the body center, $\boldsymbol{x}$ is the position along the body surface, and $\boldsymbol{u}^s(\boldsymbol{x})$ is the 'slip velocity' induced by the deformations happening along the ciliated body surface. The slip velocity can be expressed in terms of surface moments: $\boldsymbol{u}^s(\boldsymbol{x}) = \boldsymbol{E}^s \cdot \boldsymbol{x}' + \boldsymbol{B}^s : (\boldsymbol{x}'\boldsymbol{x}' - \boldsymbol{I}(x')^2) + \cdots$, where $\boldsymbol{x}' = \boldsymbol{x} - \boldsymbol{X}$, and the surface moment tensors $\boldsymbol{E}^s(t), \boldsymbol{B}^s(t)$, etc are in general functions of time and set by the swimming gait.

This moments expansion allows us the flexibility to model particular swimmers or

the interactions among many swimmers. For example, the spherical squirmers of Blake [46] and Ishikawa et al [47] invoke a quadrupolar moment $\boldsymbol{B}^s$ to achieve self-propulsion. The use of Stokesian dynamics to simulate various classes of microswimmers is given in Swan et al [48]. The only requirement for the slip velocity $\boldsymbol{u}^s$ is that it contributes no net translation or rotation to the particle (i.e., it has zero mean and zero antisymmetric first moment).

The total hydrodynamic force/torque on the swimmer can be written as

$$\begin{aligned} \mathcal{F}^H &= -\boldsymbol{R}_{\mathcal{FU}} \cdot \mathcal{U} - \underbrace{\boldsymbol{R}_{\mathcal{FE}} : \boldsymbol{E}^s - \boldsymbol{R}_{\mathcal{FB}} \odot \boldsymbol{B}^s - \cdots}_{} \\ &= \quad \mathcal{F}^{drag} \quad + \quad \mathcal{F}^{swim}, \end{aligned} \tag{1.1}$$

where we grouped the force/torque $\mathcal{F} = (\boldsymbol{F}^H, \boldsymbol{L}^H)$ and translational/angular velocities $\mathcal{U} = (\boldsymbol{U}, \boldsymbol{\Omega})$, and the hydrodynamic resistance tensors $\boldsymbol{R}_{\mathcal{FU}}, \boldsymbol{R}_{\mathcal{FE}}, \boldsymbol{R}_{\mathcal{FB}}$, etc couple the force to the velocity and to the 'squirming set' $\boldsymbol{E}^s(t), \boldsymbol{B}^s(t)$, etc.

Although we motivated this discussion using a ciliated microorganism, the same development applies for self-diffusiophoretic Janus particles which also exhibit a fluid 'slip velocity' near the particle surface due to solvent backflow induced by the flux of chemical reactants/products along the particle surface. In fact, we can generalize this structure to all classes of microswimmers by recognizing that the resistance tensors are now functions of time, rather than being fixed for the ciliates.

Equation 1.1 has been written as a sum of the hydrodynamic drag force $\mathcal{F}^{drag}$ and self-propulsive 'swim force' $\mathcal{F}^{swim}$. A microswimmer moves in the Stokes regime, so its motion is 'force-free': $\sum \mathcal{F} = \mathcal{F}^H + \mathcal{F}^{ext} = 0$, where $\mathcal{F}^{ext}$ is any external force such as gravity. In the absence of an external field, $\mathcal{F}^{ext} = 0$ and we have $\mathcal{F}^H = 0$. Using Eq 1.1, we obtain $\mathcal{F}^H = \mathcal{F}^{drag} + \mathcal{F}^{swim} = 0$ and thus the velocity of the swimmers is $\mathcal{U} = \boldsymbol{R}^{-1}_{\mathcal{FU}} \cdot \mathcal{F}^{swim}$.

For the simplest model of self-propelling spheres, the hydrodynamic resistance tensor is the Stokes drag factor $\boldsymbol{R}_{FU} = \zeta \boldsymbol{I}$, where $\zeta = 6\pi\eta a$, a is the particle size and η is the viscosity of the suspending Newtonian fluid; the swim force is $\boldsymbol{F}^{swim} = \zeta U_0 \boldsymbol{q}$, where U_0 is the intrinsic swimming speed of the swimmer and $\boldsymbol{q}$ is a unit orientation vector prescribing the direction of swimming. The orientation vector $\boldsymbol{q}$ fluctuates subject to run-and-tumble or rotational Brownian diffusion and follows directly from a torque balance. In the absence of external forces, the translational velocity of the swimmer is therefore $\boldsymbol{U} = \boldsymbol{R}^{-1}_{FU} \cdot \boldsymbol{F}^{swim} = U_0 \boldsymbol{q}$.

Equation 1.1 is the definition of the 'swim force'—one way to interpret this quantity is to measure the force required to prevent an active swimmer from moving, say by optical tweezers. In this case, the optical tweezer exerts an external force $\boldsymbol{F}^{ext}$ that exactly balances $\boldsymbol{F}^{swim}$ such that $\boldsymbol{F}^{drag} = \boldsymbol{0}$. The magnitude of the force required to hold the swimmer fixed is precisely $|\boldsymbol{F}^{ext}| = |\boldsymbol{F}^{swim}|$.

Including the effects of translational Brownian forces ($\boldsymbol{F}^{B}$), external forces ($\boldsymbol{F}^{ext}$), and interparticle interactions ($\boldsymbol{F}^{P}$) between the particles, this simple system is called the 'active Brownian particle' (ABP) model, where the force balance is $\boldsymbol{0} = -\zeta\boldsymbol{U} + \boldsymbol{F}^{swim} + \boldsymbol{F}^{B} + \boldsymbol{F}^{ext} + \boldsymbol{F}^{P}$. Because the Brownian force can be $O(10^3)$ times (or more) smaller than the self-propulsive swim force, $\boldsymbol{F}^{B}$ is often assumed to be negligible.

With an understanding of the self-propulsive forces that govern the motion of active systems, in the next section we turn our attention to the dynamic motion exhibited by active particles.

1.5 Diffusion: rotation leads to translation

Suppose we have a self-propelling swimmer of characteristic size a immersed in a continuous Newtonian solvent with viscosity η. The swimmer translates with a constant, intrinsic swim speed U_0 and tumbles with a reorientation time τ_R. The reorientation time may be from run-and-tumble motion with $\tau_R \sim 1/\omega$ where ω is the tumbling frequency and/or from the rotational Brownian motion with $\tau_R \sim 1/D_R \sim 8\pi\eta a^3/(k_B T)$—there is an equivalence between reorientations induced by run-and-tumble and rotational Brownian motion [49]. For times large compared to τ_R (i.e., swimmer has undergone many reorientation events), the swimmer's trajectory can be modeled as a random-walk process.

The diffusivity for a random-walk scales as $D \sim l^2/\tau_R$ where l is the step size. For active swimmers, the step size is the swimmer's run length $l = U_0\tau_R$ (or persistence length), which is simply the distance traveled between reorientation events. Therefore, the 'swim diffusivity' of the active body due to its self-motion scales as $D^{swim} \sim U_0^2\tau_R$. A rigorous theoretical analysis gives $D^{swim} = U_0^2\tau_R/6$ in 3D and $D^{swim} = U_0^2\tau_R/2$ in 2D for ABPs and similarly for run-and-tumble particles [22]. With the effect of translational Brownian motion, the effective translational diffusivity $D^{eff} = D_0 + U_0^2\tau_R/6$ where $D_0 = k_B T/\zeta$ is the Stokes-Einstein-Sutherland translational diffusivity. The swim diffusivity D^{swim} can be more than $O(10^3)$ larger than D_0.

Suppose we confine this swimmer with a container made of walls permeable to the

fluid but not to the swimmer (i.e., an osmotic barrier). Because of the swimmer's tendency to wander away in space given by D^{swim}, it will exert a force or a pressure on the surrounding boundaries of the box as it collides into the walls. This pressure exerted on the surrounding walls to confine the particle is precisely the physical origin of the 'swim pressure' [5]. The swim pressure is conceptually similar to the kinetic theory of gases, where molecular collisions with the container walls exert a pressure, or to the Brownian osmotic pressure exerted by molecular or colloidal solutes in solution. It is therefore an entropic quantity that is driven by the constituent's tendency to diffuse and undergo a random-walk. Although it is clear that such a swim pressure should exist, how are we to understand this pressure in basic physical quantities?

1.6 Swim pressure of active matter[1]

The virial theorem expresses the stress $\boldsymbol{\sigma}$ (or pressure) on a system in terms of the forces $\boldsymbol{F}_i$ acting on it: $\boldsymbol{\sigma} = -1/V\langle\sum_i^N \boldsymbol{x}_i\boldsymbol{F}_i\rangle$, where $\boldsymbol{x}_i$ is the position of particle i, V is the system volume, and N is the total number of particles [50]. Suppose we have a particle in Stokes flow obeying the overdamped equation of motion, $\boldsymbol{0} = -\zeta\boldsymbol{U}(t) + \boldsymbol{F}(t)$, where ζ is the hydrodynamic drag factor, $\boldsymbol{U}$ is the particle velocity, and $\boldsymbol{F}$ is any general force on the body. The position of the particle at time t is $\boldsymbol{x}(t) = \int \boldsymbol{U}(t')\,dt'$, so we obtain the stress on the particle $\boldsymbol{\sigma} = -n\langle\boldsymbol{x}\boldsymbol{F}\rangle = -n\zeta\int\langle\boldsymbol{U}(t')\boldsymbol{U}(t)\rangle\,dt' = -n\zeta\boldsymbol{D}$, where $n = N/V$ is the number density and we have written the time integral of the velocity autocorrelation as the diffusivity of the particle, $\boldsymbol{D}$.

This result demonstrates that a particle undergoing any type of random motion exerts a pressure $\Pi = -\mathrm{tr}\boldsymbol{\sigma}/3 = n\zeta D$. This general result applies for an arbitrary particle shape (where ζ may depend on particle configuration) and for any source of random motion. For passive Brownian particles where the source of random motion is the thermal energy, $D = k_BT/\zeta$, we obtain the familiar ideal-gas Brownian osmotic pressure $\Pi^B = nk_BT$. The osmotic pressure can be interpreted as a mechanical pressure resulting from the random motion induced by solvent fluctuations.

Likewise, for active particles with diffusivity $D^{swim} = U_0^2\tau_R/6$, we arrive at the

[1] See Chapter 2 for further discussion of this section.

analogous "ideal-gas" swim pressure:

$$\Pi^{swim}(\phi \to 0) = n \underbrace{(\zeta U_0^2 \tau_R/6)}$$
$$= n \ (k_s T_s), \tag{1.2}$$

where $\phi = 4\pi a^3 n/3$ is the volume fraction of active particles. As expected for dilute systems, Π^{swim} depends on the particle size only through the hydrodynamic drag factor ζ. In Eq 1.2 we have made an analogy to the Brownian osmotic pressure $\Pi^B = nk_BT$ and defined the 'activity' of the swimmers $k_sT_s \equiv \zeta U_0^2 \tau_R/6$. Because the entropic nature of D^{swim} (and by extension $\Pi^{swim} = n\zeta D^{swim}$) comes not from the thermal energy but instead from swimmer self-propulsion and reorientation, the swim pressure is entirely athermal in origin. In two dimensions, $\Pi^{swim} = n\zeta U_0^2 \tau_R/2$. To appreciate the magnitude of this swimmer activity, a $1\mu m$ swimmer traveling in water with speed $U_0 \sim 10\mu m/s$ and reorienting in time $\tau_R \sim 10s$ has an activity $k_sT_s \equiv \zeta U_0^2 \tau_R/6 \approx 4pN \cdot \mu m$. The thermal energy at room temperature is $k_BT \approx 4 \times 10^{-3} pN \cdot \mu m$, meaning that the swimmers' intrinsic self-propulsion is equivalent to approximately $1000k_BT$. In practice the intrinsic activity of active synthetic colloidal particles and living microorganisms can be even larger.

Returning to the virial theorem, we can take the forces $\boldsymbol{F}_i$ to be the swim force $\boldsymbol{F}^{swim}$ as discussed earlier and *define* the swim stress as

$$\boldsymbol{\sigma}^{swim} = -n\langle \boldsymbol{x}\boldsymbol{F}^{swim} \rangle, \tag{1.3}$$

and the swim pressure is the trace of the swim stress, $\Pi^{swim} = -\mathrm{tr}\boldsymbol{\sigma}^{swim}/3$ in 3D. Equation 1.3 defines the swim stress as the first moment of the self-propulsive swim force $\boldsymbol{F}^{swim} \sim \zeta \boldsymbol{U}_0$, and the "moment arm" is the run length of the swimmer, $\boldsymbol{x} \sim \boldsymbol{U}_0 \tau_R$. Equation 1.3 demonstrates the importance of interpreting the self-propulsion of an active particle as arising from a swim force, $\boldsymbol{F}^{swim}$. Unlike the familiar $-\langle \boldsymbol{x}_{ij}\boldsymbol{F}_{ij} \rangle$ form seen in interparticle interactions of molecular liquids, where subscripts ij indicate pairwise interactions, $-\langle \boldsymbol{x}\boldsymbol{F}^{swim} \rangle$ gives a single-particle self contribution to the stress—just like the Brownian osmotic pressure $\Pi^B = nk_BT$.

This swim pressure exists at all scales in both living (e.g., microorganisms) and nonliving active systems, and also applies to larger swimmers (e.g., fish) where inertia is important (i.e., the Reynolds number is not small). A recent study on sedimentation [51] provided an indirect measurement of the swim pressure based upon density profiles of active particles under gravity. Acoustic traps may be used to expose an active system to a near-harmonic potential well, and the restricted

swimmer motion inside the trap gives directly the swim pressure as defined via the virial theorem [52].

The swim pressure is distinct from the "hydrodynamic stresslet" that accompanies non-spherical microswimmers, [53, 47] and which scales as $n\zeta U_0 a(\boldsymbol{qq} - \boldsymbol{I}/3)$ and averages to zero for an isotropic distribution, where a is the characteristic size of the swimmer.

The swim pressure of active matter is a real, measurable mechanical pressure exerted on a confining container. Suppose we load a soft, compressible material (e.g., gel polymer network) with photo-activated synthetic colloidal particles. In the absence of light, the particles undergo thermal Brownian motion and the gel assumes an equilibrium shape, determined by a balance between the entropic force that drives the polymer to expand and the elastic force that resists expansion [54]. When the light is turned on, the particles suddenly become active and exert the swim pressure (Eq 1.2), causing the gel to expand isotropically. To make an appreciable change to the gel shape, the magnitude of the swim pressure must be larger than the shear modulus of polymer network, which in principle an be adjusted to nearly zero. For example, a dilute network of hydrated mucus (a non-Newtonian gel) has shear moduli $\sim O(0.1-10)Pa$ [55, 56]. The swim pressure exerted at 10% volume fraction of $1\mu m$ active particles in water with $U_0 \sim 10\mu m/s$ and $\tau_R \sim 10s$ is $\Pi^{swim} = n\zeta U_0^2 \tau_R/6 \approx O(1)Pa$. For soft materials with a very small shear modulus, the swim pressure can cause the gel to deform its shape. Even if the gel does not deform, it can still be translated and be steered using the active swimmers [57]. This suggests an application of active soft materials as micro- or nanomechanical devices that could have multiple applications in medicine (e.g., focused drug delivery), biophysics, and other fields. Others have analyzed the swim pressure in confinement between parallel plates [58] and along other geometric contours [59].

In addition to its practical applications, the swim pressure may be the basic underlying physical mechanism responsible for self-assembly and pattern formation in all active matter, as discussed next.

1.7 Collective behavior of active matter[2]

An early numerical work by Vicsek et al [60] showed that a minimal kinetic model for active systems may result in their directed, coherent motion, illustrating that self-motion with some nominal interaction alone is enough to observe novel forms

[2]See Chapters 2 and 4 for further discussion of this section.

of phase behavior. Aditi Simha and Ramaswamy [61] and Saintillan and Shelley [53] developed a kinetic model with hydrodynamic interactions to predict the instabilities and pattern formation in rodlike active suspensions. More recently, experiments and computer simulations [19, 49, 62, 63, 64, 65, 66] have shown that active matter self-organizes into dense and dilute phases resembling an equilibrium liquid-gas coexistence. A phase separation in a classical thermodynamic system in equilibrium may occur due to attractive interactions between the molecules. Remarkably, for active matter these collective effects can occur in the absence of any attractive forces between the particles. How can purely excluded-volume or *repulsive* interactions give rise to *attraction*?

Continuum descriptions [66, 67] and micromechanical approaches such as structure factor analysis have provided models for this peculiar behavior [64, 65, 67, 68, 69, 70]. Tailleur, Cates, and coworkers [49, 63, 71] have developed a robust theory to explain the motility-induced phase separation in active matter using a flux-based Smoluchowski analysis. They developed an accurate continuum theory by explicit coarse graining and deriving the first-order density gradient expressions for a phase-separating active system with repulsive interactions [66]. This approach was further developed by analyzing the role of dimensionality [68], where the authors invoked the first moment of the static structure factor to predict the onset of instability. By considering a density-dependent particle swim velocity, they demonstrated that an effective chemical potential and a bulk free energy can be used to establish a mapping between particle-based active Brownian simulations and their continuum model. A generic mechanism for pattern formation and instability for reproducing and interacting run-and-tumble bacteria was also presented [63], by incorporating a varying local swim speed owing to different bacterial behavior in different environments.

Redner et al [64] analyzed the structural changes associated with phase separation and developed a simple kinetic model to predict the onset of instability, which was subsequently used to analyze a mixture of active and passive particles [72]. The effect of interparticle collisions between the active particles was considered by Bialké et al [65] to derive a density-dependent effective particle swim speed. They further developed their nonlinear microrhology approach to predict the phase separation of self-propelled 2D disks [73].

Recently, an alternative approach invoking the unique mechanical pressure exerted by self-propelled bodies has been used to predict the self-assembly in active matter

[5, 6, 74, 75]. The swim pressure [5] perspective offers a convenient framework to understand the collective behavior in active systems. Below, we summarize the use of the swim pressure to predict the phase separation in a system of active Brownian particles with a homogeneous activity, and to demonstrate that this simple system engenders a pressure-volume phase diagram much like that of a van der Waals fluid.

Physically, the swim pressure is the mechanical force per unit area that a confined active particle exerts on its container, given by Eq 1.1 for a dilute active system. At higher concentrations of swimmers, the particles collide into each other and the swimmer size a enters as a new variable in the problem. The nondimensional reorientation "Péclet number" $Pe_R = U_0 a/D^{swim} = U_0 a/(U_0^2 \tau_R) = a/(U_0 \tau_R)$ is the ratio of the swimmer size a to its run length $U_0 \tau_R$, and this is a key parameter that determines the behavior of the swim pressure at higher swimmer concentrations, and the overall phase behavior of the system.

Density dependence of swim pressure

For large Pe_R the swimmers reorient rapidly and take small swim steps, behaving as if they are passive (inactive) particles subject to thermal Brownian motion with an effective activity $k_s T_s \equiv \zeta U_0^2 \tau_R/6$ [5]. As shown in Fig 1.2A, our Brownian dynamics simulations for $Pe_R \gg 1$ show that the swim pressure increases linearly with concentration. This system is analogous to passive Brownian particles, which exert the "ideal-gas" Brownian osmotic pressure $\Pi^B = nk_BT$ regardless of the concentration of particles. Thus $\Pi^{swim}(\phi, Pe_R) = nk_sT_s$ as $Pe_R \to \infty$ for all $\phi \lesssim \phi_0$ where ϕ_0 is the volume fraction at close packing. Near close packing the swimmers collide into each other before being allowed to take a swim step, so that swim pressure decreases to zero.

For small Pe_R the swimmers have run lengths large compared to their size and hinder each others' movement during collisions. Suppose we have a cluster of particles with zero net cluster velocity, i.e., individual swim velocities cancel out due to collisions. Because the cluster does not move, the constituent swimmers have no effective run length and exert zero force on the surrounding walls of the container. This continues for a time τ_R until their swimming directions change from rotational motion and the cluster breaks apart. This "clustering" behavior [49] reduces the average distance each swimmer travels between reorientations, which decreases the pressure they exert on the container walls (i.e., the swim pressure). Another interpretation is that an active swimmer in larger concentrations is less mobile and has

a smaller swim diffusivity, resulting in a smaller pressure via $\Pi^{swim} = n\zeta D^{swim}$. Therefore, for small Pe_R the swim pressure decreases as the swimmer concentration increases as shown in Fig 1.2A. This differentiates active matter from an equilibrium Brownian system, which exerts a fixed $\Pi^B = nk_BT$ of ideal-gas pressure for all ϕ.

Extending the results of a nonlinear microrheology analysis [5] the swim pressure at small Pe_R in 3D takes the form $\Pi^{swim} = nk_sT_s(1-\phi-\phi^2)$ [74]. Unlike Brownian systems where repulsive interactions (e.g., hard-sphere collisions) increase the pressure, for active matter interactions decrease the run length and therefore the swim pressure. A decreasing Π^{swim} is the principle destabilizing term that facilitates a phase transition in active systems.

Interparticle (collisional) pressure

At higher concentrations of active swimmers there is an additional contribution to the pressure due to interparticle (e.g., excluded volume) forces between the particles. Like the swim pressure and the Brownian osmotic pressure, the interparticle pressure is defined by the virial theorem: $\Pi^P = n\langle \boldsymbol{x} \cdot \boldsymbol{F}^P \rangle/3$, where $\boldsymbol{F}^P$ is the interparticle force. As shown in Fig 1.2B, Π^P necessarily increases with increasing concentration because excluded-volume collisions always result in a positive interparticle pressure, helping to stabilize the system.

For large Pe_R the swimmers behave as Brownian particles and $\Pi^P(\phi, Pe_R) = \Pi^{HS}(\phi)$, where $\Pi^{HS}(\phi)$ is the interparticle pressure of hard-sphere Brownian particles [76, 77]. Because the detailed interactions between the particles are not important [76, 77, 78], the interparticle pressure for a molecular fluid or that of a Brownian colloidal system has the same density dependence as that of active swimmers. For large Pe_R the run length $U_0\tau_R$ sets the scale of the force moment and $\Pi^P \sim n(na^3)(\zeta U_0)(U_0\tau_R) \sim nk_sT_s\phi$, analogous to the passive hard-sphere Brownian collisional pressure $\sim nk_BT\phi$.

For small Pe_R, $\Pi^P \sim n(na^3)(\zeta U_0)a$ because a swimmer is displaced by its size a upon collision, not the run length $U_0\tau_R$, and the particle size a sets the scale for the force moment. The interparticle pressure for small Pe_R in 3D can be modeled as $\Pi^P = 3nk_sT_s\phi Pe_R g(2;\phi)$ [74], where $g(2;\phi)$ is the pair-distribution function at contact [77]. This scaling is different from $\Pi^{swim} \sim n(\zeta U_0)(U_0\tau_R)$, which is a single-particle contribution and the run length $U_0\tau_R$ sets the scale for the force moment. The ratio of the interparticle pressure to the swim pressure is

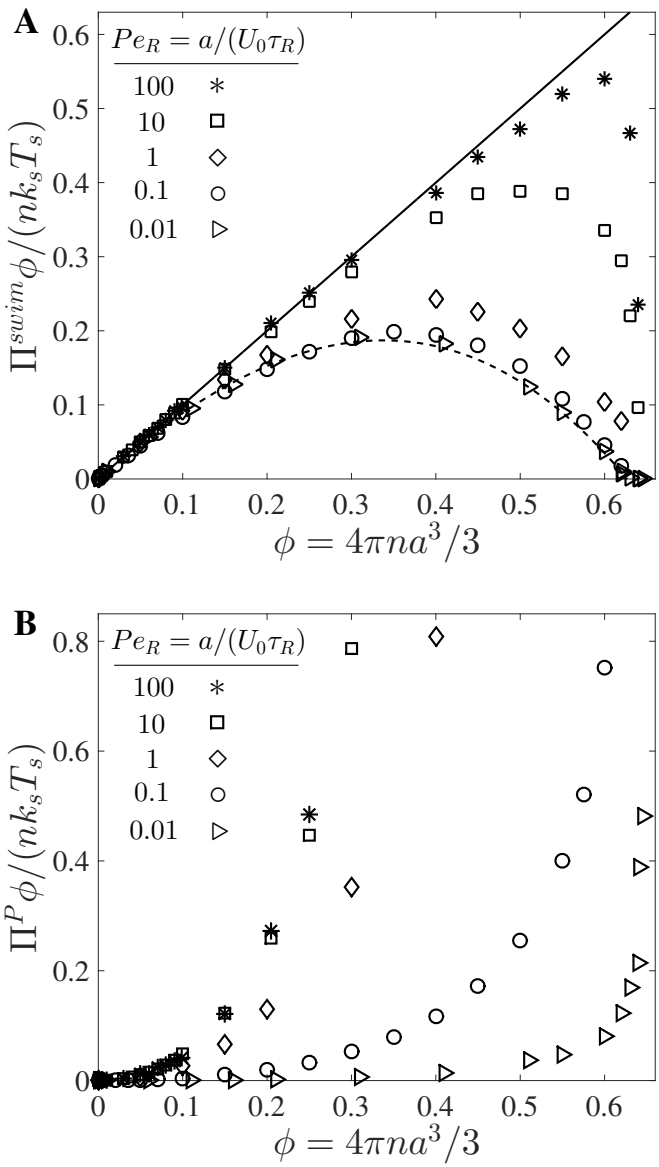

Figure 1.2: Dependence of swimmer concentration on (**A**) swim pressure and (**B**) interparticle (collisional) pressure scaled with the swim activity $k_sT_s \equiv \zeta U_0^2\tau_R/6$. Data are from Brownian dynamics simulations, where the reorientation Péclet number $Pe_R \equiv a/(U_0\tau_R)$ is the ratio of the swimmer size to its run length. In (**A**), for large Pe_R the data collapse on the solid line representing a linear increase of the active pressure with concentration, $\Pi^{swim} = nk_sT_s$. As $Pe_R \to 0$ the swim pressure decreases with increasing concentration and agrees with $\Pi^{swim} = nk_sT_s(1-\phi-\phi^2)$ (dashed curve) (Takatori and Brady, *Phys Rev E*, 2015). In (**B**), the collisional pressure increases monotonically with concentration for all Pe_R.

$\Pi^P/\Pi^{swim} \sim \phi Pe_R$, which provides an additional interpretation of the reorientation Péclet number as a balance of the two individual pressure contributions.

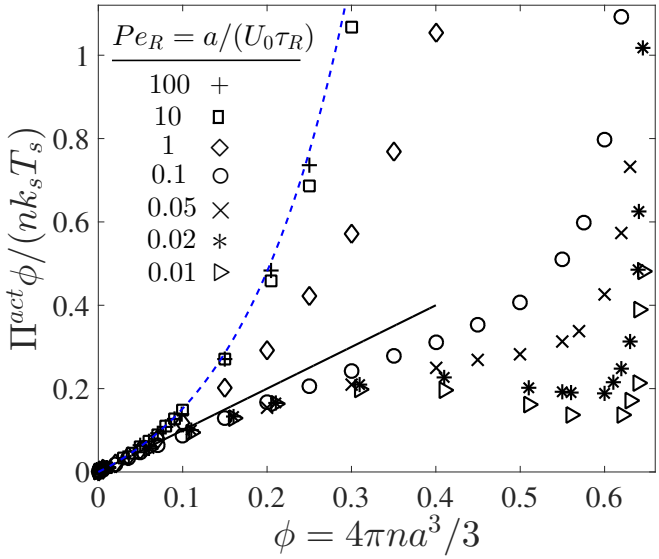

Figure 1.3: Nonequilibrium Π^{act}-ϕ phase diagram, where $\Pi^{act} = \Pi^{swim} + \Pi^{P}$ and is scaled with the swim activity $k_sT_s \equiv \zeta U_0^2\tau_R/6$. Data are from Brownian dynamics simulations, where the reorientation Péclet number $Pe_R \equiv a/(U_0\tau_R)$ is the ratio of the swimmer size to its run length. The solid line represents a linear increase of the active pressure with concentration, $\Pi^{act} = nk_sT_s$. The dashed blue curve is the Carnahan-Starling equation of state for Brownian hard-spheres. For $Pe_R < 1/3$ we observe a negative 'second virial coefficient,' and for $Pe_R \lesssim 0.03$ a non-monotonic pressure variation (analogous to a 'van der Waals loop').

Active pressure

The total pressure of active matter (in the absence of hydrodynamic interactions) is given by $P = p_f + \Pi^{act}$, where $\Pi^{act} = \Pi^{swim} + \Pi^{P}$ is the 'active pressure' and p_f is the solvent pressure (which is arbitrary for an incompressible fluid and is set to zero). Comparing Figs 1.2A and 1.2B, we have a competing contribution to the active pressure. Namely, as we increase swimmer concentration, Π^{swim} decreases (destabilizing) whereas Π^{P} increases (stabilizing). This competition may result in what would be a negative 'second virial coefficient' B_2, which implies two-body *attractions* and the possibility of a 'gas-liquid phase transition.' Attractions may give rise to a non-monotonic variation of pressure with concentration, known as a "van der Waals loop."

Remarkably, this serves as an answer to why self-assembling active systems exhibit an effective attraction despite having purely repulsive particle interactions. The clustering behavior of self-propelled particles reduces the swim pressure they contribute to the system, which destabilizes the homogeneous phase into separate dense

and dilute phases.

As shown in Fig 1.3, at low ϕ all data collapse onto the ideal-gas swim pressure given by Eq 1.2. At high Pe_R, the interparticle pressure dominates and the total pressure increases monotonically with ϕ. Because the swimmers take small swim steps and reorient rapidly for $Pe_R \gg 1$, the active pressure agrees well with the Carnahan-Starling equation of state for passive Brownian hard-spheres (see blue dashed curve in Fig 1.3). As Pe_R is reduced below ~ 0.03, we observe a non-monotonic pressure profile resembling a van der Waals loop. The decrease in Π^{act} for $Pe_R \ll 1$ is caused by the reduction in swim pressure due to the particles' tendency to form clusters, reducing the average distance they travel between re-orientations. As ϕ approaches close packing, the swim pressure decrease to zero (see Fig 1.2A) but the active pressure necessarily increases because the interparticle (excluded volume) pressure diverges to infinity (Fig 1.2B). It is in this limit where experiments and computer simulations [19, 62, 64, 65, 66, 79] have observed the self-assembly of active systems into dense and dilute phases resembling an equilibrium liquid-gas coexistence.

When designing an experiment or computer simulation, the size of the container or simulation cell must be large compared to the run length of the swimmers, $U_0\tau_R$. A smaller container artificially reduces the swim pressure because the container size enters as a new length scale in the problem and diminishes the distance the swimmers travel between reorientations [52, 58, 80].

We now understand the behavior of the active pressure for small and large values of Pe_R; in the next subsection we discuss a simple model to predict the phase separation for all values of density and Pe_R.

PVT phase diagram

Given an analytical expression for Π^{swim} and Π^{P} [74], the active pressure for small Pe_R is

$$\Pi^{act} = nk_sT_s\left(1 - \phi - \phi^2 + 3\phi Pe_R(1 - \phi/\phi_0)^{-1}\right). \tag{1.4}$$

Equation 1.4 may be treated as an equation of state, which allows the prediction of phase separation in active matter. Recently Solon et al [81] evaluated the use and validity of the active pressure as a thermodynamic equation of state, arguing that the detailed interaction of an active particle with a solid wall may impact the pressure. However, we argue that the active pressure is a state function in general, which is explained in section 1.9. For the purposes of our present discussion, we focus on

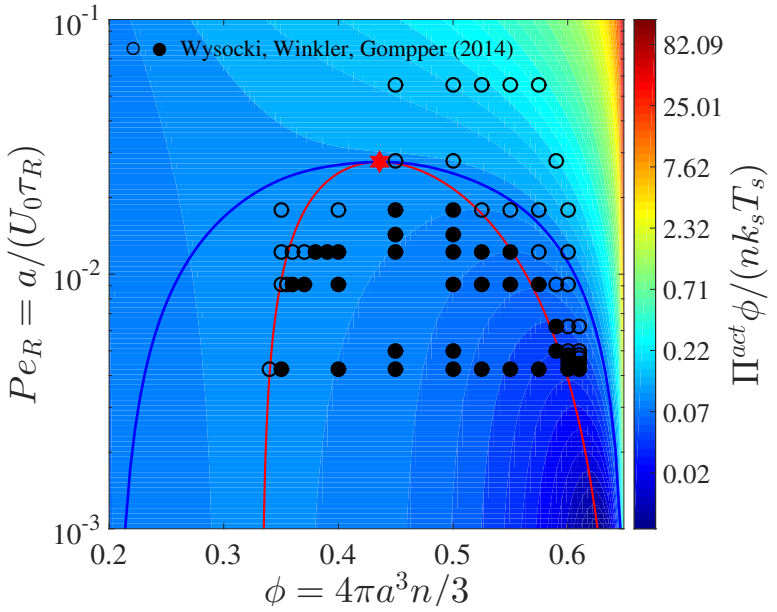

Figure 1.4: Phase diagram in the $Pe_R - \phi$ plane for a 3D active system. Colorbar represents the magnitude of the active pressure scaled with the swim activity $k_sT_s \equiv \zeta U_0^2\tau_R/6$, and the blue and red curves are the binodal and spinodal, respectively. The critical point is shown with a red star. The open and filled symbols are simulation data (Wysocki, Winkler, and Gompper, *Europhys Lett*, 2014) with a homogeneous and phased-separated state, respectively.

spherical swimmers not in confinement, so there is no such wall interaction and we can use Eq 1.4 to predict the phase behavior.

Figure 1.4 shows the phase diagram in the $Pe_R - \phi$ plane, where Eq 1.4 was used to determine the regions of stability from the spinodal condition, $\partial\Pi^{act}/\partial\phi = 0$. This is given by the red curve in Fig 1.4 that passes through the extrema of each constant-pressure isocontour ("isobar"). At the critical point (red star in Fig 1.4), $\partial\Pi^{act}/\partial\phi = \partial^2\Pi^{act}/\partial\phi^2 = 0$. In 3D the critical volume fraction $\phi^c \approx 0.44$, active pressure $\Pi^{act,c}\phi^c/(nk_sT_s) \approx 0.21$, and reorientation Péclet number $Pe_R^c \approx 0.028$, values consistent with our BD simulations and simulation data of others [82, 72, 73]. No notion of free energy is needed to obtain the spinodal and critical point—they are purely mechanical quantities.

The "binodal" or coexistence region (blue curve in Fig 1.4) is defined as the equality of the chemical potential in the dilute and dense phases. Although the thermodynamic chemical potential is defined only for equilibrium systems, we can define a nonequilibrium chemical potential for active systems using standard macroscopic

mechanical balances [5, 74]: $n(\partial\mu^{act}/\partial n) = (1-\phi)(\partial\Pi^{act}/\partial n)$. This definition, which makes no approximation other than solvent incompressibility, agrees with the true thermodynamic chemical potential for molecular or colloidal solutes in solution [54]. Active systems with a small reorientation time $\tau_R \to 0$ not only behave similarly but are equivalent in dynamics to that of passive Brownian particles. If we placed active swimmers behaving identically to passive Brownian particles behind an osmotic barrier, we would not be able to distinguish one from the other. Because the form of the chemical potential and pressure are equivalent for the two systems, we interpret μ^{act} as a natural definition and extension of the chemical potential for nonequilibrium systems, and use it to compute and define a "binodal."

Simulations of Wysocki et al [82] agree well with the spinodal of this model as shown by the location of the transition from the homogeneous (open symbols) to phase-separated (filled symbols) states. In 2D, simulation of Speck et al [73] suggest that the transition occurs near the binodal [74]. Figure 1.4, which contains no adjustable parameters, predicts that active systems prepared outside the binodal (blue curve) are stable in the homogeneous configuration and do not phase separate. Between the spinodal and binodal, the system is in a metastable state and does not spontaneously undergo a spinodal decomposition. In a simulation the system may stay in the homogeneous phase unless an artificial nucleation seed causes the system to transition to the globally-stable phase [64].

From Fig 1.4, we see that the reorientation Péclet number plays an important role in the phase behavior of active systems. In addition to a ratio of the particle size to its run length, we can use the swim activity $k_sT_s \equiv \zeta U_0^2\tau_R/6$ to rewrite the reorientation Péclet number as $Pe_R \equiv a/(U_0\tau_R) = \zeta U_0 a/(6k_sT_s)$, which is interpreted as a ratio of the interactive energy of the swimmer – force times distance, $\zeta U_0 \times a$ – to the swim activity k_sT_s.

Figure 1.4 reveals that phase separation becomes possible for small $Pe_R = \zeta U_0 a/(6k_sT_s)$, or high T_s. This is opposite to a classical thermodynamic system where phase transitions occur at low temperatures. Yet some systems like temperature-responsive polymers display a lower critical solution temperature (LCST) transition, where phase separation becomes possible at high temperatures [83]. A possible interpretation for active matter systems exhibiting an LCST is that the particle effectively becomes larger in size and thus has less space available for entropic mixing as Pe_R decreases (i.e., run length increases).

In the next section we discuss the notion of an effective 'temperature' of active

matter in the context of phase separation and provide a justification that T_s can indeed be interpreted as a temperature under certain situations.

1.8 Temperature of active matter?[3]

Because the swim pressure has been a useful concept to predict the collective behavior of active matter, a natural question and extension pertains to the temperature of active matter. Wu and Libchaber [84] observed anomalous behavior of passive Brownian particles when placed in a suspension of run-and-tumble *E. coli*, and attributed the particles' enhanced translational diffusivity to the collective motion of the bacteria. Subsequent studies like Loi et al [85] introduced an interesting notion of using passive tracer particles as a 'thermometer' to measure the 'effective temperature' of an active suspension, as many experimental, numerical, and theoretical studies reported on the enhanced hydrodynamic tracer diffusion in a bacterial system [86, 87, 88, 89, 90, 91, 92, 93]. However, the use of an effective temperature of nonequilibrium active matter is not valid in general [49], and it is unclear whether a mapping between the effective temperature and the thermodynamic temperature exists at all.

To understand the 'temperature' of active matter, we shall consider a simple experiment involving the mixing of two systems of active swimmers with a different activity, $k_sT_s \equiv \zeta U_0^2\tau_R/6$ [94]. Suppose a system of "hot" active swimmers with $(k_sT_s)_H$ is initially separated from "cold" swimmers with $(k_sT_s)_C$. When the systems are allowed to mix, the swimmers with different activities collide and displace each other, but they never share their intrinsic kinetic activity (k_sT_s) upon collisions. Even after a very long time, the system is still composed of "hot" and "cold" swimmers with no equilibration of the 'temperature,' or the activity. This is opposite to a purely passive Brownian suspension or a molecular fluid, which thermally equilibrates when systems of different temperatures mix.

For a passive tracer particle in a sea of active swimmers, the motion of the tracer depends on the swimmers' reorientation Péclet number $Pe_R \equiv a/(U_0\tau_R)$. For $Pe_R \gg 1$ the swimmers take small swim steps and they repeatedly displace the tracer particle of order the step size $\sim O(U_0\tau_R)$ upon collisions. In this limit the tracer particle can sense the activity or 'temperature' of the swimmers via collisions because the fluctuations it receives come from the swimmers' activity (plus a contribution from the solvent's thermal fluctuations), allowing it to behave as a 'ther-

[3] See Chapter 5 for further discussion of this section.

mometer' for the activity $k_sT_s = \zeta U_0^2 \tau_R/6$. In this sense a suspension of swimmers with small run lengths $U_0\tau_R < a$ can be mapped to a purely Brownian suspension with an effective 'temperature' k_sT_s[4].

In the other limit of $Pe_R \ll 1$, the swimmer collides with the tracer and continues to translate until the tracer moves completely clear of the swimmer's trajectory. The tracer receives a displacement of $\sim O(a)$ upon colliding with a swimmer, not the run length $U_0\tau_R$. Unlike the limit of $Pe_R \gg 1$, the tracer cannot act as a thermometer because it only receives a displacement of its size a, even though the swimmers actually diffuse with their swim diffusivity $D^{swim} \sim U_0^2\tau_R$. In this limit, the reorientation Péclet number $Pe_R \equiv a/(U_0\tau_R)$ is the quantity that gets shared between the swimmers via collisions [74], and the activity $k_sT_s \equiv \zeta U_0^2\tau_R/6$ cannot be mapped to the thermodynamic temperature.

Here we have focused on a simple system of active Brownian particles with a homogeneous intrinsic swim speed and reorientation time (i.e., activity), which lends itself to a thermodynamic perspective. There is also a continuum perspective which allows slow variations in space and time, and this engenders the notion of interpreting the swim force as a body force, as described next.

1.9 Swim force as an 'internal' body force

Recent discussions [81, 95] have questioned the validity of the active pressure as a true thermodynamic pressure and a state function. Solon et al [81] derived an expression for the pressure on the bounding walls of a container when a local, external torque was applied to each active particle colliding into the wall. They report that the wall pressure depends on the detailed form and nature of the local torque and conclude that the pressure of active matter thus cannot be a state function in general because the force per area on the bounding walls is not necessarily equal to the swim pressure far away from the wall, especially when polar order is present in the system.

A recent work resolved this concern by using both a global force balance and a continuum-level derivation [96]. We established in Sec 1.2 that it is permissible and essential to interpret the self-propulsion of an active particle as arising from a swim force, $\boldsymbol{F}^{swim} = \zeta U_0 \boldsymbol{q}$ for an active Brownian particle, where $\boldsymbol{q}$ is the unit orientation vector specifying the particle's direction of swimming. For an active particle in the

[4]For active Brownian particles, this contribution is in addition to the thermal k_BT that gets shared as usual as a result of translational Brownian motion.

absence of any external forces or torques, the average swim force is zero because the particle's orientation distribution is uniform: $\langle \boldsymbol{F}^{swim} \rangle = \zeta U_0 \langle \boldsymbol{q} \rangle = \boldsymbol{0}$. If we have an external orienting torque on the particles that result in polar order, then the swimming orientations are not uniform, $\langle \boldsymbol{q} \rangle \neq \boldsymbol{0}$, and thus there is a nonzero average swim force $\langle \boldsymbol{F}^{swim} \rangle \neq \boldsymbol{0}$. This nonzero average swim force may arise from an intrinsic mechanism internal to the body, so it is to be construed as an 'internal' force. Yet, this internal average swim force behaves equivalently to an external body force such as gravity [96]. Thus the true mechanical pressure exerted on a boundary is a sum of the swim pressure *plus* the 'weight' of the particles (or the average swim force), and the active pressure is indeed well-defined and independent of interactions with boundaries.

A microscopic theory [80] based upon moment expansions of the Smoluchowski equation revealed that the particle concentration and hence the force exerted on the wall depends on boundary curvature, flux conditions at the surface, etc., which agree with Solon et al [81]. Inclusion of the 'internal' body force (i.e., nonzero average swim force) into the momentum balance shows that the force per unit area on the boundary plus the integral of the internal body force is equal to the active pressure far from the boundary.

The swim pressure perspective allows researchers to analyze the effects of external forces like gravity or orienting torques in a homogeneous suspension, and then use these results to subsequently predict the inhomogeneous behavior of the active system. External gravitational fields or torques do not cause the active particles to generate their own mechanical pressure, but an external field does affect the swim pressure [57].

We motivated this development assuming that the particles have polar order and hence a nonzero $\langle \boldsymbol{F}^{swim} \rangle$. However, we may also have a density-dependent or spatially-varying intrinsic swim velocity $U_0(\boldsymbol{x})$ and reorientation time $\tau_R(\boldsymbol{x})$, due to a variation in fuel concentration, for example. This results in a nonzero $\langle \boldsymbol{F}^{swim} \rangle = -(1/n)\boldsymbol{\sigma}^{swim} \cdot \nabla \log(U_0 \tau_R)$ [94], which must then appear in the global force balance and in the continuum description to compute the pressure of active matter. Therefore, the key is to have a nonzero $\langle \boldsymbol{F}^{swim} \rangle$, not necessarily any polar order.

We have assumed that the active particles do not change their swimming speed nor reorientation time upon increasing concentration. Both synthetic Janus swimmers and biological microorganisms may alter their activity based upon confinement or local swimmer concentration, and this would add an additional complexity

and modify the swim pressure. However, the swim pressure would still be a fundamental concept to explain the phase-separating behavior of active systems.

Lastly, a microscopic perspective [80] allows any scale variation and shows the importance of another micro-length scale $\delta \sim \sqrt{D_0 \tau_R}$ that allows the swim pressure to emerge naturally. This perspective allows the swimmers' run length to be on the order of the body size (or smaller) and gives rise to interesting phenomena like the Casimir effect [97].

1.10 Conclusions

In this introduction we discussed the forces and stresses generated by active matter, and the (thermo)dynamics that results from the activity of self-propelled Brownian microswimmers. We focused on recent theoretical work predicting the fascinating collective behavior and phase separation in active systems. The nontrivial behavior of active matter such as spontaneous self-assembly and pattern formation [1, 2, 3] makes the understanding of their complex dynamics a challenging problem in the statistical physics of soft matter.

We discussed in detail about the notion that *all* active matter systems generate a swim pressure due to their self-motion. The swim pressure is distinct from, and in addition to, the "hydrodynamic stresslet" [47, 53]. For larger swimmers where the Reynolds number is not small, we also have the Reynolds (or Bernoulli) pressure contribution $\rho\langle \boldsymbol{u}' \cdot \boldsymbol{u}' \rangle$, where ρ is the density and $\boldsymbol{u}'$ is the velocity fluctuation, in addition to the swim pressure. See Chapter 8 for further detail.

An exciting future development is to analyze the extent to which the ideas presented here are applicable to larger swimmers such as fish and birds, and whether the swim pressure perspective may be used to explain large-scale flocking behavior. Another important ongoing challenge in active soft matter has been to understand the influence of solvent-mediated hydrodynamic interactions on the behavior of active systems. The simple model presented in Sec 1.7 neglected the effects of hydrodynamic interactions between the particles, which would contribute additional terms to the active pressure and affect the reorientation time. Including the effects of hydrodynamic interactions is an arduous task because the dynamics of the surrounding fluid must be incorporated into the model, in addition to that of the active particles.

On the experimental side, we foresee the use of swim pressure concepts in real-life engineering applications, such as the fabrication of novel soft materials using active swimmers. We also believe that the swim pressure may have forthcoming applica-

tions in molecular-cell biology, as the determination of the mechanical forces and stresses generated by active constituents inside a living cell may engender new discoveries in cellular morphology and function. Lastly, further experimental evidence for the intriguing behavior of active systems, such as the Casimir phenomenon or the effect of external polar or nematic fields on collective motion, is a forthcoming development in this area.

Active matter has engendered a new field of fundamental physics, materials science, and biology. Cellular biology and biophysics are becoming increasingly concerned with the mechanical forces, stresses, and (thermo)dynamics inside a living cell. New frameworks have been developed by many soft matter researchers around the world to make predictions and corroborate the fascinating nonequilibrium behaviors exhibited by active matter. Given the richness and challenges inherent in active soft matter, much work remains to elucidate the nonequilibrium dynamics of living systems and other far from equilibrium systems.

References

[1] D. J. Sumpter. *Collective animal behavior*. Princeton, New Jersey, USA: Princeton University Press, 2010.

[2] S. Ramaswamy. "The mechanics and statistics of active matter". *Ann Rev Condens Matter Phys* 1.1 (2010), pp. 323–345.

[3] J. Toner, Y. Tu, and S. Ramaswamy. "Hydrodynamics and phases of flocks". *Ann Phys* 318.1 (2005), pp. 170–244.

[4] M. C. Marchetti et al. "Hydrodynamics of soft active matter". *Rev Mod Phys* 85.3 (2013), pp. 1143–1189.

[5] S. C. Takatori, W. Yan, and J. F. Brady. "Swim pressure: Stress generation in active matter". *Phys Rev Lett* 113.2 (2014), p. 028103.

[6] X. Yang, M. L. Manning, and M. C. Marchetti. "Aggregation and segregation of confined active particles". *Soft Matter* 10.34 (2014), pp. 6477–6484.

[7] E. M. Purcell. "Life at low Reynolds number". *American Journal of Physics* 45.1 (1977), pp. 3–11.

[8] G. Taylor. "The action of waving cylindrical tails in propelling microscopic organisms". *Proc Roy Soc London Ser A* 211.1105 (1952), pp. 225–239.

[9] S. Nakata and Y. Hayashima. "Spontaneous dancing of a camphor scraping". *J Chem Soc, Faraday Trans* 94.24 (1998), pp. 3655–3658.

[10] R. F. Ismagilov, A. Schwartz, N. Bowden, and G. M. Whitesides. "Autonomous movement and self-assembly". *Angewandte Chemie International Edition* 41.4 (2002), pp. 652–654.

[11] W. F. Paxton et al. "Catalytic nanomotors: Autonomous movement of striped nanorods". *J Am Chem Soc* 126.41 (2004), pp. 13424–13431.

[12] J. R. Howse et al. "Self-motile colloidal particles: From directed propulsion to random walk". *Phys Rev Lett* 99.4 (2007), p. 048102.

[13] W. F. Paxton et al. "Catalytically induced electrokinetics for motors and micropumps". *J Am Chem Soc* 128.46 (2006), pp. 14881–14888.

[14] A. Ajdari and L. Bocquet. "Giant amplification of interfacially driven transport by hydrodynamic slip: Diffusio-osmosis and beyond". *Phys Rev Lett* 96.18 (2006), p. 186102.

[15] R. Golestanian, T. B. Liverpool, and A. Ajdari. "Designing phoretic micro- and nano-swimmers". *New J Phys* 9.5 (2007), p. 126.

[16] U. M. Córdova-Figueroa and J. F. Brady. "Osmotic propulsion: The osmotic motor". *Phys Rev Lett* 100.15 (2008), p. 158303.

[17] A. Brown and W. Poon. "Ionic effects in self-propelled Pt-coated Janus swimmers". *Soft Matter* 10.22 (2014), pp. 4016–4027.

[18] H.-R. Jiang, N. Yoshinaga, and M. Sano. "Active motion of a Janus particle by self-thermophoresis in a defocused laser beam". *Phys Rev Lett* 105.26 (2010), p. 268302.

[19] J. Palacci, S. Sacanna, A. P. Steinberg, D. J. Pine, and P. M. Chaikin. "Living crystals of light-activated colloidal surfers". *Science* 339.6122 (2013), pp. 936–940.

[20] G. Volpe, I. Buttinoni, D. Vogt, H.-J. Kümmerer, and C. Bechinger. "Microswimmers in patterned environments". *Soft Matter* 7.19 (2011), pp. 8810–8815.

[21] L. Baraban et al. "Control over Janus micromotors by the strength of a magnetic field". *Nanoscale* 5.4 (2013), pp. 1332–1336.

[22] H. Berg. *Random walks in biology*. Princeton, New Jersey, USA: Princeton University Press, 1993.

[23] J. Adler. "Chemotaxis in bacteria". *Science* 153.3737 (1966), pp. 708–716.

[24] R. Blakemore. "Magnetotactic bacteria". *Science* 190.4212 (1975), pp. 377–379.

[25] J. Armitage and K. Hellingwerf. "Light-induced behavioral responses ('phototaxis') in prokaryotes". *Photosynth Res* 76.1-3 (2003), pp. 145–155.

[26] D. Hader, R. Hemmersbach, and M. Lebert. *Gravity and the behavior of unicellular organisms*. Cambridge, United Kingdom: Cambridge University Press, 2005.

[27] X. Garcia, S. Rafaï, and P. Peyla. "Light control of the flow of phototactic microswimmer suspensions". *Phys Rev Lett* 110.13 (2013), p. 138106.

[28] J. Prost, F. Jülicher, and J. F. Joanny. "Active gel physics". *Nat Phys* 11.2 (2015), pp. 111–117.

[29] M. J. Shelley. "The dynamics of microtubule/motor-protein assemblies in biology and physics". *Ann Rev Fluid Mech* 48.1 (2016), pp. 487–506.

[30] F. Jülicher, K. Kruse, J. Prost, and J. F. Joanny. "Active behavior of the cytoskeleton". *Physics Reports* 449.1–3 (2007), pp. 3–28.

[31] J. F. Joanny and J. Prost. "Active gels as a description of the actin-myosin cytoskeleton". *HFSP Journal* 3.2 (2009), pp. 94–104.

[32] K. Kruse, J. F. Joanny, F. Jülicher, J. Prost, and K. Sekimoto. "Asters, vortices, and rotating spirals in active gels of polar filaments". *Phys Rev Lett* 92.7 (2004), p. 078101.

[33] A. J. Levine and F. C. MacKintosh. "The mechanics and fluctuation spectrum of active gels". *J Phys Chem B* 113.12 (2009), pp. 3820–3830.

[34] T. B. Liverpool. "Active gels: Where polymer physics meets cytoskeletal dynamics". *Phil Trans R Soc A* 364.1849 (2006), p. 3335.

[35] S. De Groot and P. Mazur. *Non-equilibrium thermodynamics*. New York: Dover, 1984.

[36] P. C. Martin, O. Parodi, and P. S. Pershan. "Unified hydrodynamic theory for crystals, liquid crystals, and normal fluids". *Phys Rev A* 6.6 (1972), pp. 2401–2420.

[37] C. P. Brangwynne et al. "Germline P granules are liquid droplets that localize by controlled dissolution/condensation". *Science* 324.5935 (2009), p. 1729.

[38] K. V. Kumar, J. S. Bois, F. Jülicher, and S. W. Grill. "Pulsatory patterns in active fluids". *Phys Rev Lett* 112.20 (2014), p. 208101.

[39] P. Khuc Trong, H. Doerflinger, J. Dunkel, D. St Johnston, and R. E. Goldstein. "Cortical microtubule nucleation can organise the cytoskeleton of *Drosophila oocytes* to define the anteroposterior axis". *eLife* 4 (2015), e06088.

[40] J. S. Bois, F. Jülicher, and S. W. Grill. "Pattern formation in active fluids". *Phys Rev Lett* 106.2 (2011), p. 028103.

[41] M. Mayer, M. Depken, J. S. Bois, F. Jülicher, and S. W. Grill. "Anisotropies in cortical tension reveal the physical basis of polarizing cortical flows". *Nature* 467.7315 (2010), pp. 617–621.

[42] T. Shinar, M. Mana, F. Piano, and M. J. Shelley. "A model of cytoplasmically driven microtubule-based motion in the single-celled *Caenorhabditis elegans* embryo". *Proc Natl Acad Sci U.S.A* 108.26 (2011), pp. 10508–10513.

[43] D. Kondepudi and I. Prigogine. *Modern thermodynamics: From heat engines to dissipative structures*. 2nd ed. Chichester, West Sussex, United Kingdom: John Wiley Sons, Ltd, 2014.

[44] M. Z. Bazant. "Thermodynamic stability of driven open systems and control of phase separation by electroautocatalysis". *Faraday Discussions* (2017).

[45] D. Zwicker, R. Seyboldt, C. A. Weber, A. A. Hyman, and F. Jülicher. "Growth and division of active droplets provides a model for protocells". *Nat Phys* 13.4 (2017), pp. 408–413.

[46] J. R. Blake. "A spherical envelope approach to ciliary propulsion". *J Fluid Mech* 46.01 (1971), pp. 199–208.

[47] T. Ishikawa, M. P. Simmonds, and T. J. Pedley. "Hydrodynamic interaction of two swimming model micro-organisms". *J Fluid Mech* 568 (2006), pp. 119–160.

[48] J. W. Swan, J. F. Brady, R. S. Moore, and C. 174. "Modeling hydrodynamic self-propulsion with Stokesian Dynamics. Or teaching Stokesian Dynamics to swim". *Phys Fluids* 23.7 (2011), pp. 071901–071919.

[49] M. E. Cates and J. Tailleur. "When are active Brownian particles and run-and-tumble particles equivalent? Consequences for motility-induced phase separation". *Europhys Lett* 101.2 (2013), p. 20010.

[50] H. Goldstein. *Classical mechanics*. 2nd ed. Reading, MA: Addison-Wesley, 1990.

[51] F. Ginot et al. "Nonequilibrium equation of state in suspensions of active colloids". *Phys Rev X* 5.1 (2015), p. 011004.

[52] S. C. Takatori and J. F. Brady. "Forces, stresses and the (thermo?) dynamics of active matter". *Curr Opin Colloid Interface Sci* 21 (2016), pp. 24–33.

[53] D. Saintillan and M. J. Shelley. "Instabilities, pattern formation, and mixing in active suspensions". *Phys Fluids* 20.12 (2008), pp. 123304–123315.

[54] M. Doi. *Soft matter physics*. Oxford, United Kingdom: Oxford University Press, 2013.

[55] D. S. Fudge et al. "From ultra-soft slime to hard α-keratins: The many lives of intermediate filaments". *Integr Comp Biol* 49.1 (2009), pp. 32–39.

[56] S. K. Lai, Y.-Y. Wang, D. Wirtz, and J. Hanes. "Micro- and macrorheology of mucus". *Adv Drug Deliv Rev* 61.2 (2009), pp. 86–100.

[57] S. C. Takatori and J. F. Brady. "Swim stress, motion, and deformation of active matter: Effect of an external field". *Soft Matter* 10.47 (2014), pp. 9433–9445.

[58] B. Ezhilan, R. Alonso-Matilla, and D. Saintillan. “On the distribution and swim pressure of run-and-tumble particles in confinement”. *J Fluid Mech* 781 (2015), R4.

[59] F. Smallenburg and H. Lowen. “Swim pressure on walls with curves and corners”. *Phys Rev E* 92.3 (2015), p. 032304.

[60] T. Vicsek, A. Czirók, E. Ben-Jacob, I. Cohen, and O. Shochet. “Novel type of phase transition in a system of self-driven particles”. *Phys Rev Lett* 75.6 (1995), pp. 1226–1229.

[61] R. Aditi Simha and S. Ramaswamy. “Hydrodynamic fluctuations and instabilities in ordered suspensions of self-propelled particles”. *Phys Rev Lett* 89.5 (2002), p. 058101.

[62] I. Theurkauff, C. Cottin-Bizonne, J. Palacci, C. Ybert, and L. Bocquet. “Dynamic clustering in active colloidal suspensions with chemical signaling”. *Phys Rev Lett* 108.26 (2012), p. 268303.

[63] M. E. Cates, D. Marenduzzo, I. Pagonabarraga, and J. Tailleur. “Arrested phase separation in reproducing bacteria creates a generic route to pattern formation”. *Proc Natl Acad Sci U.S.A* 107.26 (2010), pp. 11715–11720.

[64] G. S. Redner, M. F. Hagan, and A. Baskaran. “Structure and dynamics of a phase-separating active colloidal fluid”. *Phys Rev Lett* 110.5 (2013), p. 055701.

[65] J. Bialké, H. Löwen, and T. Speck. “Microscopic theory for the phase separation of self-propelled repulsive disks”. *Europhys Lett* 103.3 (2013), p. 30008.

[66] J. Stenhammar, A. Tiribocchi, R. J. Allen, D. Marenduzzo, and M. E. Cates. “Continuum theory of phase separation kinetics for active Brownian particles”. *Phys Rev Lett* 111.14 (2013), p. 145702.

[67] Y. Fily and M. C. Marchetti. “Athermal phase separation of self-propelled particles with no alignment”. *Phys Rev Lett* 108.23 (2012), p. 235702.

[68] J. Stenhammar, D. Marenduzzo, R. J. Allen, and M. E. Cates. “Phase behaviour of active Brownian particles: The role of dimensionality”. *Soft Matter* 10.10 (2014), pp. 1489–1499.

[69] R. Ni, M. A. C. Stuart, and M. Dijkstra. “Pushing the glass transition towards random close packing using self-propelled hard spheres”. *Nat Commun* 4 (2013), p. 2704.

[70] A. Baskaran and M. C. Marchetti. “Enhanced diffusion and ordering of self-propelled rods”. *Phys Rev Lett* 101.26 (2008), p. 268101.

[71] J. Tailleur and M. E. Cates. “Statistical mechanics of interacting run-and-tumble bacteria”. *Phys Rev Lett* 100.21 (2008), p. 218103.

[72] J. Stenhammar, R. Wittkowski, D. Marenduzzo, and M. E. Cates. “Activity-induced phase separation and self-assembly in mixtures of active and passive particles”. *Phys Rev Lett* 114.1 (2015), p. 018301.

[73] T. Speck, J. Bialké, A. M. Menzel, and H. Löwen. “Effective Cahn-Hilliard equation for the phase separation of active Brownian particles”. *Phys Rev Lett* 112.21 (2014), p. 218304.

[74] S. C. Takatori and J. F. Brady. “Towards a thermodynamics of active matter”. *Phys Rev E* 91.3 (2015), p. 032117.

[75] Y. Fily, S. Henkes, and M. C. Marchetti. “Freezing and phase separation of self-propelled disks”. *Soft Matter* 10.13 (2014), pp. 2132–2140.

[76] D. McQuarrie. *Statistical mechanics*. Mill Valley, California, USA: University Science Books, 2000.

[77] W. Russel, D. Saville, and W. Schowalter. *Colloidal dispersions*. Cambridge University Press, 1992.

[78] J. F. Brady. “Brownian motion, hydrodynamics, and the osmotic pressure”. *J Chem Phys* 98.4 (1993), pp. 3335–3341.

[79] I. Buttinoni et al. “Dynamical clustering and phase separation in suspensions of self-propelled colloidal particles”. *Phys Rev Lett* 110.23 (2013), p. 238301.

[80] W. Yan and J. F. Brady. “The force on a boundary in active matter”. *J Fluid Mech* 785 (2015), R1.

[81] A. P. Solon et al. “Pressure is not a state function for generic active fluids”. *Nat Phys* 11.8 (2015), pp. 673–678.

[82] A. Wysocki, R. G. Winkler, and G. Gompper. “Cooperative motion of active Brownian spheres in three-dimensional dense suspensions”. *Europhys Lett* 105.4 (2014), p. 48004.

[83] R. B. Griffiths and J. C. Wheeler. “Critical points in multicomponent systems”. *Phys Rev A* 2.3 (1970), pp. 1047–1064.

[84] X.-L. Wu and A. Libchaber. “Particle diffusion in a quasi-two-dimensional bacterial bath”. *Phys Rev Lett* 84.13 (2000), pp. 3017–3020.

[85] D. Loi, S. Mossa, and L. F. Cugliandolo. “Effective temperature of active matter”. *Phys Rev E* 77.5 (2008), p. 051111.

[86] G. Mino et al. “Enhanced diffusion due to active swimmers at a solid surface”. *Phys Rev Lett* 106.4 (2011), p. 048102.

[87] T. V. Kasyap, D. L. Koch, and M. Wu. “Hydrodynamic tracer diffusion in suspensions of swimming bacteria”. *Phys Fluids* 26.8 (2014), p. 081901.

[88] K. C. Leptos, J. S. Guasto, J. P. Gollub, A. I. Pesci, and R. E. Goldstein. "Dynamics of enhanced tracer diffusion in suspensions of swimming eukaryotic microorganisms". *Phys Rev Lett* 103.19 (2009), p. 198103.

[89] H. Kurtuldu, J. S. Guasto, K. A. Johnson, and J. P. Gollub. "Enhancement of biomixing by swimming algal cells in two-dimensional films". *Proc Natl Acad Sci U.S.A* 108.26 (2011), pp. 10391–10395.

[90] J.-L. Thiffeault and S. Childress. "Stirring by swimming bodies". *Phys Lett A* 374.34 (2010), pp. 3487–3490.

[91] M. J. Kim and K. S. Breuer. "Enhanced diffusion due to motile bacteria". *Phys Fluids* 16.9 (2004), pp. L78–L81.

[92] A. Jepson, V. A. Martinez, J. Schwarz-Linek, A. Morozov, and W. C. K. Poon. "Enhanced diffusion of nonswimmers in a three-dimensional bath of motile bacteria". *Phys Rev E* 88.4 (2013), p. 041002.

[93] A. E. Patteson, A. Gopinath, P. K. Purohit, and P. E. Arratia. "Particle diffusion in active fluids is non-monotonic in size" (2016 in review).

[94] S. C. Takatori and J. F. Brady. "A theory for the phase behavior of mixtures of active particles". *Soft Matter* 11.40 (2015), pp. 7920–7931.

[95] A. P. Solon et al. "Pressure and phase equilibria in interacting active Brownian spheres". *Phys Rev Lett* 114.19 (2015), p. 198301.

[96] W. Yan and J. F. Brady. "The swim force as a body force". *Soft Matter* 11.31 (2015), pp. 6235–6244.

[97] D. Ray, C. Reichhardt, and C. J. O. Reichhardt. "Casimir effect in active matter systems". *Phys Rev E* 90.1 (2014), p. 013019.

Chapter 2

THE SWIM PRESSURE OF ACTIVE MATTER

This chapter includes content from our previously published article:

[1] S. C. Takatori, W. Yan, and J. F. Brady. "Swim pressure: stress generation in active matter". *Phys Rev Lett* 113.2 (2014), p. 028103. DOI: 10.1103/PhysRevLett.113.028103.

2.1 Introduction

From flocks of animals and insects to colonies of living bacteria, so-called "active matter" exhibits intriguing phenomena owing to its constituents' ability to convert chemical fuel into mechanical motion. Active matter systems generate their own internal stress, which drives them far from equilibrium and thus frees them from conventional thermodynamic constraints, and by so doing they can control and direct their own behavior and that of their surrounding environment. This gives rise to fascinating behavior such as spontaneous self-assembly and pattern formation [1, 2, 3], but also makes the theoretical understanding of their complex dynamical behaviors a challenging problem in the statistical physics of soft matter.

In this chapter we identify a new principle that all active matter systems display—namely, through their self-motion they generate an intrinsic "swim stress" that impacts their dynamic and collective behavior. In contrast to thermodynamic quantities such as chemical potential and free energy, the mechanical pressure (or stress) is valid out of equilibrium because it comes directly from the micromechanical equations of motion. To motivate this new perspective, we focus on the simplest model of active matter—a suspension of self-propelled spheres of radii a immersed in a continuous Newtonian solvent with viscosity η. The active particles translate with a constant, intrinsic swim velocity $\boldsymbol{U}_0$ and tumble with a reorientation time τ_R. We do not include the effects of hydrodynamic interactions among the particles.

The origin of the swim pressure is based upon a simple notion—a self-propelled body would swim away in space unless confined by boundaries. The pressure exerted by the surrounding walls to contain the particle is precisely the swim pressure. This is similar to the kinetic theory of gases, where molecular collisions with the container walls exert a pressure. Although it is clear that such a swim pressure

should exist, what is its micromechanical origin, and how is it to be explained and expressed in basic physical quantities?

2.2 Swim Pressure

The swim pressure is the trace of the swim stress, which is the first moment of the self-propulsive force:

$$\boldsymbol{\sigma}^{swim} = -n\langle \boldsymbol{x}\boldsymbol{F}^{swim}\rangle, \tag{2.1}$$

where n is the number density of active particles, $\boldsymbol{x}$ is the absolute position, and $\boldsymbol{F}^{swim} \equiv \zeta \boldsymbol{U}_0$, where ζ is the hydrodynamic resistance coupling translational velocity to force (= $6\pi\eta a$ for an isolated sphere), and the angle brackets denote an average over all particles and over time. It is permissible for determining the stress to interpret the self-propulsion of an active particle as arising from a swim force, $\boldsymbol{F}^{swim}$ (see below). As a result, $-\langle \boldsymbol{x}\boldsymbol{F}^{swim}\rangle$ gives a single-particle self contribution to the stress. (This distinguishes Eq 2.1 from the familiar $-\langle \boldsymbol{x}_{ij}\boldsymbol{F}_{ij}\rangle$ form seen in classical analyses of molecular liquids, where subscripts ij indicate pairwise interactions.[1]) Equation 2.1 comes from the virial theorem [5], which expresses the stress (or pressure) in terms of the forces acting on a system: $\boldsymbol{\sigma} = -1/V\langle \sum_i^N \boldsymbol{x}_i\boldsymbol{F}_i\rangle$. In Eq 2.1 we take the forces $\boldsymbol{F}_i$ to be the swim force of each particle, $\boldsymbol{F}^{swim}$.

The position of a particle at time t is $\boldsymbol{x}(t) = \int \boldsymbol{U}(t')dt'$, and from the overdamped equation of motion, $\boldsymbol{0} = -\zeta\boldsymbol{U}(t) + \boldsymbol{F}(t)$. We obtain $\boldsymbol{\sigma} = -n\langle \boldsymbol{x}\boldsymbol{F}\rangle = -n\zeta \int \langle \boldsymbol{U}(t')\boldsymbol{U}(t)\rangle\, dt' = -n\zeta\boldsymbol{D}$, where the time integral of the velocity autocorrelation is the diffusivity of the particle, $\boldsymbol{D}$. A particle undergoing any type of random motion therefore exerts a pressure $\Pi = -\mathrm{tr}\boldsymbol{\sigma}/3 = n\zeta D$. This general result applies for an arbitrary particle shape (where ζ may depend on particle configuration) and for any source of random motion. Indeed, it has been used in the context of microrheology [6]. It applies equally well to Brownian particles where $D = k_BT/\zeta$, and we obtain the familiar ideal-gas Brownian osmotic pressure $\Pi^B = nk_BT$. Using the convective diffusivity of dilute active matter, $D = U_0^2\tau_R/6$ [7], we arrive at the analogous "ideal-gas" swim pressure:

$$\Pi^{swim}(\phi \to 0) = n\zeta U_0^2\tau_R/6, \tag{2.2}$$

where $\phi = 4\pi a^3 n/3$ is the volume fraction of active particles. As expected for dilute systems, Π^{swim} depends on the particle size only through the hydrodynamic drag factor ζ and is entirely athermal in origin. In two dimensions, $\Pi^{swim} = n\zeta U_0^2\tau_R/2$.

[1] Indeed, Brady [4] showed that there is no need to restrict the interaction to be pairwise, and Eq 2.1 is compatible with the traditional micromechanical definition of stress.

From Eq 2.1 the swim pressure is the average force moment, with ζU_0 the force and the "moment arm" is the run length in a reorientation time, $U_0\tau_R$.

To verify the existence of a swim pressure, we conducted Brownian dynamics (BD) simulations with active particles placed inside a simulation cell both with and without bounding walls. For now we focus on non-Brownian particles (no translational diffusion) to verify that this pressure arises solely from self-propulsion. The system was evolved following the N-particle Langevin equation: $\mathbf{0} = -\zeta(\boldsymbol{U} - \boldsymbol{U}_0) + \boldsymbol{F}^P$ and $\mathbf{0} = -\zeta_R\boldsymbol{\Omega} + \boldsymbol{L}^R$, where $\boldsymbol{U}$ and $\boldsymbol{\Omega}$ are the translational and angular velocities, ζ_R is the hydrodynamic resistance coupling angular velocity to torque, $\boldsymbol{F}^P$ is a hard-sphere interparticle force that prevents particle overlaps computed from a potential-free algorithm [8, 9], and $\boldsymbol{L}^R$ is the reorientation torque. The left-hand side is zero because inertia is negligible for colloidal dispersions.

In the absence of interparticle forces ($\boldsymbol{F}^P = \mathbf{0}$), active swimming is a force-free motion: $\zeta(\boldsymbol{U} - \boldsymbol{U}_0) = \mathbf{0}$, giving $\boldsymbol{U} = \boldsymbol{U}_0$. However, it is both permissible, and essential for computing the stress, to interpret $\zeta\boldsymbol{U}_0$ as a swim force, i.e., $\boldsymbol{F}^{swim} \equiv \zeta\boldsymbol{U}_0$, where $\boldsymbol{U}_0 = U_0\boldsymbol{q}$; U_0 is the swimming speed and $\boldsymbol{q}$ is the unit orientation vector of the swimmer. The active particle velocity then follows from $\boldsymbol{U} = \boldsymbol{F}^{swim}/\zeta = \boldsymbol{U}_0$. One way to appreciate the swim force is to suppose that we prevent an active swimmer from moving, say by optical tweezers. The force required to hold the swimmer fixed is precisely $\zeta\boldsymbol{U}_0$. This use of the swim force to compute the stress does not imply that the self-propulsive motion generates a long-range $(1/r)$ hydrodynamic velocity disturbance typical of low Reynolds number flows.

The reorientation torque has the white noise statistics $\overline{\boldsymbol{L}^R} = \mathbf{0}$ and $\overline{\boldsymbol{L}^R(0)\boldsymbol{L}^R(t)} = 2\zeta_R^2\delta(t)\boldsymbol{I}/\tau_R$. Particle orientations were updated by relating $\boldsymbol{\Omega}$ to the instantaneous orientation $\boldsymbol{q}$ [10]. Simulations were conducted with 2000 particles for at least $5\tau_R$. We varied the volume fraction ϕ and the nondimensional reorientation "Péclet number" $Pe_R = U_0a/D = U_0a/(U_0^2\tau_R) = a/(U_0\tau_R)$, which is also the ratio of the particle size a to the run length of the active particles, $U_0\tau_R$.[2] The pressure was obtained by dividing the force, calculated from the hard-sphere displacements at the wall [9], by its area, F^{wall}/A. In addition, we conducted BD simulations using periodic boundaries (without bounding walls) and used Eq 2.1 to compute the swim pressure. For a wide range of Pe_R ($= 0.01 - 100$) and small ϕ, all data collapse onto the predicted pressure, $\Pi^{swim} = n\zeta U_0^2\tau_R/6$ (see Fig 2.1). This verifies the existence

[2] We use the conventional definition of the Péclet number as advection over diffusion, but others use the inverse of this quantity.

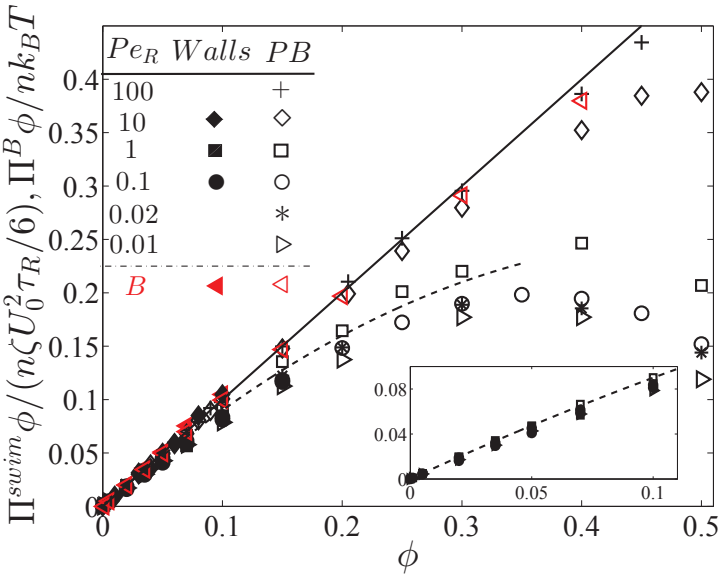

Figure 2.1: The swim, Π^{swim}, and Brownian, Π^B, pressures computed using bounding walls ("Walls") and from Eq 2.1 without walls (periodic boundaries, "PB") for various $Pe_R = a/(U_0\tau_R)$. The solid black line corresponds to a linear increase of pressure with ϕ. The dashed curve is the dilute theory expression (Eq 2.3). The inset is a magnification of the swim pressure at dilute ϕ for $Pe_R \leq 1$.

of a unique swim pressure of active matter.

The concept of confinement also applies for purely Brownian particles, where the wall pressure in this case is $\Pi^B = nk_BT$. Figure 2.1 shows the osmotic pressure of purely Brownian particles alongside the swim pressure of active matter. For active swimmers, the data (black symbols) collapse onto the line $\Pi^{swim} = n\zeta U_0^2\tau_R/6$ until around $\phi \sim 0.1$. At higher ϕ, the swim pressure decreases because the particles collide and obstruct each others' movement for a time τ_R until their swimming directions change from rotational motion. This "clustering" behavior [11] reduces the average distance they travel between reorientations and thus reduces the diffusivity and pressure (by reducing the moment arm). This differentiates active matter from an equilibrium Brownian system, which exerts a fixed $\Pi^B = nk_BT$ of ideal-gas pressure for all ϕ. For high Pe_R (small τ_R), the active particles reorient rapidly with small swim steps and behave as random walkers, so no clusters form and Π^{swim} increases linearly with ϕ until very high ϕ (~ 0.6).

The dashed curve in Fig 2.1 is our theoretical prediction of the swim pressure for small ϕ using results from nonlinear microrheology [12]. The microrheological probe particle is a swimmer that is propelled through a colloidal dispersion with

a constant swim force. Active microrheology describes our system accurately for high $Pe_s = F^{swim}/(k_BT/a)$ and a large reorientation time compared to the collisional time, i.e., $\tau_R > a/(U_0\phi)$, or $\phi > a/(U_0\tau_R) = Pe_R$. This ensures that a steady-state microstructure is achieved during the course of the swimmer's run length. Substituting the high-Pe_s results from Squires and Brady [12] (Eq 36 of their paper) into Eq 2.1, we obtain the leading-order correction to the ideal-gas swim pressure:

$$\frac{\Pi^{swim}}{n\zeta U_0^2\tau_R/6} = 1 - \phi + O(\phi^2), \tag{2.3}$$

which agrees well with our BD simulations for $\phi \lesssim 0.1$ (see inset of Fig 2.1). In contrast to Brownian systems where repulsive pair interactions (e.g., excluded volume) always increase the pressure, for active matter interactions decrease the run length and therefore the swim pressure.

The total pressure of active matter (in the absence of hydrodynamic interactions) is given by $P = p_f + \Pi^{act}$, where $\Pi^{act} = \Pi^{swim} + \Pi^P$; p_f is the solvent pressure, which is arbitrary for an incompressible fluid (plays no dynamical role and is set to zero) and Π^P is the pressure due to interparticle (e.g., excluded volume) forces, $\boldsymbol{\sigma}^P = -n\langle \boldsymbol{x}\boldsymbol{F}^P\rangle$. Following Brady [4], we computed the analytical expression for Π^P for hard-sphere particles using the results from nonlinear microrheology: $\Pi^P/(n\zeta U_0^2\tau_R/6) = 3Pe_R\phi + O(\phi^2)$. Unlike the swim pressure, the interparticle pressure scales as $n^2\zeta U_0 a^4$ since the particle size now sets the scale for the force moment. This is different from $\Pi^{swim} \sim n\zeta U_0(U_0\tau_R)$, which is a *single-particle* contribution where the run length $U_0\tau_R$ sets the scale for the force moment.

Combining this result with Eq 2.3, we obtain a nonequilibrium virial equation of state for active matter:

$$\frac{\Pi^{act}}{n\zeta U_0^2\tau_R/6} = 1 - \phi(1 - 3Pe_R) + O(\phi^2), \tag{2.4}$$

which can be rewritten as $\Pi^{act}/(n\zeta U_0^2\tau_R/6) = 1 + B_2 n + \cdots$, where $B_2 = -\pi(2a)^3(1 - 3Pe_R)/6$ is analogous to the second-virial coefficient from a classical thermodynamic system and is *negative* for $Pe_R < 1/3$. The reorientation Péclet number $Pe_R = a/(U_0\tau_R)$ is analogous to the temperature in a classical equation of state. If $Pe_R \gg 1$, then the particle takes small random steps and behaves like a Brownian walker. If $Pe_R \ll 1$, then the reorientation time is large, causing the particles to obstruct each others' paths when they collide and reduce their run lengths.

We now apply this new swim stress perspective to analyze self-assembly and phase-separation in active soft matter. Experiments and computer simulations [13, 14, 15, 16, 17, 18, 11] have shown that active matter self-organizes into dense and dilute phases resembling an equilibrium liquid-gas coexistence. Continuum descriptions [17, 19] and other microscopic approaches [15, 20, 19, 16, 21] have provided models for this behavior, but the question remains as to whether there is a simpler and more primitive explanation for the self-assembly in active matter.

From classical thermodynamics, a negative second virial coefficient B_2 (i.e., two-body attractions) implies the possibility of a gas-liquid phase transition. Attractions may give rise to a non-monotonic variation of pressure with concentration, known as a "van der Waals loop." Here we show that our simple active system has a pressure-volume phase diagram much like that of a van der Waals fluid.

We conducted BD simulations (with periodic boundary conditions) to produce the full Π^{act}-ϕ phase diagrams for different values of Pe_R. The system was initialized by placing the active particles at random configurations inside the simulation cell. For concentrated systems, we used a modified Lubachevsky-Stillinger algorithm [22]. At each time step, we followed Foss and Brady [9] to compute the interparticle stresslet $-\langle \boldsymbol{x}\boldsymbol{F}^{P}\rangle$. The swim stresslet $-\langle \boldsymbol{x}\boldsymbol{F}^{swim}\rangle$ was computed by correlating the positions of the particles with their swim force. The particle positions $\boldsymbol{x}$ are continuous across the periodic boundaries when computing $-\langle \boldsymbol{x}\boldsymbol{F}^{swim}\rangle$.

As shown in Fig 2.2, at low ϕ all data collapse onto the ideal-gas pressure given by Eq 2.2. For large Pe_R the interparticle pressure dominates and the total pressure increases monotonically with ϕ. This corroborates with Eq 2.4, which gives a positive B_2 for $Pe_R > 1/3$. As in classical thermodynamics, phase separation is possible when Pe_R is below the critical point ($\partial\Pi^{act}/\partial\phi = \partial^2\Pi^{act}/\partial\phi^2 = 0$), beyond which the system is "supercritical." As Pe_R is reduced below ~ 0.03, we observe a non-monotonic pressure profile resembling a van der Waals loop—the total pressure is lower at $\phi = 0.6$ than at $\phi = 0.3$! This decrease is caused by the reduction in swim pressure due to the particles' tendency to form clusters, reducing the average distance they travel between reorientations, i.e., reducing the moment arm $\boldsymbol{U}\tau_R$. A study of structural properties [23] corroborates with our non-monotonic pressure profiles. The probability distribution of the local volume fraction of swimmers computed using a Voronoi construction becomes bimodal for small Pe_R and finite ϕ, indicating the presence of a dilute and dense phase. As ϕ approaches close packing, $\Pi^{swim} \to 0$ but the total pressure necessarily increases because the interparticle

(excluded volume) pressure diverges to infinity.

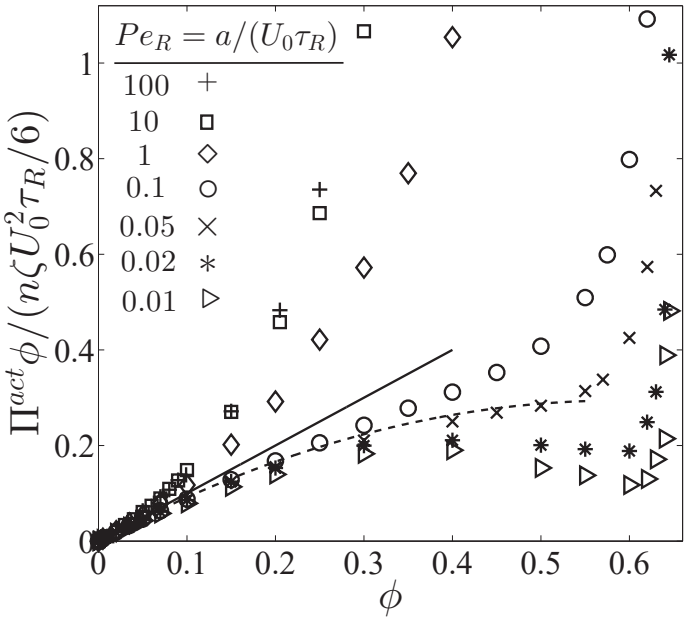

Figure 2.2: Nonequilibrium Π^{act}-ϕ phase diagram, where $\Pi^{act} = \Pi^{swim} + \Pi^{P}$. The data are from BD simulations (with periodic boundaries) and the dashed curve is the analytical theory, Eq 2.4, with $Pe_R = a/(U_0\tau_R) = 0.05$.

We now consider the effects of translational Brownian motion, which affects the interparticle pressure and contributes the dilute Brownian osmotic pressure to the active pressure: $\Pi^{act} = \Pi^{swim} + \Pi^{P} + \Pi^{B}$. The system also involves the swim Péclet number, $Pe_s = F^{swim}/(k_BT/a) = U_0a/D_0$, where $D_0 = k_BT/\zeta$ is the Stokes-Einstein-Sutherland diffusivity of an isolated Brownian particle. Physically, translational Brownian motion would tend to restore the phase-separated system back to a homogeneous state. We would no longer see non-monotonic pressure profiles as Pe_s is reduced from our non-Brownian ($Pe_s \to \infty$) system, and the Π^{act}-ϕ curve would approach the pure Brownian limit as $Pe_s \to 0$. Indeed, these qualitative predictions are corroborated by Fig 2.3, where we conducted simulations with active particles that translate by both self-propulsion and translational diffusion: $\mathbf{0} = -\zeta\boldsymbol{U} + \boldsymbol{F}^{swim} + \boldsymbol{F}^{B} + \boldsymbol{F}^{P}$, and the Brownian force has the usual properties $\overline{\boldsymbol{F}^{B}} = \mathbf{0}$ and $\overline{\boldsymbol{F}^{B}(0)\boldsymbol{F}^{B}(t)} = 2k_BT\zeta\delta(t)\boldsymbol{I}$. As shown in Fig 2.3, increasing the translational Brownian motion (decreasing Pe_s) causes the van der Waals loop to vanish and the pressure approaches the familiar osmotic pressure of Brownian particles, i.e., a monotonic increase with volume fraction. The solid curves for $Pe_s = 0.1$ and 0.01 correspond to the theoretical prediction of Brownian osmotic pressure [4] from the Carnahan-Starling equation of state, scaled appropriately by each Pe_s.

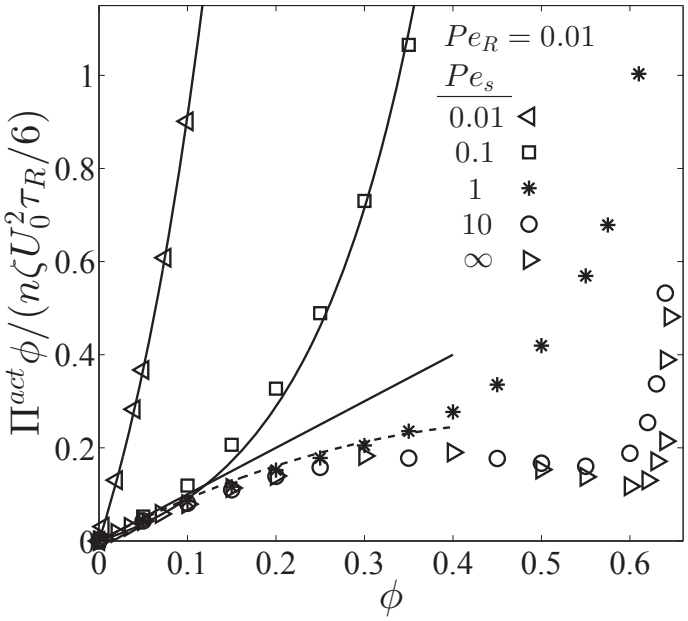

Figure 2.3: Effect of translational Brownian motion on the Π^{act}-ϕ phase diagram, where $\Pi^{act} = \Pi^{swim} + \Pi^{P} + \Pi^{B}$. The data are BD simulations for various $Pe_s = U_0 a/D_0$ with fixed $Pe_R = a/(U_0\tau_R) = 0.01$. The solid curves are theoretical expressions of osmotic pressures of Brownian particles. The dashed curve is the analytical theory, Eq 2.4.

Self-propelled particles need not be spherical nor have a constant intrinsic velocity $\boldsymbol{U}_0$ or reorientation time τ_R. We neglected hydrodynamic interactions between particles, which would contribute additional terms to the pressure and affect the reorientation time. The swim pressure is distinct from, and in addition to, the "hydrodynamic stresslet" that accompanies a class of non-spherical microswimmers [24, 25], which scales as $n\zeta U_0 a(\boldsymbol{qq} - \boldsymbol{I}/3)$ and averages to zero for an isotropic distribution. The ratio of the magnitude of the hydrodynamic stresslet over the swim pressure is Pe_R; the hydrodynamic contribution becomes negligible when phase-separation occurs at low Pe_R (see Fig 2.2).

We have allowed for any reorientation mechanism characterized solely by τ_R. If the reorientation is caused by thermal Brownian rotations, then $\tau_R = 1/D_R$, where the rotary diffusivity $D_R = k_B T/\zeta_R = k_B T/(8\pi\eta a^3)$ for an isolated sphere. In this case our $Pe_R = aD_R/U_0 = 3/(4Pe_s)$ and so the dual limits for phase separation $Pe_R \to 0, Pe_s \to \infty$ are automatically satisfied. Indeed, the ratio of the Brownian osmotic pressure to the active swim pressure $\Pi^B/\Pi^{swim} = k_B T/(\zeta U_0^2\tau_R/6) = 6Pe_R/Pe_s \ll 1$ for possible phase separation, in agreement with the results in Fig 2.3.

Through their self-motion, *all* active matter systems generate a swim pressure. The quantitative prediction of phase separation is one of many applications of the swim stress perspective. A possible application is the analysis of various biophysical systems, such as the crowded interior of a cell. For example, motor proteins moving along a microtubule will exert a tension along the tube simply because they are confined to the tube. Another application is the development of soft materials that exploit the self-organization behavior of active matter, which includes a class of artificial catalytic motors [13, 14, 26].

This swim pressure exists at all scales in both living (e.g., microorganisms) and nonliving active systems, and also applies to larger swimmers (e.g., fish) where inertia is important (i.e., the Reynolds number is not small). This swim stress is in addition to the usual Reynolds stress contribution $\rho\langle \boldsymbol{u}'\boldsymbol{u}'\rangle$, where ρ is the density and $\boldsymbol{u}'$ is the velocity fluctuation. Experimental measurement of the swim pressure requires the confining boundaries to be permeable to the solvent, just as is the case for the osmotic pressure of a solute.

Lastly, one can construct a flux model from our swim pressure perspective. The conservation of active particle number density is $\partial n/\partial t + \nabla \cdot \boldsymbol{j} = 0$, where $\boldsymbol{j} = n\boldsymbol{v}$ is the particle flux and $\boldsymbol{v}$ is the average velocity of the particles. Standard volume averaging gives a momentum balance (for negligible inertia) relating the particle flux to stress gradients: $\boldsymbol{0} = -\zeta n(\boldsymbol{v} - \boldsymbol{u})/(1 - \phi) + \nabla \cdot \boldsymbol{\sigma}^{act}$, where $\boldsymbol{\sigma}^{act} = \boldsymbol{\sigma}^{swim} + \boldsymbol{\sigma}^{P}$ and $\boldsymbol{u}$ is the volume-average velocity of the suspension. The relative flux $\boldsymbol{j}_{rel} = n(\boldsymbol{v}-\boldsymbol{u}) = (1-\phi)\nabla\cdot\boldsymbol{\sigma}^{act}/\zeta$, and the conservation of particle number density becomes an advection-diffusion equation with $\boldsymbol{D} = -(1 - \phi)(\partial\boldsymbol{\sigma}^{act}/\partial n)/\zeta$, which recovers $\boldsymbol{D} = U_0^2\tau_R\boldsymbol{I}/6$ for dilute active matter. For a thermodynamic system (slightly) out of equilibrium the driving force for motion is the gradient in the chemical potential $\nabla\mu$. From the active particle momentum balance we obtain $n(\partial\mu/\partial n) = (1 - \phi)\partial\Pi^{act}/\partial n$, which may provide the necessary generalization of the chemical potential for nonequilibrium active matter. This flux model is further developed in Chapter 4 of this thesis.

References

[1] D. J. Sumpter. *Collective animal behavior*. Princeton, New Jersey, USA: Princeton University Press, 2010.

[2] S. Ramaswamy. "The mechanics and statistics of active matter". *Ann Rev Condens Matter Phys* 1.1 (2010), pp. 323–345.

[3] J. Toner, Y. Tu, and S. Ramaswamy. “Hydrodynamics and phases of flocks”. *Ann Phys* 318.1 (2005), pp. 170–244.

[4] J. F. Brady. “Brownian motion, hydrodynamics, and the osmotic pressure”. *J Chem Phys* 98.4 (1993), pp. 3335–3341.

[5] H. Goldstein. *Classical mechanics*. 2nd ed. Reading, MA: Addison-Wesley, 1990.

[6] R. N. Zia and J. F. Brady. “Microviscosity, microdiffusivity, and normal stresses in colloidal dispersions”. *J Rheol* 56.5 (2012), pp. 1175–1208.

[7] H. Berg. *Random walks in biology*. Princeton, New Jersey, USA: Princeton University Press, 1993.

[8] D. M. Heyes and J. R. Melrose. “Brownian dynamics simulations of model hard-sphere suspensions”. *J Non-Newtonian Fluid Mech* 46.1 (1993), pp. 1–28.

[9] D. R. Foss and J. F. Brady. “Brownian Dynamics simulation of hard-sphere colloidal dispersions”. *J Rheol* 44.3 (2000), pp. 629–651.

[10] D. A. Beard and T. Schlick. “Unbiased rotational moves for rigid-body dynamics”. *Biophys J* 85.5 (2003), pp. 2973–2976.

[11] M. E. Cates and J. Tailleur. “When are active Brownian particles and run-and-tumble particles equivalent? Consequences for motility-induced phase separation”. *Europhys Lett* 101.2 (2013), p. 20010.

[12] T. M. Squires and J. F. Brady. “A simple paradigm for active and nonlinear microrheology”. *Phys Fluids* 17.7 (2005), pp. 073101–073121.

[13] I. Theurkauff, C. Cottin-Bizonne, J. Palacci, C. Ybert, and L. Bocquet. “Dynamic clustering in active colloidal suspensions with chemical signaling”. *Phys Rev Lett* 108.26 (2012), p. 268303.

[14] J. Palacci, S. Sacanna, A. P. Steinberg, D. J. Pine, and P. M. Chaikin. “Living crystals of light-activated colloidal surfers”. *Science* 339.6122 (2013), pp. 936–940.

[15] G. S. Redner, M. F. Hagan, and A. Baskaran. “Structure and dynamics of a phase-separating active colloidal fluid”. *Phys Rev Lett* 110.5 (2013), p. 055701.

[16] J. Bialké, H. Löwen, and T. Speck. “Microscopic theory for the phase separation of self-propelled repulsive disks”. *Europhys Lett* 103.3 (2013), p. 30008.

[17] J. Stenhammar, A. Tiribocchi, R. J. Allen, D. Marenduzzo, and M. E. Cates. “Continuum theory of phase separation kinetics for active Brownian particles”. *Phys Rev Lett* 111.14 (2013), p. 145702.

[18] M. E. Cates, D. Marenduzzo, I. Pagonabarraga, and J. Tailleur. “Arrested phase separation in reproducing bacteria creates a generic route to pattern formation”. *Proc Natl Acad Sci U.S.A* 107.26 (2010), pp. 11715–11720.

[19] Y. Fily and M. C. Marchetti. “Athermal phase separation of self-propelled particles with no alignment”. *Phys Rev Lett* 108.23 (2012), p. 235702.

[20] R. Ni, M. A. C. Stuart, and M. Dijkstra. “Pushing the glass transition towards random close packing using self-propelled hard spheres”. *Nat Commun* 4 (2013), p. 2704.

[21] A. Baskaran and M. C. Marchetti. “Enhanced diffusion and ordering of self-propelled rods”. *Phys Rev Lett* 101.26 (2008), p. 268101.

[22] M. Skoge, A. Donev, F. H. Stillinger, and S. Torquato. “Packing hyperspheres in high-dimensional Euclidean spaces”. *Phys Rev E* 74.4 (2006), p. 041127.

[23] A. Wysocki, R. G. Winkler, and G. Gompper. “Cooperative motion of active Brownian spheres in three-dimensional dense suspensions”. *Europhys Lett* 105.4 (2014), p. 48004.

[24] D. Saintillan and M. J. Shelley. “Instabilities, pattern formation, and mixing in active suspensions”. *Phys Fluids* 20.12 (2008), pp. 123304–123315.

[25] T. Ishikawa, M. P. Simmonds, and T. J. Pedley. “Hydrodynamic interaction of two swimming model micro-organisms”. *J Fluid Mech* 568 (2006), pp. 119–160.

[26] U. M. Córdova-Figueroa and J. F. Brady. “Osmotic propulsion: The osmotic motor”. *Phys Rev Lett* 100.15 (2008), p. 158303.

Chapter 3

ACOUSTIC TRAPPING OF ACTIVE MATTER

This chapter includes content from our previously published article:

[1] S. C. Takatori*, R. De Dier*, J. Vermant, and J. F. Brady. "Acoustic trapping of active matter". *Nat Commun* 7 (2016). DOI: 10.1038/ncomms10694.

3.1 Introduction

Confinement of living microorganisms and self-propelled particles by an external trap provides a means of analyzing the motion and behavior of active systems. Developing a tweezer with a trapping radius large compared to the swimmers' size and run length has been an experimental challenge, as standard optical traps are too weak. Here we report the novel use of an acoustic tweezer to confine self-propelled particles in two-dimensions over distances that are large compared to the swimmers' run length. We develop a near-harmonic trap to demonstrate the crossover from weak confinement, where the probability density is Boltzmann-like, to strong confinement, where the density is peaked along the perimeter. At high concentrations the swimmers crystallize into a close-packed structure, which subsequently 'explodes' as a traveling wave when the tweezer is turned off. The swimmers' confined motion provides a measurement of the swim pressure, a unique mechanical pressure exerted by self-propelled bodies.

The study of active matter systems such as swimming bacteria and molecular motors in geometrically confined environments plays an essential role in understanding many cellular and biophysical processes. Many studies have demonstrated that self-propelled bodies exhibit intriguing phenomena in confined spaces, such as accumulation at boundaries [1, 2, 3, 4, 5]. In addition to confinement by a physical boundary, confinement of active particles via a harmonic external field can engender many useful properties of active systems [6, 7, 8]. However, this has remained an experimental challenge because most biological trapping instruments are too weak to confine active systems over a large spatial extent, as swimmers' run lengths can easily exceed $100\mu m$.

In this work, we overcome this challenge by developing a custom-built acoustic tweezer to confine self-propelled Janus particles in a two-dimensional (2D) near-

harmonic trap. Analogous to optical or magnetic tweezers, acoustic traps employ sound waves to move objects to special regions of the acoustic radiation field. One or two-dimensional standing wave devices [9, 10] utilize axial radiation forces of multiple transducers and/or reflectors to manipulate objects into pressure nodes or antinodes. Unlike studies that impose a strong trap to manipulate structures and place objects at specified locations, our goal is to interrogate the motion and behavior of the trap constituents themselves (i.e., active microswimmers) under confinement.

Invoking the transverse acoustic forces of a single-beam transducer [11], in the present work we use a 2D device capable of confining active particles over a wide range of trapping forces and spatial extents of the trap, from larger than the run length of the swimmers to much smaller than it. In addition to having a significantly stronger trapping force compared to optical tweezers, acoustic traps preclude potential laser damage to biological specimens ("opticution") [12] especially for the high power intensities required for our study. Our judicious choice of the trap strength enables us to study the nonequilibrium behaviors of active particles in varying degrees of confinement: for weak traps, the probability density is Boltzmann-like and can be mapped to that of classical equilibrium Brownian systems, and for strong traps, the density is peaked along the trap perimeter. We discover that the external trap behaves as an 'osmotic barrier' confining swimmers inside the trapping region, analogous to semipermeable membranes that confine passive Brownian solutes inside a boundary. From the swimmers' restricted motion inside the trap, we calculate the unique swim pressure generated by active systems originating from the mechanical force required to confine them by boundaries. Finally, we investigate the crossover from ballistic to diffusive behavior of active microswimmers by observing the 'explosion' of an active crystal.

3.2 Results

Active Janus particles in acoustic confinement

We fabricate Janus particles (platinum/polystyrene) that swim near the interface in hydrogen peroxide solution via self-diffusiophoresis [13, 14]. These active Brownian spheres translate with an intrinsic swim velocity U_0, tumble with a reorientation time τ_R, and experience a hydrodynamic drag ζ from the surrounding continuous Newtonian fluid. The tumbling of the swimmer from rotational Brownian motion results in a random-walk process for $t > \tau_R$ with translational diffusivity

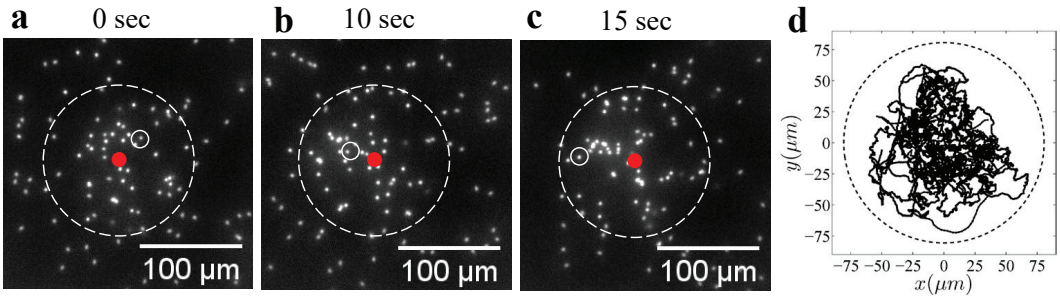

Figure 3.1: Active Janus particles in a weak acoustic trap. (**a**-**c**) Snapshots of $2\mu m$ swimmers in an acoustic trap. The solid red spot indicates the trap center and the dashed white circle delineates the outer edge of the well. The swimmer shown inside the solid white circle undergoes active Brownian motion while exploring the confines of the trap. (**d**) Two-dimensional trajectories of several particles inside the trap.

$D^{swim} = U_0^2\tau_R/2$ in 2D[1]. We choose active synthetic Janus particles as a model living system with narrow distributions in swim velocity and reorientation time, but our tweezer setup can accommodate bacteria and other biological microswimmers.

Our acoustic trap exerts a Gaussian trap force [11] with spring constant k and width w, $F^{trap}(r) = -kr\exp(-2(r/w)^2)$, which is well-approximated by a harmonic trap $F^{trap}(r) \approx -kr$ for small departures $r \ll w$. The Janus particles explore the interior of the trap with their intrinsic swimming motion; however, they are confined to remain within a circular boundary because they cannot travel beyond a certain distance from the trap center where the magnitude of their self-propulsive force equals that of the trapping force, $F^{trap}(r) = F^{swim} \equiv \zeta U_0$; F^{swim} is the swimmers' propulsive force which can be interpreted as the force necessary to hold the swimmer fixed in space. For a harmonic trap the swimmers are confined within a radius $R_c \equiv \zeta U_0/k$ of the trap center. We measure the positions and mean-square displacement (MSD) of the swimmers in both weak and strong confinement as they explore the trapping region (see Methods for further experimental detail). We also conduct Brownian dynamics (BD) computer simulations to corroborate the experimental measurements (see Methods for simulation detail).

Probability distribution

A passive Brownian particle confined in a harmonic trap has the familiar Boltzmann probability distribution: $P(r) \sim \exp(-V(r)/(\zeta D))$, where D is the translational

[1]Swimmers' translational Brownian diffusivity $D_0 = k_BT/\zeta \sim O(0.1)\mu m^2/s$ is small compared to $D^{swim} = U_0^2\tau_R/2 \sim O(100)\mu m^2/s$, and D_0 is not considered here.

diffusivity. Since the active Brownian motion of a swimmer can be interpreted as a random walk, the distribution of swimmers in a trap is also Boltzmann with the swim diffusivity $D = D^{swim} = U_0^2\tau_R/2$:

$$P(r) = \frac{k}{\pi\zeta U_0^2\tau_R}\exp\left(-\frac{kr^2}{\zeta U_0^2\tau_R}\right), \tag{3.1}$$

or by nondimensionalizing, $P(\bar{r})(U_0\tau_R)^2 = (\alpha/\pi)\exp(-\alpha\bar{r}^2)$, where $\bar{r} = r/(U_0\tau_R)$ and $\alpha \equiv k\tau_R/\zeta$ is the nondimensional trap stiffness that dictates the swimmer behavior inside the trap. For a weak trap, $\alpha < 1$, the swimmers are allowed to explore and reorient freely before reaching the 'ends' of the well (see Fig 3.1); the maximum density occurs at the trap center $r = 0$. Equation 3.1 is valid for $\alpha \lesssim 1$ since the swimmers must be allowed to undergo a random walk process within the confines of the well [8, 6]. As shown in Fig 3.2A, Eq 3.1 agrees with both experiments and BD simulations. The uniform density far away from the trap, $P(\infty)$, has been subtracted in the experiments. The active Janus particles have a range of activity levels due to variations in the platinum coating during fabrication. With a weak trap, strong swimmers are able to swim straight past the trap without getting confined, whereas the weaker swimmers struggle to escape the vicinity of the trap center. The swimmer properties (speed U_0 and reorientation time τ_R) in Eq 3.1 are the average of those particles that are confined within the trapping region.

In the other limit of a strong trap, $\alpha > 1$, the swimmer sees the 'ends' of the well before it is able to reorient (i.e., $R_c < U_0\tau_R$), so the swimmer will be stuck at R_c until it reorients and then run quickly to the other side and again wait there [7]. As shown in Fig 3.2B we observe a peak in the probability distribution near $R_c = \zeta U_0/k$, and the Boltzmann distribution no longer applies. To observe Brownian-like motion the spring must be weak, i.e., $\alpha = k\tau_R/\zeta < 1$, so that the particle can undergo a random walk before it discovers the ends of the well. Along the trap perimeter for large α, the particles are on average oriented radially outward relative to the trap center. This directional alignment is most pronounced near $r = R_c$—the particles want to swim away but the trapping force confines them to remain inside. The correlation between the distance from the trap center and the particles' orientation is directly related to the mechanical swim pressure exerted by these particles (see later subsection). Videos of active particles in confinement are available in Supplementary Movies 1-3.[2]

[2]See Supplementary Materials in ref [15].

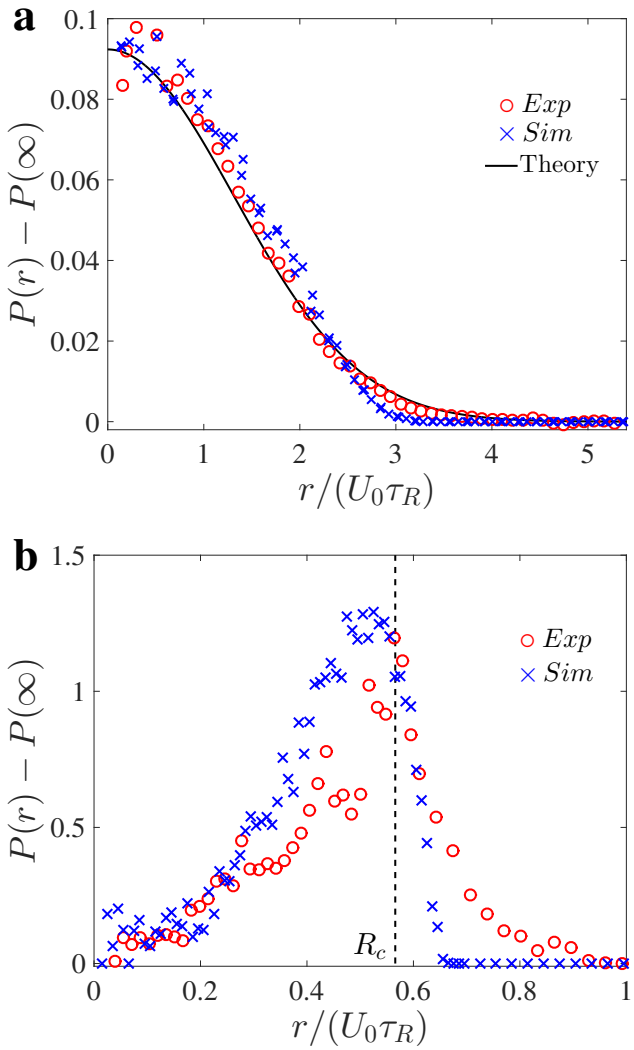

Figure 3.2: Probability distribution of confined active Janus particles. (**a**) $2\mu m$ swimmers with $\alpha \equiv k\tau_R/\zeta = 0.29$ follow a Boltzmann distribution (solid black curve is the analytical theory, Eq 3.1). (**b**) Distribution of $3\mu m$ swimmers with $\alpha = 1.76$ has a peak near $R_c = \zeta U_0/k$ (vertical dashed black line) and decreases to zero for $r > R_c$. In both (**a**,**b**), the red and blue symbols are data from experiment and Brownian dynamics simulations, respectively. Data are averages of measurements of over 500 snapshots for a duration of $50s$, each frame consisting $\approx$ 100 and 20 particles for the $\alpha = 0.29$ and $\alpha = 1.76$ cases, respectively.

Explosion of a 'swimmer-crystal'

We have focused thus far on a dilute concentration of swimmers subjected to a relatively weak trap. Using a stronger trap, all swimmers that wander within the trapping region ($\sim 150\mu m$ radius from trap center) are pulled towards the trap center and form a dense close-packed 2D crystal (see Figs 3.3**a** and 3.3**e**).

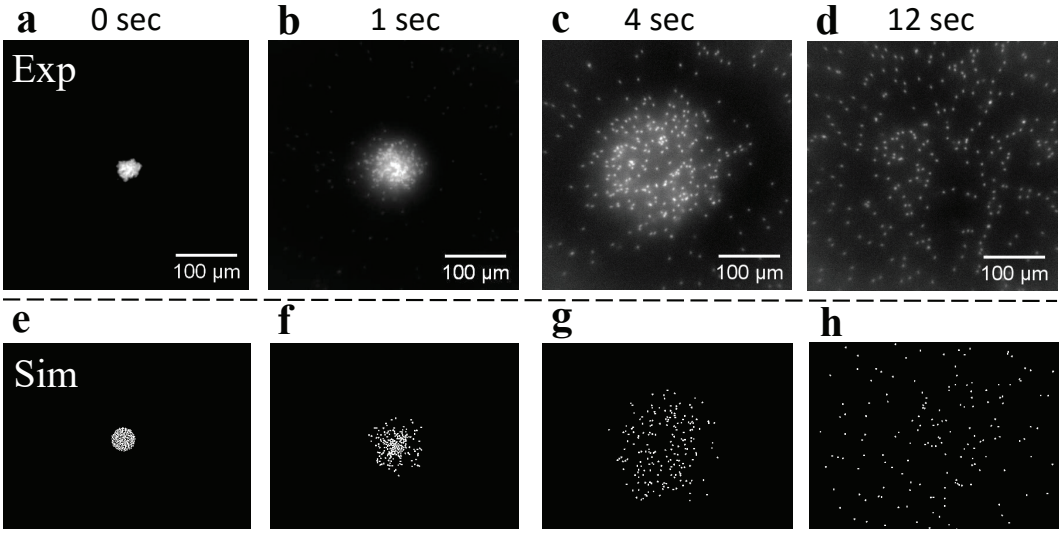

Figure 3.3: 'Explosion' of active crystal. Explosion of swimmer-crystal in (**a**-**d**) experiments and (**e**-**h**) Brownian dynamics simulations. (**a**,**e**) A strong trapping force draws the swimmers into a dense close-packed 2D crystal. (**b**,**f**) A subsequent release of the trap frees the swimmers, causing the crystal to explode. (**c**,**g**) At later times, a ballistic shock propagates outward like a traveling wave. (**d**,**h**) At long times, the swimmers spread diffusively.

When the trap is subsequently turned off, the crystal quickly 'melts' or 'explodes' and the constituent particles swim away (see progression in Fig 3.3). Videos of the accumulation, crystal formation, and melting process are available in Supplementary Movies 4-6.[3] On first glance, this process resembles the melting of an active crystal due to the constituents' sudden loss of motility [16]. Palacci et al [16] use polymer/hematite particles that self-propel and interact with each other via long-ranged phoretic attraction in the presence of blue-violet light. Due to concentration-field interaction, the particles cluster and form crystals in the presence of light. When the light is shut off, the crystal melts because the particles' motility and concentration-field interactions are turned off, and the now-passive particles spread with their translational Brownian diffusivity—the entire melting process is diffusive. In contrast, our active crystal explodes due to a sudden loss of an external trap forcing the particles together, not the slow diffusion process caused by a loss of swimmer motility. Thus, the motion of the spreading swimmers is still that of active particles—translating with speed U_0 in randomly-oriented directions that relax with the reorientation timescale τ_R.

We observe three time regimes in the explosion process. For times very short after

[3] See Supplementary Materials in ref [15].

release, only the swimmers positioned along the periphery of the crystal escape the crystal. Particles in the center obstruct each others' paths and are unable to escape the crystal, so the density is peaked at the origin (Figs 3.3**b** and 3.3**f**). During the second regime the escaped particles move ballistically outwards in the direction given by their random initial orientation. The swimmers move ballistically because they have not yet reoriented sufficiently to be diffusive (i.e., times $t \lesssim \tau_R$). The result is a depletion of particles from the origin (given the initial crystal is small; see below) and a peak in the density that propagates outward like a traveling wave (Figs 3.3**c** and 3.3**g**). Lastly, for times $t \gg \tau_R$ the swimmers have reoriented sufficiently to behave diffusively (Figs 3.3**d** and 3.3**h**) characterized by the translational diffusivity $D = D_0 + D^{swim}$ where D_0 is the Stokes-Einstein-Sutherland diffusivity and $D^{swim} = U_0^2\tau_R/2$. In this regime the spreading process is analogous to the classic diffusion of an instantaneous point source, where the transient probability distribution is

$$P(r,t) = \frac{1}{4\pi t D}\exp\left(-\frac{r^2}{4Dt}\right), \text{ for } t \gg \tau_R, \tag{3.2}$$

where t is the time after the point source is introduced and D is the translational diffusivity of the constituent "solute" particles. For the swimmer-crystal, the diffusivity of the constituent particles $D \approx D^{swim} = U_0^2\tau_R/2$.

Figure 3.4 corroborates our observations which show the three distinct time regimes in experiments and BD simulations. At short times, particles inside the crystal spread slightly faster in the experiment than the simulation, perhaps due to the sudden release of a strong acoustic force causing the particles to relax and loosen the initial packing of the crystal (see $1s$ in Fig 3.4). As predicted, Eq 3.2 is valid only for times $t \gg \tau_R$ when the explosion process is diffusive (shown as dashed curves in Fig 3.4 for comparison). This is a distinguishing feature of our explosion experiments compared to the melting of a passive Brownian crystal [16]. Because the swimmers' reorientation time can be large compared to the measurement times (as opposed to Brownian momentum relaxation times which are small), we are able to observe the crossover between ballistic and diffusive explosion of the active crystal. There is no ballistic regime for the melting of passive Brownian particles.

We conduct this experiment with different particle activities and initial crystal sizes. When the initial crystal is large and/or the swimmers reorient rapidly (i.e., τ_R is small), the ballistic shock and depletion of swimmers from the crystal origin was less noticeable. For a large initial crystal, the particles in the center must wait long times to break free of the cluster; by this time, swimmers initially positioned along

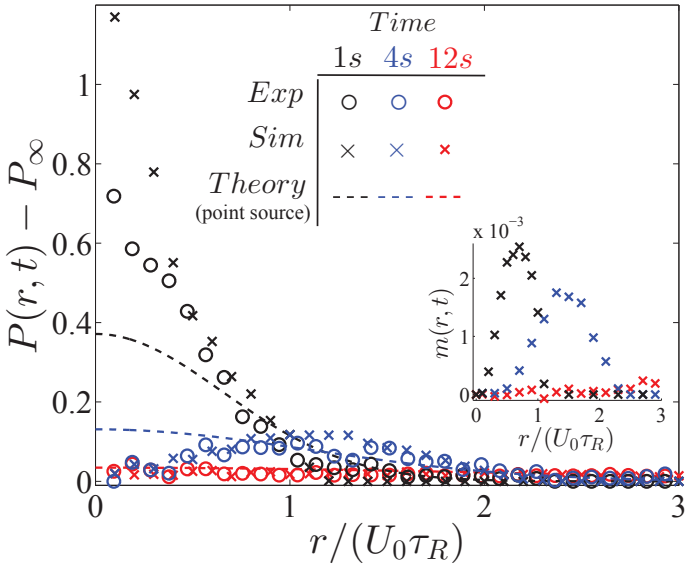

Figure 3.4: Evolution of active-crystal 'explosion.' Transient probability density of $2\mu m$ swimmers as they explode from the crystal, drawn at three representative times as described in the text. Dashed curves are the analytical theory of diffusion of a point source, Eq 3.2 (for $1s$ and $4s$, drawn as a reference for comparison), and the circles and crosses are the experiment and Brownian dynamics simulation, respectively. Inset shows the polar order of the swimmers $m(r,t)$ as the peaks spread outward. We average over 4 independent explosion measurements for a duration of $30s$ after release; each run consists of ≈ 150 spreading particles.

the crystal periphery have had enough time to reorient and explore back towards the origin to fill the void.

Inside the crystal there is an effective interaction of the concentration fields due to the swimmers' competition for 'fuel' (hydrogen peroxide). However, for a system that can be assumed to be a 2D monolayer, fuel is being supplied from the third dimension (i.e., the bulk) and thus the competition is reduced. Data near the trap center are difficult to analyze in the experiments (especially at short time) since we cannot accurately differentiate between individual particles in the large crystal. Due to the finite size of the initial crystal, theoretical prediction for diffusion of a step function (as opposed to a delta function) would appear to be more accurate at very short times after release, but Eq 3.2 is valid for $t \gg \tau_R$, so there is little difference between the two solutions in this regime.

This experiment provides a macroscopic method to measure the diffusivity of an active system using tweezers. The size or width of the spreading swimmer-crystal is related to the diffusivity by $L^2 = 2Dt$, so one can measure the size of the spreading

system (ignoring details about the motion of individual swimmers) for times $t \gg \tau_R$ to infer the diffusivity from $L \sim \sqrt{Dt}$.

These 'explosion' experiments show the development of local polar order of the swimmers as they spread outward. Orientational polar order is established when the swimmers' motion is directionally aligned. Inset of Fig 3.4 shows the average swimming orientation $m(r,t) = \|\langle \boldsymbol{q} \rangle\|(r,t)$ at three representative times, where $\boldsymbol{q} = (\cos\theta, \sin\theta)$ is a unit orientation vector defined by the swimmer's direction of self-propulsion (see Methods for further detail), and the brackets $\langle \cdot \rangle$ indicate an average over all particles at a distance r from the crystal center. One interpretation of $m(r,t)$ is the local average orientation distribution, $\langle \cos(\theta') \rangle$, where θ' is the angle of the swimmer orientation relative to the outward normal from the crystal center. Local polar order is peaked along the perimeter of the crystal, and spreads radially outward with time like a wave front. For short times when the system is ballistic, there is coherent motion of particles in the outward radial direction. This directed behavior cannot be seen for a purely passive Brownian system which exhibits 'biased-diffusion' for all times. At longer times when the crystal melts completely, there is no polar order.

Finally, a possible interpretation of the explosion process is that the particles are spreading from regions of large mechanical pressure (center of crystal) to small mechanical pressure (far away from crystal). Spatial gradients in the active mechanical pressure results in an outward flux of constituent particles [17]—in the next section we compute the unique mechanical swim pressure exerted by active systems.

Swim pressure

In addition to the probability density and diffusivity of confined swimmers, the acoustic trap can be used as a measurement of the swim pressure [17], a unique mechanical pressure that all self-propelled bodies exert as a result of their self-motion. The origin of the swim pressure is that all active bodies exert a mechanical, self-propulsive force on the surrounding boundaries that confine them per unit area, $\Pi^{swim} = F^{wall}/A$. A swimmer's self-propulsive force is given by $\boldsymbol{F}^{swim} \equiv \zeta \boldsymbol{U}_0$ where ζ is the drag factor and $\boldsymbol{U}_0$ is the swimming velocity. This is the force required to hold the swimmer fixed, at every instance in time. The swim pressure differs from the swim force, and also differs from the random thermal Brownian osmotic pressure due to the different intrinsic timescale. An active particle that col-

lides into a wall will not reorient as a result of the collision—it continues to "push" against the wall until it finally reorients from its intrinsic reorientation mechanism. These continuous collisions of magnitude F^{swim} against the wall over the time duration $t \sim O(\tau_R)$ is what gives rise to the swim pressure.

Although many theoretical studies [17, 18, 19, 20, 21, 22] have analyzed the swim pressure of active matter, there is a dearth of experimental corroboration. A recent study on sedimentation [23] gives an indirect measurement based upon density profiles of active particles under gravity. Because the acoustic trap behaves as an invisible 'semipermeable membrane' that confines the swimmers (but allows the solvent to pass through), our experiment allows us to determine the swim pressure using principles analogous to the osmotic pressure of colloidal solutes in solution.

We use the virial theorem [24] to express the swim pressure as a force moment [17]: $\Pi^{swim} = 1/(2A) \sum_i^N \langle \boldsymbol{x}_i \cdot \boldsymbol{F}_i^{swim} \rangle$ in 2D where N is the number of particles, A is the system area, and the swim forces of each particle $\boldsymbol{F}_i^{swim} \equiv \zeta_i \boldsymbol{U}_{i,0}$. As shown in the Methods, the first moment of the equation of motion for an active particle gives $\Pi^{swim} \equiv n/2\langle \boldsymbol{x} \cdot \boldsymbol{F}^{swim} \rangle = (n\zeta/4) d\langle \boldsymbol{x} \cdot \boldsymbol{x} \rangle/dt - n/2\langle \boldsymbol{x} \cdot \boldsymbol{F}^{trap} \rangle$, where n is the number density of swimmers. In the absence of the trap, $\boldsymbol{F}^{trap} = \boldsymbol{0}$, we have $\Pi^{swim} = n\zeta D^{swim}$, where we have expressed the first term on the right using the diffusivity, $D^{swim} = (1/4) d\langle \boldsymbol{x} \cdot \boldsymbol{x} \rangle/dt$. Here, the swimmer undergoes an entropic, random-walk in unbounded space with $D^{swim} = U_0^2 \tau_R/2$, giving the 'ideal-gas' swim pressure $\Pi^{swim} = n\zeta U_0^2 \tau_R/2$ [17]. In the presence of a trap force, $\boldsymbol{F}^{trap}$, the long-time diffusivity $D^{swim} = 0$ because the swimmers are confined and cannot translate in unbounded space, and the MSD achieves a constant value (i.e., does not grow with time). Therefore, at steady-state $d\langle \boldsymbol{x} \cdot \boldsymbol{x} \rangle/dt = 0$ and the acoustic trap acts as a confining force that is equal and opposite to the swim force, enabling us to determine the swim pressure via the known trap force: $\Pi^{swim} = -n/2\langle \boldsymbol{x} \cdot \boldsymbol{F}^{trap} \rangle$.

For a harmonic trap where $\boldsymbol{F}^{trap} = -k\boldsymbol{x}$, the swim pressure can be obtained directly by measuring the MSD of the swimmer inside the trap:

$$\frac{\Pi^{swim}}{n\zeta U_0^2 \tau_R/2} = \alpha \langle \overline{\boldsymbol{x}} \cdot \overline{\boldsymbol{x}} \rangle, \tag{3.3}$$

where $\alpha \equiv k\tau_R/\zeta$ and $\overline{\boldsymbol{x}} \equiv \boldsymbol{x}/(U_0 \tau_R)$ is the nondimensional position vector of the swimmer relative to the trap center. This elegant result reveals that the MSD contains information about the mechanical pressure exerted by self-propelled particles.

It comes directly from the virial theorem, where the force moment becomes a MSD for a harmonic trap.

Solving the Langevin equation analytically for a swimmer confined in a trap (see Methods), we obtain

$$\frac{\Pi^{swim}}{n\zeta U_0^2\tau_R/2} = \frac{1}{1+\alpha}. \tag{3.4}$$

The swim pressure depends only on the parameter $\alpha \equiv U_0\tau_R/R_c$, a ratio of the swimmers' run length $U_0\tau_R$ to the size of the trap $R_c = \zeta U_0/k$. Therefore this expression gives the container-size dependent swim pressure—for a weak trap, $\alpha \to 0$, and we obtain the 'ideal-gas' swim pressure $\Pi^{swim} = n\zeta U_0^2\tau_R/2$, whereas a strong trap causes the fictitious 'container' to shrink and decrease Π^{swim} because the distance the swimmers travel between reorientations decreases. Because the swim pressure is a force moment, the distance the swimmers travel between reorientations (i.e., within a time τ_R) is the 'moment arm' that determines the magnitude of the swim pressure. For a weak trap the particles are allowed to travel the full run length $U_0\tau_R$, set by the particles' intrinsic swimming speed U_0, whereas a strong trap establishes a small trap size $R_c < U_0\tau_R$ that obstructs and causes the particles to travel a distance smaller than $U_0\tau_R$.

Figure 3.5 shows the swim pressure computed in the experiments and BD simulations using Eq 3.3. The swim pressure has transient behavior for small times and we require data for times $t > \tau_R$ to observe a steady-state (see Methods). At steady-state all curves approach the theoretical prediction given by Eq 3.4.

As a swimmer wanders away from the trap center, it may explore regions of the trap that are not strictly in the linear Hookean regime. Therefore one may expect the MSD to be slightly higher than the linear theory. However, although the swimmer concentration away from the trap is dilute, near the trap center swimmers accumulate and cluster, which obstructs the motion of free swimmers trying to swim across to the other end of the trap, decreasing the MSD. Hydrodynamic interactions may also play a role near the trap center where the density of swimmers is higher. The analytical theory is valid for a dilute system of swimmers in a linear harmonic trap without hydrodynamic interactions, but we find that the linear approximations are sufficient. In addition to the MSD and Eq 3.3 (which come from a linear approximation of F^{trap}), we also compute the full correlation using a Gaussian F^{trap} (see Methods) and the results have minor quantitative differences.

We scale the swim pressure in Fig 3.5 using the average activity of the swimmers

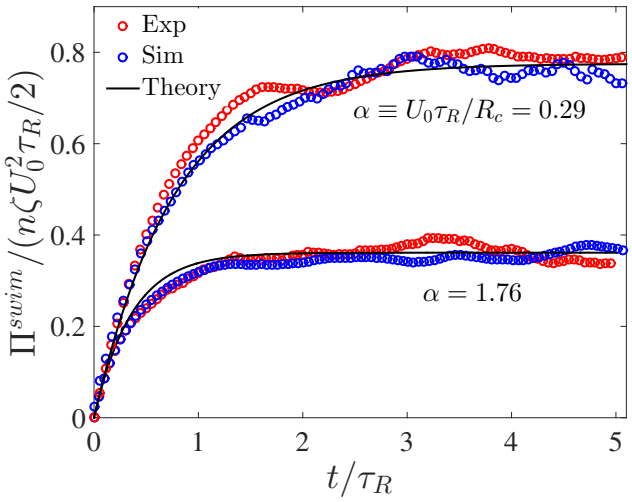

Figure 3.5: Swim pressure of Janus particles in different degrees of confinement. The parameter $\alpha \equiv U_0\tau_R/R_c$ is a ratio of the particles' run length to the trap size $R_c = \zeta U_0/k$. The solid black curves are the theoretical prediction with a harmonic trap approximation, and the red and blue symbols are results from experiments and Brownian dynamics simulations, respectively. A smaller trap size diminishes the distance the particles travel between reorientations and decreases the swim pressure. The experimental and simulation data are averages of 150 and 90 independent particle trajectories for a duration of $40s$ for the $\alpha = 0.29$ and $\alpha = 1.76$ cases, respectively.

confined within the trapping region. The number density n is given by the number of trapped particles N divided by the area of the trapping region.

When a weak trap is present for a long time ($\gtrsim$ 20 − 30 min) there is a gradual accumulation of swimmers inside the trap because those located initially far away wander near the trap and become confined. This induces a slow variation in the number density inside the trap $n(t)$ over time. We use a dilute system of swimmers (total area fraction $\phi_A \leq 0.001$) and the timescale for the change in number density ($\geq$ 5 min) is large compared to the swimmers' reorientation time ($\tau_R \sim 2 - 10s$). Since the important timescale in our problem is the swimmers' reorientation time τ_R, we only require data over a timespan of several τ_R and the effect of swimmer accumulation is negligible in our results.

3.3 Discussion

In this study, we do not observe a self-pumping state [7] induced by hydrodynamic interactions, perhaps due to the 2D dimensionality and dilute concentrations of this

study. Although we do not observe large-scale coherent motion, the precise manipulation of swimmers towards special regions may provide a method to study the collective motion of living systems in a controlled manner. Further experiments using acoustic traps may give insight into the origin of polar order, how and why living organisms align, and the advantages of such collective behavior.

Our measurement of the swim pressure may support forthcoming applications in biophysics and molecular-cell biology, as researchers are becoming increasingly concerned with the mechanical forces, pressures, and stresses generated by active constituents inside a living cell. In addition, experimental determination of the swim pressure may engender real-life engineering applications, such as fabrication of novel soft materials using active swimmers.

3.4 Methods

Equations of motion

The Langevin equation for a dilute system of swimmers in a trap is given by

$$\mathbf{0} = -\zeta \boldsymbol{U}(t) + \boldsymbol{F}^{swim} + \boldsymbol{F}^{trap}, \tag{3.5}$$

where $\boldsymbol{U}(t)$ is the velocity, ζ is the hydrodynamic drag factor, $\boldsymbol{F}^{swim} \equiv \zeta \boldsymbol{U}_0$ is the self-propulsive swim force of a swimmer, $\boldsymbol{U}_0 = U_0 \boldsymbol{q}$ is the intrinsic swim velocity of an isolated swimmer, $\boldsymbol{q}(t)$ is the swimmer's unit orientation vector defined by their swimming direction, and $\boldsymbol{F}^{trap} = -\nabla V(\boldsymbol{x})$ is the restoring force caused by the trap with potential $V(\boldsymbol{x})$. The left-hand side of Eq 3.5 is zero because inertia is negligible for a colloidal dispersion.

Transverse trapping with an acoustic tweezer results in a Gaussian trap [11] with stiffness k and width w, $\boldsymbol{F}^{trap} = -kr \exp(-2(r/w)^2)\hat{\boldsymbol{r}}$, which we independently verify. We use Janus particles in the absence of hydrogen peroxide (i.e., inactive particles) to calibrate k and w of the acoustic trap by measuring the position and velocity of the particles in the trap. For a trap with large spatial extent (large w), a linear force $\boldsymbol{F}^{trap} \approx -kr\hat{\boldsymbol{r}}$ approximates the trapping force. As a swimmer wanders far away from the focus of the trap, there is a critical radius $\sim R_c = \zeta U_0/k$ at which the swimmer cannot move any farther. At this position the swimmer's self-propulsive force $\boldsymbol{F}^{swim}$ exactly cancels the trapping force $\boldsymbol{F}^{trap}$ and the swimmer does not move. The swimmer is "stuck" in this position for a time of order $\sim \tau_R$ until the swimmer changes its orientation. The trapping force does not affect particles located far away from the trap origin because $\boldsymbol{F}^{trap}(\boldsymbol{r} \to \infty) \to \mathbf{0}$.

Experimental methods

We fabricate active Janus particles from 2 and $3\mu m$ diameter sulfate latex particles (Life Technologies, Carlsbad, CA, USA). We coat half of the particle surface with a $\sim 7nm$-thick layer of platinum using a BAL-TEC SCD 050 sputter coater (Leica Microsystems GmbH, Wetzlar, Germany). When deposited in a hydrogen peroxide solution, the particles self-propel via diffusiophoresis near the air-water interface. The particles initially deposited into the bulk rise towards the air/solution interface because the platinum half is heavy and orients with gravity. The particles swim towards the non-platinum face, and begin to move in 2D once they reach the interface. The particles at the interface do not diffuse back into the third dimension (i.e., the bulk). For the 2 and $3\mu m$ particles, they have a swim speed of $U_0 \sim 15 - 25\mu m/s$ and $\sim 8 - 15\mu m/s$ with a reorientation time of $\tau_R \sim 2 - 5s$ and $\sim 5 - 10s$, respectively. We compute the reorientation time by analyzing the swimmers' orientation autocorrelation: $\langle(\boldsymbol{q}(t) - \boldsymbol{q}(0))^2\rangle = 2(1 - \exp(-t/\tau_R))$. We verify that the swimmers undergo active Brownian motion characterized by the swim diffusivity $D^{swim} = U_0^2\tau_R/2$.

To confine the swimmers in the transverse direction we develop a custom-built acoustic tweezer setup. We excite a 0.25-inch diameter immersion type transducer (UTX Inc, Holmes, NY, USA) in a continuous sinusoidal signal at $25MHz$ with variable voltages from $0 - 10V_{pp}$ using an AM300 Dual Arbitrary Generator (Rohde & Schwarz, Munich, Germany). We immerse the transducer in the solution in an inverted position (face up to the air/solution interface) and deposit Janus particles on this interface. We adjust the focal point of the transducer at a distance of $12mm$ from the air/solution interface and hold it fixed in place throughout the experiment using an XY positioner and a tilt stage (Thorlabs Inc, Newton, NJ, USA). Although the transducer also has a radiation force in the axial direction, the effect of particles in the bulk being pushed to the interface is negligible because the Janus particles remain on the interface and do not diffuse in 3D into the bulk. We control the strength of the trap by changing the input voltage from the function generator. We connect a 50x objective (Leica Microsystems GmbH, Wetzlar, Germany) to a sCMOS digital camera (ORCA-Flash 4.0, Hamamatsu, Japan) to obtain images and a glass fiber ringlight (Volpi AG, Schlieren, Switzerland) to provide lighting. Many researchers use acoustic tweezers to generate a standing field to confine objects primarily in one dimension in acoustic pressure nodes or antinodes, depending on the properties of the objects (density, compressibility) [9]. Here we develop a 2D device which generates a near-harmonic potential using the transverse radiation forces of single

beam transducer.

We deposit Janus particles on the air-water interface of a $0.5wt\%$ hydrogen peroxide solution, and their activity remains constant for at least 1 hour (each experimental run last $\sim$ few minutes). We turn on the acoustic transducer and observe the motion of the swimmers in confinement within the trapping region. For the small voltages we apply to the transducer ($0 - 3V_{pp}$) and the particle sizes (2 and $3\mu m$) used in our swim pressure measurements, we do not detect any acoustic streaming. The acoustic tweezer exerts a Gaussian trapping force on the particles; a linear Hookean spring force approximates the trapping force since the width w is large compared to the swimmers' run lengths. We identify the center of the trap at the end of each experiment by applying a strong trapping force to collect all of the swimmers to the trap center. We use a modified particle tracking script [25] in the analysis.

Brownian dynamics simulations

In our Brownian dynamics (BD) simulations we evolve the particles following Eq 3.5. Although the concentration of swimmers far away from the trap center is dilute, we may have an accumulation of swimmers near the trap center which may obstruct the motion of free swimmers trying to swim across to the other end of the trap. To more accurately model the experimental system, our BD simulations include the interparticle force $\boldsymbol{F}^P$ in Eq 3.5. Nondimensionalizing the force by ζU_0 and position by $U_0\tau_R$, Eq 3.5 (with the interparticle force) becomes $\boldsymbol{0} = -\boldsymbol{u}(t) + \boldsymbol{q} + \overline{\boldsymbol{F}}^{trap} + \boldsymbol{F}^P$, where $\boldsymbol{u} \equiv \boldsymbol{U}/U_0$ is the particle velocity, $\overline{\boldsymbol{F}}^{trap}(\bar{r}) = -\alpha\bar{r}\exp(-2\gamma^2\bar{r}^2)\hat{\boldsymbol{r}}$ is the trapping force, $\bar{r} \equiv r/(U_0\tau_R)$ is the radial position of the swimmer, $\gamma \equiv U_0\tau_R/w$ is a ratio of the swimmers' run length to the trap width, and $\alpha \equiv \tau_R/(\zeta/k)$ is a ratio of the swimmers' reorientation time to the timescale of the trap. We can also interpret $\alpha \equiv (U_0\tau_R)/(\zeta U_0/k)$, the ratio of the swimmers' run length to the 'size' of the container (set by the trap). For Figs 3.2 and 3.5 we use $\alpha = 0.29, \gamma = 0.08$ and $\alpha = 1.76, \gamma = 0.25$ for a weak and strong trap, respectively. We vary the number of particles from $20 - 500$ to match the experimental measurements. We use a hard-disk interparticle force $\boldsymbol{F}^P = \boldsymbol{F}^{HS}$ that prevents particle overlap in our simulations [26, 27]. We evolve the swimming orientation of the swimmers $\boldsymbol{q} = (\cos\theta, \sin\theta)$ following $d\theta/dt = \sqrt{2/\tau_R}\Lambda(t)$, where $\Lambda(t)$ is a unit random deviate.

Derivation of the swim pressure in a harmonic trap

For a harmonic trapping force $\boldsymbol{F}^{trap} = -k\boldsymbol{x}$, we can solve Eq 3.5 for the position $\boldsymbol{x}(t)$ and compute the MSD:

$$\frac{\langle \boldsymbol{x}(t)\boldsymbol{x}(t)\rangle}{(U_0\tau_R)^2} = \frac{(-1+\alpha) - 2\alpha e^{-(1+\alpha)t/\tau_R} + (1+\alpha)e^{-2t/\tau_{trap}}}{\alpha(-1+\alpha^2)}\left(\frac{\boldsymbol{I}}{2}\right), \tag{3.6}$$

where $\boldsymbol{I}$ is the isotropic tensor and $\tau_{trap} = \zeta/k$ is the characteristic timescale of the trap. For small times the MSD grows quadratically in time, and for $\alpha = 0$ we obtain the long-time self diffusivity of an active swimmer: $\boldsymbol{D}^{swim} = 1/2 \lim_{t\to\infty} d\left(\langle \boldsymbol{x}(t)\boldsymbol{x}(t)\rangle_{\alpha=0}\right)/dt = U_0^2\tau_R\boldsymbol{I}/2$. Most importantly, for $\alpha \neq 0$ and times long compared to both τ_R and τ_{trap} the MSD becomes a constant

$$\lim_{t\to\infty} \frac{\langle \boldsymbol{x}(t)\boldsymbol{x}(t)\rangle}{(U_0\tau_R)^2} = \frac{1}{\alpha(1+\alpha)}\frac{\boldsymbol{I}}{2}. \tag{3.7}$$

This is a main result that we will use later.

Multiplying Eq 3.5 by $n\boldsymbol{x}$ and taking the average we obtain

$$\boldsymbol{\sigma}^{swim} \equiv -n\langle \boldsymbol{x}\boldsymbol{F}^{swim}\rangle = -\frac{n\zeta}{2}\frac{d\langle \boldsymbol{x}\boldsymbol{x}\rangle}{dt} + n\langle \boldsymbol{x}\boldsymbol{F}^{trap}\rangle, \tag{3.8}$$

where we use the definition of the swim stress $\boldsymbol{\sigma}^{swim} \equiv -n\langle \boldsymbol{x}\boldsymbol{F}^{swim}\rangle$ and n is the number density of swimmers [17]. As shown in Eq 3.7, for times long compared to both τ_R and τ_{trap} the MSD becomes a constant and its time derivative is zero: $d/dt\left(\lim_{t\to\infty}\langle \boldsymbol{x}(t)\boldsymbol{x}(t)\rangle\right) = 0$. Therefore the swim pressure $\Pi^{swim} = -\mathrm{tr}\boldsymbol{\sigma}^{swim}/2$ (in 2D) is

$$\Pi^{swim} = -\frac{n}{2}\langle \boldsymbol{x}\cdot\boldsymbol{F}^{trap}\rangle, \tag{3.9}$$

which is a general result valid in principle for any trapping force $\boldsymbol{F}^{trap}$. For a harmonic trap $\boldsymbol{F}^{trap} = -k\boldsymbol{x}$, the swim pressure can be determined from a simple MSD measurement as given in Eq 3.3 of the main text. Substituting Eq 3.7 into Eq 3.3, we obtain the theoretical result $\Pi^{swim}/(n\zeta U_0^2\tau_R/2) = (1+\alpha)^{-1}$ as given in Eq 3.4 of the main text.

For times not large compared to τ_R and τ_{trap}, the slope of MSD is not zero and the swim pressure has a transient start up period:

$$\frac{\Pi^{swim}}{n\zeta U_0^2\tau_R/2} = \frac{1}{1+\alpha}\left(1 - e^{-(\tau_R^{-1}+\tau_{trap}^{-1})t}\right). \tag{3.10}$$

This expression is exact and valid for all times t. Upon taking times $t > \tau_R$ and $t > \tau_{trap} = \zeta/k$, this result agrees with Eq 3.4. Therefore measuring the MSD $\langle \boldsymbol{x}\boldsymbol{x}\rangle$

is an easy and simple method to quantify the swim pressure in an experimental system.

For nonlinear traps with a general form of $\boldsymbol{F}^{trap}$, we must evaluate Eq 3.9 directly. For a Gaussian trap with stiffness k and width w, $\boldsymbol{F}^{trap}(r) = -kr\exp(-2(r/w)^2)\hat{\boldsymbol{r}}$, we have

$$\Pi^{swim} = \frac{n}{2}\langle kr^2 \exp(-2(r/w)^2)\rangle. \tag{3.11}$$

For a large well (large w), the trapping force becomes harmonic and we get back the previous result in Eq 3.3, where the MSD $\langle r^2\rangle$ gives the swim pressure.

References

[1] L. Rothschild. "Non-random distribution of bull spermatozoa in a drop of sperm suspension". *Nature* 198.4886 (1963), pp. 1221–1222.

[2] A. P. Berke, L. Turner, H. C. Berg, and E. Lauga. "Hydrodynamic attraction of swimming microorganisms by surfaces". *Phys Rev Lett* 101.3 (2008), p. 038102.

[3] A. Sokolov, M. M. Apodaca, B. A. Grzybowski, and I. S. Aranson. "Swimming bacteria power microscopic gears". *Proc Natl Acad Sci U.S.A* 107.3 (2010), pp. 969–974.

[4] Y. Fily, A. Baskaran, and M. F. Hagan. "Dynamics of self-propelled particles under strong confinement". *Soft Matter* 10.30 (2014), pp. 5609–5617.

[5] X. Yang, M. L. Manning, and M. C. Marchetti. "Aggregation and segregation of confined active particles". *Soft Matter* 10.34 (2014), pp. 6477–6484.

[6] Z. Wang, H.-Y. Chen, Y.-J. Sheng, and H.-K. Tsao. "Diffusion, sedimentation equilibrium, and harmonic trapping of run-and-tumble nanoswimmers". *Soft Matter* 10.18 (2014), pp. 3209–3217.

[7] R. W. Nash, R. Adhikari, J. Tailleur, and M. E. Cates. "Run-and-tumble particles with hydrodynamics: Sedimentation, trapping, and upstream swimming". *Phys Rev Lett* 104.25 (2010), p. 258101.

[8] J. Tailleur and M. E. Cates. "Sedimentation, trapping, and rectification of dilute bacteria". *Europhys Lett* 86.6 (2009), p. 60002.

[9] M. Evander and J. Nilsson. "Acoustofluidics 20: Applications in acoustic trapping". *Lab Chip* 12.22 (2012), pp. 4667–4676.

[10] X. Ding et al. "On-chip manipulation of single microparticles, cells, and organisms using surface acoustic waves". *Proc Natl Acad Sci U.S.A* 109.28 (2012), pp. 11105–11109.

[11] J. Lee et al. "Transverse acoustic trapping using a Gaussian focused ultrasound". *Ultrasound Med Biol* 36.2 (2010), pp. 350–355.

[12] M. B. Rasmussen, L. B. Oddershede, and H. Siegumfeldt. “Optical tweezers cause physiological damage to *Escherichia coli* and *Listeria* bacteria”. *Appl Environ Microbiol* 74.8 (2008), pp. 2441–2446.

[13] J. R. Howse et al. “Self-motile colloidal particles: From directed propulsion to random walk”. *Phys Rev Lett* 99.4 (2007), p. 048102.

[14] U. M. Córdova-Figueroa and J. F. Brady. “Osmotic propulsion: The osmotic motor”. *Phys Rev Lett* 100.15 (2008), p. 158303.

[15] S. C. Takatori, R. De Dier, J. Vermant, and J. F. Brady. “Acoustic trapping of active matter”. *Nat Commun* 7 (2016).

[16] J. Palacci, S. Sacanna, A. P. Steinberg, D. J. Pine, and P. M. Chaikin. “Living crystals of light-activated colloidal surfers”. *Science* 339.6122 (2013), pp. 936–940.

[17] S. C. Takatori, W. Yan, and J. F. Brady. “Swim pressure: Stress generation in active matter”. *Phys Rev Lett* 113.2 (2014), p. 028103.

[18] Y. Fily, S. Henkes, and M. C. Marchetti. “Freezing and phase separation of self-propelled disks”. *Soft Matter* 10.13 (2014), pp. 2132–2140.

[19] A. P. Solon et al. “Pressure and phase equilibria in interacting active Brownian spheres”. *Phys Rev Lett* 114.19 (2015), p. 198301.

[20] S. A. Mallory, A. Šarić, C. Valeriani, and A. Cacciuto. “Anomalous thermomechanical properties of a self-propelled colloidal fluid”. *Phys Rev E* 89.5 (2014), p. 052303.

[21] S. C. Takatori and J. F. Brady. “Swim stress, motion, and deformation of active matter: Effect of an external field”. *Soft Matter* 10.47 (2014), pp. 9433–9445.

[22] S. C. Takatori and J. F. Brady. “Towards a thermodynamics of active matter”. *Phys Rev E* 91.3 (2015), p. 032117.

[23] F. Ginot et al. “Nonequilibrium equation of state in suspensions of active colloids”. *Phys Rev X* 5.1 (2015), p. 011004.

[24] H. Goldstein. *Classical mechanics*. 2nd ed. Reading, MA: Addison-Wesley, 1990.

[25] J. C. Crocker and D. G. Grier. “Methods of digital video microscopy for colloidal studies”. *J Colloid Interface Sci* 179.1 (1996), pp. 298–310.

[26] D. R. Foss and J. F. Brady. “Brownian Dynamics simulation of hard-sphere colloidal dispersions”. *J Rheol* 44.3 (2000), pp. 629–651.

[27] D. M. Heyes and J. R. Melrose. “Brownian dynamics simulations of model hard-sphere suspensions”. *J Non-Newtonian Fluid Mech* 46.1 (1993), pp. 1–28.

Chapter 4

TOWARDS A 'THERMODYNAMICS' OF ACTIVE MATTER

This chapter includes content from our previously published article:

[1] S. C. Takatori and J. F. Brady. "Towards a thermodynamics of active matter". *Phys Rev E* 91.3 (2015), p. 032117. DOI: 10.1103/PhysRevE.91.032117.

4.1 Introduction

Self-propulsion allows living systems to display self-organization and unusual phase behavior. Unlike passive systems in thermal equilibrium, active matter systems are not constrained by conventional thermodynamic laws. A question arises however as to what extent, if any, can concepts from classical thermodynamics be applied to nonequilibrium systems like active matter. Here we use the new swim pressure perspective to develop a simple theory for predicting phase separation in active matter. Using purely mechanical arguments we generate a phase diagram with a spinodal and critical point, and define a nonequilibrium chemical potential to interpret the "binodal." We provide a generalization of thermodynamic concepts like the free energy and temperature for nonequilibrium active systems. Our theory agrees with existing simulation data both qualitatively and quantitatively and may provide a framework for understanding and predicting the behavior of nonequilibrium active systems.

Self-propulsion is a distinguishing feature of all "active matter" systems. By controlling and directing their own behavior self-propelled entities (usually, but not restricted to, living systems) can exhibit distinct phases with unusual dynamical properties [1]. These exotic behaviors are made possible because active matter is an inherently nonequilibrium system that is not bound by conventional thermodynamic constraints. A key challenge is to develop a framework for understanding the dynamic behavior and bulk properties of active matter.

While computer simulations have produced phase diagrams of active matter [2, 3, 4, 5, 6], many regions of phase space are difficult to explore because of the computational challenge of covering the parameter space. In this paper we develop a new mechanical theory for predicting the phase behavior of active systems. We also

offer suggestions on how conventional thermodynamic concepts, such as chemical potential, free energy and temperature, can be extended to provide a 'thermodynamics' of nonequilibrium active matter. At this point we are not certain whether conventional thermodynamic concepts comprise a valid and rigorous framework for studying nonequilibrium active systems. It remains uncertain to what extent, or even if, any of the concepts from classical thermodynamics are applicable to active matter. Our analysis suggests that active systems are entropically driven by a lower critical solution temperature (LCST) transition, where phase separation becomes possible with *increasing* temperature.

Here we consider a simple active matter system—a suspension of self-propelled spheres of radii a that translate with an intrinsic swim velocity $\boldsymbol{U}_0$, tumble with a reorientation time τ_R, and experience a hydrodynamic drag factor ζ from the surrounding continuous Newtonian fluid. The random tumbling results in a diffusive process for $t \gg \tau_R$ with $D^{swim} = U_0^2\tau_R/6$ in 3D. We do not include the effects of hydrodynamic interactions, and there is no polar order of the swimmers, precluding any large-scale collective motion (e.g., bioconvection). We seek to understand the phase behavior of a simple active system in which there is no large-scale coherent motion before moving on to study more complex collective behavior.

4.2 Mechanical Theory

The active pressure exerted by a system of self-propelled particles can be written as $\Pi^{act} = \Pi^{swim} + \Pi^{P}$, the sum of the "swim pressure" Π^{swim} and the interparticle (collisional) pressure Π^{P} [7]. It is permissible to add the separate contributions of the pressure in what appears to be a superposition; this is true in general for molecular, Brownian, and active systems.

The swim pressure was recently introduced as a fundamental aspect of active systems and as an aid to understand their self-assembly and phase behavior [7, 8, 9]. For a dilute system the "ideal-gas" swim pressure is $\Pi^{swim} = n\zeta D^{swim} = n\zeta U_0^2\tau_R/6$, [7]. Physically, Π^{swim} is the unique pressure exerted by self-propelled entities as they bump into the surrounding walls that confine them, analogous to the osmotic pressure of colloidal solutes. The swim pressure is an entropic quantity that arises purely from confinement, and can be computed from the first moment of the self-propulsive swim force (see Appendix).

Dimensional analysis allows us to write the swim pressure as $\Pi^{swim}(k_sT_s, \phi, Pe_R) = nk_sT_s\widehat{\Pi}^{swim}(\phi, Pe_R)$, where $k_sT_s \equiv \zeta U_0^2\tau_R/6$ defines the swimmers' "energy scale"

– force (ζU_0) $\times$ distance ($U_0\tau_R$) – and $\widehat{\Pi}^{swim}(\phi, Pe_R)$ is the nondimensional swim pressure that depends in general on the volume fraction $\phi = 4\pi a^3 n/3$ and importantly the nondimensional reorientation "Péclet number" $Pe_R = U_0 a/D^{swim} = U_0 a/(U_0^2\tau_R) = a/(U_0\tau_R)$, which is the ratio of the swimmer size a to its run length $U_0\tau_R$.[1]

For large Pe_R the swimmers reorient rapidly and take small swim steps, behaving as Brownian walkers [7]. Thus $\widehat{\Pi}^{swim}(\phi, Pe_R) = 1$ for all $\phi \lesssim \phi_0$ where ϕ_0 is the volume fraction at close packing. This system is analogous to passive Brownian particles, which exert the "ideal-gas" Brownian osmotic pressure $\Pi^B = nk_BT$ regardless of the concentration of particles.

For small Pe_R the swimmers have run lengths large compared to their size and $\widehat{\Pi}^{swim}$ decreases with ϕ because the particles hinder each others' movement. In this limit experiments and computer simulations [10, 11, 6, 12, 13, 14] have observed the self-assembly of active systems into dense and dilute phases resembling an equilibrium liquid-gas coexistence.

Extending the results of the nonlinear microrheology analysis [7] the swim pressure at small Pe_R in 3D takes the form $\widehat{\Pi}^{swim} = 1 - \phi - \phi^2$. The inclusion of a three-body term ($-\phi^2$) is based upon an empirical fit which agrees with our swim pressure data for all $Pe_R \leq 1$. Unlike Brownian systems where repulsive interactions (e.g., excluded volume) increase the pressure, for active matter interactions decrease the run length and therefore the swim pressure. The decrease in Π^{swim} is the principle destabilizing term that facilitates a phase transition in active systems.

At finite concentrations, interparticle interactions between the swimmers give rise to an interparticle (or collisional) pressure $\Pi^P(k_sT_s, \phi, Pe_R) = nk_sT_s\widehat{\Pi}^P(\phi, Pe_R)$, where $\widehat{\Pi}^P(\phi, Pe_R)$ is the nondimensional interparticle pressure. For repulsive interactions Π^P increases monotonically with ϕ and helps stabilize the system. The phase behavior of active systems is determined by a competition between a destabilizing Π^{swim} versus a stabilizing Π^P, a balance controlled by the parameter Pe_R.

For large Pe_R the swimmers behave as Brownian particles and $\widehat{\Pi}^P(\phi, Pe_R) = \widehat{\Pi}^{HS}(\phi)$, where $\widehat{\Pi}^{HS}(\phi) = 4\phi g(2;\phi)$ is the interparticle pressure of hard-sphere Brownian particles and $g(2;\phi)$ is the pair-distribution function at contact. [15, 16] The detailed interactions between the particles are not important [15, 16, 17]; a

[1] We use the conventional definition of the Péclet number as advection over diffusion, but others may use the inverse of this quantity.

hard-sphere molecular fluid's interparticle pressure has the same form – the same volume fraction dependence – as that of a Brownian system despite differences in the source of the collisions. A system of active swimmers also exhibits the same form of the interparticle pressure. Indeed, for large Pe_R the run length $U_0\tau_R$ sets the scale of the force moment and $\Pi^P \sim n^2\zeta U_0 a^3(U_0\tau_R) \sim nk_sT_s\phi$, analogous to the passive hard-sphere Brownian collisional pressure $\sim nk_BT\phi$.

For small Pe_R, $\Pi^P \sim n^2\zeta U_0 a^4 \sim nk_sT_sPe_R\phi$ since a swimmer is displaced by its size a upon collision, not the run length $U_0\tau_R$. Extending the results of [7] the interparticle pressure for small Pe_R in 3D is thus $\widehat{\Pi}^P = 3\phi Pe_R g(2;\phi)$.

For both small and large Pe_R, the pair-distribution function at contact has the form [16] $g(2;\phi) = (1-\phi/\phi_0)^{-\beta}$, and ϕ_0 and β are parameters obtained from the interparticle pressure of hard-sphere molecular fluids and/or passive Brownian particles. Simulations verify that the parameters $\phi_0 = 0.65$ and $\beta = 1$ agree independently with the collisional pressures for hard-sphere active swimmers, passive Brownian particles, and molecular fluids [16].

The active pressure is the sum of the swim and interparticle pressures[2], which for small Pe_R is

$$\Pi^{act} = nk_sT_s\left(1-\phi-\phi^2+3\phi Pe_R(1-\phi/\phi_0)^{-1}\right), \tag{4.1}$$

and which we can use to analyze phase separation in active matter. We focus on non-Brownian swimmers since the effect of translational Brownian diffusivity is small in phase-separating systems. Figure 4.1 compares the phase diagram in the $Pe_R-\phi$ plane obtained from this model to the simulation data of other studies.

The spinodal defines the regions of stability and is determined by setting $\partial\Pi^{act}/\partial\phi = 0$. This is given by the red curve in Fig 4.1 that passes through the extrema of each constant-pressure isocontour ("isobar"). No notion of free energy is needed to obtain the spinodal—it is a purely mechanical quantity.

At the critical point $\partial\Pi^{act}/\partial\phi = \partial^2\Pi^{act}/\partial\phi^2 = 0$. In 3D we find the critical volume fraction $\phi^c \approx 0.44$, active pressure $\Pi^{act,c}\phi^c/(nk_sT_s) \approx 0.21$, and Péclet number $Pe_R^c \approx 0.028$, values consistent with our BD simulations. Like the spinodal, the critical point is identified using only mechanical arguments.

The blue curve in Fig 4.1 delineates the "binodal" or coexistence regions, which we define as the equality of the chemical potential in the dilute and dense phases.

[2]Pressure p_f of the incompressible solvent is arbitrary.

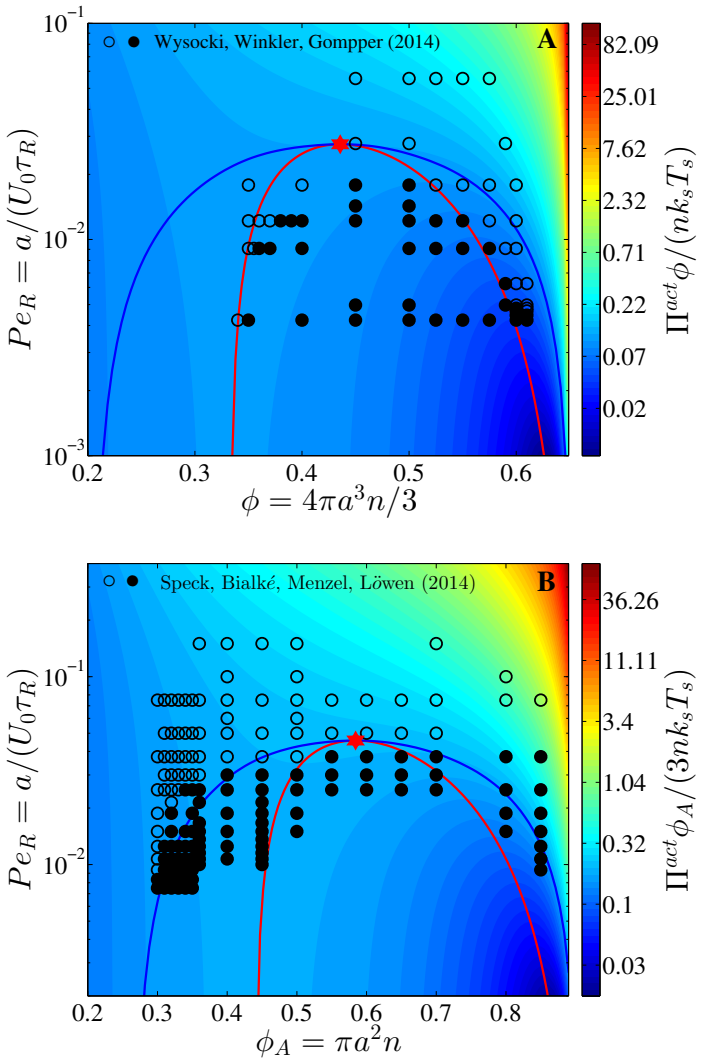

Figure 4.1: Phase diagram in the $Pe_R - \phi$ plane in (**A**) 3D and (**B**) 2D. The colorbar shows the active pressure scaled with the swim energy $k_sT_s = \zeta U_0^2\tau_R/6$, and the blue and red curves are the binodal and spinodal, respectively. The critical point is shown with a red star. The open and filled symbols are simulation data with a homogeneous and phased-separated state, respectively.

Although the thermodynamic chemical potential is defined only for equilibrium systems, one can define a nonequilibrium chemical potential for active systems using standard macroscopic mechanical balances [7]: $n(\partial\mu^{act}/\partial n) = (1-\phi)\partial\Pi^{act}/\partial n$.

This definition agrees with the true thermodynamic chemical potential for molecular or colloidal solutes in solution [18] (see Appendix). There are no approximations other than incompressibility of the solvent. Stress-induced diffusion, which

this relationship implies, has been used in the context of migration of non-Brownian particles in pressure-driven flow [19]. For $\tau_R \to 0$ active swimmers and passive Brownian particles not only behave similarly, but their dynamics are equivalent. If we placed active swimmers that behave identically to passive Brownian particles behind an osmotic barrier, we would not be able to distinguish one from the other. The form of the relationship between the chemical potential and pressure are equivalent for the two systems. We thus interpret μ^{act} as a natural definition and extension of the chemical potential for nonequilibrium systems, and use it to compute and define a "binodal."

For small Pe_R we obtain

$$\mu^{act}(k_sT_s, \phi, Pe_R) = \mu^{\theta}(k_sT_s, Pe_R) + k_sT_s \log \phi + k_sT_s \log \Gamma(\phi, Pe_R), \qquad (4.2)$$

where $\mu^{\theta}(k_sT_s, Pe_R)$ is the reference state whose form is not needed, and $\Gamma(\phi, Pe_R)$ is a nonlinear but analytic expression[3]. The second term on the right-hand side represents the entropic, "ideal-gas" contribution to the chemical potential. The third term is the nonideal term that is the analog of enthalpic attraction between the active swimmers, and is represented by the quantity $\Gamma(\phi, Pe_R)$ that resembles the fugacity coefficient in classical thermodynamics. Equation 4.2 is similar to that proposed by Cates and coworkers [20, 2] who argued that $\mu(n) = \log n + \log v(n)$, where $v(n)$ is a density-dependent swimmer velocity. Our theory gives the nonideal contribution $\Gamma(\phi, Pe_R)$ in the entire range of ϕ and Pe_R.

The chemical potential from BD simulations and the model is shown in Fig 4.2 for $Pe_R = 0.02$. It increases logarithmically at low Π^{act} and the slope changes dramatically at the coexistence point ($\Pi^{act}\phi/(nk_sT_s) \approx 0.2$). At this value of Π^{act} and Pe_R the chemical potentials are equal in the dilute and dense phases. The data in the flat van der Waals region of the $\Pi^{act} - \phi$ phase diagram (see $\phi \approx 0.25 - 0.6$ in Fig 2 of [7]) collapse onto the single coexistence point.

We can now define a "binodal" in Fig 4.1 through the equality of the chemical potential in both phases. Our theory predicts that active systems prepared outside the binodal (blue curve) are stable in the homogeneous configuration and do not phase separate. The regions between the spinodal and binodal are metastable and

[3]The nonideal term for the nonequilibrium chemical potential in Eq 4.2 is given by

$$\Gamma(\phi, Pe_R) = (1 - \phi/\phi_0)^{-3\phi_0 Pe_R} \exp\left[\phi^3 - \phi^2/2 + 3Pe_R\phi_0(1 - \phi_0)/(1 - \phi/\phi_0) - 3\phi(1 - \phi_0 Pe_R)\right].$$

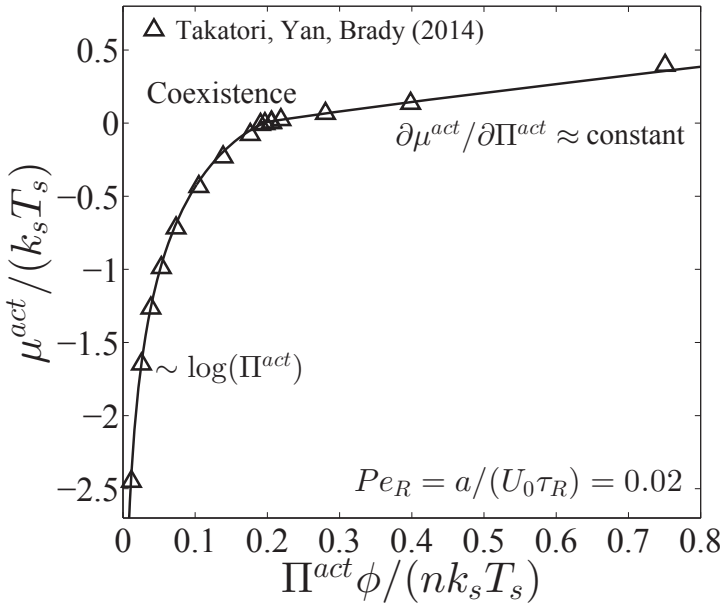

Figure 4.2: Nonequilibrium chemical potential as a function of Π^{act} for $Pe_R = a/(U_0\tau_R) = \zeta U_0 a/(6k_sT_s) = 0.02$, where $k_sT_s = \zeta U_0^2\tau_R/6$ is the swimmers' energy scale. The symbols are BD simulations (Takatori, Yan, and Brady, *Phys Rev Lett*, 2014) and the curve is the model, Eq 4.2.

a homogeneous system does not spontaneously phase separate via spinodal decomposition but can undergo a nucleation process. Nucleation times can be large and difficult to reach computationally, so artificial seeding may be required to induce phase separation [6].

As shown in Fig 4.1A in 3D the transition from the homogeneous (open symbols) to phase-separated (filled symbols) systems in the simulations of Wysocki et al [5] agree well with the spinodal of our model.

In 2D, nucleation seeds form more easily compared to 3D because active swimmers self-assemble more easily in 2D—the colliding swimmers have fewer dimensions to "escape" the cluster (e.g., consider the extreme example of a 1D system that readily clusters into a long string of swimmers). We surmise that nucleation processes are more likely to be observed in a 2D simulation prepared near the binodal curve. These observations are corroborated by Fig 4.1B where we take the swim and interparticle pressures in 2D as $\Pi^{swim}/(n\zeta U_0^2\tau_R/2) = 1 - \phi_A - 0.2\phi_A^2$ and $\Pi^P/(n\zeta U_0^2\tau_R/2) = (4/\pi)\phi_A Pe_R g(2;\phi_A)$, respectively, where $\phi_A = n\pi a^2$ is the area fraction of active swimmers and $g(2;\phi_A) = (1-\phi_A/\phi_0)^{-\beta}$ with $\phi_0 = 0.9$ and $\beta = 1$. The 2D simulation of Speck et al [3] show that the transition from the

homogeneous (open symbols) to phase-separated (filled symbols) states occur near the binodal (blue curve).

Our active pressure model agrees qualitatively and even quantitatively with the phase diagrams in Fig 4.1, as well as with those of other studies [2, 4, 6]. It should be appreciated that there are no adjustable parameters in our theory.

4.3 'Thermodynamic' Quantities

The results presented thus far come from purely micromechanical arguments with no appeal to thermodynamics. We now turn our attention towards thermodynamic properties like the free energy and temperature, which, although well-defined for an equilibrium system, have been elusive for nonequilibrium systems.

Upon carefully imposing incompressibility of the solvent, one can relate the nonequilibrium Helmholtz FE to the mechanical pressure as $\Pi^{act}(k_sT_s, \phi, Pe_R) = \phi^2 \left[\partial/\partial\phi \left((F^{act}/V)/\phi\right)\right]$, where V is the volume of the system [18]. There are again no approximations; it can be considered as the definition of the free energy for nonequilibrium active systems. Substituting the active pressure model for small Pe_R in 3D, we obtain

$$F^{act}(Pe_R < 1)/(Nk_sT_s) = \log\phi - \frac{\phi(\phi+2)}{2} - 3Pe_R\phi_0 \log(1-\phi/\phi_0) + F^{\theta}(k_sT_s, Pe_R), \tag{4.3}$$

where N is the number of active swimmers and $F^{\theta}(k_sT_s, Pe_R)$ is the reference Helmholtz FE. The first term on the right can be interpreted as the ideal entropic contribution, and the rest represent the nonideal "enthalpic" attractions between the active swimmers. For large Pe_R, the Helmholtz FE has no dependence on Pe_R: $F^{act}(Pe_R > 1)/(Nk_sT_s) = \log\phi + 4\int_0^{\phi} g(2;s)ds + F^{\theta}(k_sT_s, Pe_R)$, and has the same form as for Brownian hard-sphere systems. The Helmholtz FE Eq 4.3 has a form in agreement with Cates and coworkers [20, 2] who expressed the FE density as $f = n(\log n - 1) + \int_0^n \log\upsilon(s)ds$.

Given a chemical potential we can further define the Gibbs FE as $\mu^{act} = (\partial G^{act}/\partial N)_{N_f,\Pi^{act},T_s,Pe_R}$, where N_f is the number of solvent molecules [18]. Alternatively we can compute the Gibbs FE from the Helmholtz FE [18]: $G^{act}/(Nk_sT_s) = F^{act}/(Nk_sT_s) + \Pi^{act}/(nk_sT_s)$. Figure 4.3 shows the Gibbs FE as a function of ϕ for different values of Pe_R and fixed $\Pi^{act}\phi/(nk_sT_s) = 0.18$. As Pe_R decreases from a stable, dilute "ideal gas" phase to $Pe_R = 0.015$ with a fixed $\Pi^{act}\phi/(nk_sT_s) = 0.18$, G^{act} has a local minimum at $\phi \approx 0.6$ corresponding to the metastable dense phase (i.e., "superheated liquid") and a global minimum at

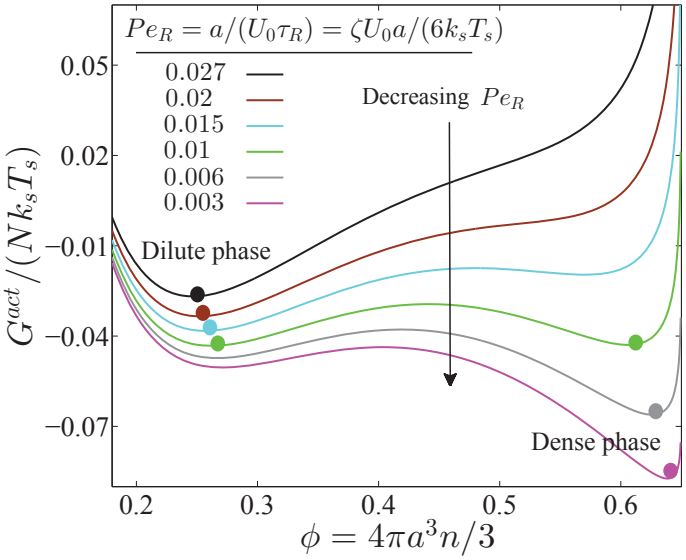

Figure 4.3: Gibbs free energy (FE) as a function of ϕ for fixed values of Pe_R and $\Pi^{act}\phi/(nk_sT_s) = 0.18$, where $k_sT_s = \zeta U_0^2\tau_R/6$. The red and blue curves are the spinodal and binodal, respectively. The black arrow points towards decreasing Pe_R at fixed Π^{act}. The filled color circles denote the stable states.

$\phi \approx 0.25$ corresponding to the stable dilute phase. At $Pe_R = 0.01$ the two minima of G^{act} are equal corresponding to the coexistence of the dilute and dense phases.

By writing the "ideal-gas" swim pressure as $\Pi^{swim} = n\zeta U_0^2\tau_R/6 = nk_sT_s$, we can identify a swimmer's energy scale as $k_sT_s = \zeta U_0^2\tau_R/6$. The reorientation Péclet number can be written as $Pe_R = a/(U_0\tau_R) = \zeta U_0 a/(6k_sT_s)$, which is interpreted as a ratio of the interactive energy of the swimmer – the energy required to displace the swimmer its size a – to the swim energy scale k_sT_s. Analogous to the Stokes-Einstein-Sutherland relation, one can interpret the swim diffusivity as $D^{swim} = k_sT_s/\zeta$, which also gives $Pe_R = U_0 a/D^{swim} \sim \zeta U_0 a/(k_sT_s)$.

From Fig 4.1 phase separation occurs for small $Pe_R = \zeta U_0 a/(6k_sT_s)$, or high T_s. This is opposite to what is typically observed in a classical thermodynamic system, where phase separation is driven by attractive enthalpic interactions and becomes possible at low temperatures. Phase separation with *increasing temperature* is uncommon but has been observed for systems driven by the lower critical solution temperature (LCST) transition [21, 22] where phase transition is dominated by entropy. As Pe_R decreases (T_s increases) and the run length of the swimmer increases, the particle effectively becomes larger in size and thus has less space available for entropic mixing.

Many studies have discussed and proposed a possible interpretation of the temperature in a nonequilibrium active matter system [23, 24, 25]. Unlike a molecular fluid particle that is able to transmit its kinetic activity to another particle upon a collision, a self-propelled swimmer cannot impart its intrinsic activity to another swimmer. In this sense the swim temperature $T_s = \zeta U_0^2 \tau_R/(6k_s)$ is different from the temperature of an equilibrium thermal fluid because each swimmer has its own unique intrinsic kinetic temperature T_s that does not get shared and equilibrated. Suppose we have a dilute suspension of completely inactive bath particles (i.e., not active swimmers nor Brownian particles). Into this we introduce a dilute concentration of active swimmers and monitor the motion of the passive bath particles. For small Pe_R the motion of the bath particles is not characterized by the swim diffusivity $D^{swim} \sim U_0^2 \tau_R$ because the bath particles get a displacement of $\sim O(a)$ upon colliding with a swimmer, not the run length $U_0 \tau_R$. Thus, the diffusivity of the bath particles is $D^{bath} \sim \phi U_0 a$, where ϕ is the volume fraction of the swimmers. The ratio of the bath to swimmer diffusivity is $D^{bath}/D^{swim} \sim \phi U_0 a/(U_0^2 \tau_R) = \phi Pe_R$, suggesting that the reorientation Péclet number is the quantity that gets shared between the swimmers and not the swim energy $k_s T_s$.

The entropy of active matter can be defined as $S^{act} = -(\partial G^{act}/\partial T_s)_{\zeta U_0 a, \Pi^{act}} = -(\partial F^{act}/\partial T_s)_{\zeta U_0 a, \phi}$. Ignoring the reference states, for large Pe_R the entropy has the same form as that for a passive Brownian system: $S^{act}(Pe_R > 1)/(Nk_s) = -\log\phi - 4\int_0^\phi g(2;s)ds$. For small Pe_R the entropy comes solely from the swim pressure: $S^{act}(Pe_R < 1)/(Nk_s) = -\log\phi + \phi(\phi+2)/2$. The entropy decreases with ϕ since the swimmers have less space available for entropic mixing.

The heat capacity can be obtained from $C_V = -T_s(\partial^2 F^{act}/\partial T_s^2)_{\phi, \zeta U_0 a}$. Aside from the reference state, substitution of the FE into this equation gives $C_V = 0$ for all ϕ at both small and large Pe_R. A possible explanation is that active matter has no true notion of the internal energy—since the swimmers cannot exchange their swim energy $k_s T_s$, there is no heat exchange between "hot" (high activity) and "cold" (low activity) active systems. There is no "first law" of thermodynamics for active matter systems.[4]

In some experimental systems the swimmers may achieve self-propulsion by consuming and converting chemical fuel into mechanical motion. Swimmers may thus decrease their intrinsic swim velocity $\boldsymbol{U}_0$ when they are in a crowded region from

[4]The actual chemical energy consumed in propelling the swimmer is dissipated into the thermal bath of the solvent. The behavior an active system depends on the activity ζU_0, not the actual energy consumed.

the lack of fuel. This is a separate and independent effect as the reduction in the actual swimmer velocity $\boldsymbol{U}$ from collisions with other swimmers, which is already reflected in Eq 4.4. Living microorganisms may possess an internal mechanism to detect changes in the local environment and alter their swim velocity or reorientation time. Hydrodynamics may also cause the drag factor to become density dependent. Our model remains applicable to swimmers with a local density-dependent intrinsic velocity $\boldsymbol{U}_0(\phi)$ and/or reorientation time $\tau_R(\phi)$. This effectively makes the swim temperature a function of the local volume fraction of active swimmers, $k_s T_s(\phi)$—decreasing the chemical fuel concentration translates to decreasing the swim temperature of the system.

As shown in the Appendix, if we allow for a density (or position) dependent intrinsic swim velocity $\boldsymbol{U}_0(\boldsymbol{x})$ and reorientation time $\tau_R(\boldsymbol{x})$, our definition of the nonequilibrium chemical potential becomes

$$n\frac{\partial \mu^{act}}{\partial n} = (1-\phi)\left[\frac{\partial \Pi^{act}}{\partial n} - \Pi^{swim}\left(\frac{\partial \log(U_0\tau_R)}{\partial n}\right)\right]. \tag{4.4}$$

Since Π^{act} was determined for a homogeneous system, Eq 4.1 still applies, but now $k_s T_s$ is also a function of ϕ.

In active systems the relevant length scale is the swimmers' run length $U_0\tau_R$ and this must to be small compared to the apparatus size in an experiment for the continuum approach to hold. In practice experiments may have non-continuum and non-local effects that may need to be considered when comparing experimental results with the thermodynamic model presented here.

In our model we neglected hydrodynamic interactions between the swimmers, which may contribute additional terms (like the "hydrodynamic stresslet" [26]) to the active pressure, affect the reorientation time, and result in additional effects like polar order of the swimmers. The ratio of the magnitudes of the hydrodynamic/polar stress to the swim stress is $\sim (n\zeta U_0 a)/(n\zeta U_0^2\tau_R) = a/(U_0\tau_R) \equiv Pe_R$; the hydrodynamic contribution becomes negligible when phase separation occurs for $Pe_R \ll 1$ (see Fig 4.1).

Much work remains to explore the implications of our 'thermodynamics' of active matter and to see if it might apply to other far from equilibrium systems.

Appendix

A: Micromechanical equations of motion

The active particle dynamics are governed by the N-particle Langevin equation

$$\mathbf{0} = -\zeta \boldsymbol{U} + \boldsymbol{F}^{swim} + \boldsymbol{F}^{P} + \sqrt{2\zeta^2 D_0}\boldsymbol{\Lambda}_T \tag{4.5}$$

$$\frac{d\boldsymbol{q}}{dt} = \sqrt{\frac{2}{\tau_R}}\boldsymbol{\Lambda}_R \times \boldsymbol{q}, \tag{4.6}$$

where $\boldsymbol{U}$ is the translational velocity, ζ is the hydrodynamic drag factor, $\boldsymbol{F}^{swim} \equiv \zeta \boldsymbol{U}_0 = \zeta U_0 \boldsymbol{q}$ is the self-propulsive swim force, U_0 is the swim speed, $\boldsymbol{q}$ is the unit vector specifying the swimmer's orientation, $\boldsymbol{F}^{P}$ is the interparticle force between the swimmers to enforce no overlap, $\boldsymbol{\Lambda}_T$ and $\boldsymbol{\Lambda}_R$ are unit random normal deviates, τ_R is the orientation time of the swimmer, and D_0 is the Stokes-Einstein-Sutherland translational diffusivity. The translational diffusivity and the reorientation dynamics are modeled with the usual white noise statistics, $\langle \Lambda_i(t) \rangle = 0$ and $\langle \Lambda_i(t)\Lambda_j(0) \rangle = \delta(t)\delta_{ij}$. The left-hand side of Eq 4.5 is zero since inertia is negligible for colloidal suspensions. In this work we neglect the translational Brownian motion of active swimmers.

For $\tau_R \to 0$ active swimmers have small run lengths compared to their size and their dynamics are equivalent to that of passive Brownian particles. Indeed, an osmotic barrier cannot distinguish between a system of passive Brownian particles and active swimmers with small τ_R. In this limit the form of the relationship between the pressure and other thermodynamic quantities (like the chemical potential) are equivalent for the two systems.

B: Swim stress

In [7] the swim stress was defined to be the first moment of the swim force

$$\boldsymbol{\sigma}^{swim} = -n\langle \boldsymbol{x}\boldsymbol{F}^{swim} \rangle, \tag{4.7}$$

where n is the number density of particles and the angle brackets denote an average over all particles and time. It is permissible for computing the stress to interpret the self-propulsion of an active swimmer as arising from a swim force, $\boldsymbol{F}^{swim} \equiv \zeta \boldsymbol{U}_0$ [7]. This use of the swim force to compute the stress does not imply that the intrinsic swim mechanism generates a long-range $(1/r)$ Stokes velocity field as does an external force [8].

The particle position at time t is $\boldsymbol{x}(t) = \int \boldsymbol{U}(t')dt'$, and from Eq 4.5 in the absence of interparticle forces (i.e., dilute suspension), we obtain $\boldsymbol{\sigma}^{swim} = -n\langle \boldsymbol{x}\boldsymbol{F}^{swim} \rangle =$

$-n\zeta \int \langle \boldsymbol{U}_0(t')\boldsymbol{U}_0(t)\rangle \, dt' = -n\zeta \boldsymbol{D}^{swim}$, where the time integral of the intrinsic velocity autocorrelation is the swim diffusivity of the swimmer, $\boldsymbol{D}^{swim}$. Using the swim diffusivity $\boldsymbol{D}^{swim} = U_0^2\tau_R\boldsymbol{I}/6$, we obtain the "ideal-gas" swim stress: $\boldsymbol{\sigma}^{swim} = -n\zeta U_0^2\tau_R\boldsymbol{I}/6$ [7]. A dilute suspension of active swimmers therefore exerts a swim pressure, $\Pi^{swim} = -\mathrm{tr}\boldsymbol{\sigma}^{swim}/3 = n\zeta U_0^2\tau_R/6$, as given in the main text.

C: Mechanical derivation of the chemical potential

The number density of active swimmers satisfies the conservation equation

$$\frac{\partial n}{\partial t} + \nabla \cdot \boldsymbol{j} = 0, \tag{4.8}$$

where $\boldsymbol{j} = n\boldsymbol{u}_p = n\langle \boldsymbol{u}\rangle + \boldsymbol{j}^{rel}$ is the particle flux, $\boldsymbol{j}^{rel} = n(\boldsymbol{u}_p - \langle \boldsymbol{u}\rangle)$ is the flux relative to the suspension average velocity $\langle \boldsymbol{u}\rangle$, which is defined as $\langle \boldsymbol{u}\rangle = \phi\boldsymbol{u}_p + (1-\phi)\boldsymbol{u}_f$, and $\boldsymbol{u}_p$ and $\boldsymbol{u}_f$ are the number averaged velocity of the swimmers and fluid at a continuum point, respectively. Due to incompressibility the suspension average velocity (particles plus the fluid) satisfies $\nabla \cdot \langle \boldsymbol{u}\rangle = 0$.

To obtain an expression for $\boldsymbol{j}^{rel}$ we have no thermodynamic arguments to rely upon (such as the free energy) so we apply an averaged macroscopic mechanical momentum balance. Following the standard Irving-Kirkwood approach for averaging over a representative volume element as was done for non-Brownian suspensions [19], we obtain

$$0 = -n\zeta(\boldsymbol{u}_p - \langle \boldsymbol{u}\rangle) + \nabla \cdot \boldsymbol{\sigma}^{act}, \tag{4.9}$$

where $\boldsymbol{\sigma}^{act} = \boldsymbol{\sigma}^{swim} + \boldsymbol{\sigma}^{P}$ and the left-hand side is zero since inertia is negligible for colloidal systems. Using the relative flux $\boldsymbol{j}^{rel} = n(\boldsymbol{u}_p - \langle \boldsymbol{u}\rangle)$ we arrive at an explicit expression for the active particle flux in terms of gradients in the active stress:

$$\boldsymbol{j}^{rel} = \frac{1}{\zeta}\nabla \cdot \boldsymbol{\sigma}^{act}. \tag{4.10}$$

No notion of a thermodynamic chemical potential or the free energy is needed to arrive at this expression. Substituting Eq 4.10 into the active particle conservation Eq 4.8, we obtain

$$\frac{\partial n}{\partial t} + \langle \boldsymbol{u}\rangle \cdot \nabla n = -\nabla \cdot \frac{1}{\zeta}\nabla \cdot \boldsymbol{\sigma}^{act}, \tag{4.11}$$

which is a convection-diffusion equation, where the diffusive nature is captured by gradients in the active stress. For a system that is macroscopically at rest, $\langle \boldsymbol{u}\rangle = \boldsymbol{0}$, and the active stress is isotropic, $\boldsymbol{\sigma}^{act} = -\Pi^{act}\boldsymbol{I}$, so Eq 4.11 becomes a diffusion equation

$$\frac{\partial n}{\partial t} = \nabla \cdot \frac{1}{\zeta}\nabla\Pi^{act}. \tag{4.12}$$

This derivation is not restricted to active systems and applies equally well to equilibrium Brownian systems, where the Brownian osmotic pressure $\Pi^B = nk_BT$ gives

$$\frac{\partial n}{\partial t} = \left(\frac{k_BT}{\zeta}\right)\nabla^2 n, \tag{4.13}$$

a familiar diffusion equation with the Stokes-Einstein-Sutherland translational diffusivity $D_0 = k_BT/\zeta$. To continue the discussion of a passive Brownian system, which *can* be rigorously related to thermodynamic quantities, one can define a chemical potential precisely from a thermodynamic treatment [18] to give

$$n\frac{\partial \mu^B}{\partial n} = (1-\phi)\frac{\partial \Pi^B}{\partial n}. \tag{4.14}$$

In a thermodynamic system slightly out of equilibrium, the particle flux relative to the suspension average velocity is driven by the chemical potential gradient $\boldsymbol{j}^{rel} = -(n/((1-\phi)\zeta))\nabla\mu^B$. Comparing this flux expression with $\boldsymbol{j}^{rel} = -(1/\zeta)\nabla\Pi^B$ (i.e., Eq 4.10 with $\boldsymbol{\sigma}^{act}$ replaced by $\boldsymbol{\sigma}^B = -\Pi^B\boldsymbol{I}$) we arrive precisely at Eq 4.14.

Therefore the mechanical derivations of the stress, momentum balance, and flux are in full agreement with thermodynamics. In fact, one can analyze an equilibrium Brownian system purely from a mechanical perspective without appealing to thermodynamics [17]. Returning to active matter systems, we can rely upon the mechanical derivation to *define* a nonequilibrium chemical potential by analogy to the quantity whose gradient would drive a flux. Repeating the connection of the relative particle flux, $\boldsymbol{j}^{rel} = -(1/\zeta)\nabla\Pi^{act}$, to gradients in this newly defined chemical potential, $\boldsymbol{j}^{rel} = -(n/((1-\phi)\zeta))\nabla\mu^{act}$, we arrive at $n(\partial\mu^{act}/\partial n) = (1-\phi)\partial\Pi^{act}/\partial n$, as used in the main text.

As mentioned in the main text, this relationship between the chemical potential and pressure are equivalent for a system of passive Brownian particles and active swimmers with small τ_R. The dynamics of swimmers with $\tau_R \to 0$ are equivalent to that of passive Brownian particles, and one cannot distinguish between the two systems using confinement by an osmotic barrier. We thus interpret μ^{act} as a natural definition and extension of the chemical potential for nonequilibrium systems, and use it to compute and define a "binodal."

D: Density-dependent swimmer activity

Suppose we have a density (or position) dependent intrinsic swim velocity $\boldsymbol{U}_0(\boldsymbol{x})$ and reorientation time $\tau_R(\boldsymbol{x})$. These may vary spatially due to a variation in fuel

concentration, for example. For a weak gradient we have

$$\boldsymbol{U}_0(\boldsymbol{x}) = U_0(\boldsymbol{x}_0)\boldsymbol{q}(\boldsymbol{x}_0) + (\nabla U_0)_{\boldsymbol{x}_0} \cdot (\boldsymbol{x} - \boldsymbol{x}_0)\boldsymbol{q}(\boldsymbol{x}_0) + U_0(\boldsymbol{x}_0)(\nabla \boldsymbol{q})_{\boldsymbol{x}_0} \cdot (\boldsymbol{x} - \boldsymbol{x}_0) + \cdots, \tag{4.15}$$

where $\boldsymbol{q}$ is the unit orientation vector of the swimmer and the ellipsis contains all higher-order gradient terms. This gives rise to a drift velocity of the swimmers due to a nonzero average swim force $\langle \boldsymbol{F}^{swim} \rangle = \langle \zeta U_0(\boldsymbol{x})\boldsymbol{q} \rangle = \zeta (\nabla U_0)_{\boldsymbol{x}_0} \cdot \langle (\boldsymbol{x} - \boldsymbol{x}_0)\boldsymbol{q}(\boldsymbol{x}_0) \rangle + \zeta U_0(\boldsymbol{x}_0) \langle (\nabla \boldsymbol{q})_{\boldsymbol{x}_0} \cdot (\boldsymbol{x} - \boldsymbol{x}_0) \rangle$, where we retain only the leading order in gradients. Using the swim stress $\boldsymbol{\sigma}^{swim} = -n\langle \boldsymbol{x}\boldsymbol{F}^{swim} \rangle = -n\langle \zeta U_0(\boldsymbol{x} - \boldsymbol{x}_0)\boldsymbol{q} \rangle$, we have

$$\langle \boldsymbol{F}^{swim} \rangle = -\frac{1}{n}\boldsymbol{\sigma}^{swim} \cdot \nabla \log(U_0 \tau_R). \tag{4.16}$$

A nonzero average swim force impacts the macroscopic flux model by contributing an additional term to the expression for the relative particle flux (see Eq 4.10):

$$\boldsymbol{j}^{rel} = \frac{1}{\zeta}\left(\nabla \cdot \boldsymbol{\sigma}^{act} + n\langle \boldsymbol{F}^{swim} \rangle \right), \tag{4.17}$$

where $\boldsymbol{\sigma}^{act} = \boldsymbol{\sigma}^{swim} + \boldsymbol{\sigma}^{P}$ is the active particle stress. Substituting for the mean swim force we obtain a constitutive relation for active systems with a drift velocity:

$$\boldsymbol{j}^{rel} = \frac{1}{\zeta}\left[\nabla \cdot \boldsymbol{\sigma}^{act} - \boldsymbol{\sigma}^{swim} \cdot \nabla \log(U_0 \tau_R) \right]. \tag{4.18}$$

For a dilute system of active swimmers, $\boldsymbol{\sigma}^{act} \approx \boldsymbol{\sigma}^{swim} = -n\zeta U_0^2 \tau_R \boldsymbol{I}/6$, and the relative flux becomes

$$\boldsymbol{j}^{rel} = -nD^{swim}\left(\nabla \log n + \nabla \log U_0 \right), \tag{4.19}$$

where $D^{swim} = U_0^2 \tau_R/6$. This result agrees with the work of Cates and coworkers [20, 13] who derived Eq 4.19 for a dilute system from consideration of the flux in a Smoluchowski analysis rather than from the swim stress perspective. And like Cates and coworkers [20, 13] for a system with zero relative particle flux, we obtain the steady-state probability density $n(\boldsymbol{x}) \sim 1/U_0(\boldsymbol{x})$. Notice that the $\nabla \log(\tau_R)$ term cancels and Eq 4.19 does not change irrespective of $\tau_R(\boldsymbol{x})$ varying with position. For the general expression (Eq 4.18) valid for all concentrations this may no longer be the case.

Repeating the connection of the relative particle flux, Eq 4.18, to gradients in the active chemical potential, $\boldsymbol{j}^{rel} = -(n/((1-\phi)\zeta))\nabla \mu^{act}$, we arrive at Eq 4.4 of the main text.

References

[1] J. Toner, Y. Tu, and S. Ramaswamy. “Hydrodynamics and phases of flocks”. *Ann Phys* 318.1 (2005), pp. 170–244.

[2] J. Stenhammar, D. Marenduzzo, R. J. Allen, and M. E. Cates. “Phase behaviour of active Brownian particles: The role of dimensionality”. *Soft Matter* 10.10 (2014), pp. 1489–1499.

[3] T. Speck, J. Bialké, A. M. Menzel, and H. Löwen. “Effective Cahn-Hilliard equation for the phase separation of active Brownian particles”. *Phys Rev Lett* 112.21 (2014), p. 218304.

[4] Y. Fily, S. Henkes, and M. C. Marchetti. “Freezing and phase separation of self-propelled disks”. *Soft Matter* 10.13 (2014), pp. 2132–2140.

[5] A. Wysocki, R. G. Winkler, and G. Gompper. “Cooperative motion of active Brownian spheres in three-dimensional dense suspensions”. *Europhys Lett* 105.4 (2014), p. 48004.

[6] G. S. Redner, M. F. Hagan, and A. Baskaran. “Structure and dynamics of a phase-separating active colloidal fluid”. *Phys Rev Lett* 110.5 (2013), p. 055701.

[7] S. C. Takatori, W. Yan, and J. F. Brady. “Swim pressure: Stress generation in active matter”. *Phys Rev Lett* 113.2 (2014), p. 028103.

[8] S. C. Takatori and J. F. Brady. “Swim stress, motion, and deformation of active matter: Effect of an external field”. *Soft Matter* 10.47 (2014), pp. 9433–9445.

[9] X. Yang, M. L. Manning, and M. C. Marchetti. “Aggregation and segregation of confined active particles”. *Soft Matter* 10.34 (2014), pp. 6477–6484.

[10] I. Theurkauff, C. Cottin-Bizonne, J. Palacci, C. Ybert, and L. Bocquet. “Dynamic clustering in active colloidal suspensions with chemical signaling”. *Phys Rev Lett* 108.26 (2012), p. 268303.

[11] J. Palacci, S. Sacanna, A. P. Steinberg, D. J. Pine, and P. M. Chaikin. “Living crystals of light-activated colloidal surfers”. *Science* 339.6122 (2013), pp. 936–940.

[12] J. Bialké, H. Löwen, and T. Speck. “Microscopic theory for the phase separation of self-propelled repulsive disks”. *Europhys Lett* 103.3 (2013), p. 30008.

[13] J. Stenhammar, A. Tiribocchi, R. J. Allen, D. Marenduzzo, and M. E. Cates. “Continuum theory of phase separation kinetics for active Brownian particles”. *Phys Rev Lett* 111.14 (2013), p. 145702.

[14] I. Buttinoni et al. “Dynamical clustering and phase separation in suspensions of self-propelled colloidal particles”. *Phys Rev Lett* 110.23 (2013), p. 238301.

[15] D. McQuarrie. *Statistical mechanics*. Mill Valley, California, USA: University Science Books, 2000.

[16] W. Russel, D. Saville, and W. Schowalter. *Colloidal dispersions*. Cambridge University Press, 1992.

[17] J. F. Brady. "Brownian motion, hydrodynamics, and the osmotic pressure". *J Chem Phys* 98.4 (1993), pp. 3335–3341.

[18] M. Doi. *Soft matter physics*. Oxford, United Kingdom: Oxford University Press, 2013.

[19] P. R. Nott and J. F. Brady. "Pressure-driven flow of suspensions: Simulation and theory". *J Fluid Mech* 275 (1994), pp. 157–199.

[20] J. Tailleur and M. E. Cates. "Statistical mechanics of interacting run-and-tumble bacteria". *Phys Rev Lett* 100.21 (2008), p. 218103.

[21] R. B. Griffiths and J. C. Wheeler. "Critical points in multicomponent systems". *Phys Rev A* 2.3 (1970), pp. 1047–1064.

[22] P. I. Freeman and J. S. Rowlinson. "Lower critical points in polymer solutions". *Polymer* 1 (1960), pp. 20–26.

[23] X.-L. Wu and A. Libchaber. "Particle diffusion in a quasi-two-dimensional bacterial bath". *Phys Rev Lett* 84.13 (2000), pp. 3017–3020.

[24] D. Loi, S. Mossa, and L. F. Cugliandolo. "Non-conservative forces and effective temperatures in active polymers". *Soft Matter* 7.21 (2011), pp. 10193–10209.

[25] M. E. Cates and J. Tailleur. "When are active Brownian particles and run-and-tumble particles equivalent? Consequences for motility-induced phase separation". *Europhys Lett* 101.2 (2013), p. 20010.

[26] D. Saintillan and M. J. Shelley. "Instabilities, pattern formation, and mixing in active suspensions". *Phys Fluids* 20.12 (2008), pp. 123304–123315.

Chapter 5

A THEORY FOR THE PHASE BEHAVIOR OF MIXTURES OF ACTIVE PARTICLES

This chapter includes content from our previously published article:

[1] S. C. Takatori and J. F. Brady. "A theory for the phase behavior of mixtures of active particles". *Soft Matter* 11.40 (2015), pp. 7920–7931. DOI: 10.1039/C5SM01792K.

5.1 Introduction

Systems at equilibrium like molecular or colloidal suspensions have a well-defined thermal energy k_BT that quantifies the particles' kinetic energy and gauges how "hot" or "cold" the system is. For systems far from equilibrium, such as active matter, it is unclear whether the concept of a "temperature" exists and whether self-propelled entities are capable of thermally equilibrating like passive Brownian suspensions. Here we develop a simple mechanical theory to study the phase behavior and "temperature" of a mixture of self-propelled particles. A mixture of active swimmers and passive Brownian particles is an ideal system for discovery of the temperature of active matter and the quantities that get shared upon particle collisions. We derive an explicit equation of state for the active/passive mixture to compute a phase diagram and to generalize thermodynamic concepts like the chemical potential and free energy for a mixture of nonequilibrium species. We find that different stability criteria predict in general different phase boundaries, facilitating considerations in simulations and experiments about which ensemble of variables are held fixed and varied.

Active matter systems like colonies of bacteria and self-propelled synthetic microswimmers are a rich area of study for soft matter. The fundamental and seemingly elementary ability of self-propulsion allows active systems to free themselves from classical thermodynamic constraints and to control their own motion and the surrounding environment. Their inherently nonequilibrium properties engender intriguing behavior such as spontaneous self-assembly and pattern formation [1, 2], making active matter a fascinating but challenging system to study.

Recently a new "swim pressure" concept was introduced—namely, all active entities exert a unique mechanical pressure owing to their self-motion [3, 4]. This perspective was applied [5] to predict the self-assembly of a suspension of active particles into regions of dense and dilute phases observed in both experiments and simulations [6, 7, 8, 9, 10]. The usefulness of the mechanical pressure to illuminate active matter's physical principles begs the question: what is the temperature of active matter? Do active swimmers "thermally equilibrate" with their surroundings? Although it is clear that the mechanical pressure can be quantified and is valid out of equilibrium, it is uncertain whether the notion of a temperature exists and can be explained in basic physical quantities.

To understand the temperature of active matter, we shall first discuss a simple experiment involving passive Brownian suspensions (i.e., no self-propulsion) which *can* be rigorously related to conventional thermodynamic quantities like the temperature and free energy. Suppose we have a purely Brownian suspension with thermal energy $(k_BT)_H$ that is separated by a thermally-insulated partition from another Brownian system with a different temperature $(k_BT)_C$, as shown in Fig 5.1. The partition is suddenly removed and the particles at different temperatures are allowed to mix. The "hot" and "cold" particles undergo many collisions, share their kinetic energy with each other, and eventually equilibrate to a common temperature $(k_BT)_{eq}$.

Now suppose we do the same mixing experiment with self-propelled swimmers at two different activity levels. For simplicity we consider self-propelled spheres of radii a that translate with an intrinsic swim speed U_0, reorient with a reorientation time τ_R, and experience a hydrodynamic drag factor ζ from the surrounding continuous Newtonian fluid. Their motion can be described as a random-walk process for times $t > \tau_R$ with a diffusivity $D^{swim} = U_0^2\tau_R/2$ in two dimensions (2D). Their characteristic "energy scale" is not the thermal energy $k_BT = \zeta D_0$ where D_0 is the Stokes-Einstein-Sutherland translational diffusivity, but comes from their self-propulsive activity, defined as $k_sT_s \equiv \zeta D^{swim} = \zeta U_0^2\tau_R/2$ (see later section for a more detailed treatment).

A system of "hot" active swimmers with $(k_sT_s)_H$ is initially separated from "cold" swimmers with $(k_sT_s)_C$ as shown in Fig 5.1. When the partition is removed, the swimmers with different activity levels spontaneously mix and undergo collisions with each other. When a swimmer collides into another swimmer, it displaces the body by its size a until they move completely clear of each others' trajectories.

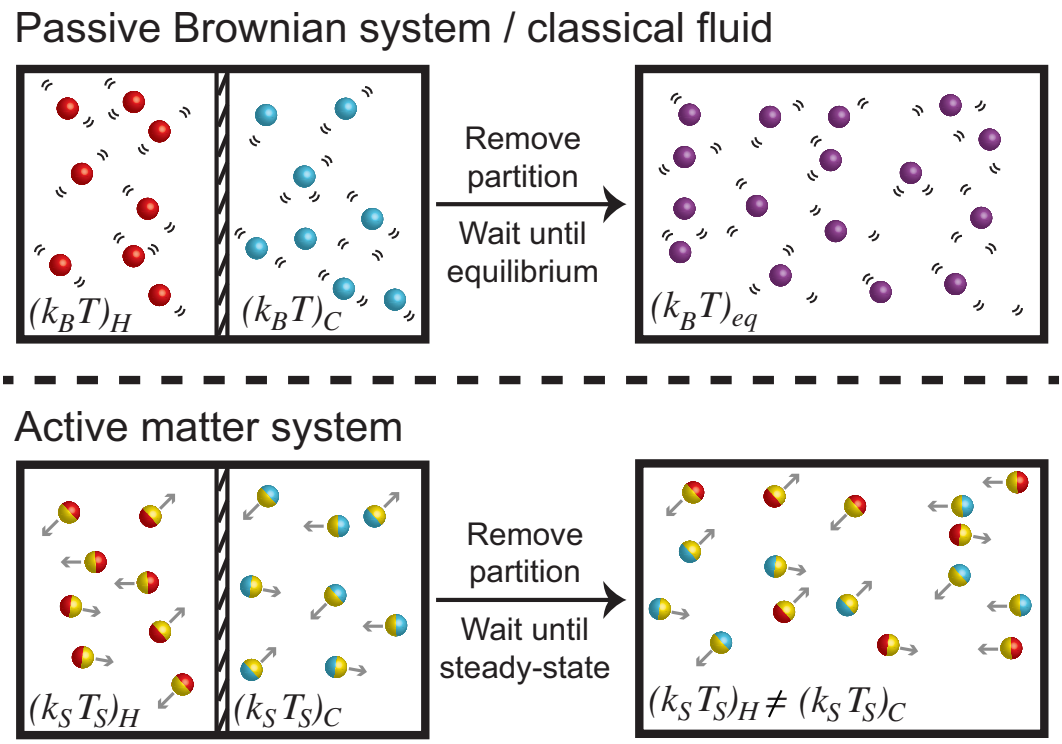

Figure 5.1: Schematic of the mixing process of purely Brownian suspensions (top) and active systems (bottom) that are initially at two different "temperatures." The Brownian particles thermally equilibrate their thermal energy k_BT whereas the active swimmers do not share their characteristic "energy scale" $k_sT_s \equiv \zeta U_0^2 \tau_R/2$.

After the collision, each swimmer then continues its motion with the *same* activity it had initially—there is no sharing of kinetic activity (k_sT_s) upon collisions. This implies that the swimmers' activity scale $k_sT_s \equiv \zeta U_0^2 \tau_R/2$ does not get shared via collisions and thus does not "equilibrate" like the temperature of a classical fluid k_BT. This simple experiment already reveals the richness and challenge to understand the "temperature" of nonequilibrium active systems.

A simple multicomponent mixture of self-propelled particles with two different activities is an ideal system to discover and study this problem in greater detail. Previous studies have provided various interpretations of the temperature in a nonequilibrium active matter system [11, 12, 13]. We discuss a new perspective by developing a mechanical pressure theory for predicting the phase behavior of a mixture of active swimmers over the entire phase space of the system. Our theory applies in general to a multicomponent suspension with swimmers of different activities, but perhaps the most straightforward mixture is that of active self-propelled particles and passive Brownian particles in a single solvent. In this mixture we must

treat active swimmers and passive particles as independent species, because their compositions vary in space due to the phase-separating behavior of active suspensions. This is true in general for multicomponent systems—in a simple polymeric solution of polyethylene in benzene, the polyethylene molecules do not all have the same number of segments or molecular weight, and thus generally need to be treated as different components. Experiments also often use mixed solvents in which the solvent composition inside a polymer coil (or gel) is in general different from the outer regions, as certain solvent species preferentially remain inside (or outside) the polymer coil [14].

We consider a simple mixture of spherical active and passive Brownian particles with equal size a; the passive particles translate by Brownian motion but are otherwise inactive (see Appendix A for the equations of motion). We do not include the effects of hydrodynamic interactions, and there is no polar order of the swimmers or any large-scale collective motion (e.g., bioconvection). We find that many new insights about the temperature of active matter can be obtained from this simple system.

In the next section we further extend the mixing example discussed above (Fig 5.1) by analyzing the effects of adding a small concentration of passive Brownian particles into an active system. We analyze the quantities that "equilibrate" in an active system by studying the collisions between a swimmer and a passive particle . In Sec 5.3 we develop a simple mechanical theory by identifying the different contributions that make up the total active pressure of the mixture. Since active matter is an inherently nonequilibrium system, we do not rely upon the thermodynamic free energy or chemical potential to predict the phase behavior of the system. Unlike these thermodynamic quantities, the mechanical stress (or pressure) is defined out of equilibrium and can be used to analyze mechanical instability of active matter. We then take our equation of state to compute what would be the nonequilibrium analogs of the free energy and chemical potential. Lastly, we analyze different stability criteria, facilitating discussion about the variables that may be held fixed and varied in experiments and computer simulations.

5.2 Do active particles "thermally" equilibrate?

From the mixing process in Fig 5.1 we learned that the characteristic activity scale of the swimmers do not equilibrate (i.e., $(k_s T_s)_H \neq (k_s T_s)_C$) unlike the thermal energy $k_B T$ of passive Brownian particles. To gain further insight into the quantities

that get shared in an active system, suppose now that we have a dilute concentration of passive bath particles in a sea of active swimmers. The motion and behavior of passive bath particles are influenced markedly by the swimmers' reorientation Péclet number $Pe_R \equiv a/(U_0\tau_R)$, a ratio of the swimmer size a to its run length $U_0\tau_R$.

Swimmers with run lengths small compared to their size ($Pe_R \gg 1$) reorient rapidly and take small swim steps behaving as Brownian walkers. When a swimmer takes a step and collides into a bath particle, the passive particle gets a displacement of order the swimmer's step size $\sim O(U_0\tau_R)$. After many such collisions, the change in the translational diffusivity of the passive bath particle is $(D^{bath} - D_0) \sim U_0(U_0\tau_R)\phi_a$, where $D_0 = k_BT/\zeta$ is the Stokes-Einstein-Sutherland diffusivity of an isolated bath particle and ϕ_a is the area (or volume in 3D) fraction of the swimmers. In this limit active swimmers repeatedly displace the bath particle by their run length $U_0\tau_R$, which allows the bath particle to sense the activity or 'temperature' of the swimmers via collisions. In other words, the bath particle behaves as a 'thermometer' of the active suspension [12], where the collisional displacements it receives from the swimmer can be used to infer the swimmers' characteristic 'energy scale' $k_sT_s = \zeta U_0^2\tau_R/2$. This activity scale is analogous to the thermal energy k_BT, the kinetic activity of passive Brownian particles, which can also be probed by analyzing the collisions between two passive particles. In this sense a suspension of swimmers with small run lengths $U_0\tau_R < a$ behaves similarly to a purely Brownian suspension with an effective 'temperature' k_sT_s. For active Brownian particles, this contribution is in addition to the thermal k_BT that gets shared as usual as a result of translational Brownian motion. However, one would not be able to distinguish between the two contributions because the dynamics of swimmers with $Pe_R \gg 1$ is equivalent to that of passive Brownian particles. If we placed active swimmers that behave identically to passive Brownian particles behind an osmotic barrier, we would not be able to distinguish one from the other. In this sense a Brownian particle can be interpreted as a "swimmer" having an extreme value of the reorientation Péclet number $Pe_R^B \to \infty$.

The swim activity k_sT_s can also be understood by comparing the statistical correlation of the self-propulsive swim force, $\boldsymbol{F}^{swim} \equiv \zeta\boldsymbol{U}_0 = \zeta U_0\boldsymbol{q}$ where $\boldsymbol{q}$ is the unit orientation vector specifying the swimmer's direction of self-propulsion, to that of the Brownian force, $\boldsymbol{F}^B$. The swim force correlation $\langle F^{swim}(t)F^{swim}(t')\rangle = (\zeta U_0)^2\langle\boldsymbol{q}(t)\boldsymbol{q}(t')\rangle = (\zeta U_0)^2\exp(-(t-t')/\tau_R)$ turns into a delta-function correlation

$\langle F^{swim}(t)F^{swim}(t')\rangle \sim (\zeta U_0)^2\tau_R\delta(t-t')$ as $\tau_R \to 0$ [15]. Recall that as $\tau_R \to 0$ the active swimmers behave as random Brownian walkers, which have the white noise statistics $\overline{F^B(t)F^B(t')} = 2k_BT\zeta\delta(t-t')$ where the overline indicates an average over the solvent fluctuations. A comparison of these two correlations again suggests that the swimmers' kinetic activity can be interpreted by $k_sT_s \equiv \zeta U_0^2\tau_R/2$.

For swimmers with run lengths large compared to their size, ($Pe_R \ll 1$), we observe a different behavior. Colliding into a bath particle, the swimmer continues to push the bath particle until it moves completely clear of the swimmer's trajectory. The bath particles receive a displacement of $\sim O(a)$ upon colliding with a swimmer, not the run length $U_0\tau_R$. Therefore the length scale associated with collisions is the swimmer size a, and the change in the long-time diffusivity of the bath particles $(D^{bath} - D_0) \sim U_0a\phi_a$. Unlike the limit of $Pe_R \gg 1$ discussed above, here the bath particles cannot probe the activity or 'temperature' of the swimmers because it only receives a displacement of its size a, even though the swimmers actually diffuse with their swim diffusivity $D^{swim} \sim U_0^2\tau_R$. The ratio of the two diffusivities $(D^{bath} - D_0)/D^{swim} \sim U_0a\phi_a/(U_0^2\tau_R) = \phi_aPe_R$, suggesting that the reorientation Péclet number $Pe_R \equiv a/(U_0\tau_R)$ is the quantity that gets shared between the swimmers via collisions for small Pe_R [5]. This implies that the swimmers' energy scale $k_sT_s = \zeta U_0^2\tau_R/2$ does not get shared in the collisions and thus does not represent the 'temperature' in the classical sense.

The bath particles' entirely different behavior for large and small Pe_R reveals the richness and challenge to understanding the 'temperature' of nonequilibrium active systems. This marked change in the quantity that gets shared in active systems is due to the capability of swimmers to have run lengths $U_0\tau_R$ that can be small or large compared to their size a. This is a key fundamental difference between the swimmers' activity k_sT_s and the thermal energy k_BT. In a classical molecular fluid, k_BT is the quantity that equilibrates because the displacements of a passive Brownian particle are small compared to its size a (or any other length scale), i.e. $Pe_R^B \equiv a/(U_B\tau_B) \to \infty$ where $U_B = D_0/a$ is the characteristic speed of a Brownian step and τ_B is its momentum relaxation timescale.

Moreover, the swimmers must continuously collide with the passive particle to impart information about their kinetic activity, k_sT_s—even after many collisions, the passive particle only possesses k_BT units of thermal energy once all collisions stop. This is in stark contrast with a molecular or kinetic fluid particle that is able to completely transmit its kinetic activity to another particle upon collisions. If a molecular

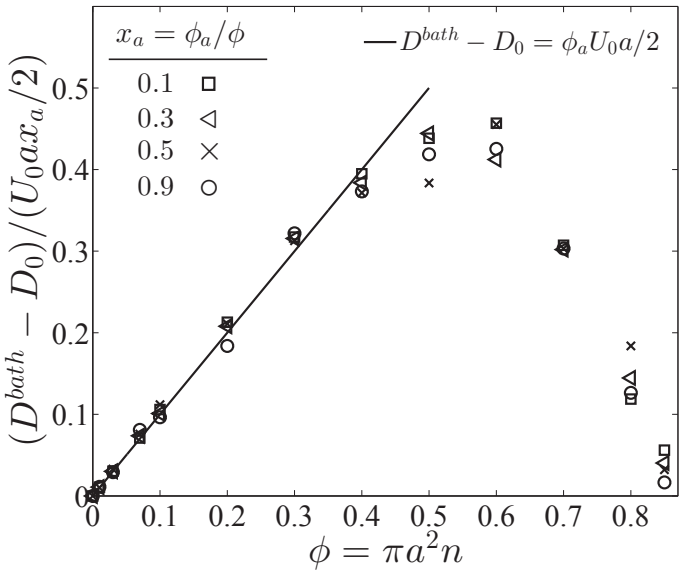

Figure 5.2: Long-time self diffusivity of a passive particle as a function of the total area fraction for different values of the active swimmer fraction x_a. The known Brownian diffusivity D_0 was subtracted from the results. The solid line is the analytical theory and symbols are Brownian dynamics (BD) simulations. All data collapse onto a single curve when the diffusivity is scaled with $U_0 a x_a/2$.

fluid particle with initially zero activity is placed inside a container full of fluid particles with energy $k_B T$, the inactive particle would collide repeatedly and eventually attain the thermal energy $k_B T$. Furthermore, it will keep its $k_B T$ activity even when the other particles are removed. In contrast, a passive particle would cease to move (aside from its translational Brownian motion) if active swimmers are removed because of the damping due to the solvent. In this sense the temperature of an active nonequilibrium fluid is not well defined, as each swimmer has its own unique intrinsic kinetic activity that does not get shared and equilibrated [5].

In pursuant of the discussion above we conducted Brownian dynamics (BD) simulations (see Appendix) and computed the long-time self diffusivity $D^{bath} = (1/2)\lim_{t\to\infty} d\langle x_d x_d\rangle/dt$, where x_d is the position of the passive bath particles. As shown in Fig 5.2, for small Pe_R we indeed find that $D^{bath} = D_0 + U_0 a\phi_a/2$ fits the data for all $\phi \lesssim 0.4$. At higher ϕ the passive particles are trapped into clusters by the swimmers and D^{bath} decays to 0. Figure 5.2 suggests that the parameter Pe_R gets shared upon swimmer collisions and not the scale $k_s T_s$.

Finally, an important concept here is that the departure induced by a swimmer is the same whether it collides into a passive particle or into another active swimmer.

In both cases the displacement due to the collision is the swimmer size a (for small Pe_R), and this is the key idea underlying the mechanical theory which we explain below.

5.3 Mechanical theory

Our theory applies in general to a mixture of active swimmers with different activity levels, but here we focus on a mixture of active swimmers and passive particles. Since a passive particle behaves equivalently to an "active" particle with a very small reorientation time and step size, this system corresponds to the limiting case of a mixture of one group of swimmers with a finite, nonzero Pe_R and another group of "swimmers" with $Pe_R \to \infty$. The general case is a mixture of active swimmers with two different, finite Pe_R^a and Pe_R^d. However, the active and passive limit is interesting from an experimental perspective because a mixture of passive and active particles is easy to make. Mixtures of swimmers with different, finite Pe_R are difficult to analyze because of the inherent variations in activity in living organisms and in synthetic self-propelled particles due to fabrication defects.

We are now in a position to derive a simple mechanical pressure theory to predict the phase behavior of a mixture of active and passive particles. The total active pressure of the mixture is given by

$$\Pi^{act} = \Pi^{swim} + \Pi_a^P + \Pi_d^P + nk_BT, \tag{5.1}$$

where Π^{swim} is the 'swim pressure,' Π_a^P and Π_d^P are the interparticle pressure contributions of the active swimmer and passive particle, respectively, and nk_BT is the Brownian osmotic pressure. It is permissible to add the separate contributions of the pressure in what appears to be a superposition; this is true in general for molecular, Brownian and active systems. Equation 5.1 is the additional pressure contribution due to the particles (both active and passive); the solvent pressure p_f is arbitrary and constant in our analyses.

In general Π^{act} is a function of $(\phi, x_a, Pe_R, k_sT_s, k_BT)$, where ϕ is the total area fraction ($\phi = \phi_a + \phi_d$), ϕ_a and ϕ_d are the area fractions of the active and passive particles, respectively, $x_a = \phi_a/\phi$ is the active swimmer composition, the reorientation Péclet number $Pe_R \equiv a/(U_0\tau_R)$ is the ratio of swimmer size a to its run length $U_0\tau_R$, $k_sT_s \equiv \zeta U_0^2\tau_R/2$ is the swimmers' characteristic 'energy scale' as discussed earlier, and k_BT is the thermal energy. We can also express the active pressure using the area fractions of the active and passive particles, $\Pi^{act}(\phi_a, \phi_d, Pe_R, k_sT_s, k_BT)$. To reduce the number of parameters, we take equal size active and passive particles

$a_a = a_d = a$ and assume that swimmer reorientation is thermally induced so that the translational and reorientational diffusivities are related via the Stokes-Einstein-Sutherland expressions: $(D_0/a^2)/\tau_R = 4/3$. Thus the ratio of the thermal energy to the swim activity is $k_BT/(k_sT_s) = 8Pe_R^2/3$. This is not a requirement; one can also vary a swim Péclet number, $Pe_s \equiv U_0 a/D_0$ in addition to the reorientation Péclet number $Pe_R \equiv a/(U_0\tau_R)$.

We now explain the independent pressure contributions in detail below. The theory is presented for 2D, but it is straightforward to generalize to 3D.

Swim pressure of active swimmers, Π^{swim}

The swim pressure is defined as the first moment of the swim force $\Pi^{swim} = -n_a\langle \boldsymbol{x} \cdot \boldsymbol{F}^{swim}\rangle/2$ (in 2D), where n_a is the number density of swimmers and the angle brackets denote an average [3]. It is permissible for computing the stress to interpret the self-propulsion of an active swimmer as arising from a swim force, $\boldsymbol{F}^{swim} \equiv \zeta \boldsymbol{U}_0$[2], where $\boldsymbol{U}_0 = U_0\boldsymbol{q}$; U_0 is the swimming speed and $\boldsymbol{q}$ is the unit orientation vector defining the swimmer's direction of self-propulsion. Physically, $\boldsymbol{F}^{swim}$ represents the force required to prevent an active swimmer from moving, for example by optical tweezers. The origin of the swim pressure stems from the notion that confined self-propelled bodies exert a pressure on the container boundaries as they collide into the surrounding walls. The same notion applies to molecular gases that collide into the container walls to exert a pressure or to colloidal solutes that collide into a semipermeable membrane to exert an osmotic pressure. The swim pressure is the "osmotic" pressure of active particles.

A dilute system of purely active swimmers exerts an 'ideal-gas' swim pressure given by $\Pi^{swim} = n_a\zeta U_0^2\tau_R/2 = n_a k_s T_s$ in 2D [3]. The swim pressure is a single-particle self contribution in which the relevant length scale (i.e. moment arm) is the swimmers' run length $U_0\tau_R$. As discussed earlier the ratio of the swimmer size a to the run length $U_0\tau_R$ is the reorientation Péclet number $Pe_R \equiv a/(U_0\tau_R)$, and this parameter impacts the phase behavior of active systems [5]. For large Pe_R the swimmers take small swim steps and behave as Brownian walkers, exerting the swim pressure $\Pi^{swim} = n_a\zeta U_0^2\tau_R/2 = n_a k_s T_s$ for all concentrations.

For small Pe_R the swimmers have large run lengths and undergo many collisions with passive particles and other swimmers in a time τ_R. The average distance trav-

[2]This however does not imply that the intrinsic swimming mechanism generates a long-range $(1/r)$ Stokes velocity field as does an external force [16, 17].

eled by a swimmer between reorientation events is reduced and the same is true for the swim pressure. Extending the results for a purely active system [5], we take (for small Pe_R)

$$\Pi^{swim} = n_a k_s T_s \left(1 - \phi - 0.2\phi^2\right), \tag{5.2}$$

where n_a is the number density of active swimmers, $k_s T_s \equiv \zeta U_0^2 \tau_R/2$ is the characteristic 'energy scale' of a swimmer. Inside the parenthesis of Eq 5.2 is the total area fraction because both active and passive particles hinder the run length of an active swimmer. Recall our discussion from Sec 5.2 that the displacement induced by a swimmer is the same whether it collides into another swimmer or a passive particle. For a dilute system $\phi \to 0$ we recover the 'ideal-gas' swim pressure $\Pi^{swim} = n_a k_s T_s$. As the area fraction increases, both passive and active particles collide and obstruct the motion of swimmers, decreasing the run length and therefore the swim pressure. The decrease in Π^{swim} is the principle destabilizing term that facilitates a phase transition in active systems. This is fundamentally different than a purely Brownian system where repulsive interactions (e.g., excluded volume) necessarily increase the pressure and have a stabilizing effect. Recall the concept that a passive Brownian particle with the thermal energy $k_B T$ is equivalent to a "swimmer" with $Pe_R^B \to \infty$. In this work we focus on small Pe_R since this is the limit that engenders interesting phase behavior in active matter.

Figure 5.3 confirms that all data from BD simulations collapse onto Eq 5.2. To better understand Eq 5.2, we can analyze the limits for large and small concentrations of active swimmers relative to passive particles. Expanding the swim pressure for small $\phi_d/\phi_a = (1 - x_a)/x_a$, we find

$$\Pi^{swim} = n_a k_s T_s \left(1 - \phi_a - 0.2\phi_a^2\right) - n_a k_s T_s (1 + 0.4\phi_a)\phi_d + O\left(\frac{\phi_d}{\phi_a}\right)^2. \tag{5.3}$$

The first term on the right is the swim pressure for a purely active system, and the second term is the leading-order correction of the hindrance provided by passive particles. As expected, it is a 2-body correction of an active swimmer colliding into a passive particle, $\sim n_a \phi_d$.

In the other limit of small concentration of active swimmers relative to passive particles (i.e., small $\phi_a/\phi_d = x_a/(1 - x_a)$), we find

$$\Pi^{swim} = n_a k_s T_s \left(1 - \phi_d - 0.2\phi_d^2\right) + O\left(\frac{\phi_a}{\phi_d}\right)^2. \tag{5.4}$$

Unlike the large active concentration limit, the reduction in the swim pressure is caused entirely by the sea of passive particles. Due to the small concentration of

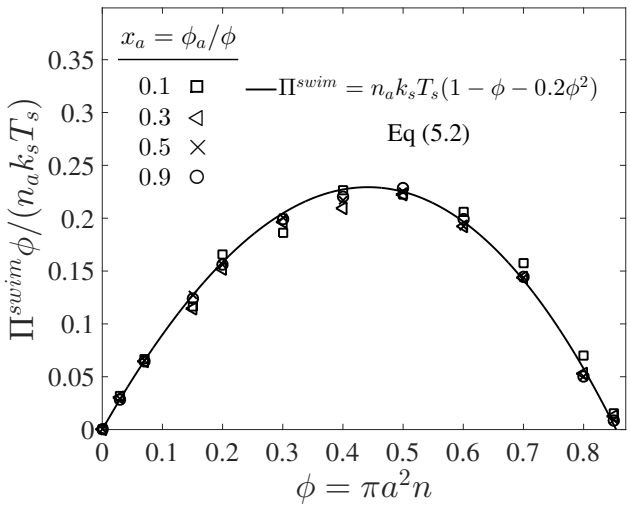

Figure 5.3: Swim pressure exerted by active swimmers in a mixture as a function of the total area fraction $\phi = \phi_a + \phi_d$ for different values of active composition $x_a = \phi_a/\phi$ and fixed $Pe_R \equiv a/(U_0\tau_R) = 0.1$. Subscripts "$a$" and "$d$" refer to active and passive particles, respectively. The solid curve is the mechanical theory Eq 5.2 and the symbols are BD simulations. The swimmer activity $k_sT_s \equiv \zeta U_0^2\tau_R/2$.

swimmers, a swimmer exerts the self-term 'ideal-gas' swim pressure $n_a k_s T_s$ but does not hinder the motion of other active swimmers.

Interparticle (collisional) pressure

In addition to the swim pressure, which is a single-particle contribution to the mechanical pressure, there is also an interparticle (or collisional) pressure arising from interactions between the particles. Since two bodies are required for an interaction (or collision for a hard-sphere potential) and the relevant length scale is the particle size a, the interparticle pressure scales as $\Pi^P \sim n^2\zeta U_0 a^3 \sim nk_sT_sPe_R\phi$, fundamentally different from the swim pressure. Furthermore, the interparticle pressure monotonically increases with concentration for a repulsive potential and helps stabilize a system. The competition between the destabilizing effect of the swim pressure and the stabilizing effect of the interparticle (or collisional) pressure controls the phase behavior of active systems. For clarity we split the interparticle pressure into two contributions—collisions induced by active swimmers and passive particles.

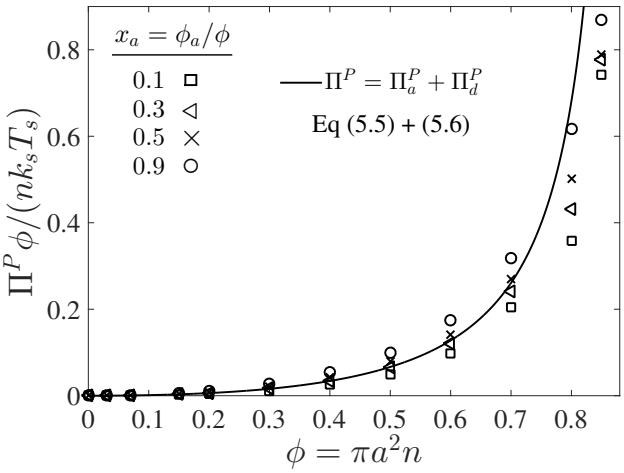

Figure 5.4: Collisional pressure exerted by active and passive particles $\Pi^P = \Pi_a^P + \Pi_d^P$ for fixed $Pe_R \equiv a/(U_0\tau_R) = 0.1$ as a function of the total area fraction $\phi = \phi_a + \phi_d$ and different values of active composition $x_a = \phi_a/\phi$. The solid curve is the mechanical theory Eq 5.5 plus Eq 5.6 for $x_a = 0.3$, and the symbols are BD simulations. We take the swimmer reorientation to be thermally induced so that $k_BT/(k_sT_s) = 8Pe_R^2/3$.

Active swimmer, Π_a^P

Extending the nonlinear microrheology analysis [3], the collisional pressure contribution for active swimmers (for small Pe_R) is

$$\Pi_a^P = n_a \left[\frac{4}{\pi} k_s T_s Pe_R + 2k_B T \right] \phi g(\phi), \tag{5.5}$$

where k_BT is the thermal energy and $g(\phi)$ is the pair-distribution function at contact. The first and second terms in the bracket are the collisional pressures due to self-propulsion and Brownian fluctuation, respectively. The former scales as $\sim n_a n\zeta U_0 a^3$ whereas the latter scales as $\sim n_a n\zeta (D_0/a) a^3$; the characteristic Brownian speed D_0/a replaces the swim speed U_0 in the collisional pressure arising from thermal noise. We again use the total area fraction in Eq 5.5 since the active swimmers impart the same departure whether they collide with a passive or an active particle. Rigorously, the pair-distribution function is different for each pair, i.e., $g_{aa}(\phi), g_{ad}(\phi)$, etc, but we assume that they are all the same and equal to $g(\phi)$ since we have taken $a_a = a_d$. We adopt $g(\phi) = (1 - \phi/\phi_0)^{-1}$, where ϕ_0 is the area fraction at close packing ($\phi_0 = 0.9$ in this study) [18, 5].

Passive particle, Π_d^P

The collisional pressure contribution of a passive particle is given by

$$\Pi_d^P = n_d \left[\frac{4}{\pi} k_s T_s Pe_R x_a + 2k_B T \right] \phi g(\phi). \tag{5.6}$$

The first term in the brackets is the interparticle pressure due to collisions with active swimmers, which scale as $n_d n_a \zeta U_0 a^3$ because these collisions are induced only by the active swimmers. The second term is the usual Brownian collisional pressure. Unlike Eq 5.5 we see that the collisional pressure of passive particles has an additional dependence on the active-swimmer fraction x_a. If there are no active swimmers (i.e., $x_a = 0$) then Eq 5.6 reduces to the usual collisional pressure of Brownian hard-spheres [19].

Figure 5.4 graphs the sum of the collisional pressures of the contributions from both active and passive particles as a function of the total area fraction. We see a dependence on the composition of active swimmers x_a especially at high area coverage. We assume that swimmer reorientation is thermally induced so that the translational and reorientational diffusivities are related via the Stokes-Einstein-Sutherland expressions, $(D_0/a^2)/\tau_R = 4/3$, and the ratio of the thermal energy to the swim activity is $k_B T/(k_s T_s) = 8Pe_R^2/3$.

5.4 Phase behavior

Experiments and computer simulations have shown that a suspension of purely active particles may self-assemble into regions of dense and dilute phases, resembling an equilibrium liquid-gas coexistence [6, 7, 8, 9, 10]. The source of this phase separation is that swimmers collide and obstruct each others' movement, causing large clusters to form at sufficiently high concentrations [13]. Now, if this active system also contained passive Brownian particles, recent computer simulations [20] and experiments [21] have shown that the composition of passive particles inside the dense cluster phase is generally larger than that in the dilute phase, as they tend to stay inside the cluster once they are pushed into one by an active swimmer. In contrast, the active swimmers prefer to swim freely in the dilute phase because their activity allows them to escape the dense clusters.

Theory and simulations have produced phase diagrams for a suspension of purely active swimmers [5, 22, 23, 15, 24, 8], but a mixture of active and passive particles is yet to be thoroughly analyzed. Recently Stenhammar et al [20] conducted Brownian dynamics simulations of a mixture of active and passive Brownian par-

ticles and used a kinetic model to locate the phase boundaries. The kinetic model based upon Redner et al [8] accurately predicts many regions of phase space, but due to the theory's inherent assumptions the lower spinodal boundary is not well characterized.

Our theory is based upon the new 'swim pressure' perspective which accurately predicts the phase behavior of a system of active swimmers [3, 5, 4]. Others have subsequently used the swim pressure to study phase-separating active systems [25, 26]. We now have Eq 5.1, an equation of state that allows us to predict the phase behavior of the active/passive mixture.

Interpreting the total density derivative of the active pressure as a global mechanical instability, $(\partial\Pi^{act}/\partial\phi)_{x_a,T_s,Pe_R} = 0$, we can identify the regions of stability in the phase diagram. This is a purely mechanical definition of the spinodal and does not rely upon thermodynamic arguments. As shown by the red curve in Fig 5.5, our prediction agrees well with Stenhammar et al's [20] simulation data. Here the spinodal and the simulation data correspond to a global dense/dilute-phase separation based upon fluctuations in the total particle–active plus passive–density. This is different from the phase separation that may occur locally within each phase, as commonly seen in immiscible polymer mixtures. There are no adjustable parameters in the comparison.

Compared to a purely active swimmer system, onset of phase transition occurs at lower Pe_R when passive particles are present. For $x_a = \phi_a/\phi = 0.5$ shown in Fig 5.5, phase transition is possible for $Pe_R \lesssim 0.025$, compared to $Pe_R \lesssim 0.04$ for a purely active system $x_a = 1$. Therefore, given a fixed total area fraction the presence of passive particles makes it more difficult for phase separation to occur, which may be an important consideration in the design of experiments of active systems.

In Sec 5.2 we discussed that the reorientation Péclet number Pe_R is the quantity that gets shared upon collisions between swimmers for $Pe_R \ll 1$. Using the swimmer activity $k_sT_s \equiv \zeta U_0^2\tau_R/2$, we can rewrite $Pe_R \equiv a/(U_0\tau_R) = \zeta U_0 a/(2k_sT_s)$, which is interpreted as the interactive energy of the swimmer $(\zeta U_0)a$ to its swim activity scale k_sT_s. In Fig 5.5 phase separation becomes possible for small Pe_R, or large k_sT_s. In contrast, phase transition in a classical thermodynamic system is usually driven by attractive enthalpic interactions and becomes possible for small k_BT (low temperatures). If k_sT_s is interpreted as the "temperature" of active matter, Fig 5.5 suggests that mixtures of active and passive particles may exhibit a lower critical

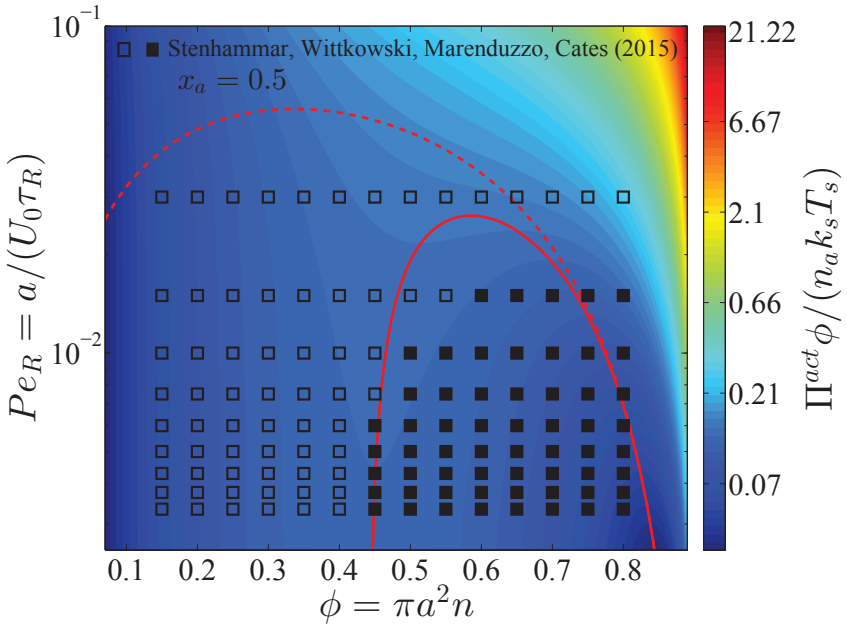

Figure 5.5: Phase diagram in the $Pe_R - \phi$ plane in 2D for a fixed active swimmer composition $x_a = 0.5$. The colorbar shows the active pressure scaled with the swim activity $k_sT_s = \zeta U_0^2\tau_R/2$. The open and filled symbols are simulation data of Stenhammar et al (Stenhammar, Wittkowski, Marenduzzo, and Cates, *Phys Rev Lett*, 2015) with a homogeneous and phased-separated state, respectively. The solid and dashed red curves are the spinodals delineating the regions of stability based upon fluctuations in the total particle density and the thermodynamic definition, respectively.

solution temperature (LCST) transition [27], commonly seen in thermosensitive polymer systems [28]. The LCST phase transition is dominated by entropy—as Pe_R decreases (k_sT_s increases), the run length of the swimmer increases, and the particle becomes effectively larger in size and has less space available for entropic mixing [5]. However, because Pe_R is the quantity that gets shared upon collisions for $Pe_R \ll 1$ (and not the activity k_sT_s), the activity k_sT_s does not play the same role as the thermal energy scale k_BT in LCST phase transitions of polymer mixtures. This further verifies that the "temperature" of active matter is an elusive quantity that does not have a direct mapping to the temperature of an equilibrium system.

5.5 Limits of active pressure

Recent experiments by Kümmel et al [21] analyzed the phase behavior of a mixture of passive particles with a small concentration of active swimmers ($\phi_a \approx 0.01$). They observed swimmers gathering and compressing the passive particles into clus-

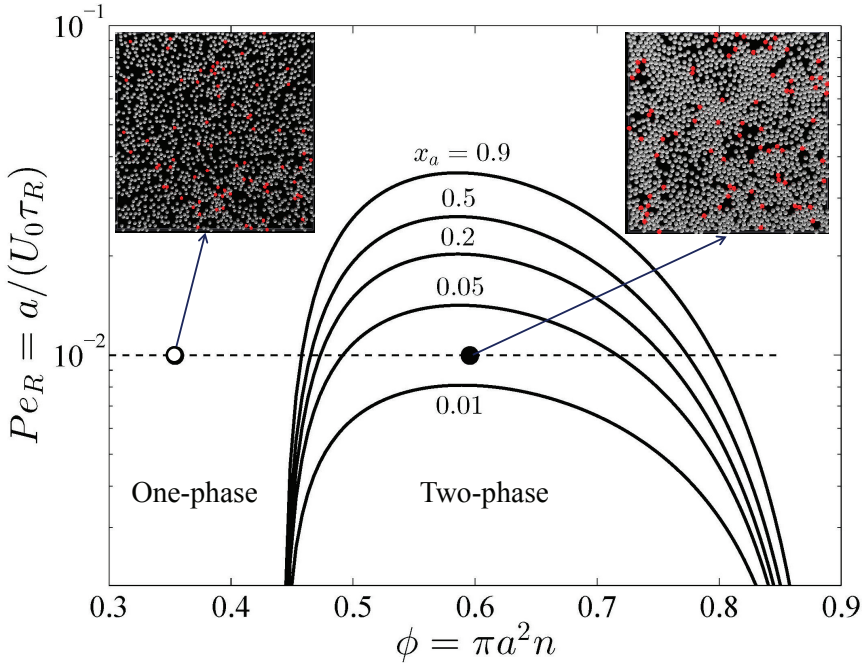

Figure 5.6: Phase diagram in the $Pe_R - \phi$ plane in 2D for different active swimmer compositions $x_a = \phi_a/\phi$. The solid curves are the spinodals delineating the regions of stability based upon fluctuations in the total particle density. The two-phase region diminishes as x_a decreases. Steady-state images from BD simulations are shown for $Pe_R = 0.01, x_a = 0.05$ at $\phi = 0.35$ (left) and $\phi = 0.6$ (right), corresponding to a homogeneous and phased-separated state, respectively. The red and white circles are the active and passive particles, respectively.

ters. By varying the concentration of passive particles, they observed a phase separation of the mixture even at very small active swimmer concentrations.

Our BD simulations agree qualitatively with the experiments [21]. The active swimmers create tunnels in the sea of passive particles, which open a path for other trailing swimmers to move through. This leads to the formation of large clusters composed of purely passive particles and individual swimmers moving in the dilute phase, as shown in simulation images in Fig 5.6. Based upon our mechanical theory, there is an equality between the Brownian collisional pressure of the dense passive clusters and the swim pressure of the dilute active swimmers compressing the crystals. A video of the BD simulation is available in the Supplementary Materials of ref [29].

To model these observations, it is instructive to analyze the limits of the active pressure for large and small concentrations of active swimmers relative to passive particles. Since the mechanical pressure exerted by a system of purely active swimmers

and purely Brownian particles is known, we can interrogate the effect of adding a small amount of passive or active particles into the suspension. This may be particularly useful for further experimental pursuits of active/passive mixtures.

In the limit of small active swimmer concentration relative to passive particles, the active pressure is

$$\Pi^{act} = \Pi^{osm} + \Pi''(\phi_d, T_s, Pe_R)\phi_a + O\left(\frac{\phi_a}{\phi_d}\right)^2, \tag{5.7}$$

where the first term on the right is the osmotic pressure of a purely Brownian suspension:

$$\Pi^{osm} = n_d k_B T \left(1 + 2\phi_d g(\phi_d)\right), \tag{5.8}$$

and the second term in Eq 5.7 is

$$\begin{aligned}\Pi''(\phi_d, T_s, Pe_R) = n_a k_s T_s \left(1 - \phi_d - 0.2\phi_d^2\right)/\phi_a + \\ 2n_d \left[\frac{4}{\pi} k_s T_s Pe_R + 2k_B T \left(2 + \frac{\phi_d}{2\phi_0} g(\phi_d)\right)\right] g(\phi_d) + n_d k_B T/\phi_d.\end{aligned} \tag{5.9}$$

In this limit, the swim pressure and swimmers' interparticle collisions appear in the leading-order correction. Taking the global density fluctuation $\partial\Pi^{act}/\partial\phi = 0$, we find that the spinodal qualitatively agrees with the experiments of Kümmel et al [21]—a lower spinodal boundary of $\phi \sim 0.45$ and the divergence of the interparticle pressure near close packing. A phase diagram in the $Pe_R - \phi$ plane for different active swimmer compositions is shown in Fig 5.6. As x_a decreases the spinodal curve lowers to smaller Pe_R because phase separation becomes more difficult to observe with a smaller fraction of swimmers. For smaller x_a, the Brownian crystals have more time to melt and dissolve into a homogeneous system, and hence the swimmer must have a small Pe_R that is in commensurate with the small x_a. Kümmel et al [21] report phase separation in swimmers with $Pe_R \approx 0.04$, but our theory suggests that Pe_R must be smaller ($Pe_R \lesssim 0.01$) for phase separation to be possible at the small concentration of active swimmers used in their study.

In the other limit of large active swimmer concentration relative to passive particles, we expect phase behavior similar to those observed in purely active suspensions [5]. The passive particles can act as nucleation sites for cluster formation, which may spark an earlier onset of phase separation. The active pressure has the form

$$\Pi^{act} = \Pi^{act}(\phi_a, \phi_d = 0, T_s, Pe_R) + \Pi'(\phi_a, T_s, Pe_R)\phi_d + O\left(\frac{\phi_d}{\phi_a}\right)^2, \tag{5.10}$$

where the first term on the right is the active pressure for a purely active swimmer suspension [5] (i.e., Eq 5.1 with $\phi_d = 0$):

$$\Pi^{act}(\phi_a, \phi_d = 0, T_s, Pe_R) = n_a k_s T_s \left(1 - \phi_a - 0.2\phi_a^2\right) + n_a \left(\frac{4}{\pi} k_s T_s Pe_R + 2k_B T\right) \phi_a g(\phi_a) + n_a k_B T, \quad (5.11)$$

and the second term in Eq 5.10 is

$$\Pi'(\phi_a, T_s, Pe_R) = -n_a k_s T_s \left(1 + 0.4\phi_a\right) + n_a \left(\frac{4}{\pi} k_s T_s Pe_R + 2k_B T\right) \left(2 + \frac{\phi_a}{\phi_0} g(\phi_a)\right) g(\phi_a) + n_a k_B T/\phi_a. \quad (5.12)$$

As expected the leading-order correction to the swim and interparticle pressures scales as $\sim n_a \phi_d$. As shown in Fig 5.6, the spinodal curve for $x_a \approx 1$ remains high because phase separation is dominated by the hindered motion of the active swimmers.

5.6 'Thermodynamic' quantities

Thermodynamic quantities like the chemical potential and free energy are defined only for equilibrium systems. However, standard macroscopic mechanical balances can be applied to define quantities that are nonequilibrium analogs for active systems [3, 5]. Here we extend the derivation of the nonequilibrium free energy and chemical potential to mixtures of active and passive particles, and interpret these quantities as a natural extension for nonequilibrium systems.

The virtual work done by an external mechanical force (i.e., stress) due to an infinitesimal change in the system volume δV is given by $\delta W = -\Pi \delta V$, where Π is the applied mechanical pressure. One can interpret this virtual work as the change in Helmholtz free energy of the system due to an applied mechanical stress, as is commonly done in elasticity theory [30]. Upon carefully imposing incompressibility of the solvent, one can relate the nonequilibrium free energy to the mechanical pressure of a multicomponent mixture as [14]

$$\Pi = -f + \sum_{i=1}^{N_c} \phi_i \frac{\partial f}{\partial \phi_i} + f(0), \quad (5.13)$$

where N_c is the number of species in the mixture and $f(0)$ is the free energy density of the pure solvent (which is arbitrary and constant in our analysis). We interpret Eq 5.13 as the definition of the free energy for nonequilibrium active systems with Π^{act}

in place of Π. For our two-component (plus the solvent) system, we have $N_c = 2$ and the nonequilibrium free energy $f^{act}(\phi_a, \phi_d, T_s, Pe_R)$ can be defined as

$$\Pi^{act} + f^{act} = \phi_a \frac{\partial f^{act}}{\partial \phi_a} + \phi_d \frac{\partial f^{act}}{\partial \phi_d}. \tag{5.14}$$

The general solution is

$$\begin{aligned} f^{act}(\phi_a, \phi_d, T_s, Pe_R) = \frac{k_s T_s}{\upsilon} \Bigg[\phi_a \log \phi_a - \phi_a \phi \left(\frac{\phi}{10} + 1 \right) - \\ 4 Pe_R \phi_0 \phi_a \log(\phi_0 - \phi) \left(\frac{1}{\pi} \left(1 + \frac{\phi_d}{\phi} \right) + \frac{4\phi}{3\phi_a} Pe_R \right) \Bigg] + \\ \frac{k_B T}{\upsilon} \left(\phi_a \log \phi_a + \phi_d \log \phi_d \right), \end{aligned} \tag{5.15}$$

where $\upsilon \equiv \pi a^2$ is the projected area of a particle. This definition for the nonequilibrium free energy agrees with the true thermodynamic free energy for molecular or colloidal solutes in solution (i.e., $f^{act}(\phi_a = 0, \phi_d, T_s, Pe_R) = f^{osm}$) [14]. To gain further insight into the free energy, in the Appendix we analyze the limits of f^{act} for our mixture for large and small concentrations of active swimmers relative to passive particles.

As done previously for a purely active system [3], we can derive the nonequilibrium chemical potential for multicomponent mixtures using purely mechanical arguments (see Appendix C). For a mixture of active and passive particles, it is given by

$$n_a \frac{\partial \mu_a^{act}}{\partial \phi} + n_d \frac{\partial \mu_d^{act}}{\partial \phi} = (1 - \phi_a - \phi_d) \frac{\partial \Pi^{act}}{\partial \phi}. \tag{5.16}$$

Again this expression agrees with the rigorous thermodynamic definition of the chemical potential for mixtures of molecular solutes in solution [14]. The chemical potential for each species i in a multicomponent system can thus be obtained from

$$\mu_i^{act} = \upsilon_i \left[\frac{\partial f^{act}}{\partial \phi_i} - \Pi^{act} \right], \tag{5.17}$$

where the reference states were absorbed into the free energy. We can invoke Eqs 5.15 and 5.1 to obtain the chemical potential for the active (μ_a^{act}) and passive (μ_d^{act}) species.

From the thermodynamics of mixtures, the stability criterion using the free energy is given by $\det(\partial^2 f / \partial \phi_i \partial \phi_j) = 0$ [14]. For our system this reduces to

$$\left(\frac{\partial^2 f^{act}}{\partial \phi_a^2} \right) \left(\frac{\partial^2 f^{act}}{\partial \phi_d^2} \right) - \left(\frac{\partial^2 f^{act}}{\partial \phi_a \partial \phi_d} \right)^2 = 0. \tag{5.18}$$

This gives us the reorientation Péclet number as a function of the active and passive concentrations, $Pe_R = Pe_R(\phi_a, \phi_d)$.

The dashed curve in Fig 5.5 is the spinodal curve using Eq 5.18 for a fixed active swimmer fraction $x_a = 0.5$. This spinodal boundary does not agree with the simulation data of Stenhammar et al [20], as Eq 5.18 predicts a different phase boundary than those observed in a simulation. The simulations reflect a global dilute/dense phase separation based upon fluctuations in the total particle (both active and passive) density. In contrast, Eq 5.18 interrogates the stability of the free energy due to fluctuations in the active particle concentration while keeping the passive particle concentration fixed, and vice versa.

This facilitates an important consideration in both experiments and simulations about which variables are held fixed and varied. Depending on the ensemble of variables that are held fixed (active swimmer density, composition, etc), the theory predicts in general different phase boundaries. To produce a phase diagram in a simulation, one typically fixes the overall swimmer composition x_a and swimmer Pe_R, and varies the total area fraction ϕ or vice versa. This corresponds to a global dense/dilute-phase separation based upon fluctuations in the total particle density, which is well described by the mechanical instability criterion $(\partial \Pi^{act}/\partial \phi)_{x_a, T_s, Pe_R} = 0$, as shown by the red solid curve in Fig 5.5.

In the experiments of Kümmel et al [21], the active swimmer area fraction ($\phi_a = 0.01$) and Péclet number ($Pe \equiv U_0\sqrt{\tau_R/D_0} = 20$) were held fixed, and the passive particle area fraction (ϕ_d) was varied. The ensemble of variables that we fix and vary must therefore be considered when we predict of the phase behavior of active mixtures. It is likely that one can conduct an experiment or simulation where the phase behavior agrees with the thermodynamic spinodal $\det(\partial^2 f/\partial\phi_i\partial\phi_j) = 0$ (red dashed curve in Fig 5.5). There remains much more to the phase portrait than the existing studies and our mechanical theory have revealed.

5.7 Conclusions

We developed a simple mechanical theory to address an important question in active matter: do active particles thermally equilibrate, and if so, what is the quantity that gets shared upon collisions? We found that the swimmers' activity $k_s T_s \equiv \zeta U_0^2 \tau_R/2$ does not have the same properties of the thermal energy $k_B T$. The swimmers' capability to have run lengths $U_0\tau_R$ small or large compared to their size a (and other length scales in the problem) distinguishes them from passive Brownian particles

whose step size is smaller than any other length scale in the system.

We discovered that for $Pe_R \equiv a/(U_0\tau_R) \ll 1$ the quantity that gets shared upon collisions is Pe_R, not the scale k_sT_s. This was seen in the simple mixing experiment in Fig 5.1 and from analyzing the motion of a passive particle as a probe to measure the kinetic activity of the swimmers (k_sT_s). The notion of the swimmers' energy k_sT_s and/or Pe_R being shared via collisions is an interesting concept that may facilitate further theoretical and experimental studies.

Another fundamental difference between an active system and a classical fluid was found by observing the motion of a passive particle in a sea of active swimmers. Even after undergoing many collisions with swimmers, the passive bath particle ceases to move (aside from its translational Brownian motion) if the swimmers are removed because of the damping by the solvent. In contrast, a passive bath particle placed inside a classical molecular or colloidal solution keeps its k_BT activity even when the other particles are removed. Because the swimmers must continuously collide into the passive bath particle to impart information about their kinetic activity, there is no "thermal equilibration" that takes place in an active suspension.

To understand the temperature and phase behavior of active matter, we studied a mixture of active and passive Brownian particles. Our theory applies more generally to a mixture of active systems with different activities. In fact, we showed that a passive Brownian particle behaves equivalently to a "swimmer" with $Pe_R \to \infty$, so the active/passive mixture corresponds to a limiting case of a mixture of active systems with different activities. A swimmer that takes small steps and reorients rapidly is indistinguishable from a purely Brownian particle if it is placed behind an osmotic barrier. For a mixture of active particles with different, finite Pe_R, we would simply write the swim and collisional pressures for each individual species $Pe_R^{(1)}, Pe_R^{(2)}$, etc. The total active pressure of the system is a sum of the contributions from all species, as in Eq 5.1.

By understanding the dependence of the active swimmer composition x_a and the total area fraction ϕ in each of the active pressure contributions, we obtained an explicit equation of state for the active/passive mixture. The key principle in deriving the equation of state was that a swimmer imparts the same displacement whether it collides into another swimmer or a passive particle. We found that the swim pressure decreases with increasing area fraction and is the destabilizing term that leads to a phase separation in active systems. In contrast, the interparticle (collisional) pressure increases monotonically with the area fraction and helps to stabilize the

suspension from phase separation. The competition between these two effects is determined by the reorientation Péclet number, $Pe_R \equiv a/(U_0\tau_R)$. The spinodal specifies the regions in the phase diagram where these two opposing effects cancel precisely, and these regions were identified in the $Pe_R - \phi$ space for our mixture.

We corroborated our theory with recent simulations [20] and experiments [21] of active/passive mixtures. Our simple model may be a useful tool for predicting phase behavior in both experiments and simulations, as many regions of phase space are difficult to explore because of experimental and computational challenges of covering the parameter space.

We found that different stability conditions give rise to different phase boundaries, facilitating considerations in simulations about which variables are held fixed and varied. The derivative of our active pressure with respect to the total area fraction predicts accurately the global dense/dilute phase transitions observed in simulations. To predict the local phase separation within the dense or dilute phase (as in immiscible polymer mixtures), a different stability criterion is required. Finally, we extended the mechanical theory to determine the nonequilibrium chemical potential and free energy for a mixture of active and passive species.

Extension of our theory to 3D and for different particle size ratios is straightforward. In 3D the characteristic activity scale becomes $k_sT_s \equiv \zeta U_0^2\tau_R/6$ instead of $\zeta U_0^2\tau_R/2$ due to the extra degree of freedom. For a mixture of particles with different sizes a and b, the pair-distribution function adjusts to different collision pairs $g_{aa}(\phi), g_{ad}(\phi)$, etc because now the particle-particle separation at contact is different. For a polydispersed active system, the large clusters are no longer crystalline and are less stable than those in a monodisperse system. Therefore the two-phase region in Fig 5.5 shrinks and shifts to smaller Pe_R.

In our model we neglected hydrodynamic interactions between the particles, which may contribute additional terms such as the "hydrodynamic stresslet" [31] to the active pressure. We also did not consider the effects of polar order and alignment of the swimmers, which are not necessary for phase-separating systems.

Appendix

A: Micromechanical equations of motion

The active particle dynamics are governed by the N-particle Langevin equation

$$\mathbf{0} = -\zeta \boldsymbol{U} + \boldsymbol{F}^{swim} + \boldsymbol{F}^{P} + \sqrt{2\zeta^2 D_0}\boldsymbol{\Lambda}_T \tag{5.19}$$

$$\frac{d\theta}{dt} = \sqrt{\frac{2}{\tau_R}}\Lambda_R, \tag{5.20}$$

where $\boldsymbol{U}$ is the translational velocity, ζ is the hydrodynamic drag factor, $\boldsymbol{F}^{swim} \equiv \zeta \boldsymbol{U}_0 = \zeta U_0 \boldsymbol{q}$ is the self-propulsive swim force, U_0 is the swim speed, θ specifies the swimmers' direction of motion $\boldsymbol{q} = (\cos\theta, \sin\theta)$, $\boldsymbol{F}^P$ is the interparticle force between the particles to enforce no overlap, $\boldsymbol{\Lambda}_T$ and Λ_R are unit random normal deviates, τ_R is the orientation time of the swimmer, and D_0 is the Stokes-Einstein-Sutherland translational diffusivity. The passive Brownian particles are governed by the same equation but without the self-propulsive force:

$$\mathbf{0} = -\zeta_d \boldsymbol{U}_d + \boldsymbol{F}^{P} + \sqrt{2\zeta_d^2 D_0}\boldsymbol{\Lambda}_T, \tag{5.21}$$

where the subscript "d" indicates a passive particle. For simplicity in this work we considered spherical particles with the same size for active and passive particles so that $\zeta = \zeta_d$. The left-hand side of Eqs 5.19 and 5.21 is zero since inertia is negligible for colloidal suspensions. A more detailed discussion concerning the origin of the swim force and the role of hydrodynamic interactions is available elsewhere [17].

B. Limits of active free energy

To gain further insight into the free energy, we analyze the limits of f^{act} for our mixture system for large and small concentrations of active swimmers relative to passive particles. Expanding the active free energy for small $\epsilon = \phi_d/\phi_a = (1 - x_a)/x_a$, we find in the limit of large active concentration

$$f^{act} = f^{act}(\phi_a, \phi_d = 0, T_s, Pe_R) + f'(\phi_a, T_s, Pe_R)\phi_d + \frac{k_B T}{\upsilon}\phi_d \log\left(\frac{\phi_d}{\phi_a}\right) + O(\epsilon^2), \tag{5.22}$$

where $\upsilon \equiv \pi a^2$ is the projected area of a particle and the first term on the right is the active free energy for a purely active system [5]:

$$f^{act}(\phi_a, \phi_d = 0, T_s, Pe_R) = \frac{k_s T_s}{\upsilon}\phi_a \left[\log\phi_a - \phi_a\left(\frac{\phi_a}{10} + 1\right) - 4Pe_R\phi_0 \log(\phi_0 - \phi_a)\left(\frac{1}{\pi} + \frac{4}{3}Pe_R\right)\right] + \frac{k_B T}{\upsilon}\phi_a \log\phi_a, \tag{5.23}$$

and the second term in Eq 5.22 is

$$f'(\phi_a, T_s, Pe_R) = \frac{k_s T_s}{\upsilon}\left[-\phi_a\left(\frac{\phi_a}{5}+1\right) - 4Pe_R\phi_0\left(\log(\phi_0-\phi_a) - \frac{\phi_a/\phi_0}{1-\phi_a/\phi_0}\right)\left(\frac{1}{\pi}+\frac{4}{3}Pe_R\right)\right] + \frac{k_B T}{\upsilon}\log\phi_a. \quad (5.24)$$

Expanding the swim pressure for small $\epsilon' = \phi_a/\phi_d = x_a/(1-x_a)$, we find in the limit of small active concentration

$$f^{act} = f^{osm} + f''(\phi_d, T_s, Pe_R)\phi_a + \frac{1}{\upsilon}(k_B T + k_s T_s)\phi_a \log\left(\frac{\phi_a}{\phi_d}\right) + O(\epsilon'^2), \quad (5.25)$$

where the first term on the right is the osmotic pressure of a purely Brownian suspension:

$$f^{osm} = \frac{k_B T}{\upsilon}\phi_d\left[\log\phi_d - \phi_0\log(\phi_0-\phi_d)\right], \quad (5.26)$$

and the second term in Eq 5.25 is

$$f''(\phi_d, T_s, Pe_R) = \frac{k_B T}{\upsilon}\left[\log\phi_d + 2\phi_0\log(\phi_0-\phi_d)\right] + \frac{k_s T_s}{\upsilon}\left[\log\phi_d - \phi_d\left(\frac{\phi_d}{10}+1\right) - \frac{8}{\pi}Pe_R\phi_0\log(\phi_0-\phi_d)\right]. \quad (5.27)$$

The influence of the swim pressure and swimmers' interparticle collisions are present in the correction term.

C. Mechanical derivation of the chemical potential for multicomponent systems

The number density of an N_c-component system[3] satisfies the conservation equation

$$\frac{\partial n}{\partial t} + \sum_{i=1}^{N_c}\nabla_i\cdot\boldsymbol{j}_i = 0, \quad (5.28)$$

where $\boldsymbol{j}_i = n_i\boldsymbol{u}_i = n_i\langle\boldsymbol{u}\rangle + \boldsymbol{j}_i^{rel}$ is the particle flux of species i, $\boldsymbol{j}_i^{rel} = n_i(\boldsymbol{u}_i - \langle\boldsymbol{u}\rangle)$ is the flux of species i relative to the suspension average velocity $\langle\boldsymbol{u}\rangle$, which is defined as $\langle\boldsymbol{u}\rangle = \sum_{i=1}^{N_c}\phi_i\boldsymbol{u}_i + (1-\phi)\boldsymbol{u}_f$, and $\boldsymbol{u}_i$ and $\boldsymbol{u}_f$ are the number averaged velocity of swimmer species i and fluid at a continuum point, respectively. The total

[3]There are $N_c + 1$ total components, including the solvent.

volume (or area) fraction of the particles is $\phi = \sum_{i=1}^{N_c} \phi_i$. Incompressibility requires the suspension-average velocity (particles plus the fluid) to satisfy $\nabla \cdot \langle \boldsymbol{u} \rangle = 0$.

We apply an averaged macroscopic mechanical momentum balance to obtain an expression for $\boldsymbol{j}_i^{rel}$. Following the standard Irving-Kirkwood approach, we obtain

$$0 = -\sum_{i=1}^{N_c} n_i \zeta_i (\boldsymbol{u}_i - \langle \boldsymbol{u} \rangle) + \nabla \cdot \boldsymbol{\sigma}^{act}, \tag{5.29}$$

where $\boldsymbol{\sigma}^{act} = \boldsymbol{\sigma}^{swim} + \boldsymbol{\sigma}^{P}$ is the active stress and the left-hand side is zero since inertia is negligible for colloidal systems. Using the relative flux $\boldsymbol{j}_i^{rel} = n_i(\boldsymbol{u}_i - \langle \boldsymbol{u} \rangle)$ we arrive at a relationship between the active particle flux and gradients in the active stress:

$$\sum_{i=1}^{N_c} \zeta_i \boldsymbol{j}_i^{rel} = \nabla \cdot \boldsymbol{\sigma}^{act}. \tag{5.30}$$

We did not rely upon the notion of a thermodynamic chemical potential or the free energy to arrive at this expression.

We can use our mechanical derivation to *define* a nonequilibrium chemical potential by analogy to the quantity whose gradient would drive a flux:

$$\boldsymbol{j}_i^{rel} = -\frac{n_i}{\zeta_i (1-\phi)} \nabla \mu_i^{act}, \tag{5.31}$$

where again $\phi = \sum_{j=1}^{N_c} \phi_j$. This definition is analogous to that of a thermodynamic system where the relative flux is driven by gradients in the thermodynamic chemical potential. Substituting Eq 5.31 into Eq 5.30 and using the definition $\Pi^{act} \equiv -\mathrm{tr}\, \boldsymbol{\sigma}^{act}/2$, we arrive at

$$\sum_{i=1}^{N_c} n_i \frac{\partial \mu_i^{act}}{\partial \phi} = (1-\phi) \frac{\partial \Pi^{act}}{\partial \phi}. \tag{5.32}$$

For a two-component (active and passive) system, we have $n_a(\partial \mu_a^{act}/\partial \phi) + n_d(\partial \mu_d^{act}/\partial \phi) = (1 - \phi_a - \phi_d)\partial \Pi^{act}/\partial \phi$, as given in the main text.

This relationship between the chemical potential and pressure is equivalent for a system of passive Brownian particles and active swimmers with small τ_R. We thus interpret μ^{act} as a natural definition and extension of the chemical potential for nonequilibrium systems.

Comparison to thermodynamics

From equilibrium thermodynamics [14], the chemical potential of species i for a multicomponent system is given by

$$\mu_i = \upsilon \left(\frac{\partial f}{\partial \phi_i} - \Pi \right), \tag{5.33}$$

where υ is the volume (or area) of a particle. The free energy is related to the osmotic pressure by

$$\phi_a \frac{\partial f}{\partial \phi_a} + \phi_d \frac{\partial f}{\partial \phi_d} = f + \Pi. \tag{5.34}$$

Taking the density derivative of both Eqs 5.33 and 5.34 and combining the results, we obtain

$$n_a \frac{\partial \mu_a}{\partial \phi} + n_d \frac{\partial \mu_d}{\partial \phi} = (1 - \phi_a - \phi_d) \frac{\partial \Pi}{\partial \phi}, \tag{5.35}$$

which is identical to Eq 5.16 of the main text, a result obtained using a mechanical derivation.

Therefore the mechanical derivations of the stress, momentum balance, and flux are in full agreement with thermodynamics.

References

[1] S. Ramaswamy. “The mechanics and statistics of active matter”. *Ann Rev Condens Matter Phys* 1.1 (2010), pp. 323–345.

[2] J. Toner, Y. Tu, and S. Ramaswamy. “Hydrodynamics and phases of flocks”. *Ann Phys* 318.1 (2005), pp. 170–244.

[3] S. C. Takatori, W. Yan, and J. F. Brady. “Swim pressure: Stress generation in active matter”. *Phys Rev Lett* 113.2 (2014), p. 028103.

[4] X. Yang, M. L. Manning, and M. C. Marchetti. “Aggregation and segregation of confined active particles”. *Soft Matter* 10.34 (2014), pp. 6477–6484.

[5] S. C. Takatori and J. F. Brady. “Towards a thermodynamics of active matter”. *Phys Rev E* 91.3 (2015), p. 032117.

[6] I. Theurkauff, C. Cottin-Bizonne, J. Palacci, C. Ybert, and L. Bocquet. “Dynamic clustering in active colloidal suspensions with chemical signaling”. *Phys Rev Lett* 108.26 (2012), p. 268303.

[7] J. Palacci, S. Sacanna, A. P. Steinberg, D. J. Pine, and P. M. Chaikin. “Living crystals of light-activated colloidal surfers”. *Science* 339.6122 (2013), pp. 936–940.

[8] G. S. Redner, M. F. Hagan, and A. Baskaran. “Structure and dynamics of a phase-separating active colloidal fluid”. *Phys Rev Lett* 110.5 (2013), p. 055701.

[9] J. Bialké, H. Löwen, and T. Speck. “Microscopic theory for the phase separation of self-propelled repulsive disks”. *Europhys Lett* 103.3 (2013), p. 30008.

[10] J. Stenhammar, A. Tiribocchi, R. J. Allen, D. Marenduzzo, and M. E. Cates. “Continuum theory of phase separation kinetics for active Brownian particles”. *Phys Rev Lett* 111.14 (2013), p. 145702.

[11] X.-L. Wu and A. Libchaber. “Particle diffusion in a quasi-two-dimensional bacterial bath”. *Phys Rev Lett* 84.13 (2000), pp. 3017–3020.

[12] D. Loi, S. Mossa, and L. F. Cugliandolo. “Non-conservative forces and effective temperatures in active polymers”. *Soft Matter* 7.21 (2011), pp. 10193–10209.

[13] M. E. Cates and J. Tailleur. “When are active Brownian particles and run-and-tumble particles equivalent? Consequences for motility-induced phase separation”. *Europhys Lett* 101.2 (2013), p. 20010.

[14] M. Doi. *Soft matter physics*. Oxford, United Kingdom: Oxford University Press, 2013.

[15] Y. Fily, S. Henkes, and M. C. Marchetti. “Freezing and phase separation of self-propelled disks”. *Soft Matter* 10.13 (2014), pp. 2132–2140.

[16] S. C. Takatori and J. F. Brady. “Swim stress, motion, and deformation of active matter: Effect of an external field”. *Soft Matter* 10.47 (2014), pp. 9433–9445.

[17] W. Yan and J. F. Brady. “The swim force as a body force”. *Soft Matter* 11.31 (2015), pp. 6235–6244.

[18] W. Russel, D. Saville, and W. Schowalter. *Colloidal dispersions*. Cambridge University Press, 1992.

[19] J. F. Brady. “Brownian motion, hydrodynamics, and the osmotic pressure”. *J Chem Phys* 98.4 (1993), pp. 3335–3341.

[20] J. Stenhammar, R. Wittkowski, D. Marenduzzo, and M. E. Cates. “Activity-induced phase separation and self-assembly in mixtures of active and passive particles”. *Phys Rev Lett* 114.1 (2015), p. 018301.

[21] F. Kümmel, P. Shabestari, C. Lozano, G. Volpe, and C. Bechinger. “Formation, compression and surface melting of colloidal clusters by active particles”. *Soft Matter* 11.31 (2015), pp. 6187–6191.

[22] J. Stenhammar, D. Marenduzzo, R. J. Allen, and M. E. Cates. “Phase behaviour of active Brownian particles: The role of dimensionality”. *Soft Matter* 10.10 (2014), pp. 1489–1499.

[23] T. Speck, J. Bialké, A. M. Menzel, and H. Löwen. “Effective Cahn-Hilliard equation for the phase separation of active Brownian particles”. *Phys Rev Lett* 112.21 (2014), p. 218304.

[24] A. Wysocki, R. G. Winkler, and G. Gompper. “Cooperative motion of active Brownian spheres in three-dimensional dense suspensions”. *Europhys Lett* 105.4 (2014), p. 48004.

[25] A. P. Solon et al. “Pressure and phase equilibria in interacting active Brownian spheres”. *Phys Rev Lett* 114.19 (2015), p. 198301.

[26] R. G. Winkler, A. Wysocki, and G. Gompper. “Virial pressure in systems of spherical active Brownian particles”. *Soft Matter* 11.33 (2015), pp. 6680–6691.

[27] R. B. Griffiths and J. C. Wheeler. “Critical points in multicomponent systems”. *Phys Rev A* 2.3 (1970), pp. 1047–1064.

[28] P. I. Freeman and J. S. Rowlinson. “Lower critical points in polymer solutions”. *Polymer* 1 (1960), pp. 20–26.

[29] S. C. Takatori and J. F. Brady. “A theory for the phase behavior of mixtures of active particles”. *Soft Matter* 11.40 (2015), pp. 7920–7931.

[30] L. Landau and E. Lifshitz. *Theory of elasticity*. 3rd ed. Vol. 7. Course of theoretical physics. Butterworth-Heinemann, 1986.

[31] D. Saintillan and M. J. Shelley. “Instabilities, pattern formation, and mixing in active suspensions”. *Phys Fluids* 20.12 (2008), pp. 123304–123315.

Chapter 6

SWIM STRESS, MOTION, AND DEFORMATION OF ACTIVE MATTER: EFFECT OF AN EXTERNAL FIELD

This chapter includes content from our previously published article:

[1] S. C. Takatori and J. F. Brady. "Swim stress, motion, and deformation of active matter: effect of an external field". *Soft Matter* 10.47 (2014), pp. 9433–9445. DOI: 10.1039/C4SM01409J.

6.1 Introduction

We analyze the stress, dispersion, and average swimming speed of self-propelled particles subjected to an external field that affects their orientation and speed. The swimming trajectory is governed by a competition between the orienting influence (i.e., taxis) associated with the external (e.g., magnetic, gravitational, thermal, nutrient concentration) field versus the effects that randomize the particle orientations (e.g., rotary Brownian motion and/or an intrinsic tumbling mechanism like the flagella of bacteria). The swimmers' motion is characterized by a mean drift velocity and an effective translational diffusivity that becomes anisotropic in the presence of the orienting field. Since the diffusivity yields information about the micromechanical stress, the anisotropy generated by the external field creates a normal stress difference in the recently developed "swim stress" tensor [1]. This property can be exploited in the design of soft, compressible materials in which their size, shape, and motion can be manipulated and tuned by loading the material with active swimmers. Since the swimmers exert different normal stresses in different directions, the material can compress/expand, elongate, and translate depending on the external field strength. Such an active system can be used as nano/micromechanical devices and motors. Analytical solutions are corroborated by Brownian dynamics simulations.

Understanding the complex dynamic behaviors of a suspension of self-propelled colloidal particles, or "active matter," has been an important but challenging problem owing to its constituents' ability to generate their own internal stress and drive the system far from equilibrium. This allows intriguing phenomena to arise that otherwise may not take place in a classical equilibrium system, like athermal self-

assembly and pattern formation [2]. Recently a new principle was introduced to study such fascinating phenomena—that is, through their self-motion all active matter systems generate an intrinsic "swim stress" that impacts their large-scale collective behavior [1]. The origin of the swim stress (or pressure) is based upon the notion that all self-propelled bodies must be confined by boundaries to prevent them from swimming away in space. The "swim pressure" is the unique pressure exerted by the swimmers as they bump into the surrounding walls that confine them. The same principle applies to molecular gases that collide into the container walls to exert a pressure or to the osmotic pressure exerted by solute molecules.

In this work we build upon this new perspective to analyze an active matter system subjected to an external field that affects its constituents' swimming orientation and speed. External fields like chemical and thermal gradients and/or the Earth's magnetic and gravitational fields can cause microorganisms to modify their swimming behavior to facilitate movement to a favorable region. For example, *E. coli* have been known to undergo chemotaxis by preferentially swimming towards (or away from) chemical gradients of nutrients (or toxins) [3]. Other examples of taxis swimmers include phototactic, [4] magnetotactic, [5] and gravitactic [6] bacteria.

External orienting fields cause the effective translational diffusivity to become anisotropic, which directly implies the existence of normal stress differences. The micromechanical stress in a dilute suspension is given by the first moment of the force, $\boldsymbol{\sigma} = -n\langle \boldsymbol{x}\boldsymbol{F} \rangle$, where n is the number density of particles and the angle brackets denote an ensemble average over all particles and time. The particle position at time t is $\boldsymbol{x}(t) = \int \boldsymbol{U}(t')\, dt'$, and from the overdamped equation of motion, $\boldsymbol{0} = -\zeta \boldsymbol{U}(t) + \boldsymbol{F}(t)$, we obtain $\boldsymbol{\sigma} = -n\langle \boldsymbol{x}\boldsymbol{F} \rangle = -n\zeta \int \langle \boldsymbol{U}(t')\boldsymbol{U}(t) \rangle\, dt' = -n\zeta \langle \boldsymbol{D} \rangle$, where ζ is the hydrodynamic drag factor and the time integral of the velocity autocorrelation is the diffusivity of the particle, $\boldsymbol{D}$. A particle undergoing any type of random motion therefore exerts a stress and a pressure, $\Pi = -\mathrm{tr}\boldsymbol{\sigma}/3 = n\zeta D$. This general result applies for Brownian particles where $D_0 = k_B T/\zeta$, leading to the familiar ideal-gas Brownian osmotic pressure $\Pi^B = nk_B T$. Using the swim diffusivity of active particles in the absence of an external field, $\langle \boldsymbol{D}^{swim} \rangle = U_0^2 \tau_R \boldsymbol{I}/6$ where U_0 is the swim speed of the active particle and τ_R is the reorientation time due to rotary Brownian motion and/or an intrinsic reorientation mechanism, we obtain the "ideal-gas" swim stress: $\boldsymbol{\sigma}^{swim} = -n\langle \boldsymbol{x}\boldsymbol{F}^{swim} \rangle = -n\zeta \langle \boldsymbol{D}^{swim} \rangle = -n\zeta U_0^2 \tau_R \boldsymbol{I}/6$, where $\boldsymbol{F}^{swim} \equiv \zeta \boldsymbol{U}_0$ is the self-propulsive force of the swimmer [1]. Although it is clear that an external field may cause the effective diffusivity and hence the swim

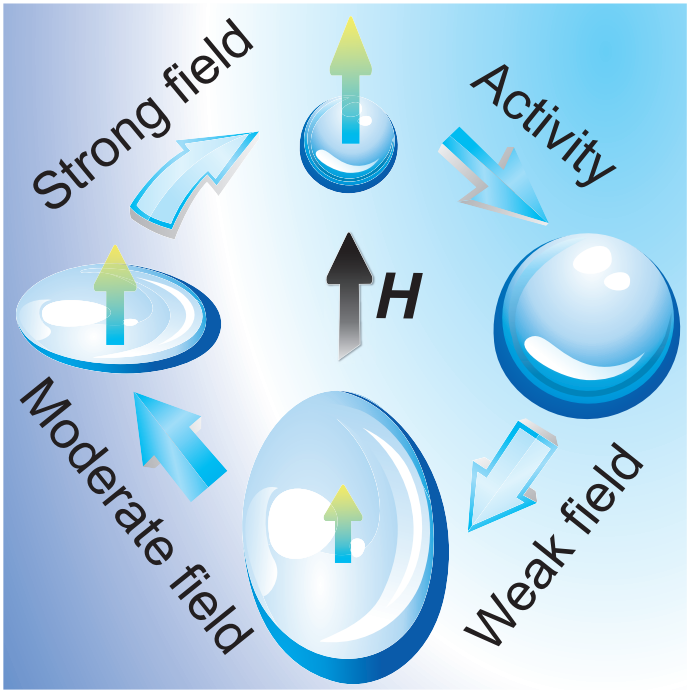

Figure 6.1: Schematic of the shape, size, and motion of a soft, compressible gel loaded with light-activated synthetic colloidal particles. When both the light and external field ($\boldsymbol{H}$) are turned on, the gel translates in the direction of the field (shown by arrows on the gel). The external field strength can be tuned to change the shape, size, and velocity of the gel.

stress to become anisotropic, how is this normal swim-stress difference generated and what are its implications on the design of novel active soft-matter materials?

To appreciate the importance of normal swim stresses, we discuss an important application of this work in the design of nano/micromechanical devices and motors. Suppose we load a soft, compressible material (e.g., gel polymer network) with light-activated synthetic colloidal particles. In the absence of light, the colloidal particles simply fluctuate due to Brownian motion, and the gel assumes some equilibrium shape as shown on the top of Fig 6.1. The equilibrium volume of the gel is determined by the balance of the force that drives the polymer to expand and mix with the solvent versus the elastic force that resists the expansion [7]. When the light is turned on, the colloidal particles become active and exert an "ideal-gas" swim pressure, $\Pi^{swim} = -\mathrm{tr}\boldsymbol{\sigma}^{swim}/3 = n\zeta U_0^2\tau_R/6$, causing the gel to expand isotropically as shown in the sketch on the right. The relative magnitudes of the swim pressure versus the shear modulus of the gel, G, determine whether the gel expands appreciably in the presence of the swimmers. In principle

the shear modulus of polymer networks can be adjusted to nearly zero. A dilute network of hydrated mucus, which behaves as a non-Newtonian gel, has shear moduli of order $\sim O(0.1 - 10)Pa$, [8, 9] but here we estimate $G \approx n_c k_B T$ where n_c is the number density of sub-chains in the network (related to the cross-link density) [7]. The energy scale associated with $1\mu m$ swimmers traveling in water with speed $U_0 \sim 10\mu m/s$ and reorienting in time $\tau_R \sim 10s$ is $\zeta U_0^2 \tau_R/6 \approx 4pN\cdot\mu m$. The thermal energy at room temperature is $k_B T \approx 4 \times 10^{-3} pN \cdot \mu m$, meaning that the swimmers' intrinsic self-propulsion is equivalent to approximately $1000 k_B T$. In practice the intrinsic activity of active synthetic colloidal particles can be even larger. The swim pressure makes an appreciable contribution to the overall size of the gel if $G/\Pi^{swim} = n_c k_B T/(n1000 k_B T) \lesssim O(1)$, or when the ratio of the polymer sub-chain density to the active-swimmer density is $n_c/n \lesssim 1000$. The swim pressure exerted at 10% volume fraction of active particles is $\Pi^{swim} = n\zeta U_0^2 \tau_R/6 \approx O(1)Pa$. For gels with a very small shear modulus, the swim pressure can cause the gel to deform its shape. As the gel expands due to the swim pressure, the concentration of swimmers decreases. The new volume of the gel is determined by the balance of the gel's expansion forces, the osmotic pressure of the polymer chains, and the swim pressure exerted by the swimmers. Even if the gel does not deform, it can still be translated and be steered using the active swimmers.

As we shall see in Section 6.6, when we apply a weak external field to the system (gel plus swimmers), the gel reacts in three ways as shown on the bottom of Fig 6.1: it expands even more due to an increase in the swim pressure; it elongates in the field direction due to a positive normal stress difference (i.e., the swimmers exert different magnitudes of normal stresses in different directions of the bounding gel network); the entire gel translates in the field direction due to the net motion of the active swimmers colliding into the gel network. Upon further increase in the external field strength, the swim pressure decreases and the normal stress difference becomes negative, which causes the gel to shrink in size, translate faster towards the field direction, and assume the shape of a thin disk as shown on the left of Fig 6.1. When the external field strength is made very high, the normal swim-stress difference and swim pressure vanish, causing the gel to return to its equilibrium shape and size but translate in the field direction.

We can make a simple estimate of the gel speed. If an active particle is tethered to a passive particle then it must drag along the passive particle as it swims. The propulsive force available to the swimmer, $\boldsymbol{F}^{swim} \equiv \zeta \boldsymbol{U}_0$, must now balance the

combined drag of the swimmer (-$\zeta \boldsymbol{U}$) and its "cargo," which is characterized by a Stokes drag coefficient ζ_C. Thus, the velocity of the combined object is $\boldsymbol{U} = \zeta \boldsymbol{U}_0/(\zeta_C + \zeta)$. If N swimmers are attached the velocity would now go as $\boldsymbol{U} = N\zeta \boldsymbol{U}_0/(\zeta_C + N\zeta)$. The same principle and estimate apply to swimmers confined to a gel. The total propulsive force available is $\boldsymbol{F} \sim nV_{gel}\zeta\langle \boldsymbol{u} \rangle$, where V_{gel} is the volume of the gel and $\langle \boldsymbol{u} \rangle$ is the mean swimmer velocity in the presence of the external field (calculated in Sections 6.4 and 6.6). This force must balance the gel and swimmers' drag $\boldsymbol{F}^{drag} = -(\zeta_{gel} + nV_{gel}\zeta)\boldsymbol{U}_{gel}$ to give $\boldsymbol{U}_{gel} \sim nV_{gel}\langle \boldsymbol{u} \rangle \zeta/\zeta_{gel}(1/(1 + nV_{gel}\zeta/\zeta_{gel}))$. The porosity and geometry of the gel would influence ζ_{gel}, but the drag is proportional to $\boldsymbol{U}_{gel}$ as in any Stokes-flow problem.

When the external field is turned off, the gel stops translating and an entire cycle is completed as depicted in Fig 6.1. Here we have assumed that the active particles are confined to the gel and that the fluid (solvent) is able to flow through the gel as needed. Instead of a gel we can also have a membrane, vesicle, fluid sack, or droplet. To ensure that the system is in osmotic balance with the solvent inside the vesicle, the surrounding membrane must be permeable to the solvent. The resistance to motion of the vesicle would now be set by the permeability of the membrane and the propulsive force determined by the number of swimmers contacting the (interior) upstream surface of the vesicle. If we had a vesicle or fluid droplet that is impermeable to the solvent, then the droplet may still deform and may also translate depending on its shape and mechanical properties of its surface or bounding membrane. A rigid object filled with fluid and swimmers would not deform nor translate; the active motion of the swimmers would set up a recirculating flow within the rigid object.

To continue in the design of nano/micromechanical devices and motors, suppose we rotate the external field by 90 degrees. For a moderate external field strength (sketched on the left of Fig 6.1), the gel reacts differently depending on the relative magnitude of the characteristic angular velocity induced by the external field, Ω_c, and the rate at which we rotate the field, Ω_{ext}. When we rotate the field slowly, $\Omega_{ext}/\Omega_c \ll 1$, the gel maintains its current shape and slowly changes its orientation with the swimmers, tracing an arc and continuing a path along the new field direction, as shown on the top of Fig 6.2. When we rotate the field quickly, $\Omega_{ext}/\Omega_c \gg 1$, the swimmers respond quickly and begin to swim in the new field direction. In this limit the gel temporarily stops translating because the swimmers do not take any swim steps between their reorientations. After the swimmers change their orienta-

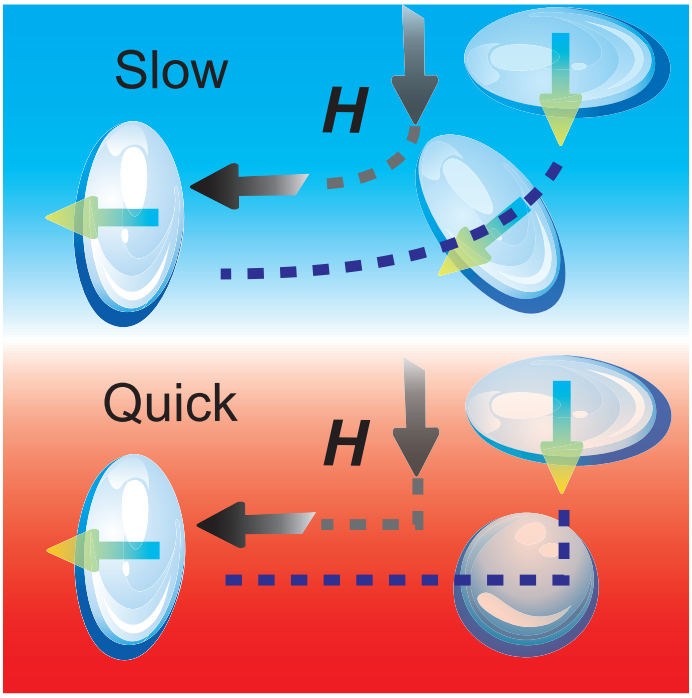

Figure 6.2: Schematic of the motion of a soft, compressible gel loaded with active particles when the external field is rotated by 90 degrees. The shape and trajectory of the gel depends on the relative rate of rotation of the field and the strength of the field.

tions toward the new field direction, the gel again assumes a disk shape and translates with the swimmers. As illustrated in Figs 6.1 and 6.2, by tuning the properties of the gel (or vesicle or drop), the activity of the swimmers, and the strength of the external orienting field, a wide range of controllable motion is possible. It is important to note that if one can measure the effective translational diffusivity of active particles in an orienting field, then the stress is known from the relationship $\boldsymbol{\sigma} = -n\zeta\langle \boldsymbol{D} \rangle$. We can thus make predictions of the shape and size of the gel based upon a simple diffusivity measurement of the swimmers.

The motion of a single particle due to an intrinsic swim force and an external force are the same. At higher concentrations or when considering the swimmer's interactions with other bodies or boundaries a distinction must be made—the intrinsic swim mechanism does not generate a long-range $1/r$ Stokes velocity field as does an external force. In our analysis we neglect hydrodynamic interactions among the particles, which would contribute additional terms to the active-particle stress and affect the reorientation time of the particles. It is important to note that the swim stress presented here is distinct and different from the "hydrodynamic

stresslet," which is also a single-particle property but scales as $\sim n\zeta U_0 a$ where a is the particle size [10, 11]. No study to date has studied the effect of an external field on the swim stress of active matter. The ratio of the magnitude of the hydrodynamic stresslet over the swim pressure is the reorientational Péclet number, $Pe_R = U_0 a/\langle D^{swim}\rangle \sim a/(U_0\tau_R)$, which compares the swimmer size a to its run length $U_0\tau_R$ [1]. The hydrodynamic contribution to the deformation of soft materials becomes negligible at low Pe_R, the regime in which many synthetic active particles operate [12, 13].

In this paper we present a micromechanical model that determines the average translational velocity, diffusivity, and swim stress of a suspension of active particles in any external field. Previous studies of the translational diffusivity of Brownian particles have used a generalized Taylor dispersion method to analyze the behavior when subjected to an external orienting field and/or a homogeneous shear flow [14, 15, 16, 17, 18]. Manela and Frankel [17] analyzed the effective translational diffusivity of dipolar swimmers subjected to a simple shear flow and an external field, and Bearon and coworkers [19, 20] extended the analysis to different flow conditions. Owing to slow numerical convergence, most studies have focused on weak external fields; in practice, however, active particles may be exposed to strong external fields, be it a chemical or thermal gradient field. As shown in this work, strong external fields are interesting because the convective enhancement to the effective translational diffusivity ($\langle D^{swim}\rangle = U_0^2\tau_R/6$) vanishes entirely. Furthermore, most studies assume a constant swimming speed of the particles, irrespective of the external field strength. In nature or in the laboratory, the local chemical and thermal environments can affect the swimming speeds of active particles. Indeed, bacteria modulate their swimming speeds when exposed to a thermal [21] or chemoattractant concentration field [22]. We address this problem by allowing the swimmers to modify their speeds based on their instantaneous orientation. Our analytical model is corroborated by Brownian dynamics (BD) simulations.

The balance between the strength of the orienting field and the effects that randomize the particle orientation is characterized by the Langevin parameter, $\chi_R = \Omega_c\tau_R$, where Ω_c is the characteristic angular velocity induced by the external field and τ_R is the reorientation time from rotary Brownian motion and/or an intrinsic reorientation mechanism. Simple dimensional reasoning provides predictions of the effect of the external field on the average swimming speed, effective translational diffusivity, and swim stress. The self-propulsive enhancement to a swim-

mer's effective translational diffusivity scales as $\langle D^{swim}\rangle \sim L_{eff}^2/\tau_R$, where L_{eff} is the effective step size. In the absence of an external field $L_{eff} \sim U_0\tau_R$, giving $\langle D^{swim}\rangle \sim U_0^2\tau_R$. With the external field in the linear response regime, the change in the effective step size, $\Delta L_{eff} \sim \chi_R U_0\tau_R$, so the change in swim stress scales as $\Delta\boldsymbol{\sigma}^{swim} = -n\zeta\langle\Delta\boldsymbol{D}^{swim}\rangle \sim -n\zeta(U_0^2\tau_R)\chi_R^2$. The average velocity along the external field scales as $\langle u_\parallel\rangle \sim L_{eff}/\tau_R \sim U_0\chi_R$, linear in the forcing. The average velocity transverse to the external field is zero for all values of χ_R: $\langle u_\perp\rangle = 0$. Thus, $\langle\boldsymbol{D}\rangle \sim D_0 + U_0^2\tau_R/6(1 + O(\chi_R^2))$ and $\boldsymbol{\sigma}^{swim} \sim -n\zeta U_0^2\tau_R/6(1 + O(\chi_R^2))$ and is anisotropic.

For $\chi_R \gg 1$, the external field is so strong that the swimmers spend most of their time oriented along the field. This suggests that the average swimmer velocity is $\langle u_\parallel\rangle \sim U_0(1 - \chi_R^{-1})$; the instantaneous swimmer velocity is the same as the average velocity, minus a small $O(\chi_R^{-1})$ correction. The effective translational diffusivity depends on the fluctuation of the swimmers' instantaneous speed from the average speed. This gives the effective step size, $L_{eff} \sim (\langle u\rangle - U_0)\tau_R$. Parallel to the external field we thus have $\sigma_\parallel^{swim} = -n\zeta\langle D_\parallel^{swim}\rangle \sim -n\zeta U_0^2\tau_R\chi_R^{-3}$. In the transverse direction, the average velocity is zero so a small fluctuation in an individual swimmer's perpendicular motion affects the dispersion more strongly than small fluctuations along the external field. This suggests that the swimmer's perpendicular velocity decays more slowly, as $u_\perp \sim O(\chi_R^{-1/2})$, giving $\sigma_\perp^{swim} = -n\zeta\langle D_\perp^{swim}\rangle \sim -n\zeta U_0^2\tau_R\chi_R^{-2}$. Interestingly, under strong external fields the swim stress and diffusivity tend to zero.

In the next section, we formulate an expression for the average translational flux, from which we deduce the swim stress and the average translational velocity and diffusivity. In section 6.3, we derive the evolution equations governing the orientation distribution and fluctuation fields. A similar approach has been used to study two-body collisions in nonlinear microrheology [23], which we extend here into orientation space. In part 6.4, we consider our first example of swimmers with uniform speeds. We build up our BD simulation framework in section 6.5 to verify the analytical theory. To obtain a more complete description, in section 6.6 we allow the swimming speeds to vary with orientation and field strength.

6.2 Average swimmer motion

We focus on the motion of a single active Brownian particle that swims in a quiescent fluid with an orientation-dependent velocity $\boldsymbol{u}(\boldsymbol{q})$, where the unit vector $\boldsymbol{q}$

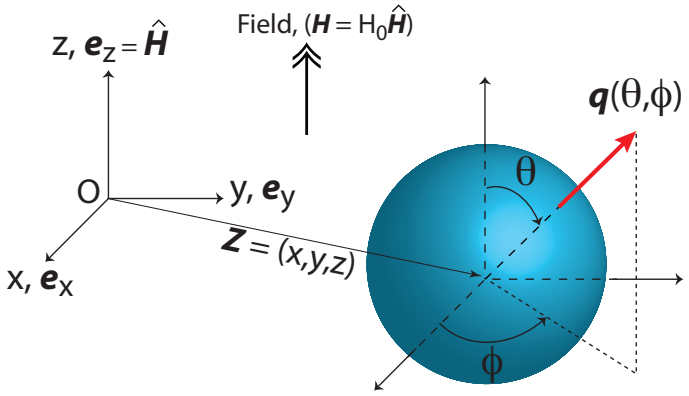

Figure 6.3: Definition sketch of an active particle at position $\boldsymbol{z}$ with orientation $\boldsymbol{q}$ in an external field, $\boldsymbol{H}$.

specifies its orientation. The swimming velocity can be a result of intrinsic self-propulsion from a living microorganism or an activated synthetic catalytic particle [2, 24]. The particle also undergoes random thermal motion with a translational diffusivity $\boldsymbol{D}_0$, and reorients due to rotary Brownian motion and/or an intrinsic mechanism (e.g., flagella), characterized by a reorientation time τ_R. For torqued swimmers like gravitactic or magnetotactic bacteria, the external field induces an orientation-dependent torque on the particle, $\boldsymbol{L}^{ext}(\boldsymbol{q})$. In contrast, force and torque-free swimmers like phototactic bacteria or other microorganisms undergoing chemotaxis or thermotaxis may possess an internal mechanism (e.g., biological sensor) to reorient themselves along the field. Our general analysis remains valid whether the reorientation is induced by an external torque or as a result of an intrinsic particle property. The dynamics of an active particle is contained in $P(\boldsymbol{z},\boldsymbol{q},t|\boldsymbol{z}_0,\boldsymbol{q}_0,t_0)$, the conditional probability of finding the particle at position $\boldsymbol{z}$ and orientation $\boldsymbol{q}$ at time t, given that it was at $\boldsymbol{z}_0$ and $\boldsymbol{q}_0$ at time t_0. This probability density obeys the Smoluchowski equation

$$\frac{\partial P}{\partial t} + \nabla \cdot \boldsymbol{j}_T + \nabla_q \cdot \boldsymbol{j}_R = 0, \tag{6.1}$$

where the translational and rotary fluxes are given by, respectively,

$$\boldsymbol{j}_T = \boldsymbol{u}(\boldsymbol{q})P - \boldsymbol{D}_0 \cdot \nabla P, \tag{6.2}$$

$$\boldsymbol{j}_R = \boldsymbol{\omega}(\boldsymbol{q})P - \frac{1}{\tau_R}\nabla_q P, \tag{6.3}$$

where $\boldsymbol{\omega}(\boldsymbol{q})$ is the orientation-dependent angular velocity of the swimmer, $\boldsymbol{D}_0$ is its Brownian translational diffusivity, and ∇ and ∇_q are the physical-space and orientation-space gradient operators, respectively.

We are interested in times $t > \tau_R$ in which all orientations have been sampled. To this end, we follow Zia and Brady [23] and introduce the Fourier transform with respect to position, denoted by $\widehat{\ }$. Averaging Eqs 6.1 and 6.2 over orientation space, we obtain

$$\frac{\partial \hat{n}(\boldsymbol{k},t)}{\partial t} + i\boldsymbol{k} \cdot \langle \widehat{\boldsymbol{j}_T} \rangle = 0, \tag{6.4}$$

$$\langle \widehat{\boldsymbol{j}_T} \rangle = \int \boldsymbol{u} \hat{P} \, d\boldsymbol{q} - \boldsymbol{D}_0 \cdot i\boldsymbol{k}\hat{n}, \tag{6.5}$$

where $\hat{n}(\boldsymbol{k},t) \equiv \int \hat{P}(\boldsymbol{k},\boldsymbol{q},t) \, d\boldsymbol{q}$ is the local number density of active particles. We introduce $\hat{P}(\boldsymbol{k},\boldsymbol{q},t) = g(\boldsymbol{k},\boldsymbol{q},t)\hat{n}(\boldsymbol{k},t)$, and focus on the orientation distribution through the structure function $g(\boldsymbol{k},\boldsymbol{q},t)$. For the long-time self-diffusion we consider the short wave vector (long length scale) limit [23] and thus expand for small $\boldsymbol{k}$: $g(\boldsymbol{k},\boldsymbol{q},t) = g_0(\boldsymbol{q},t) + i\boldsymbol{k} \cdot \boldsymbol{d}(\boldsymbol{q},t) + O(\boldsymbol{k}\boldsymbol{k})$. The field g_0 is the orientation distribution function, and $\boldsymbol{d}$ is the probability-weighted displacement or fluctuation of a particle about its mean velocity (i.e., the strength and direction of the swimmer's displacement due to the external field). Readers familiar with Brenner's [25] generalized Taylor dispersion theory will notice that g_0 and $\boldsymbol{d}$ are similar to his P_0^∞ and $\boldsymbol{B}$ fields, respectively. Introducing this expansion into Eq 6.5, we obtain the mean particle translational flux:

$$\langle \widehat{\boldsymbol{j}_T} \rangle = \hat{n} \left[\langle \boldsymbol{u} \rangle - i\boldsymbol{k} \cdot \langle \boldsymbol{D} \rangle \right], \tag{6.6}$$

where the average translational velocity and diffusivity are, respectively,

$$\langle \boldsymbol{u} \rangle = \int \boldsymbol{u}(\boldsymbol{q}) g_0 \, d\boldsymbol{q}, \tag{6.7}$$

$$\langle \boldsymbol{D} \rangle - \boldsymbol{D}_0 = \langle \boldsymbol{D}^{swim} \rangle = \int \left(\langle \boldsymbol{u} \rangle - \boldsymbol{u}(\boldsymbol{q}) \right) \boldsymbol{d} \, d\boldsymbol{q}. \tag{6.8}$$

In Eq 6.8 the term $\langle \boldsymbol{u} \rangle$ was inserted to emphasize that it is the velocity fluctuation that generates dispersion.

In the Introduction we derived a direct relationship between the translational diffusivity and the micromechanical stress: $\boldsymbol{\sigma} = -n\zeta \langle \boldsymbol{D} \rangle$. Substituting Eq 6.8 into this expression gives the stress generated by the active particle, $\boldsymbol{\sigma} = \boldsymbol{\sigma}^B + \boldsymbol{\sigma}^{swim}$, where we identify the Brownian osmotic stress as $\boldsymbol{\sigma}^B = -n\zeta \boldsymbol{D}_0 = -nk_BT\boldsymbol{I}$, and the swim stress as the convective enhancement to the diffusivity (right-hand side of Eq 6.8):

$$\boldsymbol{\sigma}^{swim} = -n\zeta \int \left(\langle \boldsymbol{u} \rangle - \boldsymbol{u}(\boldsymbol{q}) \right) \boldsymbol{d} \, d\boldsymbol{q}. \tag{6.9}$$

Equations 6.7 to 6.9 are the main results we wish to determine. The swim pressure is given by $\Pi^{swim} = -\text{tr}\boldsymbol{\sigma}^{swim}/3$ and is interpreted as the average normal swim stress (i.e., the confinement forces) necessary to prevent an active body from swimming away in space [1].

6.3 Non-equilibrium orientation and fluctuation fields

We now develop the evolution equations governing the orientation-distribution function g_0 and the fluctuation field $\boldsymbol{d}$ for use in Eqs 6.7 to 6.9. From the Smoluchowski Eq 6.1, $g(\boldsymbol{k},\boldsymbol{q},t)$ satisfies

$$\frac{\partial g}{\partial t} + \nabla_q \cdot (\boldsymbol{\omega}(\boldsymbol{q})g) - \frac{1}{\tau_R}\nabla_q^2 g = g\, i\boldsymbol{k} \cdot [\langle \boldsymbol{u} \rangle - \boldsymbol{u}(\boldsymbol{q}) - i\boldsymbol{k} \cdot (\langle \boldsymbol{D} \rangle - \boldsymbol{D}_0)], \qquad (6.10)$$

where g is finite on the unit sphere and is normalized: $\int g(\boldsymbol{k},\boldsymbol{q},t)\, d\boldsymbol{q} = 1$.

To proceed we need a form of $\boldsymbol{\omega}(\boldsymbol{q})$, the rotary velocity that reorients the biased swimmer along the external field or gradient, $\boldsymbol{H}$. For force and torque-free swimmers, like microorganisms undergoing phototaxis, chemotaxis, and/or thermotaxis, we assume that they possess an intrinsic mechanism (e.g., biological sensor) to reorient themselves along $\boldsymbol{H}$. A simple expression for the rotary velocity that models this behavior is $\boldsymbol{\omega}(\boldsymbol{q}) = \Omega_c \boldsymbol{q} \times \hat{\boldsymbol{H}}$, where Ω_c is the magnitude of the angular velocity and $\hat{\boldsymbol{H}}$ is the unit vector along the field. This expression implies that the swimmer attains the maximum rotary velocity when $\boldsymbol{q} \perp \hat{\boldsymbol{H}}$ and zero rotary velocity when $\boldsymbol{q} \parallel \hat{\boldsymbol{H}}$. Another common class of swimmers, like magnetotactic or gravitactic bacteria, reorient themselves owing to a torque induced by the external field, $\boldsymbol{\omega}(\boldsymbol{q}) = \boldsymbol{M}_R \cdot \boldsymbol{L}^{ext}$, where $\boldsymbol{M}_R$ is the rotary mobility tensor. Following Brenner and Condiff [26], one can show that this leads to the same expression as that of the torque-free swimmers. This implies that the detailed reorientation mechanism is unimportant, and both types of swimmers can be modeled with the same expression for the rotary velocity. When analyzing the motion of a single particle, there is no distinction between rotation caused by an external torque and motion arising inherently from the swimmer.

The equations are made dimensionless by scaling $\boldsymbol{u} \sim U_0, \boldsymbol{\omega}(\boldsymbol{q}) \sim \Omega_c$, and $\boldsymbol{d} \sim U_0\tau_R$. Using the small-$\boldsymbol{k}$ expansion and considering a spherical particle with a constant, isotropic Brownian diffusivity, the steady-state orientation distribution function satisfies a convection-diffusion equation:

$$\nabla_q^2 g_0 - \chi_R \nabla_q \cdot \left[(\boldsymbol{q} \times \hat{\boldsymbol{H}}) g_0 \right] = 0, \qquad (6.11)$$

with $\int g_0 \, d\boldsymbol{q} = 1$, and $\chi_R \equiv \Omega_c \tau_R$ is the Langevin parameter. The $\boldsymbol{d}$-field satisfies a similar equation, but is forced by deviations from the mean velocity:

$$\nabla_q^2 \boldsymbol{d} - \chi_R \nabla_q \cdot \left[(\boldsymbol{q} \times \hat{\boldsymbol{H}}) \boldsymbol{d} \right] = -g_0 \left(\langle \boldsymbol{u} \rangle - \boldsymbol{u}(\boldsymbol{q}) \right). \tag{6.12}$$

6.4 Uniform swimming velocity

In this section, we assume all particles have the nondimensional swim velocity $\boldsymbol{u}(\boldsymbol{q}) = \boldsymbol{q}$. We shall see in section 6.6 that allowing the speed to change with orientation leads to additional interesting dispersive effects. Equations 6.11 and 6.12 have exact analytical solutions, but we first consider the limiting behaviors at low and high χ_R.

$\chi_R \ll 1$ limit

As shown in Appendix A, we apply a regular perturbation to obtain $g_0(\boldsymbol{q}) = 1/(4\pi) + \hat{\boldsymbol{H}} \cdot \boldsymbol{P}_1(\boldsymbol{q}) \chi_R/(4\pi) + \hat{\boldsymbol{H}}\hat{\boldsymbol{H}} : \boldsymbol{P}_2(\boldsymbol{q}) \chi_R^2/(12\pi) + O(\chi_R^3)$, where $\boldsymbol{P}_n(\boldsymbol{q})$ are the n^{th}-order tensor surface spherical harmonics [27]. This is identical to Almog and Frankel's [15] result who considered the sedimentation of axisymmetric non-centrosymmetric particles by gravity. Whether the orienting torque is caused by shape-dependent gravitational settling or from dipole-induced alignment, the orientation distribution is the same.

Substituting this solution into Eq 6.7, the average translational velocity of the swimmers at low χ_R is

$$\langle \boldsymbol{u} \rangle = \frac{1}{3} \chi_R \hat{\boldsymbol{H}} + O(\chi_R^3). \tag{6.13}$$

The average velocity increases linearly with χ_R, as predicted from simple scaling arguments. As $\chi_R \to 0$ the orientation distribution becomes uniform, resulting in no net swimming speed.

To obtain a leading-order correction in the swim stress and translational diffusivity, we must proceed to the $O(\chi_R^2)$ $\boldsymbol{d}$-field problem. Substituting the $\boldsymbol{d}$-field solution (see Appendix A) into Eqs 6.8 and 6.9, we obtain the swim diffusivity and stress for $\chi_R \ll 1$:

$$\boldsymbol{\sigma}^{swim} = -n\zeta \langle \boldsymbol{D}^{swim} \rangle = -\frac{n\zeta U_0^2 \tau_R}{6} \left[\boldsymbol{I} - \frac{6}{5} \chi_R^2 \left(\frac{7}{27} \hat{\boldsymbol{H}}\hat{\boldsymbol{H}} + \frac{1}{8} \left(\boldsymbol{I} - \hat{\boldsymbol{H}}\hat{\boldsymbol{H}} \right) \right) \right] + O(\chi_R^4). \tag{6.14}$$

We have adopted the transversely isotropic form, where $\hat{\boldsymbol{H}}\hat{\boldsymbol{H}}$ and $\boldsymbol{I} - \hat{\boldsymbol{H}}\hat{\boldsymbol{H}}$ correspond to the parallel and perpendicular components relative to the field direction, respectively. As $\chi_R \to 0$ we recover the "ideal-gas" swim pressure,

$\Pi^{swim} = n\zeta U_0^2 \tau_R/6$ [1]. The first effect of the external field appears at $O(\chi_R^2)$, in agreement with our scaling arguments in the Introduction. Notice that the external field causes a decrease in the translational diffusivity, in contrast to the increase seen in the sedimentation problem [15]. The dispersion decreases here because the particles now swim collectively toward $\hat{\boldsymbol{H}}$, reducing their tendency to take random swim steps.

$\chi_R \gg 1$ limit

A singular perturbation scheme is required for $\chi_R \gg 1$ because the problem separates into an outer and inner region. Near $\mu \equiv \hat{\boldsymbol{H}} \cdot \boldsymbol{q} \approx 1$ there is an orientation-space boundary layer and the angular coordinate is rescaled as $\hat{\mu} = (1 - \mu)\chi_R \sim O(1)$. To leading order, g_0 and $\boldsymbol{d}$ are zero in the outer region because the orientation of the swimmer is confined to a $1/\chi_R$-thick "cone" around $\mu \approx 1$. As shown in Appendix B, the leading-order boundary-layer solution to Eq 6.11 is $g_0(\hat{\mu}; \chi_R) = \chi_R e^{-\hat{\mu}}/(2\pi) + O(1)$. As $\chi_R \to \infty$, the orientation distribution approaches a delta-function peaked at $\hat{\mu} = 0$, confining the swimming trajectory to a narrow "cone" about the field direction. From Eq 6.7, the average translational velocity is $\langle \boldsymbol{u} \rangle = \left(1 - \chi_R^{-1}\right) \hat{\boldsymbol{H}}$. To leading order, all swimmers move along the field direction, $\hat{\boldsymbol{H}}$, at the same speed, U_0.

The $\boldsymbol{d}$-field problem is resolved into a direction parallel ($d_\parallel$) and perpendicular ($d_\perp$) to the external field. The swim diffusivity and stress for $\chi_R \gg 1$ are

$$\boldsymbol{\sigma}^{swim} = -n\zeta \langle \boldsymbol{D}^{swim} \rangle = -n\zeta U_0^2 \tau_R \left[\frac{1}{2} \chi_R^{-3} \hat{\boldsymbol{H}} \hat{\boldsymbol{H}} + \chi_R^{-2} \left(\boldsymbol{I} - \hat{\boldsymbol{H}} \hat{\boldsymbol{H}} \right) \right]. \tag{6.15}$$

As $\chi_R \to \infty$, the swim stress vanishes entirely, including the "ideal-gas" pressure $\Pi^{swim} = n\zeta U_0^2 \tau_R/6$ that was present at low χ_R (see Eq 6.14). Since all particles are oriented along a $1/\chi_R$-thick "cone" about the field, each particle swims at the same velocity U_0 towards the same direction, resulting in a vanishingly small dispersion. Since it is the random diffusion of a particle that gives rise to a swim pressure, $\Pi^{swim} = n\zeta \mathrm{tr} \langle \boldsymbol{D}^{swim} \rangle/3$, a small diffusivity results in a small swim pressure. Another way to understand this is to suppose that the bounding walls in a simulation cell were translating with the average particle velocity, $\langle \boldsymbol{u} \rangle$. As $\chi_R \to \infty$, all particles are swimming with the same speed in the same direction so no confinement pressure is required to contain the particles inside the simulation cell [1].

Exact solution for arbitrary χ_R

As given in Appendix C, the solution to Eq 6.11 for arbitrary χ_R is

$$g_0(\mu;\chi_R) = \frac{\chi_R}{4\pi \sinh \chi_R} e^{\mu\chi_R}, \tag{6.16}$$

where $\mu \equiv \hat{\boldsymbol{H}} \cdot \boldsymbol{q}$ as before in the domain $-1 \leq \mu \leq 1$. From Eq 6.7, the average translational velocity for arbitrary χ_R is

$$\langle \boldsymbol{u} \rangle = \left(\coth \chi_R - \chi_R^{-1} \right) \hat{\boldsymbol{H}} \equiv \mathcal{L}(\chi_R) \hat{\boldsymbol{H}}, \tag{6.17}$$

where $\mathcal{L}(\chi_R)$ is the Langevin function. As expected, the average perpendicular velocity is zero for all χ_R. We resolve the corresponding displacement field in Eq 6.12 into the parallel and perpendicular directions. As shown in Appendix C, the parallel direction has an exact solution. In the perpendicular direction, we expand our solution as a series of associated Legendre polynomials. Finally, the effective translational diffusivity and swim stress are obtained from Eqs 6.8 and 6.9.

6.5 Brownian dynamics (BD) simulations

The motion of active particles in an external field can also be analyzed via BD simulations. The system follows the N-particle Langevin equations: $\boldsymbol{0} = -\zeta(\boldsymbol{U} - \boldsymbol{U}_0) + \boldsymbol{F}^B$ and $\boldsymbol{0} = -\zeta_R \boldsymbol{\Omega} + \boldsymbol{L}^{ext} + \boldsymbol{L}^R$, where $\boldsymbol{U}$ and $\boldsymbol{\Omega}$ are the translational and angular velocities, $\boldsymbol{F}^{swim} \equiv \zeta \boldsymbol{U}_0$ is the self-propulsive force, $\boldsymbol{F}^B$ is the Brownian force, ζ_R is the hydrodynamic resistance coupling angular velocity to torque, and $\boldsymbol{L}^{ext}$ and $\boldsymbol{L}^R$ are the torques induced by the external field and rotary Brownian motion and/or an intrinsic reorientation mechanism, respectively. The left-hand sides are zero because inertia is negligible for colloidal dispersions.

The Brownian force and reorientation torque have the white noise statistics $\overline{\boldsymbol{F}^B} = \boldsymbol{0}$, $\overline{\boldsymbol{F}^B(0)\boldsymbol{F}^B(t)} = 2k_BT\zeta\delta(t)\boldsymbol{I}$, $\overline{\boldsymbol{L}^R} = \boldsymbol{0}$, and $\overline{\boldsymbol{L}^R(0)\boldsymbol{L}^R(t)} = 2\zeta_R^2\delta(t)\boldsymbol{I}/\tau_R$. Particle orientations were updated by relating $\boldsymbol{\Omega}$ to the instantaneous orientation $\boldsymbol{q}$ [28]. We varied the Langevin parameter χ_R and analyzed the motion of a single active particle for over 4000 realizations and for at least $100\tau_R$.

The average translational velocity and diffusivity are given by $\langle \boldsymbol{u} \rangle = d\langle \boldsymbol{x} \rangle/dt$ and $\langle \boldsymbol{D} \rangle = \lim_{t\to\infty} d\langle \boldsymbol{x}'\boldsymbol{x}' \rangle/(2dt)$, where $\boldsymbol{x}' = \boldsymbol{x} - \langle \boldsymbol{u} \rangle \Delta t$ is the displacement of the swimmer from the mean motion. The swim stress was computed from $\boldsymbol{\sigma}^{swim} = -n\zeta\langle \boldsymbol{x}'\boldsymbol{F}^{swim'} \rangle$, where $\boldsymbol{F}^{swim'} = \boldsymbol{F}^{swim} - \langle \boldsymbol{F}^{swim} \rangle$. The average swim force over all realizations, $\langle \boldsymbol{F}^{swim} \rangle$, must be subtracted to account for the drift velocity of the particles caused by the external field.

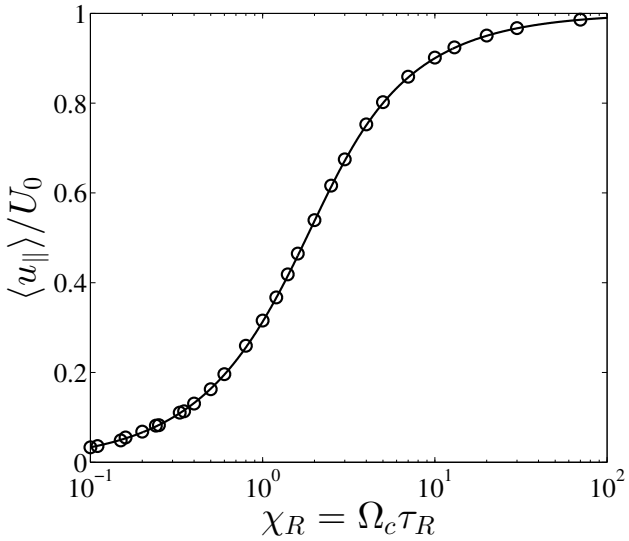

Figure 6.4: Average translational velocity along the external field as a function of χ_R. The solid curve is the exact analytical solution, and the circles are data from Brownian dynamics (BD) simulations.

Results

Both the asymptotic and exact solutions of the Smoluchowski equation and BD simulation results are presented here together. Figure 6.4 shows the nondimensional average swimmer velocity along the external field as a function of χ_R. The average velocity increases linearly following Eq 6.13 for low χ_R, and approaches 1 as $\chi_R \to \infty$. There is no average speed transverse to the external field.

In the BD simulations, the swim stress was computed using two methods. One approach is to use the definition of the swim stress, $\boldsymbol{\sigma}^{swim} = -n\langle \boldsymbol{x'F}^{swim'} \rangle$ (shown in circles in Fig 6.5). The alternative method is to first calculate the long-time self diffusivity of an active particle and then obtain the swim stress using the relationship $\boldsymbol{\sigma}^{swim} = -n\zeta\langle \boldsymbol{D}^{swim} \rangle$ (shown in squares). The two methods give identical results, verifying that for a single particle the stress is indeed directly related to the diffusivity, $\boldsymbol{\sigma} = -n\zeta\langle \boldsymbol{D} \rangle$. Here we present results for the stress, but the effective translational diffusivity can be obtained by simply dividing the stress by $-n\zeta$.

For $\chi_R \ll 1$, the swim stress reduces to the ideal-gas swim pressure [1]. The swim stress then decreases as $\sim O(\chi_R^2)$ following Eq 6.14. At intermediate values of χ_R (≈ 2), the curves decline as $\sim O(\chi_R^{-1})$, which means that the dispersion is controlled by convective rotation, i.e., $\boldsymbol{\sigma}^{swim} \sim -n\zeta U_0^2 \tau_R \chi_R^{-1} \sim -n\zeta U_0^2/\Omega_c$. The diffusivity continues to decay at high χ_R following Eq 6.15. An interesting feature

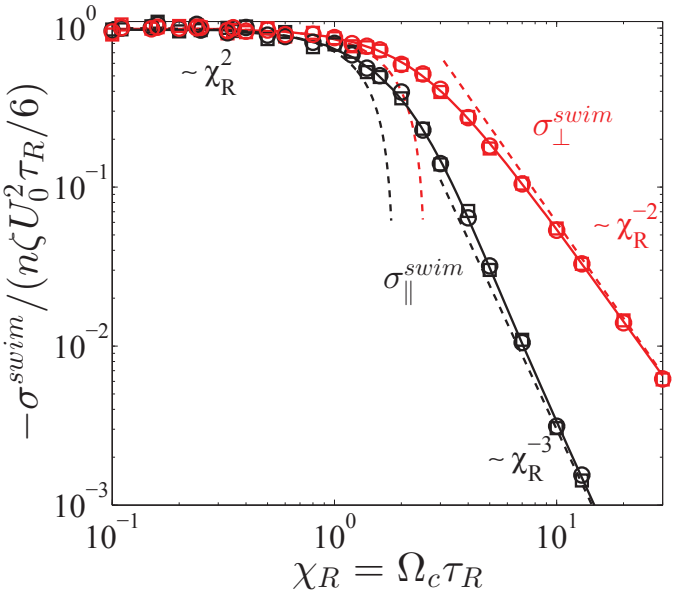

Figure 6.5: The swim stress in the parallel (in black) and perpendicular (in red) directions as a function of χ_R, computed in the simulations from $\boldsymbol{\sigma}^{swim} = -n\langle \boldsymbol{x'F}^{swim'}\rangle$ (in circles) and also from first obtaining the effective translational diffusivity and then using $\boldsymbol{\sigma}^{swim} = -n\zeta\langle \boldsymbol{D}^{swim}\rangle$ (in squares). The solid and dashed curves are the exact and asymptotic analytical solutions, respectively.

at high χ_R is the faster decay of $\sigma_\parallel^{swim} \sim O(\chi_R^{-3})$ than $\sigma_\perp^{swim} \sim O(\chi_R^{-2})$. This can be explained by considering the driving force for dispersion, $\Delta\boldsymbol{u} = \langle \boldsymbol{u}\rangle - \boldsymbol{u}(\boldsymbol{q})$. Gradients in $\Delta\boldsymbol{u}$ determine the driving force for dispersion: $d\Delta u_\parallel/d\hat{\mu} \sim \chi_R^{-1}$ and $d\Delta u_\perp/d\hat{\mu} \sim \chi_R^{-1/2}\hat{\mu}^{-1/2}$. The parallel direction has a small driving force for all $\hat{\mu}$ because an individual particle's instantaneous velocity is the same as the mean, $\langle u_\parallel\rangle$. A very large fluctuation is required to generate an appreciable contribution to the parallel diffusivity. In contrast, the gradient is maximized at $\hat{\mu} = 0$ in the perpendicular direction because the mean transverse velocity is zero. A small fluctuation in the perpendicular direction contributes more to the dispersion than in the parallel direction, so $\sigma_\parallel^{swim}$ decays faster than does $\sigma_\perp^{swim}$.

Figure 6.5 shows that the swim stress tensor is anisotropic, which allows us to identify the first normal swim-stress difference: $N_1 = \sigma_\parallel^{swim} - \sigma_\perp^{swim}$. Remarkably, this normal swim-stress difference is a *single-particle* property that arises uniquely from the biased motion of an active particle. As shown in Fig 6.6, N_1 goes to zero for $\chi_R \to 0$ since the swim stress tensor becomes isotropic. It also goes to zero for $\chi_R \to \infty$ because the swim stress decays to zero in both the parallel and perpendicular directions (see Eq 6.15). It reaches a maximum at intermediate

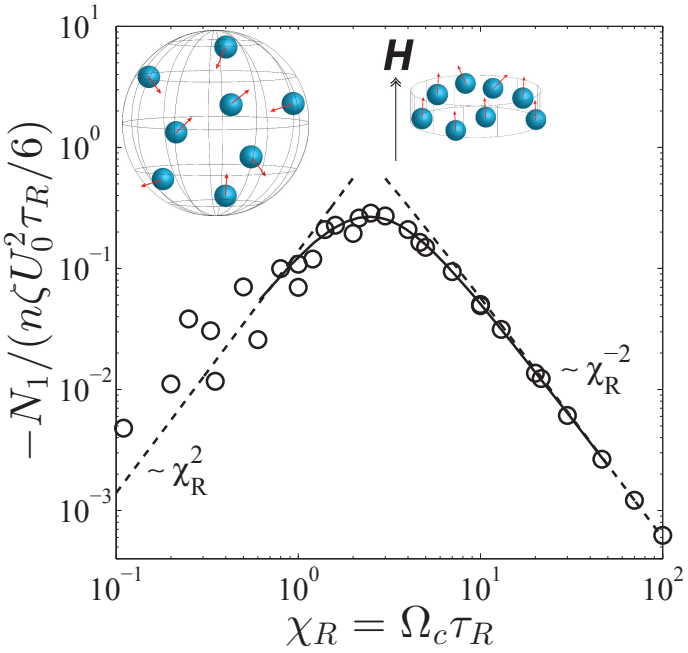

Figure 6.6: The first normal swim-stress difference, $N_1 = \sigma_{\parallel}^{swim} - \sigma_{\perp}^{swim}$, as a function of χ_R. The circles are results from BD simulations, and the solid and dashed curves are the exact and asymptotic analytical solutions, respectively. The illustration shows an instantaneous configuration of the swimmers under a weak (sketch on left) and moderate (on right) external field.

values of χ_R owing to the rapid decay of the swim stress in the parallel direction ($\sigma_{\parallel}^{swim} \sim O(\chi_R^{-3})$). Due to axisymmetry the second normal swim-stress difference is zero for all χ_R.

An anisotropic $\boldsymbol{\sigma}^{swim}$ means that the confining force required to contain the swimmers by the bounding walls would be different in the parallel and perpendicular directions. The swim pressure represents the average of the normal swim stresses (i.e., confinement pressure) exerted on the bounding walls: $\Pi^{swim} = -\mathrm{tr}\boldsymbol{\sigma}^{swim}/3$ [1]. As shown in Fig 6.7, the swim pressure approaches the "ideal-gas" value as $\chi_R \to 0$: $\Pi^{swim} = n\zeta U_0^2\tau_R/6$. At higher χ_R, the swim pressure decreases since the external field confines the swimming trajectories along the field direction, reducing the confinement pressure on the surrounding walls.

Since normal stress differences indicate how a soft material might elongate or shrink, results from Figs 6.6 and 6.7 can be exploited in the design of various novel active soft materials. Using the results of this section we can now describe how a polymer network (e.g., a gel) loaded with active particles with uniform swim speeds behaves in the presence of an external field. In the absence of the external field, the

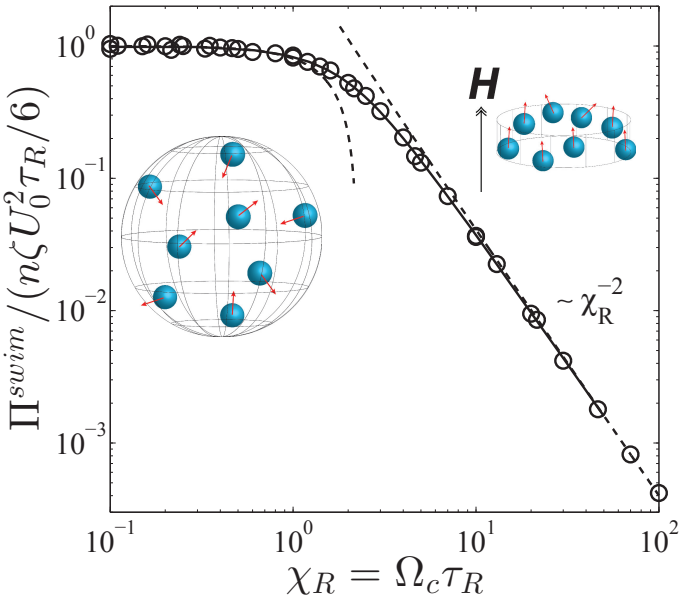

Figure 6.7: The swim pressure, $\Pi^{swim} = -\mathrm{tr}\boldsymbol{\sigma}^{swim}/3$, as a function of χ_R. The circles are results from BD simulations, and the solid and dashed curves are the exact and asymptotic analytical solutions, respectively. The illustration shows an instantaneous configuration of the swimmers under a weak (sketch on left) and moderate (on right) external field.

active particles exert an equal magnitude of normal stress in all directions of the gel, namely $\boldsymbol{\sigma}^{swim} = -n\zeta U_0^2\tau_R\boldsymbol{I}/6$. Upon turning on the external field, the gel shrinks due to the decrease in swim pressure (see Fig 6.7), assumes the shape of a thin 3D disk due to the negative normal stress difference (see Fig 6.6), and the gel translates due to the average velocity of the swimmers (see Fig 6.4). Such a device can be used as a mechanical device/motor where its shape, size, and motion can be carefully tuned by an external field. The gel behavior discussed in the Introduction (Fig 6.1) is for non-uniform swim speeds of the particles, which we discuss in Section 6.6. It is important to note that if one can measure the effective translational diffusivity of active particles in an orienting field, then the stress is known from the relationship $\boldsymbol{\sigma} = -n\zeta\langle\boldsymbol{D}\rangle$. We can thus make predictions of the shape and size of the gel based upon a simple diffusivity measurement of the swimmers.

6.6 Nonuniform swimming velocity

The swimming speeds of bacteria have been shown to change when exposed to chemical [22] and thermal [21] gradients. To this end, we now consider the effects of nonuniform swimming speeds on the swim stress and the average translational

velocity and diffusivity. Specifically, we allow the swimmers' speed to vary with their orientation relative to the external field, $\boldsymbol{q}\cdot\boldsymbol{H}$. Consider the swimming velocity

$$\boldsymbol{u}(\boldsymbol{q}) = \boldsymbol{q}\left(1 + u'(\alpha H_0\hat{\boldsymbol{H}}\cdot\boldsymbol{q})\right), \tag{6.18}$$

where $u'(\alpha H_0\hat{\boldsymbol{H}}\cdot\boldsymbol{q})$ is a dimensionless perturbed velocity relative to the uniform speed, U_0. We introduce α as an intrinsic particle property relating the external field strength, H_0, to the translational velocity.

The g_0 solution is identical to Eq 6.16 since the orientation distribution is independent of $\boldsymbol{u}(\boldsymbol{q})$. However, the $\boldsymbol{d}$-field differs because the driving force $\Delta\boldsymbol{u} = \langle\boldsymbol{u}\rangle - \boldsymbol{u}(\boldsymbol{q})$ is different. Equation 6.12 now becomes

$$\nabla_q^2\boldsymbol{d} - \chi_R\nabla_q\cdot\left[\left(\boldsymbol{q}\times\hat{\boldsymbol{H}}\right)\boldsymbol{d}\right] = -g_0\left[\langle\boldsymbol{u}\rangle - \boldsymbol{q}\left(1 + u'(\alpha H_0\hat{\boldsymbol{H}}\cdot\boldsymbol{q})\right)\right], \tag{6.19}$$

where

$$\langle\boldsymbol{u}\rangle = \int g_0\left[\boldsymbol{q}\left(1 + u'(\alpha H_0\hat{\boldsymbol{H}}\cdot\boldsymbol{q})\right)\right]d\boldsymbol{q}. \tag{6.20}$$

The swim diffusivity and stress become

$$\boldsymbol{\sigma}^{swim} = -n\zeta\langle\boldsymbol{D}^{swim}\rangle = -n\zeta U_0^2\tau_R\int\left[\langle\boldsymbol{u}\rangle - \boldsymbol{q}\left(1 + u'(\alpha H_0\hat{\boldsymbol{H}}\cdot\boldsymbol{q})\right)\right]\boldsymbol{d}\;d\boldsymbol{q}. \tag{6.21}$$

Equations 6.19-6.21 are the only changes required to account for nonuniform swimming speeds. With a choice of $u'(\alpha H_0\hat{\boldsymbol{H}}\cdot\boldsymbol{q})$, the problem statement is complete. Here we consider a linear relationship for the velocity perturbation: $u'(\alpha H_0\hat{\boldsymbol{H}}\cdot\boldsymbol{q}) = \alpha H_0\hat{\boldsymbol{H}}\cdot\boldsymbol{q}$. A swimmer's velocity is now

$$\boldsymbol{u}(\boldsymbol{q}) = \boldsymbol{q}\left[1 + \alpha H_0(\boldsymbol{q}\cdot\hat{\boldsymbol{H}})\right], \tag{6.22}$$

which may be a more complete description than the uniform-speed case considered earlier. When oriented along $\hat{\boldsymbol{H}}$, the swimmer increases its speed, and when oriented antiparallel to $\hat{\boldsymbol{H}}$, it decreases its speed.

Substituting Eqs 6.22 and 6.16 into Eq 6.20, the average velocity is

$$\langle\boldsymbol{u}\rangle = \hat{\boldsymbol{H}}\left[\coth\chi_R - \chi_R^{-1} + \alpha H_0\left(1 - 2\chi_R^{-1}\coth\chi_R + 2\chi_R^{-2}\right)\right]. \tag{6.23}$$

Comparing with Eq 6.17, we see that the average velocity increases by the last term in parentheses on the right-hand side. At low χ_R, the mean velocity of the swimmers is

$$\langle\boldsymbol{u}\rangle = \hat{\boldsymbol{H}}\left(\frac{1}{3}\alpha H_0 + \frac{1}{3}\chi_R + \frac{2}{45}\alpha H_0\chi_R^2 + O(\chi_R^3)\right). \tag{6.24}$$

The first term on the right-hand side represents a mean drift velocity arising from the perturbed velocity. At high χ_R, the swimmers are strongly oriented along the field direction, so the average velocity approaches $U_0(1 + \alpha H_0)$ following Eq 6.22.

An analytic solution of Eq 6.19 for arbitrary χ_R and αH_0 is available in Appendix D, but here we analyze the behavior at low and high χ_R. At low χ_R, a regular perturbation scheme gives the swim stress $\boldsymbol{\sigma}^{swim} = -n\zeta \left[\langle D_{\parallel}^{swim}\rangle \hat{\boldsymbol{H}}\hat{\boldsymbol{H}} + \langle D_{\perp}^{swim}\rangle(\boldsymbol{I} - \hat{\boldsymbol{H}}\hat{\boldsymbol{H}})\right]$, where

$$\langle D_{\parallel}^{swim}\rangle = U_0^2\tau_R\left[\left(\frac{1}{6} + \frac{2}{135}(\alpha H_0)^2\right) + \frac{2\chi_R}{27}\alpha H_0 - \chi_R^2\left(\frac{7}{135} - \frac{(\alpha H_0)^2}{189}\right)\right] + O(\chi_R^3), \tag{6.25}$$

$$\langle D_{\perp}^{swim}\rangle = U_0^2\tau_R\left[\left(\frac{1}{6} + \frac{1}{90}(\alpha H_0)^2\right) + \frac{\chi_R}{18}\alpha H_0 - \chi_R^2\left(\frac{1}{40} - \frac{59(\alpha H_0)^2}{22680}\right)\right] + O(\chi_R^3). \tag{6.26}$$

As $\alpha H_0 \to 0$, the results reduce to the uniform-speed solution considered earlier. The striking feature is that the dispersion *increases* at small χ_R, unlike the uniform-velocity case (compare with Eq 6.14). Since the swimmers oriented towards the field move faster than those oriented away from the field, we see an enhanced dispersion (and swim stress) at low to intermediate χ_R. As we shall see from the exact solution, the swim stresses in both parallel and perpendicular directions continue to increase and reach a maximum at intermediate χ_R.

Another key difference is the anisotropic swim stress at $\chi_R = 0$; the parallel diffusion is larger ($2/135$ versus $1/90$ for $\alpha H_0 = 1$). The average drift velocity from Eq 6.24 increases the effective translational diffusivity above $U_0^2\tau_R/6$ even at $\chi_R = 0$. This drift velocity may help explain the observed migration of bacteria along a temperature gradient [21].

At high χ_R, the behavior is similar to the uniform-velocity case. Since all particles are oriented along the external field, the effect of swimming-speed nonuniformity becomes negligible and the particles swim in the same direction with the same speed. The swim stress at high χ_R is

$$\boldsymbol{\sigma}^{swim} = -n\zeta U_0^2\tau_R\left[\frac{1}{2}(1 + 2\alpha H_0)^2\chi_R^{-3}\hat{\boldsymbol{H}}\hat{\boldsymbol{H}} + (1 + \alpha H_0)^2\chi_R^{-2}(\boldsymbol{I} - \hat{\boldsymbol{H}}\hat{\boldsymbol{H}})\right]. \tag{6.27}$$

The swim stress as a function of χ_R for $\alpha H_0 = 1$ is shown in Fig 6.8A. The instantaneous swimming speed is twice the uniform speed when the swimmer is oriented along the field ($2U_0$) and zero when oriented in the opposite direction. The swim

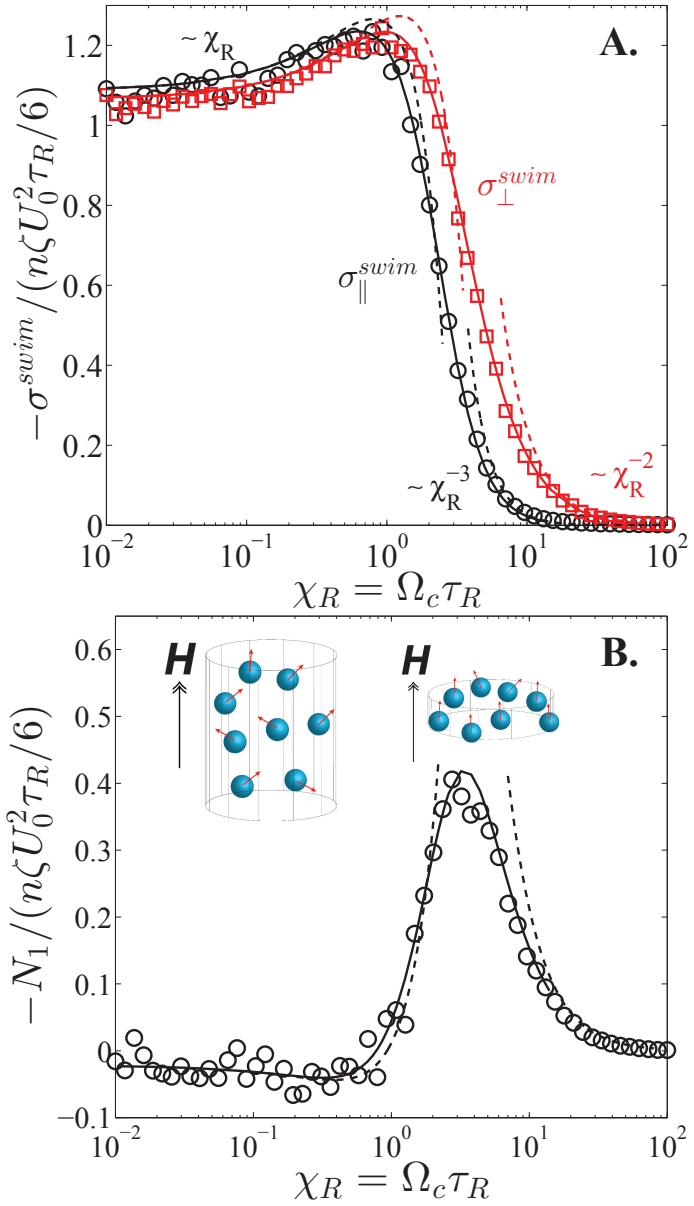

Figure 6.8: (**A**.) Swim stress in the parallel (in black) and perpendicular (in red) directions as a function of χ_R for $\alpha H_0 = 1$. The αH_0 parameter allows the swimming speed to vary with particle orientation. (**B**.) First normal swim-stress difference. The illustration shows an instantaneous configuration of the swimmers under a weak (sketch on left) and moderate (on right) external field. In both (**A**) and (**B**), the solid curves are the exact solutions, and the dashed curves are the asymptotic solutions. In (**A**) BD simulation results are shown in circles and squares for the parallel and perpendicular directions, respectively.

stress increases at low to moderate χ_R and reaches a maximum at $\chi_R^{max} = 0.60$ and $\chi_R^{max} = 0.95$ in the parallel and perpendicular directions, respectively. We

see maxima because the field redistributes the orientations *and* modifies the swimming speeds. This is different from the uniform-speed case where the field affected only the swimming orientations. As shown in Fig 6.8B, the normal swim-stress difference is non-monotonic and also changes in sign from negative to positive at $\chi_R \approx 0.8$.

We saw in Fig 6.7 that an external field that affects the particles' swimming orientation (but not their speed) resulted in a monotonically decreasing swim pressure with χ_R. As shown in Fig 6.9, the swim pressure becomes non-monotonic when both the particles' swimming orientation and speed are affected by the external field. This is interesting because an external field can give a non-monotonic pressure profile at the single-particle level (i.e., an infinitely dilute system).

In the Introduction we discussed an important application of loading a soft, compressible gel with active particles. Here we support the description of Fig 6.1 with our results. When the colloidal particles are inactive, the gel assumes some equilibrium shape as shown on the top of Fig 6.1. Activating the colloidal particles causes the gel to swell due to the "ideal-gas" swim pressure of the active particles, $\Pi^{swim} = n\zeta U_0^2 \tau_R/6$. Since the shear modulus of polymer networks can be adjusted over a wide range (in principle to nearly zero) and the intrinsic activity of the swimmers can be made much larger than the thermal energy, $\zeta U_0^2 \tau_R \gg k_B T$, the swim pressure can make an appreciable contribution to the overall size of the gel.

When we then apply a weak external field (i.e., $\chi_R < 1$), the gel expands even more due to increased swim pressures (see Fig 6.9), elongates due to positive normal stress differences (see Fig 6.8B), and translates due to the net motion of the active swimmers (see Eq 6.24) within the gel. When we increase the external field strength ($1 < \chi_R \ll \infty$), the swim pressure decreases and the normal stress difference becomes negative (Fig 6.8B graphs $-N_1$), which causes the gel to shrink in size, translate faster towards the field direction, and assume the shape of a thin disk as shown on the left of Fig 6.1. When the external field strength becomes very high ($\chi_R \to \infty$), the normal swim-stress difference and swim pressure vanish, causing the gel to return to its equilibrium shape and size but translate in the field direction. When the external field is turned off, the gel stops translating and an entire cycle is completed as depicted in Fig 6.1. Each transformation of the gel is corroborated by our calculations and BD simulations.

Allowing the swimming speeds to vary with orientation introduces features similar to the sedimentation problem considered by Brenner [14] and Almog and Frankel

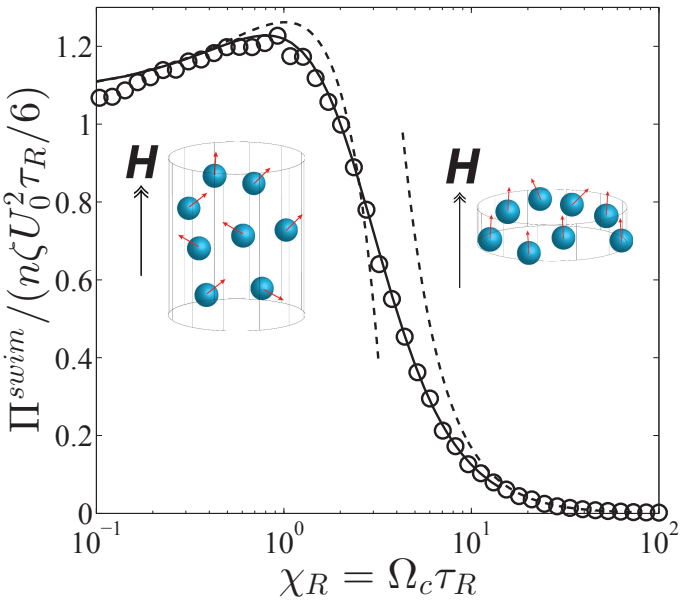

Figure 6.9: The swim pressure, $\Pi^{swim} = -\mathrm{tr}\boldsymbol{\sigma}^{swim}/3$, as a function of χ_R for $\alpha H_0 = 1$. The circles are results from BD simulations, and the solid and dashed curves are the exact and asymptotic analytical solutions, respectively. The illustration shows an instantaneous configuration of the swimmers under a weak (sketch on left) and moderate (on right) external field.

[15]. In the effective translational diffusivity (Eqs 6.25 and 6.26), the terms involving $(\alpha H_0)^2$ are identical to those by Almog and Frankel [15]. When analyzing the motion of a single particle, there is no distinction between a motion caused by an external force (i.e., gravity) and a motion arising from intrinsic particle activity (i.e., swim force). Therefore, the perturbation $u' = \alpha H_0 \hat{\boldsymbol{H}} \cdot \boldsymbol{q}$ in the modified velocity expression is similar to adding a contribution from an external force, $\boldsymbol{M}(\boldsymbol{q}) \cdot \boldsymbol{F}^{ext}$, where $\boldsymbol{M}(\boldsymbol{q})$ is the orientation-dependent mobility and $\boldsymbol{F}^{ext}$ is the external force. Of course, one could assume an expression of $u'(\alpha H_0 \hat{\boldsymbol{H}} \cdot \boldsymbol{q})$ that is different from the linear relationship (Eq 6.22) considered here, and the results would no longer be the same as the sedimentation problem. Therefore, for a single particle the sedimentation problem is a special case of our general formulation.

6.7 Conclusions

We have introduced a new approach to understand and compute the active stress in a system of self-propelled bodies. All active matter systems generate a unique swim pressure through their intrinsic self-motion. Here we used this swim stress perspective to analyze the effect of an external field on the motion and deformation

of active matter. We saw that the external field engendered anisotropic stresses, meaning that the swimmers experience a different confining force in the parallel and perpendicular directions. This lead directly to the shrinking/expanding, elongating, and translating of soft, compressible materials that are loaded with active particles. The external field can thus be used to manipulate the shape and size of soft materials such as a gel or perhaps a biological membrane. Another important application may be the analysis of various biophysical systems, such as the interior of a cell. Molecular motors that activate the cytoskeleton must exert a swim pressure on the cell owing to their self-motion along a track.

Our analysis remains valid for non-spherical particles with a varying swim velocity $\boldsymbol{U}_0$ and/or reorientation time τ_R. Here we focused on a dilute system of swimmers, but inclusion of two-body effects in the Smoluchowski Eq 6.1 is straightforward. At finite volume fractions, the particle size, a, would enter in the form of a nondimensional rotary Péclet number, $Pe_R = U_0 a/\langle D^{swim}\rangle \sim a/(U_0\tau_R)$, which compares the swimmer size a to its run length $U_0\tau_R$. With the inclusion of translational Brownian motion, all three parameters must be varied in the analysis: $\chi_R = \Omega_c\tau_R$, $Pe_R = a/(U_0\tau_R)$, and the swim Péclet number $Pe_s = U_0 a/D_0$.

In our analysis we neglected hydrodynamic interactions among the particles, which would contribute additional terms to the active-particle stress and affect the reorientation time of the particles due to translation-rotation coupling. It is important to note that the swim stress is distinct and different from the "hydrodynamic stresslet", which is also a single-particle property but scales as $\sim n\zeta U_0 a$ [10, 11]. As mentioned before, the motion of a single particle due to an intrinsic swim force and an external force are the same. At higher concentrations or when considering the swimmer's interactions with other bodies or boundaries a distinction must be made—the intrinsic swim mechanism does not generate a long-range $1/r$ Stokes velocity field as does an external force.

Here we focused on a dilute system of active particles, but at higher concentrations active systems have been known to exhibit unique collective behavior [2, 29]. The swim pressure presented here remains valid and appropriate for hydrodynamically interacting active systems, but one needs to carefully examine the individual contributions to the active stress. A single particle hydrodynamic contribution to the stress is of the form $\sim n\zeta a\boldsymbol{U}$, which, while important, is much smaller by a factor of $U_0\tau_R/a$ than the swim pressure. A complete study would need to consider the effects of both the swim and hydrodynamic stresses. We believe that the experimen-

tal, numerical, and theoretical analyses of active systems may need to be revisited in light of the new swim stress concept.

Experimentally, the precise manipulation of colloids using external fields is critical in many applications, like the targeted transport and delivery of specific chemicals [30]. Active-matter systems are ideal candidates for understanding dynamic self-assembly and developing synthetic structures. For example, dipolar particles subjected to a magnetic or electric field have been shown to form patterns [30, 31, 32]. Self-assembly and clustering behavior in active matter have been analyzed from the swim stress perspective [1], and it would be straightforward to extend these ideas to self-propelled particles that are biased by an external orienting field.

Appendix

A: Low-χ_R limit

A regular perturbation expansion of Eqs 6.11 and 6.12 assumes solutions of the form $g_0(\boldsymbol{q};\chi_R) = g_0^{(0)}(\boldsymbol{q}) + g_0^{(1)}(\boldsymbol{q})\chi_R + g_0^{(2)}(\boldsymbol{q})\chi_R^2 + O(\chi_R^3)$ and $\boldsymbol{d}(\boldsymbol{q};\chi_R) = \boldsymbol{d}^{(0)}(\boldsymbol{q}) + \boldsymbol{d}^{(1)}(\boldsymbol{q})\chi_R + \boldsymbol{d}^{(2)}(\boldsymbol{q})\chi_R^2 + O(\chi_R^3)$.

Substituting these into Eq 6.11 of the text, the leading-order orientation distribution function $g_0^{(0)}$ satisfies $\nabla_q^2 g_0^{(0)} = 0$ and $\int g_0^{(0)}\, d\boldsymbol{q} = 1$. The solution is the uniform distribution, $g_0^{(0)} = 1/4\pi$. The $O(\chi_R)$ problem is $-\hat{\boldsymbol{H}}\cdot\boldsymbol{q}/(2\pi) = \nabla_q^2 g_0^{(1)}$ with $\int g_0^{(1)}\, d\boldsymbol{q} = 0$. From Brenner [27], vector spherical surface harmonics satisfy

$$\nabla_q^2 \boldsymbol{P}_n(\boldsymbol{q}) = -n(n+1)\boldsymbol{P}_n(\boldsymbol{q}). \tag{6.28}$$

We hence substitute the trial solution $g_0^{(1)} = \boldsymbol{P}_1(\boldsymbol{q})\cdot\boldsymbol{a}_1$ into Eq 6.28, and obtain $\boldsymbol{a}_1 = \hat{\boldsymbol{H}}/4\pi$. Thus, the solution is $g_0^{(1)} = \hat{\boldsymbol{H}}\cdot\boldsymbol{P}_1(\boldsymbol{q})/(4\pi)$. The $O(\chi_R^2)$ problem is solved similarly: $\nabla_q^2 g_0^{(2)} = -\hat{\boldsymbol{H}}\hat{\boldsymbol{H}} : \boldsymbol{P}_2(\boldsymbol{q})/(2\pi)$ with $\int g_0^{(2)}\, d\boldsymbol{q} = 0$. The solution is $g_0^{(2)} = \hat{\boldsymbol{H}}\hat{\boldsymbol{H}} : \boldsymbol{P}_2(\boldsymbol{q})/(12\pi)$. Substitution of these three contributions into the perturbation expansion, we arrive at the solution in the text.

A similar procedure for the $\boldsymbol{d}$-field gives

$$\boldsymbol{d} = -\frac{1}{8\pi}\boldsymbol{P}_1(\boldsymbol{q}) - \frac{5\chi_R}{72\pi}\hat{\boldsymbol{H}}\cdot\boldsymbol{P}_2(\boldsymbol{q}) + \frac{\chi_R^2}{\pi}\left(\frac{29}{1440}\hat{\boldsymbol{H}}\hat{\boldsymbol{H}}\cdot\boldsymbol{P}_1(\boldsymbol{q}) - \frac{13}{720}\hat{\boldsymbol{H}}\hat{\boldsymbol{H}} : \boldsymbol{P}_3(\boldsymbol{q}) - \frac{3}{160}\boldsymbol{P}_1(\boldsymbol{q})\right) + O(\chi_R^3). \tag{6.29}$$

As in the force-induced microrheology problem considered by Zia and Brady [23], the $O(1)$ solution for $\boldsymbol{d}$ is the same as the $O(\chi_R)$ problem for g_0. In the linear-response regime, the problems are identical whether the swimmers are reoriented

by the external field (g_0) or by thermal energy k_BT ($\boldsymbol{d}$) and the same holds true when the reorientation is athermal with τ_R.

B: High-χ_R limit

The problem is singular in the $\chi_R \gg 1$ limit, so we expand the solution in the inner region as $g_0(\hat{\mu};\chi_R) = \chi_R g_0^{(0)}(\hat{\mu}) + g_0^{(1)}(\hat{\mu}) + O(\chi_R^{-1})$. Substituting into Eq 6.11 of the text, the leading-order solution satisfies

$$\frac{d}{d\hat{\mu}}\left[\hat{\mu}\left(g_0^{(0)} + \frac{dg_0^{(0)}}{d\hat{\mu}}\right)\right] = 0, \tag{6.30}$$

with $\int_0^{2\pi}\int_0^{\infty} g_0^{(0)}(\hat{\mu})\, d\hat{\mu}\, d\phi = 1$. For the fluctuation field, we separate the solution into scalar components parallel and perpendicular to $\hat{\boldsymbol{H}}$ as $\boldsymbol{d}(\mu,\phi;\chi_R) = d_\parallel(\mu;\chi_R)\hat{\boldsymbol{H}} + d_\perp(\mu;\chi_R)(\boldsymbol{e}_x\cos\phi + \boldsymbol{e}_y\sin\phi)$, where $\boldsymbol{e}_x$ and $\boldsymbol{e}_y$ are unit vectors in the x and y directions, respectively (see Fig 6.3). We assume subject to posteriori verification that $d_\parallel$ and $d_\perp$ are only a function of μ. Substituting the scaled $\hat{\mu}$ variable into Eq 6.12, we obtain

$$\frac{d}{d\hat{\mu}}\left[\hat{\mu}\left(d_\parallel + \frac{dd_\parallel}{d\hat{\mu}}\right)\right] = -\frac{1}{4\pi}e^{-\hat{\mu}}\chi_R^{-1}\,(\hat{\mu}-1)\,, \tag{6.31}$$

$$\frac{d}{d\hat{\mu}}\left[\hat{\mu}\left(d_\perp + \frac{dd_\perp}{d\hat{\mu}}\right)\right] - \frac{d_\perp}{4\hat{\mu}} = \frac{\sqrt{2}}{4\pi}\chi_R^{-1/2}e^{-\hat{\mu}}\hat{\mu}^{1/2}. \tag{6.32}$$

The leading nonzero solution is of order $d_\parallel \sim O(\chi_R^{-1})$ and $d_\perp \sim O(\chi_R^{-1/2})$. In the parallel direction, the solution is $d_\parallel(\hat{\mu};\chi_R) = \chi_R^{-1}e^{-\hat{\mu}}(\hat{\mu}-1)/(4\pi) + O(\chi_R^{-2})$, which satisfies both the regularity and normalization conditions. In the perpendicular direction, we obtain $d_\perp(\hat{\mu};\chi_R) = -\chi_R^{-1/2}\hat{\mu}^{1/2}e^{-\hat{\mu}}/(\sqrt{2}\pi) + O(\chi_R^{-1})$. Using boundary-layer coordinates, the effective translational diffusivity is computed from

$$\langle\boldsymbol{D}\rangle - \boldsymbol{D}_0 = \langle\boldsymbol{D}^{swim}\rangle = \pi U_0^2\tau_R\int_0^{\infty}\Big[2\chi_R^{-2}(1-\hat{\mu})d_\parallel\hat{\boldsymbol{H}}\hat{\boldsymbol{H}} + \sqrt{2}\chi_R^{-3/2}d_\perp\hat{\mu}^{1/2}\left(\boldsymbol{I}-\hat{\boldsymbol{H}}\hat{\boldsymbol{H}}\right)\Big]\,d\hat{\mu}. \tag{6.33}$$

C: Exact solution for arbitrary χ_R: Uniform speeds

We rewrite Eq 6.11 as

$$\frac{d}{d\mu}\left[(1-\mu^2)\frac{dg_0}{d\mu}\right] - \chi_R\frac{d}{d\mu}\left[(1-\mu^2)g_0\right] = 0, \tag{6.34}$$

where $\mu \equiv \hat{\boldsymbol{H}}\cdot\boldsymbol{q}$. Twice integrating and invoking the normalization and regularity conditions (finite $dg_0/d\mu$ and g_0 at $\mu = \pm 1$), we arrive at Eq 6.16 of the text.

The corresponding displacement field is broken into the parallel and perpendicular components. The solution in the parallel direction is

$$d_{\parallel}(\mu;\chi_R) = \frac{e^{\mu\chi_R}}{8\pi(\sinh\chi_R)^2}\Big[\cosh(\chi_R)\log\left(\frac{1-\mu}{1+\mu}\right) - \sinh(\chi_R)\log\left(1-\mu^2\right) + e^{\chi_R}Ei\left(-\chi_R(\mu+1)\right) - e^{-\chi_R}Ei\left(\chi_R(1-\mu)\right)\Big] + A_{\parallel}e^{\mu\chi_R}, \quad (6.35)$$

where $Ei(t)$ is the exponential integral $Ei(t) \equiv \int_{-\infty}^{t} e^{-\zeta}/\zeta \; d\zeta$, and $A_{\parallel}$ is the normalization constant:

$$A_{\parallel} = -\frac{\chi_R}{16\pi(\sinh\chi_R)^3}\int_{-1}^{1} e^{\mu\chi_R}\Big[\cosh(\chi_R)\log\left(\frac{1-\mu}{1+\mu}\right) - \sinh(\chi_R)\log\left(1-\mu^2\right) + e^{\chi_R}Ei\left(-\chi_R(\mu+1)\right) - e^{-\chi_R}Ei\left(\chi_R(1-\mu)\right)\Big]d\mu. \quad (6.36)$$

In the perpendicular direction, the solution is expanded as $d_{\perp} = \sum_{n=1}^{\infty} C_n P_n^1(\mu)$. The coefficients C_n are found by solving a tridiagonal matrix problem:

$$-\chi_R\frac{(n+1)(n-1)}{2n-1}C_{n-1} + n(n+1)C_n + \chi_R\frac{n(n+2)}{2n+3}C_{n+1} = b_n, \quad (6.37)$$

with $C_0 = 0$, and the forcing coefficients b_n are given by

$$b_n = -\frac{2n+1}{2n(n+1)}\int_{-1}^{1} g_0(\mu;\chi_R)\sqrt{1-\mu^2}P_n^1 \, d\mu. \quad (6.38)$$

From Eq 6.9, the swim diffusivity and stress are

$$\boldsymbol{\sigma}^{swim} = -n\zeta\langle\boldsymbol{D}^{swim}\rangle = -n\zeta U_0^2\tau_R\pi\int_{-1}^{1}\Big[2d_{\parallel}\left(\coth\chi_R - \chi_R^{-1} - \mu\right)\hat{\boldsymbol{H}}\hat{\boldsymbol{H}} + d_{\perp}\sqrt{1-\mu^2}\left(\boldsymbol{I} - \hat{\boldsymbol{H}}\hat{\boldsymbol{H}}\right)\Big]d\mu, \quad (6.39)$$

where only the diagonal terms contribute to the quadrature. In the perpendicular direction, the convenience of using associated Legendre polynomials is evident in

$$\begin{aligned}\sigma_{\perp}^{swim} &= -n\zeta U_0^2\tau_R\pi\int_{-1}^{1}\sum_{n=1}^{\infty}C_nP_n^1(\mu)P_1^1(\mu)\,d\mu \\ &= -\frac{4\pi}{3}n\zeta U_0^2\tau_R C_1. \end{aligned} \quad (6.40)$$

D: Exact solution for arbitrary χ_R: Nonuniform speeds

Resolving Eq 6.19 into the parallel and perpendicular components, the exact $\boldsymbol{d}$-field solution in the parallel direction is

$$d_{\parallel} = \frac{e^{\mu\chi_R}}{8\pi(\sinh\chi_R)^2}\Bigg\{\left(1-\frac{2\alpha H_0}{\chi_R}\right)\Bigg[\cosh(\chi_R)\log\left(\frac{1-\mu}{1+\mu}\right) - \sinh(\chi_R)\log\left(1-\mu^2\right) + e^{\chi_R}Ei\left(-\chi_R(\mu+1)\right) - e^{-\chi_R}Ei\left(\chi_R(1-\mu)\right)\Bigg] - 2\alpha H_0\mu\sinh\chi_R\Bigg\} + \tilde{A}_{\parallel}e^{\mu\chi_R}, \quad (6.41)$$

where $\tilde{A}_{\parallel}$ is found from the normalization constraint to be

$$\tilde{A}_{\parallel} = -\frac{\chi_R}{16\pi(\sinh\chi_R)^3}\int_{-1}^{1} e^{\mu\chi_R}\Bigg\{\left(1-\frac{2\alpha H_0}{\chi_R}\right)\times \Bigg[\cosh(\chi_R)\log\left(\frac{1-\mu}{1+\mu}\right) - \sinh(\chi_R)\log\left(1-\mu^2\right) + e^{\chi_R}Ei\left(-\chi_R(\mu+1)\right) - e^{-\chi_R}Ei\left(\chi_R(1-\mu)\right)\Bigg] - 2\alpha H_0\mu\sinh\chi_R\Bigg\}d\mu. \quad (6.42)$$

Substitution of this equation into Eq 6.9 gives the swim stress in the parallel direction.

In the perpendicular direction, the form of the solution is the same as before (Eq 6.37) except the forcing coefficients b_n are given by

$$b_n = -\frac{2n+1}{2n(n+1)}\int_{-1}^{1} g_0(\mu;\chi_R)\sqrt{1-\mu^2}\,(1+\alpha H_0\mu)\,P_n^1\,d\mu. \quad (6.43)$$

The tridiagonal matrix problem is solved for the coefficients C_{n-1}, C_n, and C_{n+1}. The effective translational diffusivity in the perpendicular direction is given by

$$\langle D_{\perp}\rangle = 4\pi U_0^2\tau_R\left(\frac{1}{3}C_1 + \frac{1}{5}\alpha H_0 C_2\right), \quad (6.44)$$

where we have used the orthogonality of the associated Legendre functions $P_1^1 = -\sqrt{1-\mu^2}$ and $P_2^1 = -3\mu\sqrt{1-\mu^2}$ to evaluate the integral.

References

[1] S. C. Takatori, W. Yan, and J. F. Brady. “Swim pressure: Stress generation in active matter”. *Phys Rev Lett* 113.2 (2014), p. 028103.

[2] S. Ramaswamy. “The mechanics and statistics of active matter”. *Ann Rev Condens Matter Phys* 1.1 (2010), pp. 323–345.

[3] J. Adler. “Chemotaxis in bacteria”. *Science* 153.3737 (1966), pp. 708–716.

[4] J. Armitage and K. Hellingwerf. “Light-induced behavioral responses (‘phototaxis’) in prokaryotes”. *Photosynth Res* 76.1-3 (2003), pp. 145–155.

[5] R. Blakemore. “Magnetotactic bacteria”. *Science* 190.4212 (1975), pp. 377–379.

[6] D. Hader, R. Hemmersbach, and M. Lebert. *Gravity and the behavior of unicellular organisms*. Cambridge, United Kingdom: Cambridge University Press, 2005.

[7] M. Doi. *Soft matter physics*. Oxford, United Kingdom: Oxford University Press, 2013.

[8] D. S. Fudge et al. “From ultra-soft slime to hard α-keratins: The many lives of intermediate filaments”. *Integr Comp Biol* 49.1 (2009), pp. 32–39.

[9] S. K. Lai, Y.-Y. Wang, D. Wirtz, and J. Hanes. “Micro- and macrorheology of mucus”. *Adv Drug Deliv Rev* 61.2 (2009), pp. 86–100.

[10] D. Saintillan and M. J. Shelley. “Instabilities, pattern formation, and mixing in active suspensions”. *Phys Fluids* 20.12 (2008), pp. 123304–123315.

[11] T. Ishikawa, M. P. Simmonds, and T. J. Pedley. “Hydrodynamic interaction of two swimming model micro-organisms”. *J Fluid Mech* 568 (2006), pp. 119–160.

[12] I. Theurkauff, C. Cottin-Bizonne, J. Palacci, C. Ybert, and L. Bocquet. “Dynamic clustering in active colloidal suspensions with chemical signaling”. *Phys Rev Lett* 108.26 (2012), p. 268303.

[13] J. Palacci, S. Sacanna, A. P. Steinberg, D. J. Pine, and P. M. Chaikin. “Living crystals of light-activated colloidal surfers”. *Science* 339.6122 (2013), pp. 936–940.

[14] H. Brenner. “Taylor dispersion in systems of sedimenting nonspherical brownian particles. I. Homogeneous, centrosymmetric, axisymmetric particles”. *J Colloid Interface Sci* 71.2 (1979), pp. 189–208.

[15] Y. Almog and I. Frankel. “Effects of fore-aft asymmetry on the sedimentation and dispersion of axisymmetric Brownian particles”. *J Colloid Interface Sci* 157.1 (1993), pp. 60–71.

[16] M. A. Bees, N. A. Hill, and T. J. Pedley. “Analytical approximations for the orientation distribution of small dipolar particles in steady shear flows”. *J Math Biol* 36.3 (1998), pp. 269–298.

[17] A. Manela and I. Frankel. “Generalized Taylor dispersion in suspensions of gyrotactic swimming micro-organisms”. *J Fluid Mech* 490 (2003), pp. 99–127.

[18] T. J. Pedley and J. O. Kessler. “A new continuum model for suspensions of gyrotactic micro-organisms”. *J Fluid Mech* 212 (1990), pp. 155–182.

[19] R. N. Bearon, A. L. Hazel, and G. J. Thorn. “The spatial distribution of gyrotactic swimming micro-organisms in laminar flow fields”. *J Fluid Mech* 680 (2011), pp. 602–635.

[20] R. N. Bearon, M. A. Bees, and O. A. Croze. “Biased swimming cells do not disperse in pipes as tracers: A population model based on microscale behaviour”. *Phys Fluids* 24.12 (2012), pp. 121902–121920.

[21] M. Demir and H. Salman. “Bacterial thermotaxis by speed modulation”. *Biophys J* 103.8 (2012), pp. 1683–1690.

[22] R. R. Vuppula, M. S. Tirumkudulu, and K. V. Venkatesh. “Chemotaxis of *Escherichia coli* to L-serine”. *Phys Biol* 7.2 (2010), p. 026007.

[23] R. N. Zia and J. F. Brady. “Single-particle motion in colloids: Force-induced diffusion”. *J Fluid Mech* 658 (2010), pp. 188–210.

[24] U. M. Córdova-Figueroa and J. F. Brady. “Osmotic propulsion: The osmotic motor”. *Phys Rev Lett* 100.15 (2008), p. 158303.

[25] H. Brenner and D. Edwards. *Macrotransport processes*. Butterworth-Heinemann Limited, 1993.

[26] H. Brenner and D. W. Condiff. “Transport mechanics in systems of orientable particles. IV. Convective transport”. *J Colloid Interface Sci* 47.1 (1974), pp. 199–264.

[27] H. Brenner. “The Stokes resistance of an arbitrary particle. III: Shear fields”. *Chem Engng Sci* 19.9 (1964), pp. 631–651.

[28] D. A. Beard and T. Schlick. “Unbiased rotational moves for rigid-body dynamics”. *Biophys J* 85.5 (2003), pp. 2973–2976.

[29] J. Toner, Y. Tu, and S. Ramaswamy. “Hydrodynamics and phases of flocks”. *Ann Phys* 318.1 (2005), pp. 170–244.

[30] A. Snezhko and I. S. Aranson. “Magnetic manipulation of self-assembled colloidal asters”. *Nat Mater* 10.9 (2011), pp. 698–703.

[31] M. V. Sapozhnikov, Y. V. Tolmachev, I. S. Aranson, and W. K. Kwok. “Dynamic self-assembly and patterns in electrostatically driven granular media”. *Phys Rev Lett* 90.11 (2003), p. 114301.

[32] M. E. Leunissen, H. R. Vutukuri, and A. van Blaaderen. “Directing colloidal self-assembly with biaxial electric fields”. *Adv Mater* 21.30 (2009), pp. 3116–3120.

Chapter 7

SUPERFLUID BEHAVIOR OF ACTIVE SUSPENSIONS FROM DIFFUSIVE STRETCHING

This chapter includes content from our previously published article:

[1] S. C. Takatori and J. F. Brady. "Superfluid behavior of active suspensions from diffusive stretching". *Phys Rev Lett* 118.1 (2017), p. 018003. DOI: 10.1103/PhysRevLett.118.018003.

7.1 Introduction

Current understanding is that the non-Newtonian rheology of active matter suspensions is governed by fluid-mediated hydrodynamic interactions associated with active self-propulsion. Here we discover an additional contribution to the suspension shear stress that predicts both thickening and thinning behavior, even when there is no nematic ordering of the microswimmers with the imposed flow. A simple micromechanical model of active Brownian particles in homogeneous shear flow reveals the existence of off-diagonal shear components in the swim stress tensor, which are independent of hydrodynamic interactions and fluid disturbances. Theoretical predictions from our model are consistent with existing experimental measurements of the shear viscosity of active suspensions, but also suggest new behavior not predicted by conventional models.

Shear rheology of suspensions containing self-propelled bodies at low Reynolds numbers has been studied intensively during the past several years. Conventional models predict that fluid disturbances induced by active self-propulsion help to 'stretch' or 'contract' the fluid along the extensional axis of shear, resulting in large deviations in the effective shear viscosity of the suspension relative to that of the embedding medium [1, 2, 3]. In this work, we demonstrate that intrinsic self-propulsion engenders a 'shear swim stress' that affects the rheology of active systems in previously unreported ways. The swim stress is a 'diffusive' stress generated by self-propulsion and is distinct from, and in addition to, the hydrodynamic stress resulting from fluid-mediated hydrodynamic interactions.

Earlier [4, 5] we derived a direct relationship between the translational diffusivity $\boldsymbol{D}$ and the stress generated by a dilute suspension of particles: $\boldsymbol{\sigma} = -n\zeta\boldsymbol{D}$, where

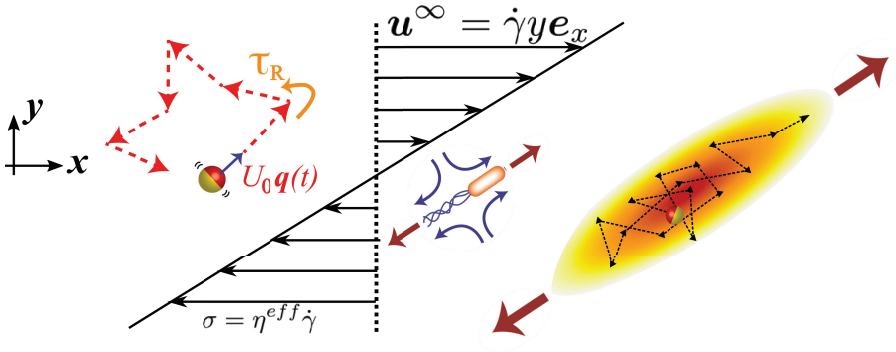

Figure 7.1: Schematic of active particles with swimming speed U_0 and reorientation time τ_R in simple shear flow with fluid velocity $u_x^{\infty} = \dot{\gamma} y$, where $\dot{\gamma}$ is the magnitude of shear rate. The unit vector $\boldsymbol{q}(t)$ specifies the particle's direction of self-propulsion. Diffusion of active particles along the extensional axis of shear acts to 'stretch' the fluid and reduce the effective shear viscosity, similar to the effect that the hydrodynamic stress plays for pusher-type microorganisms.

n is the particle number density and ζ is the hydrodynamic drag coefficient. The effective translational diffusivity of a dilute active system is $\boldsymbol{D}^{swim} = U_0^2 \tau_R \boldsymbol{I}/6$ for times $t > \tau_R$, where U_0 and τ_R are the swimming speed and reorientation time of the particle, respectively. This gives directly the unique mechanical swim stress exerted by active particles, $\boldsymbol{\sigma}^{swim} = -n\zeta \boldsymbol{D}^{swim} = -n\zeta U_0^2 \tau_R \boldsymbol{I}/6$, which has been used to predict the phase behavior of self-assembling active matter [4, 6, 7, 8]. The swim stress is analogous to the osmotic Brownian stress of passive particles.

In shear flow, particle motion in the flow gradient direction couples to advective drift in the flow direction (Fig 7.1), resulting in nonzero off-diagonal components in the long-time particle diffusivity, $D_{xy} \neq 0$. This directly implies the existence of a nonzero shear component in the swim stress tensor, $\sigma_{xy}^{swim} = -n\zeta D_{xy}^{swim}$. In this work, we discover that $D_{xy}^{swim} > 0$ for small shear rates, which gives $\sigma_{xy}^{swim} < 0$ and a decrease in the effective shear viscosity of active suspensions below that of the surrounding solvent for pusher, puller, and neutral-type microswimmers. As shown in Fig 7.1, diffusion of active particles along the extensional axis of shear acts to 'stretch' the fluid and reduce the effective shear viscosity, analogous to the effect of the hydrodynamic stress generated by pusher microorganisms. Whereas the swim pressure represents the mechanical confinement of diffusing active particles [4], a nonzero shear swim stress represents the mechanical stress required to prevent shear deformation of the suspension.

7.2 Micromechanical model

To motivate this new perspective, we consider a single rigid active particle that swims with a fixed speed U_0 in a direction specified by a body-fixed unit orientation vector $\boldsymbol{q}$, which relaxes with a timescale τ_R due to rotational Brownian motion (see Fig 7.1). The particle is immersed in a continuous Newtonian solvent with viscosity η_0. We analyze the dynamics of the particle in steady simple shear flow $\boldsymbol{u}^\infty = \dot{\gamma} y \boldsymbol{e}_x$, where $\dot{\gamma}$ is the magnitude of shear rate. The Smoluchowski equation governing the probability distribution $P(\boldsymbol{x}, \boldsymbol{q}, t)$ is

$$\frac{\partial P}{\partial t} + \nabla \cdot \boldsymbol{j}_T + \nabla_q \cdot \boldsymbol{j}_R = 0, \tag{7.1}$$

where the translational and rotational fluxes are given by, respectively [9, 10, 11],

$$\boldsymbol{j}_T = (\boldsymbol{u}^\infty + U_0 \boldsymbol{q})\, P, \tag{7.2}$$

$$\boldsymbol{j}_R = \dot{\gamma}\, (\boldsymbol{q} \cdot \boldsymbol{\Lambda} + B(\boldsymbol{I} - \boldsymbol{qq})\boldsymbol{q} : \boldsymbol{E})\, P - \frac{1}{\tau_R} \nabla_q P. \tag{7.3}$$

In Eq 7.3, the antisymmetric and symmetric velocity-gradient tensors $\boldsymbol{\Lambda}$ and $\boldsymbol{E}$ are nondimensionalized by $\dot{\gamma}$, and $\nabla_q \equiv \partial / \partial \boldsymbol{q}$ is the orientation-space gradient operator. The dynamics of the particle are controlled by a balance between shear-induced particle rotations and the particle's intrinsic reorientation time, given by a shear Péclet number $Pe \equiv \dot{\gamma} \tau_R$. The constant scalar $B = ((a/b)^2 - 1)/((a/b)^2 + 1)$, where a and b are the semi-major and minor radii of the particle, respectively; $B = 0$ for a spherical particle. The terms in Eq 7.2 are the advective contributions from ambient fluid flow and intrinsic self-propulsion of the swimmer. The Stokes-Einstein-Sutherland translational diffusivity, $\boldsymbol{D}_0$, is omitted in Eq 7.2, since the magnitude of the self-propulsive contribution $D^{swim} = U_0^2 \tau_R / 6$ may be $O(10^3)$ larger (or more) than D_0 for many active swimmers of interest.

Following established procedures [5, 10, 12] (see Appendix), we obtain the steady solution to Eqs 7.1-7.3 for times $t > \tau_R$ and $t > \dot{\gamma}^{-1}$ when all orientations have been sampled; the resulting solution gives the effective translational diffusivity, hydrodynamic stress, and swim stress. As shown in Fig 7.2, fluid shear introduces anisotropy and nonzero off-diagonal components in the particle diffusivity. The asymptotic solution at small shear rates is $\boldsymbol{D}^{swim} / (U_0^2 \tau_R / 6) = \boldsymbol{I} + Pe(1 + B)\boldsymbol{E}/2 + O(Pe^2)$. In the flow direction, D_{xx}^{swim} initially increases with a correction of $O(Pe^2)$ due to increased sampling of fluid streamlines in the flow gradient direction, but decreases to zero as $Pe \to \infty$ because the particle simply spins around with little translational movement. This non-monotonic behavior was also seen in the dispersion

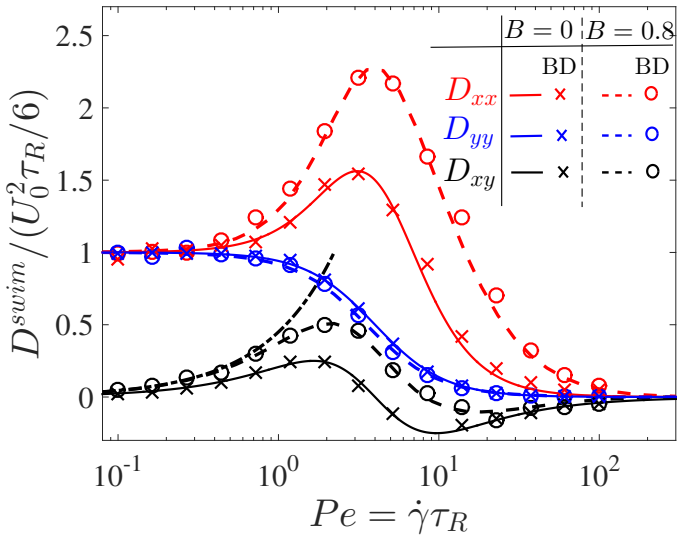

Figure 7.2: Swim diffusivity as a function of shear Péclet number for two different values of geometric factor B ($B = 0$ sphere; $B = 0.8$ ellipsoid). Solid and dashed curves are theoretical solutions, and the symbols are Brownian dynamics (BD) simulation results. Dash-dotted curve for D_{xy} is the small-Pe solution for $B = 0.8$.

of active particles in an external field [5] and sedimentation of noncentrosymmetric Brownian particles [13]. In the flow gradient direction, D_{yy}^{swim} decreases monotonically with increasing Pe. In the vorticity direction, D_{zz}^{swim} is unaffected by shearing motion and is constant for all Pe.

Most interestingly, the off-diagonal diffusivity D_{xy}^{swim} is nonzero, $O(Pe)$ for small Pe, non-monotonic, and negative for intermediate values of Pe. Random diffusion in the gradient direction, D_{yy}^{swim}, allows the particle to traverse across streamlines, which couples to the advective drift in the flow direction to give a non-monotonic off-diagonal shear diffusivity (see schematic in Fig 7.1). In an experiment or computer simulation, calculation of shear-induced diffusivity requires attention because advective drift translates the particles in the flow direction, resulting in Taylor dispersion with mean-squared displacements that do not grow linearly with time [14].

A nonzero off-diagonal swim diffusivity implies the presence of a shear swim stress from $\sigma_{xy}^{swim} = -n\zeta D_{xy}^{swim}$. From Fig 7.2 we see that $D_{xy}^{swim} > 0$ for small Pe, which gives $\sigma_{xy}^{swim} < 0$ and the effective shear viscosity of the suspension decreases below that of the surrounding solvent. In addition to an indirect calculation of the stress via the diffusivity, we can also compute it directly using the virial expression for the stress. The Langevin equation governing the motion of a single swimmer in simple

shear flow (without translational Brownian motion) is $\mathbf{0} = -\zeta(\boldsymbol{U} - \boldsymbol{u}^{\infty}) + \boldsymbol{F}^{swim}$, where $\boldsymbol{u}^{\infty} = \dot{\gamma} y \boldsymbol{e}_x$, and $\boldsymbol{F}^{swim} \equiv \zeta \boldsymbol{U}_0$ is the self-propulsive swim force of the particle [4].

The swim stress is the first moment of the force, $\boldsymbol{\sigma}^{swim} \equiv -n \left\langle \left[\boldsymbol{x} \boldsymbol{F}^{swim} \right]^{sym} \right\rangle$, where $[\cdot]^{sym}$ is the symmetric part of the tensor. The angle brackets denote an average over all particle configurations, $\langle (\cdot) \rangle = \int (\cdot) P(\boldsymbol{x}, \boldsymbol{q}) d\boldsymbol{x} d\boldsymbol{q}$ where $P(\boldsymbol{x}, \boldsymbol{q})$ is the steady solution to Eqs 7.1-7.3. It is important to ensure symmetry in the swim stress because angular momentum conservation requires the stress to be symmetric in the absence of body couples. Direct calculation of the swim stress via the virial definition (see Appendix) gives results identical to those obtained from the diffusivity-stress relationship; Brownian dynamics simulations also corroborate our result. In our simulations, the particles were evolved following the Langevin equation given above, in addition to the rotational dynamics, $d\boldsymbol{q}/dt = \dot{\gamma} \left(\boldsymbol{q} \cdot \boldsymbol{\Lambda} + B(\boldsymbol{I} - \boldsymbol{q}\boldsymbol{q}) \boldsymbol{q} : \boldsymbol{E} \right) + \sqrt{2/\tau_R} \boldsymbol{\Gamma}_R \times \boldsymbol{q}$, where $\boldsymbol{\Gamma}_R$ is a unit random normal deviate: $\overline{\boldsymbol{\Gamma}_R(t)} = 0$ and $\overline{\boldsymbol{\Gamma}_R(t) \boldsymbol{\Gamma}_R(0)} = \delta(t) \boldsymbol{I}$. Results from simulations were averaged over 10^4 independent particle trajectories for times long compared to τ_R and $\dot{\gamma}^{-1}$.

Until this work, only the normal components of the swim stress (i.e., σ_{ii}^{swim} where $i = x, y, z$) have been studied [4, 5, 6, 7, 8, 15, 16, 11, 17, 18, 19, 20, 21, 22, 23], which give the average pressure required to confine an active body inside of a bounded space. We discover here that the off-diagonal *shear* swim stress, σ_{xy}^{swim}, provides a new physical interpretation of the non-Newtonian shear rheology of active matter.

From continuum mechanics, we have $\nabla \cdot \boldsymbol{\sigma} = \mathbf{0}$ and $\nabla \cdot \boldsymbol{u} = 0$, where $\boldsymbol{\sigma}$ is the total stress of the suspension and $\boldsymbol{u}$ is the suspension-average velocity. The stress can be written as $\boldsymbol{\sigma} = -p_f \boldsymbol{I} + 2\eta_0 \dot{\gamma} \left(1 + 5\phi/2\right) \boldsymbol{E} + \boldsymbol{\sigma}^{act}$, where p_f is the fluid pressure, η_0 is the viscosity of the continuous Newtonian solvent, ϕ is the volume fraction of particles ($= 4\pi a^3 n/3$ for spheres), $5\phi/2$ is the Einstein shear viscosity correction that is present for all suspensions (taking the result for spherical particles in this work), and the active stress is the contribution due to self-propulsion of the particles, $\boldsymbol{\sigma}^{act} = \boldsymbol{\sigma}^{H} + \boldsymbol{\sigma}^{swim}$.

The hydrodynamic stress is $\boldsymbol{\sigma}^{H} = n\boldsymbol{S}^{H} = n\sigma_0^{H} \left(\langle \boldsymbol{q}\boldsymbol{q} \rangle - \boldsymbol{I}/3 \right)$, where $\boldsymbol{S}^{H}$ is the hydrodynamic stresslet associated with the swimmers' permanent force dipole, and σ_0^{H} is its magnitude which scales as $\sigma_0^{H} \sim \zeta U_0 a$ ($\sigma_0^{H} < 0$ for 'pushers,' $\sigma_0^{H} > 0$ for 'pullers') [1, 24, 25]. For swimmers with an isotropic orientation distribution,

$\langle \boldsymbol{qq} \rangle = \boldsymbol{I}/3$, the hydrodynamic stress makes no contribution to the suspension stress. The hydrodynamic stress is present in the model by Saintillan [1] and is the only contribution that has been considered in the literature.

The main contribution of this work is the identification and inclusion of an off-diagonal shear component in the swim stress, $\boldsymbol{\sigma}^{swim} \equiv -n \left\langle \left[\boldsymbol{x} \boldsymbol{F}^{swim} \right]^{sym} \right\rangle$. The swim force of an active Brownian particle is $\boldsymbol{F}^{swim} \equiv \zeta U_0 \boldsymbol{q}$, so we obtain $\boldsymbol{\sigma}^{swim} = -n\zeta U_0^2 \tau_R \left\langle [\overline{\boldsymbol{x}} \boldsymbol{q}]^{sym} \right\rangle$, where nondimensional position $\overline{\boldsymbol{x}} = \boldsymbol{x}/(U_0 \tau_R)$.

It is important to distinguish and differentiate the swim stress from the hydrodynamic stress. First, $\boldsymbol{\sigma}^{swim}$ is an entropic term because it arises from the random walk process associated with active swimming and tumbling, whereas $\boldsymbol{\sigma}^{H}$ comes from fluid-mediated hydrodynamics and the multipole moments generated by self-propulsion. Naturally, this leads to a different scaling of the swim stress $\boldsymbol{\sigma}^{swim} \sim (n\zeta U_0)(U_0 \tau_R)$ compared to the hydrodynamic stress $\boldsymbol{\sigma}^{H} \sim (n\zeta U_0)a$. The relevant length scale of the swim stress is the swimmer run length, $U_0 \tau_R$, as opposed to the hydrodynamic stress that scales with the swimmer size a (see schematic in Fig 7.1).

In addition to the two terms above, we know from passive Brownian suspensions that non-spherical particles like polymers and liquid crystals can generate a shear stress from flow-induced particle alignment or stretching [26, 27]. Compared with the swim stress, the magnitudes of these terms are $O(k_B T/(k_s T_s))$, where $k_s T_s \equiv \zeta U_0^2 \tau_R/6$ is the activity scale associated with self-propulsion [6]. For most microswimmers of interest, $k_B T/(k_s T_s) \lesssim O(10^{-3})$, so these terms are not included in this work.

7.3 Effective shear viscosity of active fluids

For steady simple shear flow, the shear stress is constant across every plane, and we obtain $\sigma_{xy} = \sigma = \eta^{eff} \dot{\gamma}$, where the effective viscosity of the suspension is

$$\frac{\eta^{eff}}{\eta_0} = 1 + \frac{5}{2}\phi + \frac{\sigma_{xy}^{H} + \sigma_{xy}^{swim}}{\eta_0 \dot{\gamma}}, \tag{7.4}$$

where $\sigma_{xy}^{H} = n\sigma_0^{H} \langle q_x q_y \rangle$ and $\sigma_{xy}^{swim} = -n(\langle x F_y^{swim} \rangle + \langle y F_x^{swim} \rangle)/2$. For the active Brownian particle model with swim force $\boldsymbol{F}^{swim} \equiv \zeta U_0 \boldsymbol{q}$, we obtain $\sigma_{xy}^{swim} = -n\zeta U_0^2 \tau_R (\langle \overline{x} q_y \rangle + \langle \overline{y} q_x \rangle)/2$, where $\overline{x}$ and $\overline{y}$ are nondimensionalized by the run length $U_0 \tau_R$.

Active spherical particles that do not establish macroscopic orientational order with the imposed flow do not generate a hydrodynamic stress, $\sigma_{xy}^{H} = 0$, but can exert a

nonzero swim stress, giving, for all Pe (see Appendix),

$$\frac{\eta^{eff}}{\eta_0} = 1 + \frac{5}{2}\phi - \frac{3\phi}{16}\left(\frac{1}{Pe_R}\right)^2 \left(\frac{1-(Pe/4)^2}{[1+(Pe/4)^2]^2}\right). \tag{7.5}$$

The reorientation Péclet number $Pe_R \equiv a/(U_0\tau_R)$ is a ratio of the particle size a to the swimmer run length $U_0\tau_R$. For small Pe and Pe_R, η^{eff} is smaller than the Newtonian viscosity of the surrounding solvent, η_0. With increasing Pe, η^{eff} increases and becomes larger than η_0, until a maximum is reached at intermediate Pe. As $Pe \to \infty$, the particles spin around in place without taking a step, so η^{eff} approaches a constant given by the solvent's viscosity plus the Einstein correction. This non-monotonic behavior has not been predicted previously because conventional models do not include the swim stress.

For non-spherical particles, the hydrodynamic drag tensor varies with the orientation as $\boldsymbol{\zeta} = \zeta_\parallel \boldsymbol{qq} + \zeta_\perp(\boldsymbol{I} - \boldsymbol{qq})$, where $\zeta_\parallel$ and $\zeta_\perp$ are the parallel and perpendicular components, respectively. We assume here that the direction of self-propulsion is aligned with the body-fixed axisymmetric polar axis, $\boldsymbol{U}_0 = U_0\boldsymbol{q}$, so the swim diffusivity-stress relationship becomes $\boldsymbol{\sigma}^{swim} = -n\zeta_\parallel \boldsymbol{D}^{swim}$.

Analytical solutions to Eqs 7.1-7.3 are not available for non-spherical particles, so a perturbation analysis for small Pe gives the swim stress $\boldsymbol{\sigma}^{swim}/(n\zeta_\parallel U_0^2\tau_R/6) = -\boldsymbol{I} - Pe(1+B)\boldsymbol{E}/2 + O(Pe^2)$, and the hydrodynamic stress $\boldsymbol{\sigma}^H/(n\sigma_0^H) = BPe\boldsymbol{E}/15 + O(Pe^2)$. Substituting these results into Eq 7.4, we obtain the effective shear viscosity for small Pe:

$$\frac{\eta^{eff}(Pe\to 0)}{\eta_0} = 1 + \frac{5}{2}\phi - \left(-\frac{1}{5}B\alpha Pe_R + \frac{1+B}{4}\right)\frac{3\phi}{4Pe_R^2}K\left(\frac{a}{b}\right), \tag{7.6}$$

where α is a parameter associated with the force dipole magnitude, defined as $\alpha \equiv \sigma_0^H/(\zeta_\parallel U_0 a)$, K is the shape factor in the hydrodynamic drag coefficient in the parallel component $\zeta_\parallel = 6\pi\eta_0 bK$, and a and b are the semi-major and minor radii of an ellipsoidal particle, respectively. The constant scalar $B = ((a/b)^2-1)/((a/b)^2+1)$; $B = 0$ for a spherical particle.

Figure 7.3 compares the effective shear viscosity from our micromechanical model (Eq 7.4) with the experiments of López et al [28]. Physical properties of the *E. coli* bacteria used in our model were taken from their work [28], with swimming speed $U_0 = 20\mu m/s$, reorientation time $\tau_R = 4.8s$, body length $2a = 1.7\mu m$, and body diameter $2b = 0.5\mu m$, which give the hydrodynamic drag shape factor $K = 1.5$ and geometric coefficient $B = 0.88$. Particle reorientations are modeled in Eq 7.3 as

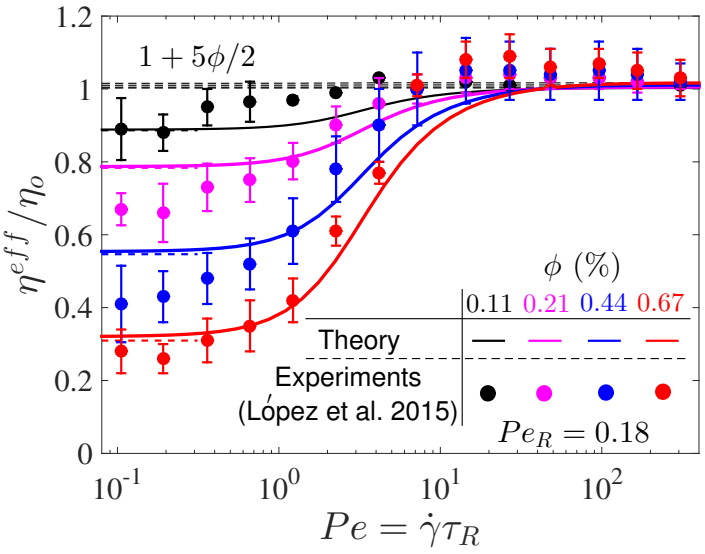

Figure 7.3: Comparison of our model, Eq 7.4, with shear experiments of López et al (López, Gachelin, Douarche, Auradou, and Clément, *Phys Rev Lett*, 2015) with motile *E. coli* bacteria at different concentrations. Horizontal dashed lines for small Pe are the analytical solutions of Eq 7.6.

a diffusive Brownian process using the run-and-tumble equivalence [29], so τ_R is consistent with that reported by López et al [28], which is a directional persistence time based on the bacteria tumble frequency, $1/\omega = \tau_R/2 = 2.4s$. The reorientation Péclet number based on the swimmer body length a yields negative effective shear viscosity predictions, so we have adopted the length scale associated with the force dipole strength of the *E. coli*, $l_d = 17.7\mu m$ from Lopez et al [28], which gives $Pe_R = l_d/(U_0\tau_R) \approx 0.18$. The force dipole parameter $\alpha \equiv \sigma_0^H/(\zeta_{\|}U_0 a) \approx -15$, which is based on the reported force dipole strength of the bacteria [28], $\sigma_0^H = -3.8 \pm 1.0 \times 10^{-18} Pa \cdot m^3$.

In the results of Fig 7.3, the ratio $\sigma_{xy}^{swim}/(\sigma_{xy}^{swim} + \sigma_{xy}^{H}) \approx 0.5$ for small Pe and all bacteria concentrations, which quantifies the importance of the swim stress. For swimmers with $Pe_R \ll 1$ such as puller microalgae *C. Reinhardtii*, the hydrodynamic stress plays a negligibly small role and the swim stress dominates. Figure 7.4 compares our model with the experimental data of Rafaï et al [30], who measured the effective shear viscosity of a suspension containing *C. Reinhardtii*. Physical properties of the microalgae used in our model were taken from their work [30], with swimming speed $U_0 = 40\mu m/s$, reorientation time $\tau_R = 3.5s$, and body radius $a = 5\mu m$, giving $Pe_R \equiv a/(U_0\tau_R) \approx 0.035$. This motile microorganism has

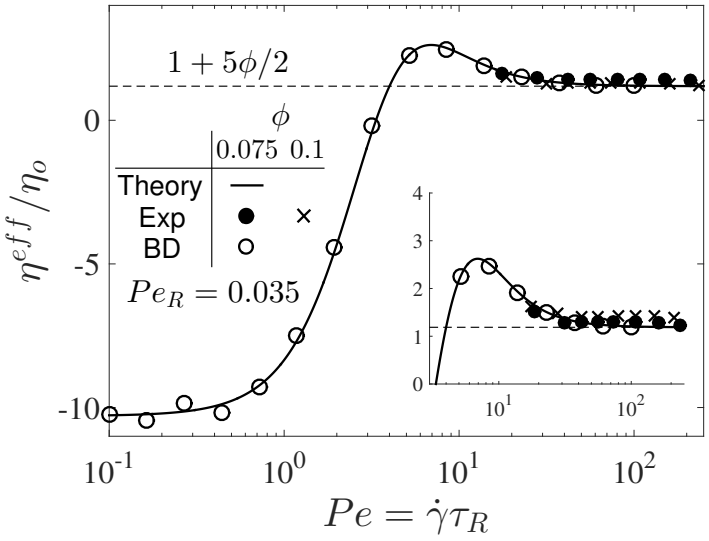

Figure 7.4: Effective suspension viscosity of spherical active particles at dilute concentrations and reorientation Péclet number $Pe_R \equiv a/(U_0\tau_R) = 0.035$. Filled circles and crosses at large Pe are experimental data of Rafaï et al (Rafaï, Jibuti, and Peyla, *Phys Rev Lett*, 2010) using 'puller' microalgae *C. Reinhardtii*. The solid curve is the analytical theory of Eq 7.5, and the open circles are BD simulation results. *Inset:* Magnification at large Pe to show agreement with experiments.

a spherical body but can align with an imposed flow, perhaps due to rheotaxis or small asymmetry arising from the two flagella used for self-propulsion. The solid curve in Fig 7.4 is the analytical theory of Eq 7.5 which does not involve the hydrodynamic stress. We obtain good agreement with experimental data and Brownian dynamics simulations, which demonstrates the importance of the shear swim stress for active systems with small reorientation Péclet numbers.

Results in Fig 7.4 suggest new behavior not predicted by conventional models. Previous studies [28, 3, 1, 2] have predicted that puller-type microorganisms like *C. Reinhardtii* increase the effective suspension viscosity above that of the suspending fluid because the hydrodynamic stress is positive for pullers, $\sigma_0^H > 0$. However, the swim stress predicts both thickening and thinning behavior, an increase and decrease of the effective viscosity, for pushers, pullers, and even particles that generate no hydrodynamic stress. Shear thickening and thinning are seen for small Pe_R; they are also present in Fig 7.3 but the magnitudes are too small to see. Because the swim stress is large in magnitude compared to the hydrodynamic stress for systems with $Pe_R \ll 1$, the effective shear viscosity decreases below η_0 at small shear rates regardless of the swimmer shape or hydrodynamic stress. Further exper-

iments with puller microorganisms at small shear rates are needed to verify if the effective viscosity decreases below the solvent viscosity.

In Fig 7.4, we observe a "negative" effective shear viscosity for small Pe, which means that a shear stress must be applied in a direction opposing the flow to maintain a fixed shear rate. The spontaneous onset of active diffusion of particles along the extensional axis of shear can result in a negative effective shear viscosity, analogous to that of active nematics for 'pusher' swimmers (see Fig 7.1). For a constant shear stress experiment, a reduction in effective viscosity would trigger the shear rate to increase, so a self-regulating processes would preclude a negative viscosity. For active suspensions with a larger concentration of particles, we must include an additional stress contribution from interparticle interactions between the swimmers, $\boldsymbol{\sigma}^P = -n\langle \boldsymbol{x}_{ij}\boldsymbol{F}^P_{ij}\rangle$. Our simulations reveal that the interparticle stress has a negligible effect for the dilute concentrations studied in this work. The force moment for the interparticle stress scales as the particle size, so its contribution is $O(Pe_R)$ smaller than the swim stress.

7.4 Appendix

We consider a single rigid Brownian active particle that swims in a Newtonian fluid with a fixed speed U_0 in a direction specified by a body-fixed unit orientation vector $\boldsymbol{q}$, which relaxes with a timescale τ_R due to rotational Brownian motion. We analyze the dynamics of this active particle in a steady simple shear flow described by a constant and uniform velocity-gradient tensor $\dot{\boldsymbol{\Gamma}}$.

The dynamics of the active particle is described by $P(\boldsymbol{x},\boldsymbol{q},t)$, the conditional probability of finding the particle at position $\boldsymbol{x}$ with orientation $\boldsymbol{q}$ at time t. As given in the main text, the Smoluchowski equation governs the probability distribution,

$$\frac{\partial P}{\partial t} + \nabla \cdot \boldsymbol{j}_T + \nabla_q \cdot \boldsymbol{j}_R = 0, \tag{7.7}$$

where the translational and rotational fluxes are given by, respectively,

$$\boldsymbol{j}_T = \left(\boldsymbol{x} \cdot \dot{\boldsymbol{\Gamma}} + U_0\boldsymbol{q}\right) P, \tag{7.8}$$

$$\boldsymbol{j}_R = \dot{\gamma}\left(\boldsymbol{q} \cdot \boldsymbol{\Lambda} + B(\boldsymbol{I} - \boldsymbol{qq})\boldsymbol{q} : \boldsymbol{E}\right) P - \frac{1}{\tau_R}\nabla_q P. \tag{7.9}$$

The dimensionless tensors $\boldsymbol{\Lambda}$ and $\boldsymbol{E}$ are the antisymmetric and symmetric contributions of the velocity-gradient tensor $\overline{\dot{\boldsymbol{\Gamma}}} = \dot{\boldsymbol{\Gamma}}/\dot{\gamma}$, where $\dot{\gamma}$ is the magnitude of shear rate, $\boldsymbol{I}$ is the isotropic tensor, and $\nabla \equiv \partial/\partial\boldsymbol{x}$ and $\nabla_q \equiv \partial/\partial\boldsymbol{q}$ are the physical-space and orientation-space gradient operators, respectively. The operator $\nabla_q \equiv \partial/\partial\boldsymbol{q}$

is not to be confused with the operator $\mathcal{R} \equiv \boldsymbol{q} \times \partial/\partial \boldsymbol{q}$. The constant scalar $B = ((a/b)^2 - 1)/((a/b)^2 + 1)$, where a and b are the semi-major and minor axis of the particle, respectively; $B = 0$ for a spherical particle. For microorganisms like gravitactic, magnetotactic, and phototactic bacteria, the rotational flux has an additional term incorporating the effects of an external torque or field.

From Eqs 7.7-7.9 we arrive at a convection-diffusion equation for the structure function $g(\boldsymbol{k},\boldsymbol{q},t)$, defined as $\widehat{P}(\boldsymbol{k},\boldsymbol{q},t) = g(\boldsymbol{k},\boldsymbol{q},t)\widehat{n}(\boldsymbol{k},t)$, where $\widehat{\cdot}$ represents the Fourier transform with respect to position, $\boldsymbol{k}$ is the wave vector, and $\widehat{n}(\boldsymbol{k},t) \equiv \int \widehat{P}(\boldsymbol{k},\boldsymbol{q},t)\, d\boldsymbol{q}$ is the Fourier transform of the local number density of active particles. We expand in the short wave vector limit $g(\boldsymbol{k},\boldsymbol{q},t) = g_0(\boldsymbol{q},t) + i\boldsymbol{k} \cdot \boldsymbol{d}(\boldsymbol{q},t) + O(\boldsymbol{k}\boldsymbol{k})$. Physically, g_0 is the orientation distribution field of the active particle and $\boldsymbol{d}$ is the probability-weighted fluctuation field of a particle about its mean velocity.

For an active particle in a simple shear flow, $\boldsymbol{u}^\infty = \dot{\gamma} y \boldsymbol{e}_x$, the nondimensional evolution equations governing the orientation-distribution function g_0 and the fluctuation field $\boldsymbol{d}$ are, respectively:

$$-\nabla_q^2 g_0 + Pe \nabla_{\boldsymbol{q}} \cdot (\boldsymbol{q} \cdot \boldsymbol{\Lambda} + B(\boldsymbol{I} - \boldsymbol{q}\boldsymbol{q})\boldsymbol{q} : \boldsymbol{E})\, g_0 = 0, \tag{7.10}$$

$$-\nabla_q^2 \boldsymbol{d} + Pe \nabla_{\boldsymbol{q}} \cdot (\boldsymbol{q} \cdot \boldsymbol{\Lambda} + B(\boldsymbol{I} - \boldsymbol{q}\boldsymbol{q})\boldsymbol{q} : \boldsymbol{E})\, \boldsymbol{d} + Pe \boldsymbol{d}_y \delta_{xy} = g_0 \left(\boldsymbol{q} - \langle \boldsymbol{q} \rangle\right). \tag{7.11}$$

The shear Péclet number $Pe \equiv \dot{\gamma}\tau_R$ balances the magnitude of the shear rate and the particle's intrinsic reorientation time. In the $\boldsymbol{d}$-field equation, the last term on the left, $Pe\boldsymbol{d}_y\delta_{xy}$, is the convective drift of the fluctuation field and is present only in the x-direction. The right side of Eq 7.11 is the forcing due to the orientation distribution, where $\langle \boldsymbol{q} \rangle = \int \boldsymbol{q} g_0(\boldsymbol{q}) d\boldsymbol{q}$. The conditions on g_0 and $\boldsymbol{d}$ are that they are finite and normalized: $\int g_0\, d\boldsymbol{q} = 1$ and $\int \boldsymbol{d}\, d\boldsymbol{q} = 0$.

By solving Eqs 7.10 and 7.11, we can compute the average translational velocity, $\langle \boldsymbol{u} \rangle = U_0 \int \boldsymbol{q} g_0\, d\boldsymbol{q}$, and effective translational diffusivity of the particle:

$$\langle \boldsymbol{D} \rangle = \boldsymbol{D}^{swim} = (U_0^2 \tau_R) \int [\boldsymbol{q}\boldsymbol{d}]^{sym}\, d\boldsymbol{q}, \tag{7.12}$$

where $\boldsymbol{d}$ is nondimensionalized by the swimmer run length $U_0\tau_R$ and $[\cdot]^{sym}$ denotes the symmetric part of the tensor.

Exact analytical solutions to Eqs 7.10 and 7.11 are available [10] for spherical particles ($B = 0$), which govern the orientation distribution function g_0 and the fluctu-

ation field $\boldsymbol{d} = d_x\boldsymbol{e}_x + d_y\boldsymbol{e}_y + d_z\boldsymbol{e}_z$:

$$g_0 = 1/(4\pi), \tag{7.13}$$

$$d_x = \frac{1}{\pi(Pe^2+16)^2}\left[-\frac{Pe}{2}(3Pe^2-16)\cos\phi + 2(5Pe^2+16)\sin\phi\right]\sin\theta, \tag{7.14}$$

$$d_y = \frac{1}{\pi(Pe^2+16)}\left(\frac{Pe}{2}\sin\phi + 2\cos\phi\right)\sin\theta, \tag{7.15}$$

$$d_z = \frac{1}{8\pi}\cos\theta. \tag{7.16}$$

Anisotropy in the fluctuation field is apparent in the flow (x), gradient (y), and vorticity (z) directions. Substituting Eqs 7.14 - 7.16 into Eq 7.12, the nonzero elements of the swim diffusivity $\widehat{\boldsymbol{D}}^{swim} = \boldsymbol{D}^{swim}/(U_0^2\tau_R/6)$ are:

$$\widehat{D}_{xx}^{swim} = \frac{1 + 5Pe^2/16}{\left[1 + (Pe/4)^2\right]^2} \tag{7.17}$$

$$\widehat{D}_{xy}^{swim} = \widehat{D}_{yx}^{swim} = \frac{Pe}{4}\left\{\frac{1-(Pe/4)^2}{\left[1+(Pe/4)^2\right]^2}\right\} \tag{7.18}$$

$$\widehat{D}_{yy}^{swim} = \frac{1}{1+(Pe/4)^2} \tag{7.19}$$

$$\widehat{D}_{zz}^{swim} = 1. \tag{7.20}$$

These analytical results are plotted in Fig 2 of the main text. Results for non-spherical particles for arbitrary Pe require a numerical solution to Eqs 7.10 and 7.11.

In an experiment or computer simulation, calculation of shear-induced diffusivity is nontrivial because advective drift translates the particles in the flow direction. We cannot simply take the time derivative of the mean-square displacement, $\langle \boldsymbol{x}\boldsymbol{x}\rangle$, because these quantities in general do not grow linearly with time due to Taylor dispersion. Furthermore, cross-correlations between advective drift in the flow direction and a random walk in the gradient direction give a nonzero contribution [15]. For example, to compute the flow-gradient component of the diffusivity, D_{xy}, from the displacements, one must use

$$D_{xy} = \frac{1}{2}\frac{d\langle x(t)y(t)\rangle}{dt} - \frac{1}{2}\dot{\gamma}\langle y(t)y(t)\rangle. \tag{7.21}$$

The second term demonstrates that a random walk in the flow gradient direction, $\langle y(t)y(t)\rangle$, allows an active particle to sample new streamlines in the flow direction to give a nonzero D_{xy}. We can use a similar expression to compute D_{xx} [15].

Using the relationship between the swim diffusivity and the swim stress, we have

$$\boldsymbol{\sigma}^{swim} = -n\zeta \boldsymbol{D}^{swim} = -(n\zeta U_0^2 \tau_R) \int [\boldsymbol{qd}]^{sym} \; d\boldsymbol{q}. \tag{7.22}$$

Therefore, computing the effective translational diffusivity is equivalent to measuring the stress (or pressure) generated by the particle. For spherical active particles, we can simply multiply Eqs 7.17-7.20 by $(n\zeta)$ to obtain the swim stress. When there is no nematic ordering of the microswimmers with the imposed flow, $g_0 = 1/(4\pi)$, and the hydrodynamic stress is $\boldsymbol{\sigma}^H = n\boldsymbol{S}^H = n\sigma_0^H(\langle \boldsymbol{qq} \rangle - \boldsymbol{I}/3) = \boldsymbol{0}$.

In addition to an indirect calculation of the micromechanical stress via the diffusivity, we can also compute it directly using the virial expression. Here we compute individual components of the swim stress for a spherical particle in a dilute system. From the overdamped Langevin equations, the motion of a non-Brownian particle in simple shear flow is given by

$$\frac{dx}{dt} = q_x + Pe \; y \tag{7.23}$$

$$\frac{dy}{dt} = q_y, \tag{7.24}$$

where $\boldsymbol{q} = (q_x, q_y, q_z)^T$ is the unit orientation vector in the direction of self-propulsion, $Pe \equiv \dot{\gamma}\tau_R$ is the shear Péclet number, and length and time are nondimensionalized by the swimmer's run length $U_0\tau_R$ and τ_R, respectively. Solving these equations, we obtain $y(t) = \int_0^t q_y(t')dt'$ and $x(t) = \int_0^t q_x(t')dt' + Pe \int_0^t \int_0^{t'} q_y(t'')dt''dt'$.

We can now directly compute every component in the swim stress tensor $\boldsymbol{\sigma}^{swim} = -n\langle \left[\boldsymbol{x}\boldsymbol{F}^{swim}\right]^{sym} \rangle$, where $\boldsymbol{F}^{swim} = \zeta U_0 \boldsymbol{q}$ for active Brownian particles. We obtain

$$\frac{\sigma_{xx}^{swim}}{-n\zeta U_0^2 \tau_R} = \int_0^t \langle q_x(t')q_x(t) \rangle dt' + Pe \int_0^t \int_0^{t'} \langle q_y(t'')q_x(t) \rangle dt''dt' \tag{7.25}$$

$$\frac{\sigma_{xy}^{swim}}{-n\zeta U_0^2 \tau_R} = \frac{1}{2} \int_0^t \left[\langle q_x(t')q_y(t) \rangle + \langle q_y(t')q_x(t) \rangle \right] dt' + Pe \int_0^t \int_0^{t'} \langle q_y(t'')q_y(t) \rangle dt''dt' \tag{7.26}$$

$$\frac{\sigma_{yy}^{swim}}{-n\zeta U_0^2 \tau_R} = \int_0^t \langle q_y(t')q_y(t) \rangle dt'. \tag{7.27}$$

The first term on the right of Eq 7.25 is the 'self-term' and is equal to $(1 + (Pe/4)^2)^{-1}/6$ (for spheres), which come from the constant angular velocity imposed on the particle due to the shear flow. The second term is the cross-correlation between a random walk in the y-direction and the advective flow in the x-direction. In Eq 7.26, the second integral on the right shows that random motion in the y-direction, $D_{yy}^{swim} \sim \langle q_y(t'')q_y(t)\rangle$, can induce a shear component. The orientation correlations in Eqs 7.25-7.27 can be computed by solving the angular Langevin equation governing the time evolution of $\boldsymbol{q}(t)$ (see main text). The resulting solutions give

$$\frac{\sigma_{xx}^{swim}}{-n\zeta U_0^2\tau_R/6} = \frac{1 + 5Pe^2/16}{\left(1 + (Pe/4)^2\right)^2} \tag{7.28}$$

$$\frac{\sigma_{xy}^{swim}}{-n\zeta U_0^2\tau_R/6} = \frac{Pe}{4}\left[\frac{1 - (Pe/4)^2}{\left(1 + (Pe/4)^2\right)^2}\right] \tag{7.29}$$

$$\frac{\sigma_{yy}^{swim}}{-n\zeta U_0^2\tau_R/6} = \frac{1}{1 + (Pe/4)^2}. \tag{7.30}$$

The solutions we have obtained using the virial expression are identical to those obtained using the generalized Taylor dispersion theory in Eqs 7.17-7.19. We again find that the relationship between the mechanical stress and the effective translational diffusivity, $\boldsymbol{\sigma} = -n\zeta\boldsymbol{D}$, is true in general for dilute systems with any source of random motion.

References

[1] D. Saintillan. "The dilute rheology of swimming suspensions: A simple kinetic model". *Exp Mech* 50.9 (2010), pp. 1275–1281.

[2] M. C. Marchetti et al. "Hydrodynamics of soft active matter". *Rev Mod Phys* 85.3 (2013), pp. 1143–1189.

[3] Y. Hatwalne, S. Ramaswamy, M. Rao, and R. A. Simha. "Rheology of active-particle suspensions". *Phys Rev Lett* 92.11 (2004), p. 118101.

[4] S. C. Takatori, W. Yan, and J. F. Brady. "Swim pressure: Stress generation in active matter". *Phys Rev Lett* 113.2 (2014), p. 028103.

[5] S. C. Takatori and J. F. Brady. "Swim stress, motion, and deformation of active matter: Effect of an external field". *Soft Matter* 10.47 (2014), pp. 9433–9445.

[6] S. C. Takatori and J. F. Brady. "Towards a thermodynamics of active matter". *Phys Rev E* 91.3 (2015), p. 032117.

[7] S. C. Takatori and J. F. Brady. “A theory for the phase behavior of mixtures of active particles”. *Soft Matter* 11.40 (2015), pp. 7920–7931.

[8] S. C. Takatori and J. F. Brady. “Forces, stresses and the (thermo?) dynamics of active matter”. *Curr Opin Colloid Interface Sci* 21 (2016), pp. 24–33.

[9] M. A. Bees, N. A. Hill, and T. J. Pedley. “Analytical approximations for the orientation distribution of small dipolar particles in steady shear flows”. *J Math Biol* 36.3 (1998), pp. 269–298.

[10] A. Manela and I. Frankel. “Generalized Taylor dispersion in suspensions of gyrotactic swimming micro-organisms”. *J Fluid Mech* 490 (2003), pp. 99–127.

[11] W. Yan and J. F. Brady. “The force on a boundary in active matter”. *J Fluid Mech* 785 (2015), R1.

[12] R. N. Zia and J. F. Brady. “Single-particle motion in colloids: Force-induced diffusion”. *J Fluid Mech* 658 (2010), pp. 188–210.

[13] Y. Almog and I. Frankel. “Effects of fore-aft asymmetry on the sedimentation and dispersion of axisymmetric Brownian particles”. *J Colloid Interface Sci* 157.1 (1993), pp. 60–71.

[14] A. Sierou and J. F. Brady. “Shear-induced self-diffusion in non-colloidal suspensions”. *J Fluid Mech* 506 (2004), pp. 285–314.

[15] S. C. Takatori, R. De Dier, J. Vermant, and J. F. Brady. “Acoustic trapping of active matter”. *Nat Commun* 7 (2016).

[16] W. Yan and J. F. Brady. “The swim force as a body force”. *Soft Matter* 11.31 (2015), pp. 6235–6244.

[17] X. Yang, M. L. Manning, and M. C. Marchetti. “Aggregation and segregation of confined active particles”. *Soft Matter* 10.34 (2014), pp. 6477–6484.

[18] S. A. Mallory, A. Šarić, C. Valeriani, and A. Cacciuto. “Anomalous thermomechanical properties of a self-propelled colloidal fluid”. *Phys Rev E* 89.5 (2014), p. 052303.

[19] B. Ezhilan, R. Alonso-Matilla, and D. Saintillan. “On the distribution and swim pressure of run-and-tumble particles in confinement”. *J Fluid Mech* 781 (2015), R4.

[20] A. P. Solon et al. “Pressure and phase equilibria in interacting active Brownian spheres”. *Phys Rev Lett* 114.19 (2015), p. 198301.

[21] R. G. Winkler, A. Wysocki, and G. Gompper. “Virial pressure in systems of spherical active Brownian particles”. *Soft Matter* 11.33 (2015), pp. 6680–6691.

[22] R. G. Winkler. “Dynamics of flexible active Brownian dumbbells in the absence and the presence of shear flow”. *Soft Matter* 12.16 (2016), pp. 3737–3749.

[23] F. Smallenburg and H. Lowen. “Swim pressure on walls with curves and corners”. *Phys Rev E* 92.3 (2015), p. 032304.

[24] D. Saintillan and M. J. Shelley. “Instabilities, pattern formation, and mixing in active suspensions”. *Phys Fluids* 20.12 (2008), pp. 123304–123315.

[25] D. Saintillan and M. J. Shelley. “Instabilities and pattern formation in active particle suspensions: Kinetic theory and continuum simulations”. *Phys Rev Lett* 100.17 (2008), p. 178103.

[26] E. J. Hinch and L. G. Leal. “Constitutive equations in suspension mechanics. Part 2. Approximate forms for a suspension of rigid particles affected by Brownian rotations”. *J Fluid Mech* 76.01 (1976), pp. 187–208.

[27] C.-C. Huang, R. G. Winkler, G. Sutmann, and G. Gompper. “Semidilute polymer solutions at equilibrium and under shear flow”. *Macromolecules* 43.23 (2010), pp. 10107–10116.

[28] H. M. López, J. Gachelin, C. Douarche, H. Auradou, and E. Clément. “Turning bacteria suspensions into superfluids”. *Phys Rev Lett* 115.2 (2015), p. 028301.

[29] M. E. Cates and J. Tailleur. “When are active Brownian particles and run-and-tumble particles equivalent? Consequences for motility-induced phase separation”. *Europhys Lett* 101.2 (2013), p. 20010.

[30] S. Rafaï, L. Jibuti, and P. Peyla. “Effective viscosity of microswimmer suspensions”. *Phys Rev Lett* 104.9 (2010), p. 098102.

Chapter 8

INERTIAL EFFECTS ON THE STRESS GENERATION OF ACTIVE COLLOIDS

We analyze the effects of finite particle inertia on the mechanical pressure (or stress) exerted by a suspension of self-propelled bodies. The magnitude of particle inertia is characterized by the Stokes number St_R, defined as the ratio of the active swimmers' momentum relaxation time to their reorientation time. We maintain negligible fluid inertia so that the fluid motion satisfies the steady Stokes equation. Through their self-motion swimmers of all scales exert a unique 'swim stress' and 'Reynolds stress' that impacts their large-scale behavior. We find that particle inertia plays a similar role as confinement in overdamped Brownian systems, where the reduced run length decreases the swim pressure and affects the phase behavior of active systems. Although the swim and Reynolds stresses vary with St_R, the sum of the two contributions is independent of St_R for all values of particle inertia. This points to an important concept when computing stresses in computer simulations of nonequilibrium systems—the Reynolds stress and the virial stress must both be calculated to obtain the total stress generated by a system. For dilute active swimmers, the total stress generation is the same regardless of the swimmers' size and mass, and we provide a simple method to compute the active pressure exerted by larger self-propelled bodies where particle inertia is important.

8.1 Introduction

Active matter systems constitute an intriguing class of materials whose constituents have the ability to self-propel, generate internal stress, and drive the system far from equilibrium. Because classical thermodynamic concepts do not rigorously apply to nonequilibrium active matter, recent work has focused on invoking the mechanical pressure (or stress) as a framework to understand the complex dynamic behaviors of active systems [1, 2, 3, 4, 5, 6]. In particular, active swimmers exert a unique "swim pressure" as a result of their self propulsion [1]. A physical interpretation of the swim pressure is the unique pressure (or stress) exerted by the swimmers as they bump into the surrounding boundaries that confine them, similar to molecular or colloidal solutes that collide into the container walls to exert an osmotic pressure. The swim pressure is a purely entropic, destabilizing quantity [7] that can explain

the self-assembly and phase separation of a suspension of self-propelled colloids into dilute and dense phases that resemble an equilibrium gas-liquid coexistence [8, 9, 10, 11, 12, 13].

Existing studies of the pressure of active systems [1, 14, 7, 4, 5, 3, 6] have focused on overdamped systems where swimmer inertia is neglected (i.e, the particle Reynolds number is small). However, the swim pressure has no explicit dependence on the body size and may exist at all scales including larger swimmers (e.g., fish, birds) where particle inertia is not negligible [1]. The importance of particle inertia is characterized by the Stokes number, $St_R \equiv (M/\zeta)/\tau_R$, where M is the particle mass, ζ is the hydrodynamic drag factor, and τ_R is the reorientation time of the active swimmer. Here we analyze the role of nonzero St_R on the mechanical stress exerted by a system of self-propelled bodies and provide a natural extension of existing pressure concepts to swimmers with finite inertia.

We consider a suspension of self-propelled spheres of radii a that translate with an intrinsic swim velocity $\boldsymbol{U}_0$, tumble with a reorientation time τ_R, and experience a hydrodynamic drag factor ζ from the surrounding continuous Newtonian fluid. The random tumbling results in a diffusive process for time $t \gg \tau_R$ with $D^{swim} = U_0^2\tau_R/6$ in 3D. An isolated active particle generates a swim pressure $\Pi^{swim} = n\zeta D^{swim} = n\zeta U_0^2\tau_R/6$, where n is the number density of active particles. We do not include the effects of hydrodynamic interactions, and there is no macroscopic polar order of the swimmers or any large-scale collective motion (e.g., bioconvection).

From previous work [15, 2, 16, 17], we know that geometric confinement of overdamped active particles plays a significant role in their dynamics and behavior. Confinement from potential traps, physical boundaries, and collective clustering can reduce the average run length and swim pressure of the particles. We have shown experimentally [15] that active Brownian particles trapped inside a harmonic well modifies the swim pressure to $\Pi^{swim} = (n\zeta U_0^2\tau_R/2)\,(1+\alpha)^{-1}$ in 2D, where $\alpha \equiv U_0\tau_R/R_c$ is a ratio of the run length, $U_0\tau_R$, to the size of the trap, R_c. For weak confinement, $\alpha \ll 1$, we obtain the 'ideal-gas' swim pressure of an isolated swimmer. For strong confinement, $\alpha \gg 1$, the swim pressure decreases as $\Pi^{swim}/(n\zeta U_0^2\tau_R/2) \sim 1/\alpha$. Confinement reduces the average distance the swimmers travel between reorientation events, which results in a decreased swim pressure.

In this work, we find that particle inertia plays a similar role as confinement by

reducing the correlation between the position and self-propulsive swim force of the swimmers. In addition to the swim pressure, active swimmers exert the usual Reynolds pressure contribution associated with their average translational kinetic energy. For swimmers with finite particle inertia we find that the sum of the swim and Reynolds pressure is the relevant quantity measured by confinement experiments and computer simulations. We also study systems at finite swimmer concentrations and extend our existing mechanical pressure theory to active matter of any size or mass.

An important consequence of this work pertains to the computation of mechanical stresses of colloidal suspensions at the appropriate level of analysis. Consider the Brownian osmotic pressure of molecular fluids and Brownian colloidal systems, $\Pi^B = nk_BT$, where n is the number density of particles and k_BT is the thermal energy. At the Langevin-level analysis where mass (or inertia) is explicitly included, the Reynolds stress or the autocorrelation of the velocity fluctuation, $-\langle \rho \boldsymbol{U}\boldsymbol{U} \rangle$, is the source of the Brownian osmotic pressure. The virial stress or the moment of the Brownian force, $-n\langle \boldsymbol{x}\boldsymbol{F}^B \rangle$, is identically equal to zero due to delta-function statistics imposed for the Brownian force. However, at the overdamped Fokker-Planck or Smoluchowski level where inertia is not explicitly included, the virial stress $-n\langle \boldsymbol{x}\boldsymbol{F}^B \rangle$ is the source of the Brownian osmotic pressure, whereas the Reynolds stress is zero. The important point is that the sum of the Reynolds and virial stresses gives the correct Brownian osmotic pressure at both levels of analysis, as it must be since the osmotic pressure of colloidal Brownian suspensions is $\Pi^B = nk_BT$ whether or not inertia is explicitly included in the analysis.

We report in this work that an identical concept applies for active swimmers. The virial stress arising from the correlation between the particle position and its 'internal' force, $-n\langle \boldsymbol{x}\boldsymbol{F} \rangle$, is a term that is separate and in addition to the Reynolds stress associated with their average translational kinetic energy. Interestingly, the mechanical stress generated by active swimmers has a nonzero contribution from both the Reynolds and virial stresses because the internal force associated with self-propulsion has an autocorrelation that is not instantaneous in time and instead decays over a finite timescale modulated by the reorientation time of the active swimmer, τ_R: $\langle \boldsymbol{F}^{swim}(t)\boldsymbol{F}^{swim}(0) \rangle \sim e^{-2t/\tau_R}$. If one were to incorporate the solvent relaxation timescale, τ_S, into the Brownian force (e.g., $\langle \boldsymbol{F}^B(t)\boldsymbol{F}^B(0) \rangle \sim e^{-2t/\tau_S}$), the Brownian osmotic stress would also have a nonzero contribution from both the $-\langle \rho \boldsymbol{U}'\boldsymbol{U}' \rangle$ and $-n\langle \boldsymbol{x}\boldsymbol{F}^B \rangle$ terms, with their sum equal to $\boldsymbol{\sigma}^B = -nk_BT\boldsymbol{I}$ for all τ_S.

A distinguishing feature of active swimmers compared with passive Brownian particles is that their direction of self-propulsion can relax over large timescales, and that the 'internal' swim force autocorrelation cannot in general be described by a delta-function in time.

This raises an important concept about the calculation of stresses in computer simulations of molecular fluids or Brownian colloidal systems. As stated above, the delta-function statistics for the Brownian force autocorrelation give the virial force moment $-n\langle \boldsymbol{x}\boldsymbol{F}^B\rangle \equiv \boldsymbol{0}$, and the Reynolds stress is the only nonzero term that one needs to calculate in a simulation to obtain the Brownian osmotic pressure. However, active systems generate nonzero contributions from both the Reynolds and virial stresses that must be calculated in a simulation. This is especially important when adapting existing molecular dynamics software packages to compute the stresses of active systems and other nonequilibrium systems.

8.2 Swim stress

All self-propelled bodies exert a swim pressure, a unique pressure associated with the confinement of the active body inside a bounded domain [1]. The swim pressure is the trace of the swim stress, which is defined as the first moment of the self-propulsive force, $\boldsymbol{\sigma}^{swim} = -n\langle \boldsymbol{x}\boldsymbol{F}^{swim}\rangle$, where n is the number density of swimmers, $\boldsymbol{x}$ is the position, and $\boldsymbol{F}^{swim}$ is the swimmer's self-propulsive swim force [1]. For the active Brownian particle model, the swim force can be written as $\boldsymbol{F}^{swim} = \zeta U_0 \boldsymbol{q}$ where $\boldsymbol{q}$ is a unit vector specifying the swimmer's direction of self-propulsion. For a dilute suspension of active particles with negligible particle inertia the "ideal-gas" swim stress is given by $\boldsymbol{\sigma}^{swim} = -n\zeta U_0^2 \tau_R \boldsymbol{I}/6 = -nk_sT_s\boldsymbol{I}$, where we define $k_sT_s \equiv \zeta U_0^2\tau_R/6$ as the swimmer's "energy scale" (force (ζU_0) $\times$ distance ($U_0\tau_R$)). The swim pressure (or stress) is entropic in origin and is the principle destabilizing term that facilitates a phase transition in active systems [7].

In the absence of any external forces, the motion of an active Brownian particle is governed by the Langevin equations:

$$M\frac{\partial \boldsymbol{U}}{\partial t} = -\zeta(\boldsymbol{U} - \boldsymbol{U}_0) + \sqrt{2\zeta^2 D_0}\boldsymbol{\Lambda}_T, \tag{8.1}$$

$$I\frac{\partial \boldsymbol{\Omega}}{\partial t} = -\zeta_R\boldsymbol{\Omega} + \sqrt{\frac{2\zeta_R^2}{\tau_R}}\boldsymbol{\Lambda}_R, \tag{8.2}$$

where M and I are the particle mass and moment-of-inertia, $\boldsymbol{U}$ and $\boldsymbol{\Omega}$ are the translational and angular velocities, ζ_R is the hydrodynamic drag factor coupling angu-

lar velocity to torque, $\sqrt{2\zeta^2 D_0}\boldsymbol{\Lambda}_T$ and $\sqrt{2\zeta_R^2/\tau_R}\boldsymbol{\Lambda}_R$ are the Brownian translational force and rotational torque, respectively, $\boldsymbol{\Lambda}_T$ and $\boldsymbol{\Lambda}_R$ are unit random normal deviates, $\tau_R \sim 1/D_R$ is the reorientation timescale set by rotational Brownian motion, and D_0 is the Stokes-Einstein-Sutherland translational diffusivity. The translational diffusivity and the reorientation dynamics are modeled with the usual white noise statistics, $\langle\Lambda_i(t)\rangle = 0$ and $\langle\Lambda_i(t)\Lambda_j(0)\rangle = \delta(t)\delta_{ij}$. The swimmer orientation $\boldsymbol{q}(t)$ is related to the angular velocity by the kinematic relation $\boldsymbol{\Omega}\times\boldsymbol{q} = d\boldsymbol{q}/dt$. The translational and angular velocities may be combined into a single vector, $\mathcal{U} = (\boldsymbol{U},\boldsymbol{\Omega})^T$, and similarly for the force and torque, $\mathcal{F} = (\boldsymbol{F},\boldsymbol{L})^T$, to obtain a general solution to the system of ordinary differential equations [18]. Although a general solution is available for any particle mass and moment-of-inertia, inclusion of nonzero moment-of-inertia leads to calculations that are analytically involved. For convenience and to make analytical progress, here we summarize the case of zero moment-of-inertia ($I = 0$) and focus on finite mass ($St_R \equiv (M/\zeta)/\tau_R \neq 0$) to elucidate the effects of inertia on the dynamics of active matter.

We can solve Eqs 8.1 and 8.2 for the swimmer configuration $(\boldsymbol{x}(t),\boldsymbol{q}(t))$, and calculate the swim stress. As shown in the Appendix, the swim stress for arbitrary particle inertia is

$$\boldsymbol{\sigma}^{swim} = -nk_sT_s\left(\frac{1}{1+2St_R}\right)\boldsymbol{I}, \tag{8.3}$$

where we have taken times $t > \tau_M$ and $t > \tau_R$, $\tau_M \equiv M/\zeta$ is the swimmer momentum relation time, energy scale $k_sT_s \equiv \zeta U_0^2\tau_R/6$, and $St_R \equiv \tau_M/\tau_R = (M/\zeta)/\tau_R$ is the Stokes number. For $St_R = 0$ we recover the "ideal-gas" swim pressure for an overdamped system: $\Pi^{swim} = -\mathrm{tr}\boldsymbol{\sigma}^{swim}/3 = n\zeta U_0^2\tau_R/6 = nk_sT_s$ [1]. This is precisely the mechanical force per unit area that a dilute system of confined active micro-swimmers exert on its surrounding container [1, 4, 5].

Notice in the other limit as $St_R \to \infty$, $\boldsymbol{\sigma}^{swim}$ vanishes. Physically, the magnitude of the swim stress decreases because inertia may translate the swimmer in a trajectory that is different from the direction of the swim force, reducing the correlation $\langle\boldsymbol{x}\boldsymbol{F}^{swim}\rangle$ between the moment arm $\boldsymbol{x}$ and the orientation-dependent swim force $\boldsymbol{F}^{swim} = \zeta U_0\boldsymbol{q}$. Our earlier work [15] showed that active particles confined by an acoustic trap exert a swim pressure that is reduced by a factor of $(1+\alpha)^{-1}$, where $\alpha \equiv U_0\tau_R/R_c$ is the degree of confinement of the swimmer run length relative to the size of the trap R_c. Equation 8.3 has a reduction in the swim pressure by a similar factor, $(1+2St_R)^{-1}$, suggesting that particle inertia plays a similar role as confine-

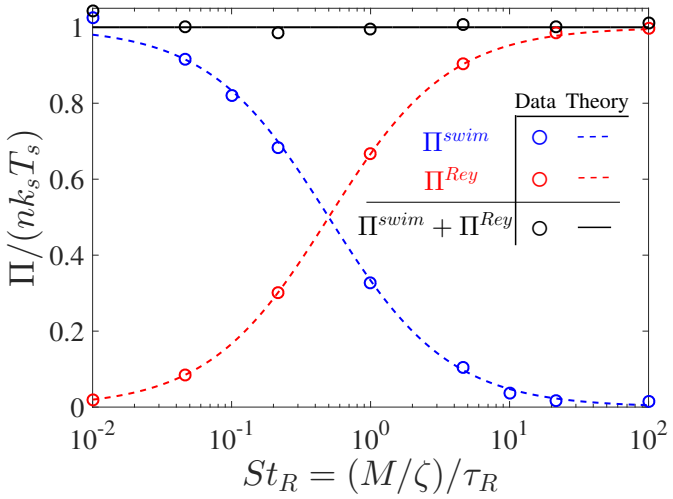

Figure 8.1: Swim and Reynolds pressures of a dilute system of swimmers with finite inertia, where $\Pi = -\mathrm{tr}\boldsymbol{\sigma}/3$. The red ($\Pi^{swim}$) and blue ($\Pi^{Rey}$) curves and symbols are the analytical theory of Eqs 8.3 and 8.4 and simulation data, respectively. The solid black line is the sum of the swim and Reynolds stresses. The Brownian osmotic pressure $\Pi^B = nk_BT$ has been subtracted from Π^{Rey}.

ment by reducing the correlation between the position and self-propulsive direction of the swimmers.

Confinement imposed by particle inertia decreases the average run length of the swimmer to $(U_0\tau_R - \Delta x')$, where $\Delta x' = U_0\Delta t$ is the distance over which inertia translates the swimmer along a trajectory that is different from the direction of its swim force, and the time over which this occurs scales with the inertial relaxation time, $\Delta t \sim M/\zeta$. Substituting these terms into the virial expression for the swim pressure, we obtain $\Pi^{swim} \sim n\langle \boldsymbol{x} \cdot \boldsymbol{F}^{swim} \rangle \sim n\zeta U_0^2\tau_R(1 - (M/\zeta)/\tau_R)$. Using the definition of the Stokes number $St_R \equiv (M/\zeta)/\tau_R$ and for small St_R, we can rewrite the swim pressure as $\Pi^{swim} \sim n\zeta U_0^2\tau_R(1 + St_R)^{-1}$. Aside from the factor of 2 in the denominator (which arises from spatial dimensionality), this scaling argument agrees with Eq 8.3 and shows that particle inertia plays a confining role in the swim pressure.

8.3 Reynolds stress

For systems with finite particle inertia, an additional stress contribution arises owing to particle acceleration: the Reynolds stress. This term is seen in Bernoulli's equation and is associated with the average translational kinetic energy of a particle, $\boldsymbol{\sigma}^{Rey} = -nM\langle \boldsymbol{U}\boldsymbol{U} \rangle$. This contribution was not included in previous studies since

overdamped active systems have no particle mass, $M = 0$ (i.e., $St_R = (M/\zeta)/\tau_R = 0$). As shown in the Appendix, we can use the solution to Eqs 8.1 and 8.2 to obtain the Reynolds stress for arbitrary St_R, given by

$$\boldsymbol{\sigma}^{Rey} = -nk_BT\boldsymbol{I} - nk_sT_s\left(\frac{1}{1+1/(2St_R)}\right)\boldsymbol{I}, \tag{8.4}$$

which is a sum of the Brownian osmotic stress $\boldsymbol{\sigma}^B = -nk_BT\boldsymbol{I}$ and a self-propulsive contribution that depends on St_R. For an overdamped system where $St_R = 0$, the self-propulsive contribution to the Reynolds stress vanishes, justifying the neglect of this term in previous studies of overdamped systems. Mallory et al [5] calculated the analytical expression of the Reynolds stress, Eq 8.4, but not the swim stress, Eq 8.3; the mechanical pressure they measured from the walls of an enclosing container is the sum of the Reynolds and swim pressures.

Notice that the Brownian osmotic stress, $\boldsymbol{\sigma}^B = -nk_BT\boldsymbol{I}$, arises solely from the Reynolds stress and not from taking the virial moment of the Brownian force, $\langle \boldsymbol{x}\boldsymbol{F}^B\rangle$. As stated earlier, this is precisely because of the delta-function statistics imposed for the Brownian force in the Langevin-level analysis where mass is explicitly included: $\langle \boldsymbol{F}^B(t)\boldsymbol{F}^B(0)\rangle = 2k_BT\zeta\delta(t)\boldsymbol{I}$. In contrast, the active stress has a nonzero contribution from both the Reynolds and swim stresses because the swim force autocorrelation is a decaying exponential modulated by the reorientation timescale τ_R: $\langle \boldsymbol{F}^{swim}(t)\boldsymbol{F}^{swim}(0)\rangle \sim e^{-2t/\tau_R}$. If one were to model the Brownian force autocorrelation as one that relaxes over a finite solvent relaxation timescale, $\langle \boldsymbol{F}^B(t)\boldsymbol{F}^B(0)\rangle \sim e^{-2t/\tau_S}$, then we would obtain nonzero contributions from both the Reynolds and virial stresses, with their sum equal to $\boldsymbol{\sigma}^B = -nk_BT\boldsymbol{I}$ for all τ_S.

When computing stresses in computer simulations of molecular fluids or colloidal systems, it is important to remember that the virial stress arising from the correlation between the particle position and its 'internal' force, $-n\langle \boldsymbol{x}\boldsymbol{F}\rangle$, is a term that is separate and in addition to the Reynolds stress, $\boldsymbol{\sigma}^{Rey} = -nM\langle \boldsymbol{U}\boldsymbol{U}\rangle$. This is true in general for passive colloidal systems and is not unique to active swimmers. Some care is required when computing stresses in computer simulations, as systems may have nonzero contributions from both the Reynolds and virial stresses that must be calculated separately.

For a dilute suspension, the stress exerted by an active swimmer is the sum of the swim and Reynolds stresses. Adding Eqs 8.3 and 8.4, we find

$$\boldsymbol{\sigma}^{swim} + \boldsymbol{\sigma}^{Rey} = -n(k_BT + k_sT_s)\boldsymbol{I}. \tag{8.5}$$

Remarkably, the Stokes number St_R disappears. The magnitude of the swim pressure that decreases with increasing St_R cancels exactly the increase in the magnitude of the Reynolds stress. This verifies that swimmers of all scales exert the pressure, nk_sT_s, regardless of their mass and inertia. We conducted simulations where the dynamics of active Brownian particles were evolved following Eqs 8.1 and 8.2 using the velocity verlet algorithm [19], and the results are shown in Fig 8.1. Results from the simulations agree with our theoretical predictions in Eqs 8.3 - 8.5. In an experiment or simulation, the average mechanical pressure exerted on a confining boundary gives Eq 8.5, the sum of the swim and Reynolds pressures, and not their separate values.

In the presence of a nonzero moment-of-inertia, there is another dimensionless Stokes number, $St_I \equiv (I/\zeta_R)/\tau_R$, which is a ratio of the inertial reorientation timescale, $\tau_I = I/\zeta_R$, and the swimmers' intrinsic reorientation timescale, τ_R. Similar to the translational Stokes number St_R that does not appear in Eq 8.5, the moment-of-inertia is not expected to appear explicitly in the total stress generated by an active swimmer.

8.4 Finite concentrations

The results thus far are for a dilute suspension of active swimmers. At finite concentrations, experiments and computer simulations have observed unique phase behavior and self-assembly in active matter [8, 9, 10, 11, 12, 13]. Recently a new mechanical pressure theory was developed to provide a phase diagram and a natural extension of the chemical potential and other thermodynamic quantities to nonequilibrium active matter [7].

At finite concentrations of swimmers, dimensional analysis shows that the nondimensional swim and Reynolds stresses depend in general on $(St_R, \phi, Pe_R, k_sT_s/(k_BT))$, where $\phi = 4\pi a^3 n/3$ is the volume fraction of active swimmers and $Pe_R \equiv a/(U_0\tau_R)$ is the reorientation Péclet number—the ratio of the swimmer size a to its run length $U_0\tau_R$. The ratio $k_sT_s/(k_BT)$ quantifies the magnitude of the swimmers' activity ($k_sT_s \sim \zeta U_0^2\tau_R$) relative to the thermal energy k_BT; this ratio can be a large quantity for typical micro-swimmers.

From previous work on overdamped active systems with negligible particle inertia [1], we know that Pe_R is a key parameter controlling the phase behavior of active systems. For large Pe_R the swimmers reorient rapidly and take small swim steps, behaving as Brownian walkers; the swimmers thus do not clump together to form

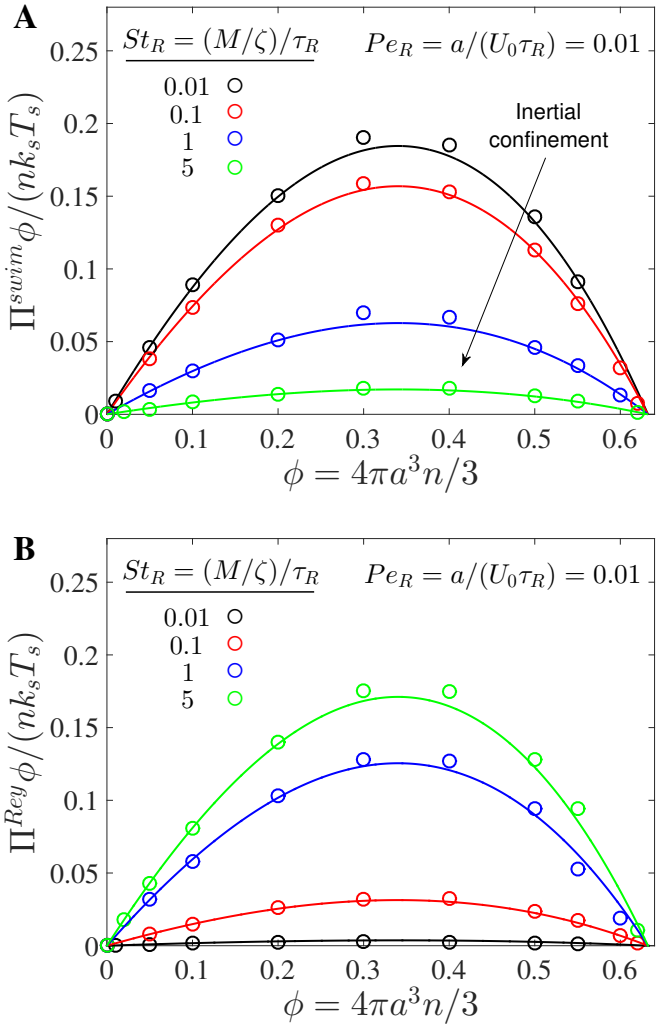

Figure 8.2: (**A**) Swim pressure, Π^{swim}, and (**B**) Reynolds pressure, Π^{Rey}, as a function of volume fraction of particles, ϕ, for different values of $St_R \equiv (M/\zeta)/\tau_R$ and a fixed reorientation Péclet number, $Pe_R \equiv a/(U_0\tau_R) = 0.01$. The symbols and solid curves are the simulation data and analytical theory, respectively. The Brownian osmotic pressure $\Pi^B = nk_BT$ has been subtracted from the Reynolds pressure.

clusters and the system remains homogeneous. For small Pe_R the swimmers obstruct each others' paths when they collide for a time τ_R until they reorient. This decreases the run length of the swimmers between reorientation events and causes the system to self-assemble into dense and dilute phases resembling an equilibrium liquid-gas coexistence.

As reported previously for $St_R = 0$ [1, 7], for small Pe_R the swim pressure decreases with increasing swimmer concentration. To verify how finite particle inertia affects the swim pressure at larger concentrations, we conducted simulations by evolving the motion of active particles following Eqs 8.1 and 8.2, with an additional hard-sphere interparticle force $\boldsymbol{F}^P$ that prevents particle overlaps using a potential-free algorithm [20]. Care was taken to ensure that the simulation time step was small enough to preclude unwanted numerical errors associated with resolution of particle collisions. We varied the simulation time step from $dt/\tau_R = 10^{-5} - 10^{-3}$ and found a negligible difference in our results. As shown in Fig 8.2A, for finite St_R the data from our simulations are well described by the expression $\Pi^{swim} = nk_sT_s(1 - \phi - \phi^2)/(1 + 2St_R)$, which is simply a product of a volume fraction dependence and a Stokes number dependence of Eq 8.3. The volume fraction dependence $(1 - \phi - \phi^2)$ was used previously to model the phase behavior of active matter [7]. In addition to using a potential-free algorithm to model hard-sphere particles, we have also tested a short-ranged, repulsive Weeks-Chandler-Andersen potential with an upper cut-off at particle separation distances of $r = 2^{1/6}(2a)$. Using this softer potential, the swim pressure does not exhibit a concentration dependence of $(1-\phi-\phi^2)$ because the effective radius of the particles decreases as the system becomes denser, meaning that colliding particles exhibit increasingly large overlaps. Increasing particle inertia (i.e., larger St_R) also changed the effective particle size. As previously stated [21], one must use care when soft potentials are used to model hard-sphere particle collisions because the effective particle size may depend on system parameters (like Pe_R and St_R).

The clustering of swimmers reduces their translational velocity autocorrelation, $\langle \boldsymbol{UU} \rangle$, and hence decreases the Reynolds pressure. As shown in Fig 8.2B, our simulations show that the Reynolds pressure decreases with concentration, increases with St_R, and is well described by the expression $\Pi^{Rey} = nk_sT_s(1 - \phi - \phi^2)/(1 + 1/(2St_R)) + nk_BT$.

The sum of the swim and Reynolds stresses is given by

$$\Pi^{swim} + \Pi^{Rey} = nk_BT + nk_sT_s(1 - \phi - \phi^2), \tag{8.6}$$

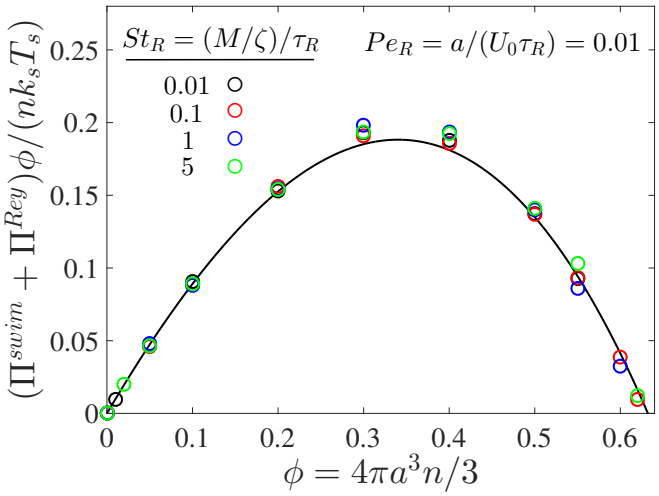

Figure 8.3: Sum of swim and Reynolds pressures, $\Pi^{swim} + \Pi^{Rey} = -\text{tr}(\boldsymbol{\sigma}^{swim} + \boldsymbol{\sigma}^{Rey})/3$, as a function of volume fraction of particles ϕ for different values of $St_R \equiv (M/\zeta)/\tau_R$ and a fixed reorientation Péclet number, $Pe_R \equiv a/(U_0\tau_R) = 0.01$. The symbols and solid curve are the simulation data and analytical theory of Eq 8.6, respectively. The Brownian osmotic pressure $\Pi^B = nk_BT$ has been subtracted from the total pressure.

which again has no dependence on neither St_R nor Pe_R, even at finite ϕ. Equation 8.6 is corroborated by our simulations as shown in Fig 8.3. This result implies that the existing mechanical pressure theory [7] developed for overdamped systems can be used directly for swimmers with finite Stokes numbers, as long as we include the Reynolds stress contribution into the active pressure. Inclusion of the Reynolds stress is critical, as confinement experiments and computer simulations measure the total active pressure, including both the swim and Reynolds contributions.

In addition to the swim and Reynolds stresses, interparticle interactions between the swimmers at finite concentrations give rise to an interparticle stress, $\boldsymbol{\sigma}^P(St_R, \phi, Pe_R, k_sT_s/(k_BT))$. For repulsive interactions, the interparticle (or collisional) pressure, $\Pi^P = -\text{tr}\boldsymbol{\sigma}^P/3$, increases monotonically with concentration and helps to stabilize the system. As shown in Fig 8.4, we find that the expression $\Pi^P/(nk_sT_s) = 3Pe_R\phi g(\phi)/(1 + 0.5St_R)$ agrees with the simulation data for a fixed value of $Pe_R = 0.01$, where $g(\phi) = (1 - \phi/\phi_0)^{-1}$ is the pair distribution function at particle contact, and $\phi_0 = 0.65$ is a parameter obtained from the interparticle pressure of hard-sphere molecular fluids [7]. We can add Π^P to Eq 8.6 to construct phase diagrams of a system of inertial swimmers, which are qualitatively similar to those presented in [7] for small values of St_R.

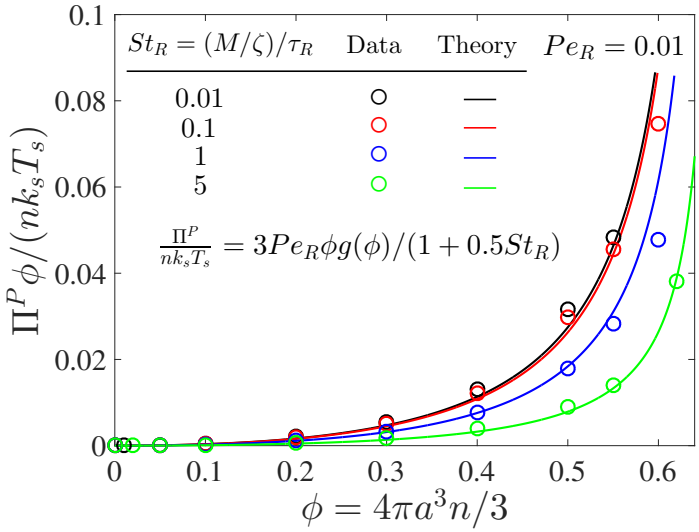

Figure 8.4: Interparticle collisional pressure, Π^P, as a function of volume fraction of particles, ϕ, for different values of $St_R \equiv (M/\zeta)/\tau_R$ and a fixed reorientation Péclet number, $Pe_R \equiv a/(U_0\tau_R) = 0.01$. The symbols and solid curves are the simulation data and analytical expression, respectively.

As shown by Batchelor [22], there may be an additional contribution to the particle stress arising from local fluctuations in acceleration, $\boldsymbol{f}'$, and is given by $-(1/V)\sum\int_{V_p}\rho\boldsymbol{f}'\boldsymbol{r}dV$, where V is the volume of the suspension (fluid plus particles), V_p is the volume of an individual particle, ρ is the uniform density of the suspension, $\boldsymbol{r}$ is a position vector (or the moment arm) from the particle center, and the summation is over the number of particles in the volume V. For a dilute system of rigid particles, this term arises only from solid body rotation of the particle and takes the form $\int_{V_p}\boldsymbol{f}'\boldsymbol{r}dV = (4\pi a^5/15)(\boldsymbol{\Omega}_P\boldsymbol{\Omega}_P - \boldsymbol{\Omega}_P\cdot\boldsymbol{\Omega}_P\boldsymbol{I})$, where $\boldsymbol{\Omega}_P$ is the average angular velocity of the rigid particle of size a. Here the active swimmers have no average angular velocity, so there is no stress arising from local fluctuations in acceleration for dilute active systems of rigid particles.

8.5 Conclusion

Here we presented a mechanical pressure theory for active Brownian particles with finite inertia. We neglected hydrodynamic interactions between the swimmers, which may contribute additional terms (like the “hydrodynamic stresslet" [23]) to the active pressure, and result in large-scale coherent motion of the constituents. The ratio of the magnitudes of the hydrodynamic stress to the swim stress is $\sigma^H/\sigma^{swim} \sim (n\zeta U_0 a)/(n\zeta U_0^2\tau_R) = a/(U_0\tau_R) \equiv Pe_R$. The hydrodynamic stress

contribution becomes negligible when phase-separation occurs at low Pe_R.

We assumed that the surrounding fluid obeys the steady Stokes equations, which may not be true for larger swimmers that propel themselves using fluid inertia. However, the concepts of the swim and Reynolds stress apply for swimmers with a nonlinear hydrodynamic drag factor, $\zeta_{inertia}(|\boldsymbol{U}|)$, where $|\boldsymbol{U}|$ is the magnitude of the swimmer velocity. For example, a self-propelled body may experience a fluid drag that is quadratic in the velocity $\boldsymbol{F}^{drag} \sim \zeta_{inertia}(|\boldsymbol{U}|)\boldsymbol{U} \sim (\rho_s a^2 |\boldsymbol{U}|)\boldsymbol{U}$, where ρ_s is the fluid density and a is the characteristic size of the body. The nondimensional Langevin equations would become $d\boldsymbol{U}/dt = -A|\boldsymbol{U}|(\boldsymbol{U} - \boldsymbol{q})$, where $\boldsymbol{q}$ is the orientation vector of the swimmer and $A = \rho_s a^2 U_0 \tau_R / M \sim (1/St_R)(\zeta_{inertia}/(\eta a))$ is the relevant quantity that must be varied.

8.6 Appendix

Integrating Eq 8.1 twice in time, we obtain the position of the swimmer,

$$\boldsymbol{x}(t) = \boldsymbol{x}(0) + \boldsymbol{U}(0)\tau_M \left(1 - e^{-t/\tau_M}\right) + \int_0^t \left(U_0 \boldsymbol{q}(t') + \sqrt{2D_0}\boldsymbol{\Lambda}_T(t')\right)\left(1 - e^{-(t-t')/\tau_M}\right) dt', \quad (8.7)$$

where $\boldsymbol{x}(0)$ and $\boldsymbol{U}(0)$ are the arbitrary initial position and velocity, respectively, $\tau_M \equiv M/\zeta$ is the momentum relaxation time, U_0 is the intrinsic swimmer velocity, $\boldsymbol{q}$ is the unit orientation vector of the swimmer, and $\boldsymbol{\Lambda}_T$ is a unit random deviate. Integrating Eq 8.2 and using the kinematic relation, $\boldsymbol{\Omega} \times \boldsymbol{q} = d\boldsymbol{q}/dt$, we obtain

$$\frac{d\boldsymbol{q}}{dt} = \boldsymbol{\Omega}(0) \times \boldsymbol{q}(t) e^{-t/\tau_I} + \frac{1}{\tau_I}\sqrt{\frac{2}{\tau_R}} \int_0^t \boldsymbol{\Lambda}_R(t') \times \boldsymbol{q}(t') e^{-(t-t')/\tau_I}\, dt', \quad (8.8)$$

where $\boldsymbol{\Omega}(0)$ is the initial angular velocity, $\tau_I = I/\zeta_R$ is the angular momentum relaxation time, and $\boldsymbol{\Lambda}_R$ is a unit random deviate. Equation 8.8 is of the form $dq_i/dt = A_{ik}(t)q_k$, where $A_{ik}(t)$ is a coefficient matrix. The general solution of Eq 8.8 is $q_i(t) = q_k(0) e^{\int_0^t A_{ik}(t')\, dt'}$, where $q_k(0)$ is an arbitrary initial orientation of the swimmer.

We are interested in the orientation autocorrelation

$$\langle q_i(t) q_n(t') \rangle = \frac{1}{3}\delta_{nk} \langle e^{\int_{t'}^t A_{ik}(t'')dt''} \rangle, \quad (8.9)$$

where $A_{ik}(t) = \epsilon_{ijk}\left(\Omega_j(0)e^{-t/\tau_I} + \sqrt{2/(\tau_R\tau_I^2)}\int_0^t \Lambda_j(t') e^{-(t-t')/\tau_I} dt'\right)$ is the coefficient matrix, and $\boldsymbol{\epsilon}$ is the unit alternating tensor. In the limit of small angular

momentum relaxation time, $\tau_I \to 0$, we obtain $A_{ik}(t) = \sqrt{2/\tau_R}\epsilon_{ijk}\Lambda_j(t)$, and

$$\langle q_i(t)q_n(t')\rangle = \frac{1}{3}\delta_{in}e^{-2(t-t')/\tau_R}. \tag{8.10}$$

Notice that as $\tau_R \to 0$ the autocorrelation becomes a delta function and the swimmer reorients rapidly and behaves as a Brownian walker.

Using Eqs 8.7, 8.10, and the swim force $\boldsymbol{F}^{swim} \equiv \zeta U_0 \boldsymbol{q}$, the swim stress is given by

$$\boldsymbol{\sigma}^{swim} = -n\langle \boldsymbol{x}\boldsymbol{F}^{swim}\rangle = \frac{n}{3}\zeta U_0^2 \boldsymbol{I}\left[\frac{\tau_R}{2}\left(1-e^{-2t/\tau_R}\right) - \frac{1}{2/\tau_R+1/\tau_M}\left(1-e^{-(2/\tau_R+1/\tau_M)t}\right)\right], \tag{8.11}$$

where we have used that $\langle \boldsymbol{x}(0)\boldsymbol{F}^{swim}(t)\rangle = \langle \boldsymbol{U}(0)\boldsymbol{F}^{swim}(t)\rangle = \langle \boldsymbol{F}^{swim}(t')\boldsymbol{\Lambda}_T(t)\rangle = \boldsymbol{0}$. Taking times $t > \tau_M$ and $t > \tau_R$, we obtain Eq 8.3 of the main text.

Following a similar procedure, the Reynolds stress is given by

$$\begin{aligned}\boldsymbol{\sigma}^{Rey} = -nM\langle \boldsymbol{U}\boldsymbol{U}\rangle = -nM\langle \boldsymbol{U}(0)\boldsymbol{U}(0)\rangle e^{-2t/\tau_M} - \\ \frac{nM}{3}\left(\frac{U_0}{\tau_M}\right)^2 \boldsymbol{I}\left\{\frac{1}{2/\tau_R+1/\tau_M}\left[\frac{\tau_M}{2}\left(1-e^{-2t/\tau_M}\right) - \right.\right. \\ \left.\frac{1}{-2/\tau_R+1/\tau_M}\left(e^{-(2/\tau_R+1/\tau_M)t} - e^{-2t/\tau_M}\right)\right] + \\ \left.\frac{1}{-2/\tau_R+1/\tau_M}\left[-\frac{\tau_M}{2}\left(1-e^{-2t/\tau_M}\right) + \frac{1}{2/\tau_R+1/\tau_M}\left(1-e^{-(2/\tau_R+1/\tau_M)t}\right)\right]\right\} - \\ nk_BT\left(1-e^{-2t/\tau_M}\right)\boldsymbol{I}.\end{aligned} \tag{8.12}$$

Taking times $t > \tau_M$ and $t > \tau_R$, we obtain the Reynolds stress as given in Eq 8.4 of the main text.

References

[1] S. C. Takatori, W. Yan, and J. F. Brady. "Swim pressure: Stress generation in active matter". *Phys Rev Lett* 113.2 (2014), p. 028103.

[2] S. C. Takatori and J. F. Brady. "Forces, stresses and the (thermo?) dynamics of active matter". *Curr Opin Colloid Interface Sci* 21 (2016), pp. 24–33.

[3] F. Ginot et al. "Nonequilibrium equation of state in suspensions of active colloids". *Phys Rev X* 5.1 (2015), p. 011004.

[4] X. Yang, M. L. Manning, and M. C. Marchetti. "Aggregation and segregation of confined active particles". *Soft Matter* 10.34 (2014), pp. 6477–6484.

[5] S. A. Mallory, A. Šarić, C. Valeriani, and A. Cacciuto. “Anomalous thermomechanical properties of a self-propelled colloidal fluid”. *Phys Rev E* 89.5 (2014), p. 052303.

[6] A. P. Solon et al. “Pressure and phase equilibria in interacting active Brownian spheres”. *Phys Rev Lett* 114.19 (2015), p. 198301.

[7] S. C. Takatori and J. F. Brady. “Towards a thermodynamics of active matter”. *Phys Rev E* 91.3 (2015), p. 032117.

[8] I. Theurkauff, C. Cottin-Bizonne, J. Palacci, C. Ybert, and L. Bocquet. “Dynamic clustering in active colloidal suspensions with chemical signaling”. *Phys Rev Lett* 108.26 (2012), p. 268303.

[9] J. Palacci, S. Sacanna, A. P. Steinberg, D. J. Pine, and P. M. Chaikin. “Living crystals of light-activated colloidal surfers”. *Science* 339.6122 (2013), pp. 936–940.

[10] G. S. Redner, M. F. Hagan, and A. Baskaran. “Structure and dynamics of a phase-separating active colloidal fluid”. *Phys Rev Lett* 110.5 (2013), p. 055701.

[11] J. Bialké, H. Löwen, and T. Speck. “Microscopic theory for the phase separation of self-propelled repulsive disks”. *Europhys Lett* 103.3 (2013), p. 30008.

[12] J. Stenhammar, A. Tiribocchi, R. J. Allen, D. Marenduzzo, and M. E. Cates. “Continuum theory of phase separation kinetics for active Brownian particles”. *Phys Rev Lett* 111.14 (2013), p. 145702.

[13] M. E. Cates, D. Marenduzzo, I. Pagonabarraga, and J. Tailleur. “Arrested phase separation in reproducing bacteria creates a generic route to pattern formation”. *Proc Natl Acad Sci U.S.A* 107.26 (2010), pp. 11715–11720.

[14] S. C. Takatori and J. F. Brady. “Swim stress, motion, and deformation of active matter: Effect of an external field”. *Soft Matter* 10.47 (2014), pp. 9433–9445.

[15] S. C. Takatori, R. De Dier, J. Vermant, and J. F. Brady. “Acoustic trapping of active matter”. *Nat Commun* 7 (2016).

[16] W. Yan and J. F. Brady. “The force on a boundary in active matter”. *J Fluid Mech* 785 (2015), R1.

[17] B. Ezhilan, R. Alonso-Matilla, and D. Saintillan. “On the distribution and swim pressure of run-and-tumble particles in confinement”. *J Fluid Mech* 781 (2015), R4.

[18] E. J. Hinch. “Application of the Langevin equation to fluid suspensions”. *J Fluid Mech* 72.3 (1975), pp. 499–511.

[19] M. Allen and D. Tildesley. *Computer simulation of liquids*. Oxford, UK: Clarendon Press, 1989.

[20] D. M. Heyes and J. R. Melrose. “Brownian dynamics simulations of model hard-sphere suspensions”. *J Non-Newtonian Fluid Mech* 46.1 (1993), pp. 1–28.

[21] J. Stenhammar, D. Marenduzzo, R. J. Allen, and M. E. Cates. “Phase behaviour of active Brownian particles: The role of dimensionality”. *Soft Matter* 10.10 (2014), pp. 1489–1499.

[22] G. K. Batchelor. “The stress system in a suspension of force-free particles”. *J Fluid Mech* 41.03 (1970), pp. 545–570.

[23] D. Saintillan and M. J. Shelley. “Instabilities, pattern formation, and mixing in active suspensions”. *Phys Fluids* 20.12 (2008), pp. 123304–123315.